

University of Strathclyde

Department of Naval Architecture, Ocean and
Marine Engineering

**The Development of Intelligent Hull Forms of
Large Ships for Energy Efficient
Transportation**

Kurt Mizzi

A thesis presented in fulfilment of the
requirements for the degree of Doctor of
Philosophy

2020

This thesis is the result of the author's original research. It has been composed by the author and has not been previously submitted for examination which has led to the award of a degree.

The copyright belongs to the author under the terms of the United Kingdom Copyright Acts as qualified by University of Strathclyde Regulation 3.50. Due acknowledgement must always be made of the use of any material contained in, or derived from, this thesis.

Signed:

Date:

Acknowledgements

This PhD research has been no easy journey. Throughout the writing of this dissertation I have received a great deal of support and assistance. I would therefore like to take this opportunity to acknowledge and thank those individuals who were instrumental to the completion of this thesis.

First and foremost, I would like to thank my supervisor Prof. Osman Turan for giving me the opportunity to carry out this research and providing invaluable guidance along the way. He was always present to assist and remind me of the bigger picture. I would like to thank him for providing this opportunity to conduct my research and complete my dissertation. Furthermore, I would like to express my gratitude for my secondary supervisor, Prof. Panagiotis Kaklis, as well as other colleagues who have been fundamental to the knowledge exchange during the research.

I would also like to express my appreciation to Dr. Yigit Demirel, Matthias Maasch, Dr. Tahsin Tezdogan, Prof. Noriyuki Sasaki and Prof. Mehmet Atlar, who all helped me develop professionally and academically providing continuous support throughout my studies. Their excellent collaboration and co-operation were second to none.

I would also like to thank and single out my friend, Michaela Abela, for assisting in proofreading this thesis. I would also like to mention my colleagues at the University of Strathclyde and friends for their continuous support and motivation. I would also like to take this opportunity to thank my family, in particular my parents, Edwin and Roseanne Mizzi, for always believing in me, supporting me and making all this possible. Without their support, this opportunity would have not been possible. Their wise counsel and sympathetic ear were crucial to the completion of this thesis.

Contents

List of Figures	vi
List of Tables.....	x
Abstract	xiii
1 Introduction.....	15
1.1 Introduction	15
1.2 General Perspective.....	15
1.3 Background of the Problem.....	18
1.4 Statement of the problem	21
1.5 Research Design.....	25
1.6 Structure of this Thesis.....	29
1.7 Significance of the Study	31
1.8 Chapter Summary and Conclusion.....	31
2 Critical Review	32
2.1 Introduction	32
2.2 Literature & Critical Review	34
2.3 Key Findings & Areas Requiring Investigation.....	82
2.4 Chapter Summary and Conclusion.....	85
3 Study Procedure & Strategy.....	86
3.1 Introduction	86
3.2 Hull-Propeller Interaction Optimisation Procedure	87
3.3 Geometry.....	89
3.4 Chapter Summary & Conclusion	96
4 CFD Modelling for Hull-Propeller Performance Prediction.....	97
4.1 Introduction	97

4.2	Open Water Propeller Tests	99
4.3	Virtual Towing Hull Tests.....	106
4.4	Self-Propulsion Tests	125
4.5	Full-Scale Accuracy Comparison.....	136
4.6	Chapter Summary and Conclusion.....	144
5	Hull-Propeller Performance Analysis Techniques.....	146
5.1	Introduction	146
5.2	Hull-Propeller Performance Analysis Techniques	147
5.3	Chapter Summary and Conclusions	154
6	Hull- Stern Optimisation.....	155
6.1	Introduction	155
6.2	Optimisation Procedure Outline & Methodology	157
6.3	Results and Discussion.....	167
6.4	Chapter Summary and Conclusions	181
7	Full-Scale Design Optimisation of PBCF.....	183
7.1	Introduction	183
7.2	Optimisation Framework.....	184
7.3	Parametric Model	185
7.4	Optimisation	186
7.5	Results & Discussion	191
7.6	Physics of PBCF.....	195
7.7	Additional Comments	199
7.8	Chapter Summary and Conclusion.....	201
8	ESD Performance Impact in Different Scale Environments.....	202
8.1	Introduction	202
8.2	Performance and Fluid Flow Behaviour at Different Scales.....	203

8.3	ESD Impact at Different Scales.....	209
8.4	Chapter Summary and Conclusion.....	238
9	Analysing ESD Combinations	240
9.1	Introduction	240
9.2	Approach & Methodology	241
9.3	Towing performance Analyses: Resistance	243
9.4	Propelled Performance Analyses: Resistance, Thrust & Torque	246
9.5	Analyses of ESD Behaviour.....	249
9.6	Propulsive Performance Analyses.....	251
9.7	Wake Analyses	255
9.8	Chapter Summary and Conclusion.....	260
10	Discussion	262
10.1	Introduction	262
10.2	Achievement of Research Aims and Objectives	262
10.3	General Discussion with Novelties and Contributions to the Field	266
10.4	Future Study Recommendations	272
10.5	Chapter Summary and Conclusion.....	273
11	Conclusion & Summary.....	274
11.1	Introduction	274
11.2	Conclusions	274
11.3	Chapter Summary and Conclusion.....	276
	References	277
	Research Outputs	293

List of Figures

Figure 1. CO ₂ Emissions and Fuel Consumption by Ship Types	16
Figure 2. Carbon Dioxide Projection by 2050	17
Figure 3. Ship Energy Losses	19
Figure 4. Study Procedure.....	29
Figure 5. Energy Efficiency	33
Figure 6. Turbulence Models	45
Figure 7. Propeller Wake	55
Figure 8. Total Wake Components	56
Figure 9. Average Mean Nominal Wake	57
Figure 10. Wake Generation	58
Figure 11. Boundary Layer Development	58
Figure 12. Wake Scaling	62
Figure 13. Wake Scaling Effects with Retrofitted ESDs	64
Figure 14. ESD Categories.....	66
Figure 15. Pre-Swirl Stator and Becker Mewis Duct	68
Figure 16. Kappel, CLT Propellers and CRPP	69
Figure 17. PBCF, Asymmetric Rudder and Rudder Bulb	71
Figure 18. Comparison Nominal Wake Field for Model-Scale and Full-Scale	77
Figure 19. Components of Hull Resistance	80
Figure 20. Study Breakdown.....	86
Figure 21. PPTC Propeller	89
Figure 22. CAESES Propeller.....	90
Figure 23. JBC Geometry	91
Figure 24. RSBC Geometry	92
Figure 25. Operational Profile Analyses	94
Figure 26. Speed & Draught Frequency	94
Figure 27. Draught Frequency per Specific Popular Speeds	96
Figure 28. Surface Mesh	102
Figure 29. Boundary Conditions Configuration.....	103

Figure 30: PPTC Open Water Characteristics	104
Figure 31. Model–Scale JBC Wave Profile	107
Figure 32. Convective Courant Number	108
Figure 33. Wake Field CC Model Study.....	110
Figure 34. Wave Cut Comparison.....	111
Figure 35. Static vs DFBI Impact Study	113
Figure 36. Surface Mesh	114
Figure 37. Mesh Refinements: Side & Top	115
Figure 38. Prism Layer Blending	116
Figure 39. Wall Y+ for Case 2 & 3	116
Figure 40. Dimensions of Free Surface.....	117
Figure 41. Domain Boundary Conditions	118
Figure 42. Grid Dependency Study.....	119
Figure 43. Comparison of Experimental Results and Numerical Results	122
Figure 44. Wave Profile Comparison.....	123
Figure 45. Visual Y+ of Propeller and Hull.....	126
Figure 46. Convective Courant Numbers (<i>Case5</i>).....	126
Figure 47. Propeller Surface Mesh.....	127
Figure 48. Rotating Region	127
Figure 49. Y+ Values of Hull and Propeller	128
Figure 50. Propeller Prism Layer	129
Figure 51. Full-Scale Propeller Open Water Characteristics	137
Figure 52. Difference in Propeller Characteristics.....	140
Figure 53. Common Propeller Characteristics	141
Figure 54. Wake Shadow Area	149
Figure 55. Single and Double Wake Peak Width Definition	151
Figure 56. Wake Non-Uniformity Criterion	152
Figure 57. BSRA Output.....	149
Figure 58. Energy Components Results Format	153
Figure 59. Coupled Optimisation Framework	158
Figure 60. Parametric Foil	162
Figure 61. Basic Ship Curve Definition & Parameter Distribution	162

Figure 62. RSBC Parametric Hull.....	163
Figure 63. RSBC SAC Analyses.....	164
Figure 64. Design Variables.....	165
Figure 65. WAT Graphical User Interface	165
Figure 66. Wake Probe Evaluation Workflow	167
Figure 67. Exploration Output	168
Figure 68. Design Variables Correlations.....	170
Figure 69. Wake Non-Uniformity vs Resistance	171
Figure 70. Wake Fraction vs Resistance	172
Figure 71. Wake Fraction vs Wake Non-Uniformity	173
Figure 72. Wake Non-Uniformity vs Total Resistance: <i>Dakota07 Des01</i>	175
Figure 73. Mean Wake Fraction vs Total Resistance: <i>Dakota07 Des01</i>	175
Figure 74. Mean Wake Fraction vs Total Resistance: <i>Sobol02 Des33</i>	176
Figure 75. Wake Non-Uniformity vs Total Resistance: <i>Sobol02 Des33</i>	176
Figure 76. Mean Wake Fraction vs Total Resistance: <i>Dakota04 Des02</i>	177
Figure 77. Wake Non-Uniformity vs Total Resistance: <i>Dakota04 Des02</i>	177
Figure 78. Mean Wake Fraction vs Total Resistance: <i>Dakota04 Des02</i>	178
Figure 79. Wake Non-Uniformity vs Total Resistance: <i>Dakota04Des02</i>	178
Figure 80. Optimisation Framework.....	184
Figure 81. PBCF Geometry.....	185
Figure 82. Quasi-Random Sequence.....	187
Figure 83. Local Optimum.....	187
Figure 84. Optimisation Algorithm.....	187
Figure 85. Surface Mesh for CAESES Propeller with PBCF	189
Figure 86. Y+ Histogram (<i>Model and Full Scale Respectively</i>)	190
Figure 87. Y+ Values & Figure 88: Mesh Refinement.....	191
Figure 89. Boundary Conditions	191
Figure 90. CAESES Open Water Characteristics	192
Figure 91: Quasi Random Designs	193
Figure 92. KT Optimal Design Candidate	193
Figure 93. KQ Optimal Design Candidate.....	194
Figure 94. Angular Fin Position Variations	195

Figure 95. Pressure Distribution	196
Figure 96. Boss Cap Tip Pressure Drop.....	198
Figure 97. Hub Vortex	199
Figure 98. Wake Analyses	213
Figure 99. Velocity Definitions.....	216
Figure 100. Wall Shear Stress: Towing (<i>Flow Separation Comparison</i>)	220
Figure 101. Wake Velocity Distribution (<i>Flow separation Comparison</i>)	221
Figure 102. Limiting Streamlines for Baseline Design and Duct Design without Duct Visualisation: <i>Towing</i>	221
Figure 103. Wall Shear Stress: Self-Propulsion (<i>Flow Separation Comparison</i>) ...	222
Figure 104. Limiting Streamlines for Baseline Design and Duct Design: <i>Self-Propulsion</i>	222
Figure 105. Separation Around Duct at Maximum Width of the Duct.....	223
Figure 106. Velocity Flow Vectors (<i>Top View</i>).....	223
Figure 107. Velocity Flow Vectors (<i>Profile View</i>)	224
Figure 108. Kinetic Energy Losses: <i>Towing Conditions</i>	225
Figure 109. Kinetic Energy Losses: <i>Self-Propulsion Conditions</i>	226
Figure 110. Full-Scale Velocity Flow Vectors (<i>Bottom View</i>)	235
Figure 111. Full-Scale Velocity Flow Vectors (<i>Profile View</i>).....	235
Figure 112. Kinetic Energy Losses: <i>Towing Conditions</i>	236
Figure 113. Kinetic Energy Losses: <i>Self-Propulsion Conditions</i>	237
Figure 114. Open Water Tests	242
Figure 115. ESD Geometry.....	243
Figure 116. Duct & Fin Components.....	250

List of Tables

Table 1. PPTC Parameters	89
Table 2. CAESES Parameters	90
Table 3. JBC Particulars.....	91
Table 4. RSBC Particulars	93
Table 5. Most Frequent Operational Conditions.....	95
Table 6. Validation and Verification Cases	98
Table 7. MRF vs Sliding Mesh	101
Table 8. Steady vs Unsteady	101
Table 9. Mesh Size Comparison for PPTC Model-Scale Propeller.....	104
Table 10. Calculation of the Discretisation Error for K_T and K_Q Values	105
Table 11. Sink & Trim CFD Model Comparison	111
Table 12. PL No. & Mesh Size	114
Table 13. Refinement Details.....	114
Table 14. Grid Dependency Study	119
Table 15. Case2: Grid Convergence Study for C_T	120
Table 16. Case 2: Validation for C_T	120
Table 17. Case3: Grid Convergence Study for C_T	121
Table 18. Case 3: Validation for C_T	121
Table 19. Case4: Grid Convergence Study for C_T	121
Table 20. Case 2 with Duct Validation	123
Table 21. JBC w/Duct Wake Contour Comparison.....	124
Table 22. PL. No & Mesh Size (<i>Self-Propulsion</i>)	129
Table 23. Self-Propulsion Grid Dependency Study.....	130
Table 24. Case5: Grid Convergence Study for K_T	131
Table 25. Case 5: Validation for K_T	131
Table 26. Case 5: Grid Convergence Study for K_Q	131
Table 27. Case 5: Validation for K_Q	131
Table 28. Case 5: Grid Convergence Study for C_T	131
Table 29. Case 5: Validation for C_T	131

Table 30. JBC No Duct Wake Contour Comparison (<i>Self-Propulsion</i>)	132
Table 31. JBC w/Duct Wake Contour Comparison (<i>Self-Propulsion</i>)	134
Table 32. Powering Performance (<i>No Duct</i>).....	138
Table 33. Propulsive Performance Comparison (<i>No Duct</i>)	139
Table 34. Propulsive Performance Comparison (<i>No Duct</i>)	141
Table 35. Powering Performance (<i>With Duct</i>).....	142
Table 36. Propulsive Performance Comparison (<i>With Duct</i>).....	142
Table 37. Propulsive Performance Comparison (<i>With Duct</i>).....	143
Table 38. Hull-Propeller Analysis Techniques	147
Table 39. Self-Propulsion Comparison Analyses	179
Table 40. Design Variables	186
Table 41. Wall Y+ Study	190
Table 42. Sample of Sobol Design Results.....	193
Table 43. Energy Efficiency Gain.....	194
Table 44. Optimal Design Parameters	195
Table 45. Performance Breakdown.....	196
Table 46. Performance Difference after PBCF Installation.....	197
Table 47. Propulsion Performance Scaling	205
Table 48. Wake Scaling Analyses @ Propeller Plane (<i>Towing</i>).....	205
Table 49. Wake Scaling @ Propeller Plane (<i>Towing</i>)	206
Table 50. Wake Scaling @ 0.0375Lpp (<i>Self-Propulsion</i>)	207
Table 51. Wake Scaling Analyses @ 0.117Lpp (<i>Self-Propulsion</i>).....	207
Table 52. Wake Scaling @ 0.0168Lpp (<i>Self-Propulsion</i>)	207
Table 53. Wall Shear Stress Analyses Scaling effects.....	208
Table 54. Performance: <i>Towing</i>	209
Table 55. Performance: <i>Self-Propulsion</i>	209
Table 56. Resistance Breakdown: <i>Towing</i>	210
Table 57. Resistance Breakdown: <i>Self-Propulsion</i>	211
Table 58. Thrust and Torque Breakdown: <i>Self-Propulsion</i>	211
Table 59. Wake Analyses @ Propeller Plane (<i>Towing</i>).....	214
Table 60. Flow Field Behaviour @ Propeller Plane (<i>Towing</i>).....	215
Table 61. Velocity Comparisons.....	217

Table 62. Wake Analyses @ 0.117Lpp (<i>Self-Propulsion</i>).....	217
Table 63. Flow Filed behaviour @ 0.117Lpp (<i>Self-Propulsion</i>)	218
Table 64. Flow Field behaviour Post-Propeller (<i>Self-Propulsion</i>).....	219
Table 65. Kinetic Energy Losses: <i>Towing Conditions</i>	224
Table 66. Kinetic Energy Losses: <i>Self-Propulsion Conditions</i>	225
Table 67. Performance: <i>Towing</i>	227
Table 68. Performance: <i>Self-Propulsion</i>	228
Table 69. Resistance Breakdown: <i>Towing</i>	229
Table 70. Resistance Breakdown: <i>Self-Propulsion</i>	229
Table 71. Thrust and Torque Breakdown: <i>Self-Propulsion</i>	229
Table 72. Full-Scale Wake Analyses @ Propeller Plane (<i>Towing</i>)	230
Table 73. Flow Field Behaviour @ Propeller Plane (<i>Towing</i>).....	231
Table 74. Full-Scale Wake Analyses @ 0.117Lpp (<i>Self-Propulsion</i>)	232
Table 75. Full-Scale Flow Filed behaviour @ 0.117Lpp (<i>Self-Propulsion</i>).....	232
Table 76. Full- Scale Flow field behaviour Post-Propeller (<i>Self-Propulsion</i>).....	233
Table 77. Full-Scale Wall Shear Stress Analyses	234
Table 78. Kinetic Energy Losses: <i>Towing Conditions</i>	236
Table 79. Kinetic Energy Losses: <i>Self-Propulsion Conditions</i>	237
Table 80. Kinetic Energy Losses: <i>Model-Scale vs Full -Scale</i>	237
Table 81. ESD Combinations.....	241
Table 82. Resistance Breakdown: <i>Towing</i>	244
Table 83. Understanding Resistance in Towing	245
Table 84. Resistance, Thrust and Torque Breakdown: <i>Self-Propulsion</i>	246
Table 85. Understanding Resistance in Self-propulsion	247
Table 86. ESD Analyses (<i>Drag</i>)	249
Table 87. Propulsion Performance Analyses	252
Table 88. Wake Analyses @ propeller Plane (<i>Towing</i>).....	255
Table 89. Flow Field Behaviour @ Propeller Plane (<i>Towing</i>).....	255
Table 90. Flow Field Behaviour @ Post- Propeller Plane (<i>Self-Propulsion</i>)	258

Abstract

It is not usual that the interests of ship owners are aligned with maritime legislation requirements with the incentives to make ships more efficient. Owners seek to reduce the ship operating costs whilst entities, such as the IMO, push for a more environment friendly marine industry.

A ship's efficiency can be improved by optimising the hull form and/or by installing Energy Saving Devices (ESD) in order to improve the hydrodynamic performance and fluid flow of a vessel. These two areas are not new to the industry and have been investigated using various methods, including computational fluid dynamics (CFD) procedures. The use of CFD for ship performance analyses is becoming more popular in the maritime industry due to its cost-effective capabilities. The continuous development of numerical simulation (CFD) as well as high performance computing opens doors to new areas of investigation and allows research to further study topics that have been previously looked into as well as research questions that have never been explored.

The general aim of this PhD thesis is to contribute to the body of knowledge by shedding light on improving the hydrodynamic performance of large ships for energy efficient transportation. This was achieved by accomplishing a series of objectives and case studies that addressed various research questions.

This study initially proposes an intelligent state-of-the-art methodology for predicting and enhancing the hull-propeller interaction of a vessel using numerical techniques (CFD), optimisation procedures and high-performance computing to identify optimal stern designs as well as understanding the physics and impact of Energy Saving Device/s that could help improve the stern flow characteristics.

The CFD method, that was used to predict the performance for all the various case studies, was validated and verified using well established procedures. The implementation of the recently available curvature correction feature in the numerical model and its enhanced wake prediction capabilities were clearly demonstrated.

Moreover, various types of post-processing CFD analyses that were deemed useful to understand the hydrodynamic performance of a vessel were listed and outlined.

A practical full-scale stern form optimisation procedure for a bulk carrier was developed and demonstrated. Furthermore, whether the quality of a nominal wake can provide any insight into the propeller performance of a vessel was investigated and evaluated.

With regards to the case studies investigating Energy Saving Devices, Propeller Boss Cap Fins were analysed in open water full-scale conditions to understand the physics, function and working principles of such technologies. A state-of-the-art full-scale PBCF optimisation procedure was also demonstrated. The performance of a Wake Equalising Duct at different scale conditions was investigated and compared. The study indicated that the duct is not as effective in full-scale. The reasons and findings were thoroughly discussed and outlined.

The thesis also focused on the research questions regarding the installation of multiple Energy Saving Devices on a ship system. Whether the benefits are directly cumulative or whether the ESDs affect the flow regimes of one another? Thus, a case study was carried out by investigating seven combinations using PBCF, a duct and stator fins. The performance of each condition was clearly outlined, discussed and explained.

This author believes that this study has exhibited and proven the ability and applicability of computational fluid dynamics (CFD) to better understand the hydrodynamics of a ship system and improve hull-propeller interaction dynamics. The studies and research in this thesis contribute to the industry as well as academia by shedding more light on large ship hydrodynamic systems.

1 Introduction

1.1 Introduction

This chapter introduces the setting for this thesis identifying the motivations behind the research. A thorough overview of the hydrodynamic performance of large ships was presented, and specific gaps in the marine body of knowledge were identified, creating a motive for this study. The research strategy was then presented, highlighting the aims and objectives together with the respective research questions to be addressed.

1.2 General Perspective

1.2.1 Operational Costs and Maritime Legislation

Ships are known to be one of the most popular and efficient modes of bulk transportation, contributing to around 90% of international trade, thus allowing globalisation and communication between different countries. Ship operations and resultant fuel consumption lead to emissions, in particular greenhouse gases. This was a principal concern stated by the 2007 Intergovernmental Panel on Climate Change (IPCC, 2008). A recent GHG study (2015), conducted by IMO reported that 796 million tonnes of CO₂ were emitted by international shipping during 2012 making up 2.2% of the global emissions. This recorded a decrease from 2007 when 885 million tonnes of CO₂ were recorded. This suggests that preventive measures in place are proving useful. It was estimated that international shipping generated around 18.6 million and 10.6 million tonnes of NO_x and SO_x annually making carbon dioxide the most important gas emitted by ships. In addition, total fuel consumptions and carbon dioxide emissions were studied across all ship types identifying containers and bulk carriers to be the highest consumers and pollutants (Figure 1). Although shipping emission volumes seem minor, their absolute values are significant and if not addressed, are likely to increase drastically in the coming years with the increase in the world seaborne trade.

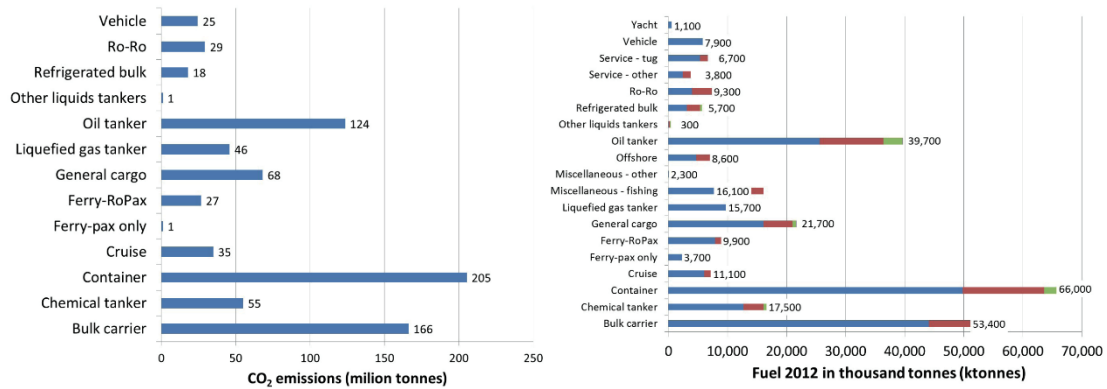


Figure 1. CO₂ Emissions and Fuel Consumption by Ship Types (IMO, 2015)

A projection outlined by Fang (2013), indicated an increase of the world seaborne trade in the near future, predicting it to double by 2030. This increase in shipping volume will lead to an increase in ship emissions. IMO's second GHG study indicated that in the absence of policies, by the year 2050, ship emissions could multiply by a factor of around 2 to 3 times that of current levels. This was then overshadowed by the third IMO study (2015) which projected the increase of emissions between 50% and 250% by 2050 depending on the future economic and energy developments thus depicting different scenarios (Figure 2). These studies identify a problematic issue which requires attention and recognition as it is a growing concern which must be addressed. The need to improve energy efficiency to minimise emissions from the shipping sector is vital.

Surprisingly, these ambitions are commonly shared with ship owners seeking to reduce fuel costs. Although this might not be an important factor at present due to the significantly low fuel prices, it will definitely raise concerns if the bunker prices resort back to higher ranges. This is demonstrated by Hansen and Dinham-Peren (2014) who outline that with the increase of fuels costs, a vessel's fuel consumption becomes a ship owner's prime concern which also boils down to the energy efficiency of the vessel.

In the year 2000, various research institutes collaborated together to carry out a study for the International Maritime Organisation (IMO) indicating the motivation and need to reduce shipping GHG. The study (IMO, 2009) was extended in 2009 by the IMO as they identified the potential energy efficiency improvements that could be attained using various measures. The different methods were classified under three categories namely; Technical, Operational and Market Based Measures (MBM) using the Energy Efficiency Design Index (EEDI) criteria and the Ship Energy Efficiency Management Plan (SEEMP). The study outlined that if such measures were implemented, energy efficiency levels could increase by 25% to 75%.

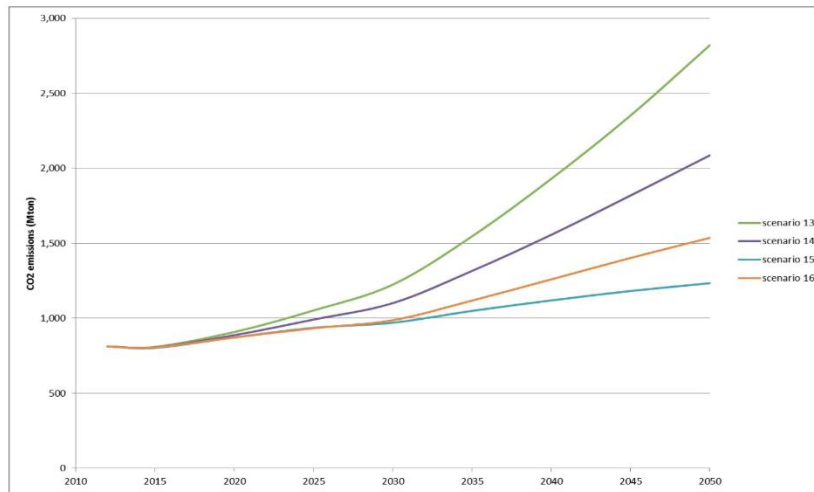


Figure 2. Carbon Dioxide Projection by 2050 (IMO, 2015)

1.2.2 EEDI

The Marine Environmental Protection Committee (MEPC), a specialised group of the IMO, developed the so-called Energy Efficiency Design Index (EEDI) as a tool to control and lower ship emissions. This was adopted as a mandatory measure during the 62nd MEPC meeting in July 2011. It is an index that compares the volume of carbon dioxide a ship emits in relation to the cargo it transports and can be expressed as transport work capacity. This is used to restrict the designed energy efficiency of the ship before building it by providing a calculation for the predicted carbon emissions emitted compared to the useful work done by the ship (i.e. tonnes of cargo transported per nautical mile).

The first international ship energy efficiency regulations entered into force in 2013 with a phased implementation plan (IMO, 2014) that will see the restrictions become more stringent over the coming years. The EEDI provides a strong incentive for the shipping industry to improve fuel consumption efficiency with updated technical improvements. Failing to meet the requirements may lead to the detention of ships, fined or even forbidden to trade. This has brought about the need for improving energy efficiency for environmental benefits and will also help reduce operational costs during difficult maritime economic cycles (Stopford, 2008).

The EEDI is a simple formula that estimates the carbon emission of a vessel per tonne mile. It is an index developed to allow for the assessment of a ship's performance and carbon footprint. Compliance is attained by comparing the attained EEDI of the vessel to corresponding baseline values that have been stated by the IMO. The restriction of the calculated EEDI value is

assigned depending on the ship type and size. Therefore, various baselines for different ship categories have been proposed. The EEDI is represented by the equation (1) below.

$$\text{EEDI} = \frac{\text{Main Engines Emissions} + \text{Auxiliary Engines Emissions} + \text{Shaft Motors Emissions} + \text{Efficiency Technologies}}{\text{Capacity} \cdot \text{Reference Speed}} \quad (1)$$

The EEDI equation takes into consideration the emissions from the main engine, auxiliary engine, shaft/motors and any other technologies that influence the mechanical energy efficiency of the vessel. These are expressed as a ratio of the transport work carried out by the vessel, which is expressed by the volume of cargo /deadweight and the design speed of the vessel. Therefore, in order to reduce the EEDI value, one has to try minimising the nominator and maximising the denominator. This can be addressed in a number of ways.

The speed of the vessel, in particular, has a significant impact on the EEDI and fuel consumption. This is because the speed is exponentially related to the required propulsive power. Significant savings make it easy to understand why there is substantial interest in slow steaming, especially when fuel prices escalate. This being said, it should be noted that the ship speed varies according to the market demands and expectations. These criteria should be reconsidered regularly to reflect realistic ship operations since it has a direct impact on the EEDI.

Various solutions have been outlined, generally trying to minimise the installed power or to maximise the cargo weight of a vessel. However, it was clearly specified by the IMO, that any changes made should not inhibit the safety of the vessel, (IMO, 2009): “Safety should not be compromised”. Although shipping is known to be the most efficient mode of commercial transportation per tonne of cargo, several design and operational methods have been identified with the potential to increase ship energy efficiency (IMO, 2009).

1.3 Background of the Problem

1.3.1 Energy Efficient Ship Design

The IMO has outlined various methods addressing these issues that can help reduce energy losses. The various technical measures proposed generally relate to resistance, machinery and

propulsion systems also highlighting the potential energy efficiency improvement in each area related to the extent of losses. IMO's second GHG study presents a table (Figure 3) indicating typical losses of energy and a breakdown for the different areas of the vessel for different types of vessels.

	Tanker/bulk		Container		General cargo		RoPax	
Speed (knots)	15.6	10.9	21.2	15.5	13.4	9.5	20.1	14.7
Bunker	100	100	100	100	100	100	100	100
Engine								
Exhaust	25.5	28.4	25.0	28.0	25.5	28.4	25.5	28.4
Shaft	49.3	45.4	50.5	46.5	49.3	45.4	49.3	45.4
Heat	25.2	26.2	24.5	25.5	25.2	26.2	25.2	26.2
Propulsion								
Propeller loss	16.3	14.3	15.6	13.0	19.7	15.3	15.5	14.4
Propulsion power	32.1	30.2	33.7	32.4	28.1	28.8	32.6	29.9
Transmission loss	1.0	0.9	1.3	1.2	1.5	1.4	1.2	1.1
Propeller								
Axial loss	6.3	5.3	4.8	3.5	8.8	5.6	4.8	4.3
Rotational loss	3.9	3.4	5.3	3.9	6.0	4.5	5.0	4.7
Frictional loss	6.0	5.7	5.5	5.6	4.9	5.2	5.7	5.4
Hull								
Wave generation	6.4	4.1	8.6	3.9	12.8	5.9	5.3	3.9
Air resistance	0.6	0.6	1.0	1.1	0.7	1.0	1.0	0.9
Hull friction	16.2	16.6	13.9	15.6	8.3	12.0	15.9	14.7
Residual resistance	2.7	1.9	1.8	1.4	2.8	3.2	2.2	1.4
Weather and waves	6.2	6.9	8.4	10.3	3.5	6.7	8.3	9.1

Figure 3. Ship Energy Losses (IMO, 2009)

As can be seen from Figure 3 above, a ship's energy is lost from various areas of the ship system with hull and propulsion factors being significant contributors. This is in agreement with another report published by Fathom (Lockley et al., 2011) that suggests that the main losses of a hull-propeller hydrodynamic system are those related to the generation of waves at the pressure peaks along the hull, the generation of flow due to the surface friction and the propulsion losses. These issues have thus driven research to focus on challenges such as optimising hull designs, propeller performance and the stern flow characteristics, also known as the hull-propeller interaction.

When focusing on hull design and hull-propeller optimisation, we refer to the modification of the hull forms, the selection of the appropriate propeller or the installation of various Energy Saving Devices in order to improve the hydrodynamic system and fluid flow of a vessel. When designing the after body of ships, the designer aims to minimise the resistance of the vessel and maximise the propulsive efficiency. Having said this, one should also be aware of the

unacceptable propeller induced levels of vibration that the resultant design might generate. All these three objectives tend to conflict each other, making the optimisation of hull-propeller performance challenging.

There are various methods that can help improve the stern flow field of a ship with all approaches being applicable to new builds and some of those methods such as the installation of retrofitting devices, which are applicable to existing vessels. Common ways of hydrodynamic improvement are generally associated with bulbous bow design, stern form design, hull form and the installation of energy saving devices. In summary, these technologies address the following hydrodynamic characteristics:

- Bulbous Bow Design: Waves
- Stern Design: Directs the fluid flow into the Propeller
- Hull Design: Flow along the hull
- ESD: Improve propulsive efficiency and wake characteristics depending on the technology.

All these factors will have an impact on the resistance, propulsion efficiency and resultant delivered power of the vessel. It is for this reason that design and optimisation approaches have been developed over the years in order to improve the energy efficiency of the vessel to reduce operational cost and also meet recent EEDI requirements.

The shape or type of the aft end of a vessel plays a crucial role in the stern flow characteristics. Higher block coefficient vessels with a bulbous stern tend to generate higher viscous resistance due to the generation of vortices, thus requiring a higher effective power. Such bulky vessels generally provide a better propulsive coefficient (QPC) and produce a high non-uniform wake resulting in significant propeller excited vibrations (PEV). Therefore, when it comes to optimising such vessels, the key is to try to improve or maintain the propulsive performance and reduce the PEV by improving the velocity distribution in the wake flow.

Although hull designs can be modified to improve flow characteristics and reduce drag, retrofitting technologies, also known as Energy Saving Devices, can be additionally installed to direct or accelerate stern flow thus generating a more uniform wake field into the propeller improving propeller efficiency as well as resulting in other benefits such as the reduction of pressure fluctuations.

1.3.2 Energy Saving Devices

Hydrodynamics based Energy Saving Devices (ESDs) are usually retrofitting devices that can be installed on vessels to improve the propulsion and hull-propeller interaction efficiencies. They can be installed on optimised new hulls as well as existing vessels by means of retrofitting (Hansen et al., 2011). A wide range of ESDs have been developed through the years with different features, types and working principles. These devices can be generally classified into three different categories; Pre-swirl, Post-swirl and added features to the propeller.

Recently a large amount of experimental and numerical ESD research has been carried out. Various studies (e.g. Kawamura (2012), Hansen (2011), Atlar (1998) and Schuiling (2013)) suggest that the installation of ESDs on a ship can result in a significant improvement in energy efficiency. As specified by Hooijmans et al. (2010), ESDs are designed to improve the flow around the hull, and the wake/propeller inflow. They can also be designed to recover energy leaving the ship system. On-going research focuses on maximising the energy efficiency potential of these devices through design improvements. With the increased availability of computational power and advances in numerical tools and modelling software, the use of optimisation procedures are becoming more and more popular to identify the potential energy efficiency savings that ESDs provide.

Nevertheless, the availability and reliability of many ESDs that can be used to reduce the EEDI value and increase energy efficiency remain uncertain. There is a lack of confidence in their use within the industry because efficiency gains are small and extremely difficult to assess by full-scale measurements as well as model tests. Furthermore, there is ambiguity regarding the compatibility with different ship types and the benefits involved when installing multiple energy saving devices.

1.4 Statement of the problem

Having provided insight into the background of the problem, specific gaps in the body of knowledge have been identified and listed below. The issues that require further investigation are considered as motivating drivers for this study. Once these have been clearly identified and highlighted, the research design and strategy, including aims and objectives, will be outlined addressing each of these gaps.

1. Numerical ship optimisation procedures generally aim to improve performance factors such as resistance or power without taking into consideration wake analyses or propeller-induced vibrations. As explained in the previous section (1.3), propulsion performance, wake characteristics and propeller excited vibrations are vital elements in the aft body design of a vessel. Such criteria are generally investigated for the best design candidates after the optimisation process to determine whether the designs are satisfactory. Capturing wake distribution velocities using numerical procedures require high computational power, experienced CFD users and considerable running time. In addition, most optimisation processes carry out the investigation at model scale and in towing conditions. Model-scale simulations do not capture ship behaviour appropriately due to Froude scaling phenomena resulting in misleading results (Hans-Jurgen Heinke, 2011). Furthermore, analysing the performance of a vessel in self-propulsion conditions is more realistic and meaningful than towing conditions giving an indication of propulsive performance. One particular study (Khorasanchi et al., 2013) indicated that the benefits of an ESD in towing conditions turned out to provide poor performance in self-propulsion conditions. That being said, self-propulsion simulations at full scale require significant computational power making optimisation procedures with many design variants very expensive and impractical. Therefore, there is need for a smart and feasible process to optimise the performance of a vessel using more practical full-scale towing simulations that also give insight into the propulsive performance of the ship by also taking wake field characteristics into consideration. To the best of the author's knowledge, research on RANS multi-objective optimization of hull drag in towing conditions at full-scale is scarce and incompletely reported in the literature. It does not include topics like validation/verification studies and multi-objective strategies to also improve wake quality characteristics. It would be interesting to investigate whether the outcome of such a process (best design) would improve the self-propulsion performance and whether such a procedure can provide a feasible compromise to optimise the vessel's energy efficiency and reduce pressure vibrations.
2. Energy Saving Devices are not new technologies and have been on the market for quite some time. Various authors have reviewed ESDs in the past, e.g. (Blaurock, 1990), all outlining various improvements and gains achieved by the different technologies that seem promising. However, ESD gains are relatively small and extremely difficult to evaluate not only by model tests but also during sea trial measurements. Improper

extrapolation of model test results due to scaling issues, together with correction factors associated with sea trials and the disconcertingly great natural variation between the performances of sister ships, create uncertainties in accuracy when determining the gain or performance of such devices. Furthermore, the benefits achieved when installing similar ESDs on different ship types, forms and speeds, vary significantly, leaving ship operators disappointed with large expenditure. Therefore, the reliability and guarantee of energy savings for such devices remain an issue, and continuous research should be carried out and encouraged to support their reliability (Mizzi et al., 2015).

- a. One of the more popular ESDs is the Propeller Boss Cap Fins (PBCF) with MOL Techno-Trade Ltd. claiming to have installed over 3000 of these technologies. They are easy to retrofit, relatively cheap and claim to provide beneficial energy savings. Although these retrofitting technologies are not new to the market and have been well established over the years, most PBCF analyses and research has been carried out at model-scale through model tests or basic CFD methods. As previously mentioned, these methods could lead to misleading results or inaccurate energy-saving claims. With the availability of more advanced computational techniques, the author understands that further detailed analyses of such technologies in full-scale conditions are required outlining their physics and function.

- b. Since the Reynolds number is considerably higher for full-scale ships when compared to the model-scale scenarios, scale effect issues are a prime concern during ESD analyses. Some researches (e.g. Hansen (2011) and Kawamura (2012)) have shown that ESDs are more efficient at full-scale than those determined from model tests. The boundary layer is relatively thinner in full-scale flows than in model test conditions. The wake fraction is, therefore, larger in model tests than in full scale. ESDs that function within the boundary layer result in different performance behaviour between both scales. Flow separation is generally delayed in full scale, and vortices encounter higher damping. Thus, ship wakes and velocity profiles in the propeller plane are significantly changed. Vortices from bilge or struts are much weaker sometimes disappearing in full-scale simulations. It is therefore vital to understand the scaling issues of retrofitting technologies and more importantly being able to accurately predict

their performance in full-scale conditions. The author understands and highlights that although some literature focusing on ESD scaling using CFD methods has been previously published, further understanding and contribution to knowledge in this field is required. The continuous developments of CFD techniques allow for better analyses and in-depth investigation of the issue. With the available state-of-the-art CFD methods and high computational power (HPC), there is a need to analyse the impact of Energy Saving Devices in different scale conditions with regards to performance, wake analyses and pressure excited vibrations. This would help contribute to the body of knowledge of the ESD community.

- c. The installation of more than one Energy Saving Device aboard a vessel is not so common. The low cost and ease of retrofit of such technologies make ESD economic feasible options that are worth looking into and investigating. A few case studies and applications have paired up technologies, but these are limited and do not delve into great technical detail. The different types of ESDs are varied with many options available, paving the way for many windows of opportunity to investigate multiple combinations. When installing a combination of compatible ESDs, (e.g. a pre-swirl device with a post-swirl device), it should be noted that the total energy efficiency is not simply cumulative (Jens Ring Nielsen, 2012). This is because some ESDs affect the flow regimes of other technologies and can reduce the total effectiveness. The efficiency of one ESD cannot be easily subtracted or added from the total efficiency. Some ESDs are compatible with each other and can be simultaneously retrofitted to obtain a higher benefit whilst others can be detrimental when used in conjunction. Such issues have not been thoroughly researched and published, requiring more input by focusing efforts on analysing the impacts of installing a combination of technologies in full-scale environments. As previously mentioned, current computational capabilities and enhanced expertise allows for the analyses of such retrofitting technologies in full-scale self-propulsion conditions investigating their impact on performance, wake characteristics and pressure excited vibrations.

1.5 Research Design

1.5.1 Research Aims

The main aim of this PhD thesis is to improve the hydrodynamic performance of large ships for energy efficient transportation. In particular, the idea is to propose an intelligent state-of-the-art methodology and process for enhancing the hull-propeller interaction of a vessel using numerical techniques, optimisation procedures and high-performance computing to identify optimal stern designs for particular vessels as well as any necessary Energy Saving Device/s that could help improve the stern flow characteristics. This was achieved by accomplishing a series of objectives that are addressing necessary research questions thus contributing to the academic body of knowledge.

1.5.2 Research Objectives

- To carry out an extensive literature review on hull-propeller interaction modelling techniques and design methods to improve the performance, including the modification of stern forms and use of ESDs in order to identify gaps in the literature.
- To validate and verify numerical procedures of ship performance analyses in towing and self-propulsion conditions, to accurately measure performance criteria and capture wake characteristics as well as wave cut analyses. The implementation of the newly available curvature correction feature for better turbulence modelling and hence, its enhanced wake prediction capabilities is also demonstrated.
- Prior to carrying out these objectives, a systematic ESD analytic process will be developed. The literature on ESD analyses will be thoroughly reviewed, and the best methods would be adopted to compile a checklist on analysing ESD technologies in-depth. This analytical process would then be used to analyse the impact of ESDs for different case studies.
- To develop and demonstrate a practical full-scale stern form optimisation procedure and evaluate whether it can be considered to be a feasible alternative to computationally

expensive full-scale self-propulsion optimisations. The development for such a process would require the following tasks:

- The design of a fully parametric bulk carrier vessel based on a case study vessel that is currently in operation.
 - To further develop an automatic wake analyses code by implementing the BSRA wake criteria (Maasch et al., 2019).
 - To set up the interaction framework between the parametric modeller, CAESES, and the numerical solver, Star-CCM+, on a high performance-computing platform to perform a multi-objective optimisation to improve the drag, wake non-uniformity and the wake fraction in full scale towing conditions using CFD.
 - To carry out the optimisation procedure in two parts whereby the process is initiated by submitting batch designs for CFD analyses and is later followed by the use of an optimisation algorithm to generate design variants.
 - To shortlist the best design candidates from the optimisation pool based on drag and wake characteristics and analysed them in self-propulsion conditions to evaluate their ultimate power performance, wake quality and propeller excited vibrations (PEV).
-
- To analyse the physics behind PBCF in a full-scale environment and contribute to understanding the function and working principles of such a retrofitting technology. Furthermore, a state-of-the-art full-scale PBCF optimisation procedure using high fidelity methods in open water conditions is to be proposed and demonstrated. Net energy savings and any beneficial effects are to be highlighted and explained in detail.
 - To analyse the performance differences of ESDs between different scales conditions (i.e. full-scale and model-scale). A case study would be carried out on a typical bulk carrier by analysing its performance with and without a well-established ESD (Duct) both in model-scale and full-scale conditions. Differences in results will be investigated, highlighted and explained.

- To develop a further understanding of ESD combination effects in-full scale environments by investigating their impact on performance, wake characteristics and propeller excited vibrations. The aim is to select a combination of three compatible technologies and study all 7 possible configurations on a case study bulk carrier vessel in self-propulsion conditions. Most of the ESD analytical process and checklist developed in the previous task would also be carried out for all the respective combinations. The idea behind the checklist is that it adopts and transfers all the knowledge and skills from the previous tasks to carry out this novel study with the highest standard and quality contributing to the lack of knowledge in this field.

1.5.3 Research Questions

All the aforementioned outlined objectives were devised in a way to better understand hull-propeller interaction phenomenon and more specifically to comprehend ESD combination effects. Although all the tasks are carried out to create a strong bases for the main study and novelty, i.e. ESD combination analyses, each objective or investigation addresses a specific research question derived from the challenges previously outlined in section 1.4. The research questions that are addressed by this PhD study are outlined below. Each question is directly related to the statement of the problem, identifying the motivation to investigate such issues.

- 1) Considering that optimisation techniques using full-scale self-propulsion simulations are not feasible, what is a good compromise and good alternative to such methods? What would be the outcome of a multi-objective stern form optimisation using full-scale towing simulations to improve the drag and wake field characteristics concurrently? Would the performance of the optimal design candidate provided by the optimisation process improve in self-propulsion conditions? Can such a solution be considered a good alternative? What are the pros and cons of such a process? *(Addresses Problem 1.)*
- 2) Extensive research on PBCF has been carried out at model-scale. What are the actual energy savings and benefits from installing PBCF in full-scale conditions, and how do they function in such environments? *(Addresses Problem 2.a)*

- 3) With the use of more currently available analyses techniques, what can be deduced regarding the differences in ESD function and working principles between different scale environments? (*Addresses Problem 2.b*)

- 4) What are the effects and influences of installing two or more ESDs on a vessel in a full-scale environment? Using current state-of-the-art techniques and analyses, what are the impacts of these retrofitting technologies when installed simultaneously in relation to power performance and wake characteristics? Do they influence, interrupt or interact with the flow regimes, functions and working principles of one another? Are the energy savings directly cumulative, and are there any adverse consequences? Can the use of current capabilities shed more light onto this subject that is a necessity in the ESD community (*Addresses Problem 2.c*)

1.5.4 Research Strategy

The research approach for this PhD study was devised and carried out in a way to develop an in-depth understanding of the performance and impact of Energy Saving Devices when installed simultaneously on-board full-scale ships using state-of-the-art CFD procedures. Initial sub-studies were carried out in order to address specific research questions and contribute to the body of knowledge as well as develop the expertise and skills required in order to carry out the main study to the highest quality of standard. The methodology consists of 5 major modules with each designed to satisfy an objective or contribute to a research question. The diagram below (Figure 4) represents the schematic flow of the study procedure. It should be noted that Module 2 (Stern Form design) can be applied to new ships, whereas the installation of Energy Saving Devices is applicable to both new and existing vessels.

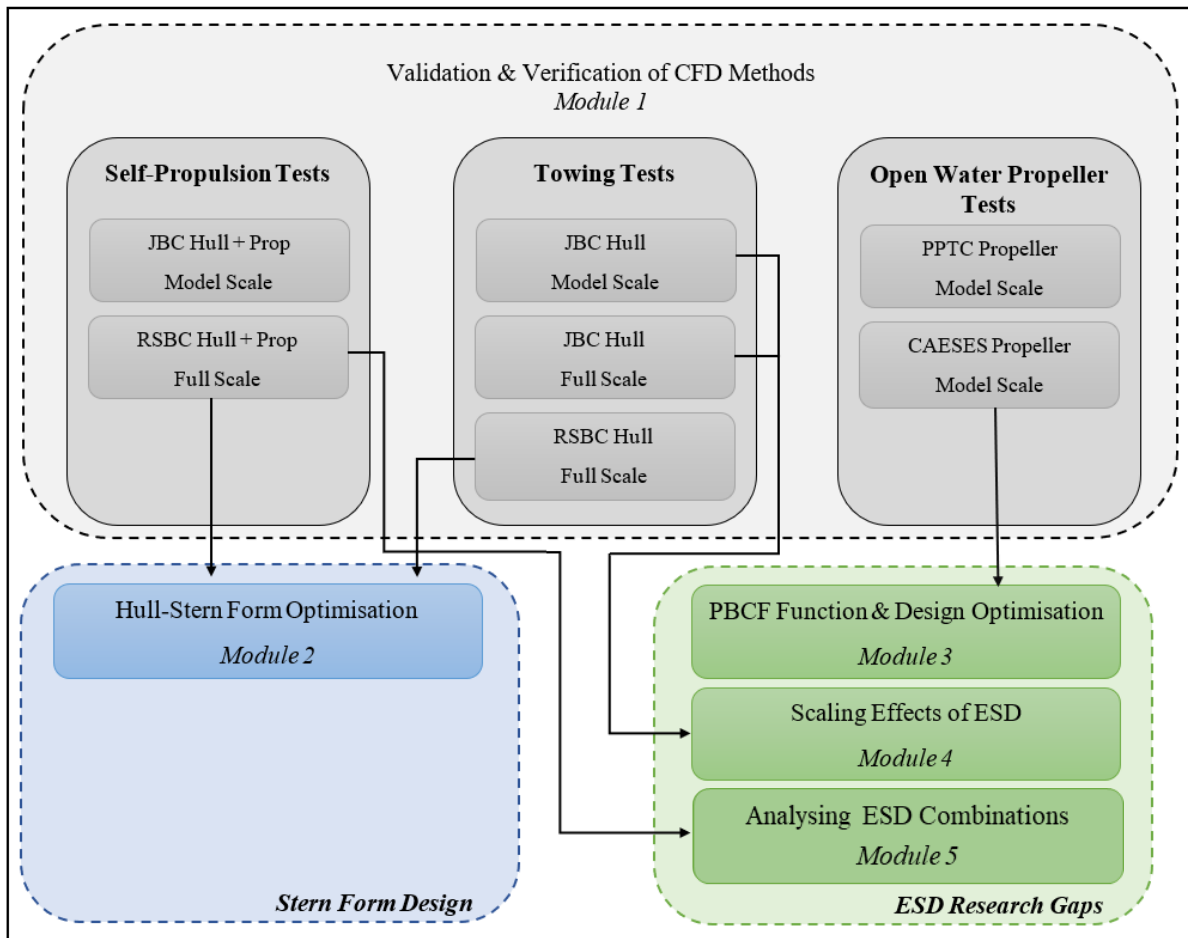


Figure 4. Study Procedure

1.6 Structure of Thesis

This thesis is presented in nine chapters, most of which follow the same format consisting of an introduction, methodology, results and discussion. The structure of this thesis is summarised below:

- Chapter 2 sheds some light on selected background information as well as theoretical details about the fundamentals of the subjects covered throughout this study, presenting a literature review from a critical point of view. (Critical Review)
- Chapter 3 outlines the approach and strategy of the study, together with the workflow and procedure. Each module is briefly explained, identifying their contribution to the research.

- Chapter 4 presents a validation and verification study for the CFD simulation models used throughout this study, ensuring that the numerical solver works accordingly and accurately. (Module 1)
- Chapter 5 presents the compiled checklist and process for ESD analyses which are carried out in various case studies to analyse the impact of ESDs
- Chapter 6 proposes and demonstrates the developed state-of-the-art hull-stern form optimisation procedure explaining the automation process, the parametric design of the case study ship, the codes developed to evaluate wake characteristics and PEV criteria, the study itself and the results explained and discussed. (Module 2)
- Chapter 7 investigates and explains the performance of PBCF in full-scale conditions outlining their function and highlighting their working principles in such environments. Furthermore, a PBCF design optimisation procedure is demonstrated and the results and outcomes discussed accordingly. (Module 3)
- Chapter 8 presents the study that was carried out to analyse the performance and impact of ESDs between different scale environments highlighting the major differences. (Module 4)
- Chapter 9 demonstrates the investigation carried out to analyse the impacts and consequences of installing a combination of retrofitting technologies simultaneously, in relation to power performance, wake characteristics and pressure excited vibrations. The shortlisted ESDs, which were used for the case studies, are presented, and each possible configuration was examined through the pre-defined ESD analytical process that were later discussed in detail in the following chapters. (Module 5)
- Chapter 10 and 11 present the discussion and conclusion of the PhD study. The prior section will outline the outcomes of this thesis and its state-of-the-art contributions, demonstrating how well the aims and objectives were achieved. Concluding remarks together with recommendations for future avenues of research are then highlighted in the chapter to follow.

1.7 Significance of the Study:

The importance, purpose and significance of this PhD study is to develop a better understanding of ship stern flow behaviour, thus contributing to the body of knowledge. Not only is the physics and function behind stern designs, Energy Saving Devices and stern wake flow characteristics better understood, but the energy efficiency of a vessel is enhanced by making it more environmentally friendly whilst at the same time reducing operational costs for the shipowner. As such, we would be able to provide ship owners with accurate information for them to make educated decisions on installing ESDs. In addition, the study aims to improve the reliability and trust of the use of CFD during design procedures as well as the installation of Energy Saving Devices on large vessels. Having a better understanding of hull-propeller flow interaction and the flow mechanisms of ESDs is crucial for shipowners seeking to invest in such retrofitting technologies.

1.8 Chapter Summary and Conclusion

This chapter presented and identified the research gaps and motivation behind this study outlining the aim and objectives of this thesis, including the research strategy and design.

2 Critical Review

2.1 Introduction

Chapter 2 presents an extensive literature and critical review explaining the background and context behind the research of this study. It also demonstrates how this PhD research addresses the bigger picture and contributes to the requirements of the academic body of knowledge by identifying gaps in the current state of the art.

In very broad terms, as the title of this PhD suggests, the study focuses on the intelligent development of hydrodynamic ship systems for energy efficient design outcomes (Figure 5). More specifically, the study aims to enhance the understanding behind hull–propeller interactions of high block coefficient ships and the use of Energy Saving Devices to improve vessel performance. These ambitions are achieved by carrying out various case studies including a novel state-of-the-art stern form optimisation procedure, wake quality analyses, PBCF analyses, retrofitting technology impacts at different scales and in off-design conditions together with various ESD combinations and configurations.

The main core elements of the study include parametric modelling of ship design, a validated and verified numerical CFD solver to predict the flow, wake field analyses and ESD studies whilst also briefly touching on automation and optimisation. It was therefore deemed appropriate to carry out an extensive review with particular emphasis on the following topics highlighting the important cornerstones of the subjects:

- Numerical Ship Performance Prediction & Design Procedures (2.2.1)
- Wake Field Analyses (2.2.2)
- Energy Saving Devices (2.2.3)

Since the study does not contribute towards optimisation algorithms and parametric modelling methods but simply makes use of these highly developed techniques for the research, these subjects did not require a comprehensive review but are only briefly mentioned with the other topics in an interdisciplinary manner.

Each topic will be reviewed in a critical manner while presenting any literature that might be considered relevant to the study (2.2). The key findings and cornerstones are then explicitly presented, also highlighting the relevant research gaps and areas that require investigation (2.3).

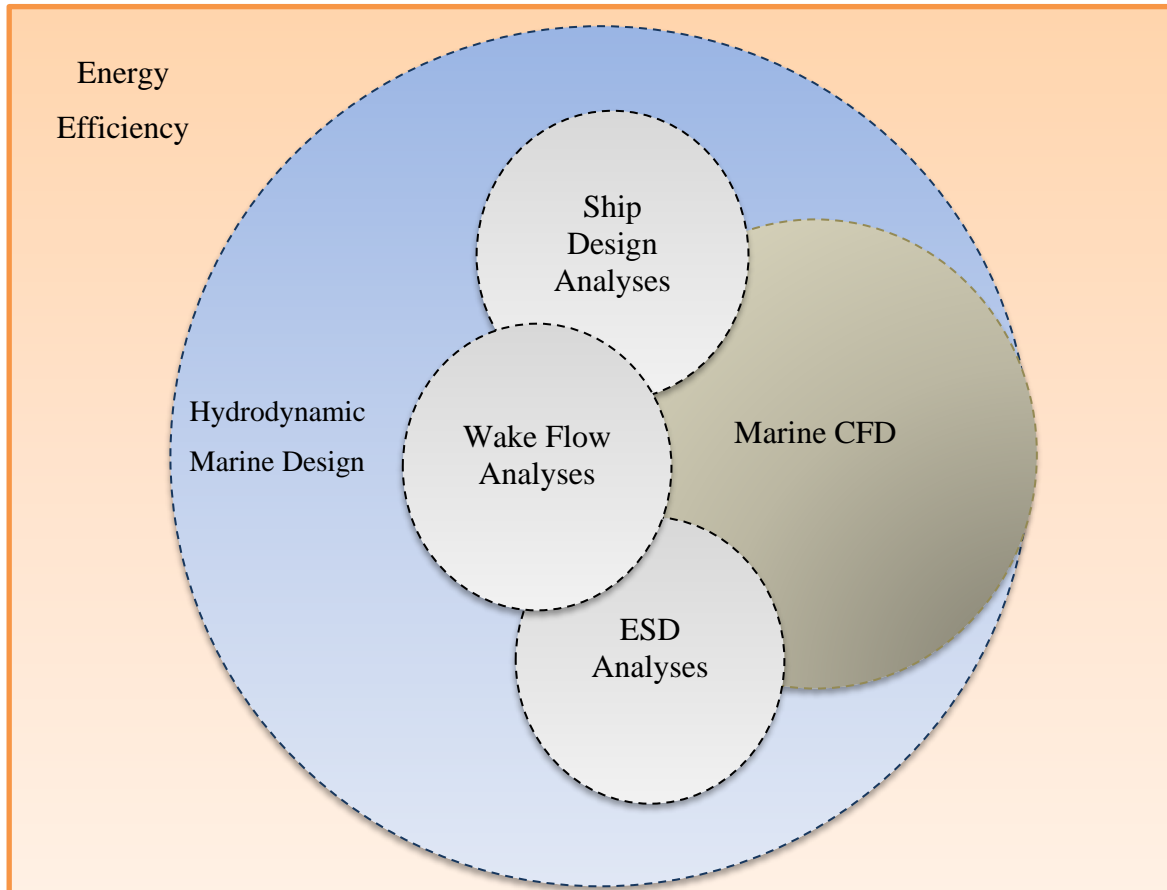


Figure 5. Energy Efficiency

2.2 Literature & Critical Review

2.2.1 Numerical Ship Performance Prediction & Design Procedures

2.2.1.1 Introduction of CFD in the Marine Industry

Back in the day, before CFD techniques were introduced, ship design procedures involved experimental test measurements. Towing tank methods have been adopted and approved for a while now, making them well-acknowledged within the marine industry. Despite their popularity, they are still considered to be time-consuming and costly, thus limiting engineers to test a few design variants. Not to mention the number of stakeholders required to carry out such experimentation and the issues associated with scaling during data extrapolation. Such concerns, together with others from different engineering disciplines, have motivated engineers to numerically solve or virtually simulate physical applications using code or software to determine and measure any desired quantities. This, in turn, led to the development of various numerical solvers such as Finite Element Analysis (FEA) and Computational Fluid Dynamics (CFD). The former is used to carry out structural analyses while the latter is used to calculate and predict fluid flow characteristics. CFD has been adopted by ship designers and is used for hydrodynamic analyses to investigate and predict ship performance and flow behaviour.

During the very early stages of CFD, limited power capacity restricted approaches to more common potential flow methods. Such an approach did not take into account the viscous effects of the fluid, which resulted in the loss of accuracy for some applications. Thereafter, with the introduction of viscous flow solvers, although more accurate, simulations were time-consuming and computationally expensive thus constraining the cell count number of mesh sizes to model scale which brought about similar error to experimental results. This also prevented the detailed representation of the geometry and proper prediction of physics. Furthermore, simulations took longer to converge, implying that analytical studies and variations were limited, and optimization procedures were not really an option.

The use of simplified approaches, which find it difficult to capture complex flow phenomena, were commonly adopted. However, with the advance in computational power, RANS based CFD simulations became more feasible, thus allowing the use of various turbulence models and other features (Larsson et al., 2003). Till this very day, numerical solvers are continuously being developed to enhance accuracy and predict further detail and phenomena. This being

said, full-scale simulations are still considered a challenge due to the resources required by the solver to compute high cell size numbers. However, the development of certain methods such as mesh refinement regions, whereby the cell sizes are finer in particular areas of interest, have facilitated a reduction in mesh numbers thus allowing for the possibility to investigate ship flow at full scale (Visonneau, 2005). Recent improvements have also initially introduced Direct Eddy Simulations (DES), Large Eddy Simulations (LES) and Direct Numerical Simulation (DNS) methods that are useful for investigating cavitation behaviour (Fureby, 2008, Stern et al., 2012, Bhushan et al., 2013, Carrica et al., 2010). However, these are not popular due to their computational demand.

With the introduction and development of high-performance computing, more advanced numerical methods are being introduced together with the various post-processing capabilities that allow the user to analyse data in further detail in an easy and user-friendly manner. The advances and developments in numerical software generally require a higher computational demand. Consequently, it is vital that both fields work together to understand each other's needs and limitations and that they strive to enhance numerical techniques and push the boundaries of science.

2.2.1.2 CFD development in the Marine Industry

Economic and feasibility benefits have pushed computational fluid dynamics to become more popular and common in the marine industry. That is why there is a continuous, ongoing focus on improving CFD marine applications for better-developed and more efficient simulation-based design tools with enhanced capabilities. This is evident in the progress that marine CFD has made over the years, particularly over the last decade.

Going back 30 years, integral methods were more common and generally constrained to 2D applications in order to simplify any complexities associated with 3D. Soon after, the three-dimensional boundary layer finite difference methods were developed. However, these were unable to capture the thick boundary layers and flow separation phenomena (Stern et al., 1989). Partially Parabolic approaches were later developed (Stern et al., 1988) followed by RANS solvers with viscous-inviscid interaction for non-zero Froude numbers (Tahara et al., 1992) and this then developed into more complex large domain RANSE methods which utilised free surface tracking capabilities (Tahara and Stern, 1996).

Further improvements involved enhanced turbulent and propulsion modelling including features like overset mesh and multi-block grids. More worthy features such as free surface capturing capabilities and dynamic overset grids were then introduced (Carrica et al., 2007). To better simulate and capture turbulence, URANS and DES methods were recently developed (Metcalf et al., 2006) together with other useful technologies such as 6 DOF modelling, wall functions, controllers for manoeuvring, capsizing predictions and sliding mesh interaction for rotating propellers. Computational performance is also a crucial part of the current simulation-based design and next generation high fidelity SBD tools (Bhushan et al., 2011). All these developments allowed for various marine applications to be carried out such as resistance, self-propulsion and open water virtual test simulations to investigate parameters such as drag, torque, thrust, wave cuts, wake flow details and more.

2.2.1.3 CFD Theory

The use of CFD in the marine industry is primarily focused on hydrodynamics trying to simulate and understand the fluid behaviour around the vessel and its influence on the body. Global pressures and fluid velocities are computed in a three-dimensional system, thus allowing the forces and moments acting on the vessel to be measured. The airflows around the body (aerodynamics) are in some cases also analysed but such simulations are not very popular for commercial ships.

In hydrodynamics, studies focus on simulating two working fluids; water and air. They are generally treated as Newtonian fluids and are also assumed to be isothermal and incompressible due to their low Mach numbers. The conservation laws of physics are represented by fluid flow governing equations known as the incompressible Navier-Stokes equations:

Continuity equations:

$$\frac{\partial \rho}{\partial t} + \nabla \cdot (\rho \mathbf{U}) = 0 \quad (2)$$

Momentum Equations:

$$\text{- X component: } \frac{\partial \rho}{\partial t} + \nabla \cdot (\rho \mathbf{u}) = -\frac{\partial p}{\partial x} + \frac{\partial \tau_{xx}}{\partial x} + \frac{\partial \tau_{yx}}{\partial y} + \frac{\partial \tau_{zx}}{\partial z} + \rho f_x \quad (3)$$

$$\text{- Y component: } \frac{\partial \rho}{\partial t} + \nabla \cdot (\rho \mathbf{v}) = -\frac{\partial p}{\partial y} + \frac{\partial \tau_{xy}}{\partial x} + \frac{\partial \tau_{yy}}{\partial y} + \frac{\partial \tau_{zy}}{\partial z} + \rho f_y \quad (4)$$

$$\text{- Z component: } \frac{\partial \rho}{\partial t} + \nabla \cdot (\rho \mathbf{w}) = -\frac{\partial p}{\partial z} + \frac{\partial \tau_{xz}}{\partial x} + \frac{\partial \tau_{yz}}{\partial y} + \frac{\partial \tau_{zz}}{\partial z} + \rho f_z \quad (5)$$

Energy Equations:

$$\begin{aligned} \frac{\partial}{\partial t} \left(\rho \left(e + \frac{U^2}{2} \right) \right) + \nabla \cdot \left(\rho \mathbf{U} \left(e + \frac{U^2}{2} \right) \right) = & \quad (6) \\ \rho \dot{q} + \frac{\partial}{\partial x} \left(k \frac{\partial T}{\partial x} \right) + \frac{\partial}{\partial y} \left(k \frac{\partial T}{\partial y} \right) + \frac{\partial}{\partial z} \left(k \frac{\partial T}{\partial z} \right) - \frac{\partial (u p)}{\partial x} - \frac{\partial (v p)}{\partial y} \\ & - \frac{\partial (w p)}{\partial z} + \frac{\partial (u \tau_{xx})}{\partial x} + \frac{\partial (v \tau_{yx})}{\partial y} + \frac{\partial (w \tau_{zx})}{\partial z} \\ & + \frac{\partial (u \tau_{xy})}{\partial x} + \frac{\partial (v \tau_{yy})}{\partial y} + \frac{\partial (w \tau_{zy})}{\partial z} + \frac{\partial (u \tau_{xz})}{\partial x} \\ & + \frac{\partial (v \tau_{yz})}{\partial y} + \frac{\partial (w \tau_{zz})}{\partial z} + \rho f U \end{aligned}$$

The above five transport equations with seven unknowns require the use of another two equations in order to be solved.

Density to Temperature:

$$\rho = \rho(T, p) \quad (7)$$

Pressure:

$$h = h(T, p) \quad (8)$$

Since hydrodynamics considers and assumes the incompressibility of fluid flow, these equations are further simplified into the following:

Continuity:

$$\frac{\partial \rho}{\partial t} + \nabla \cdot (\rho \mathbf{U}) = 0 \quad (9)$$

Momentum Equations:

$$\text{- X component:} \quad \rho \frac{Du}{Dt} = - \frac{\partial p}{\partial x} + \mu \nabla^2 u + \rho \cdot f_x \quad (10)$$

$$\text{- Y component:} \quad \rho \frac{Dv}{Dt} = - \frac{\partial p}{\partial y} + \mu \nabla^2 v + \rho \cdot f_y \quad (11)$$

$$\text{- Z component:} \quad \rho \frac{Dw}{Dt} = - \frac{\partial p}{\partial z} + \mu \nabla^2 w + \rho \cdot f_z \quad (12)$$

Where ρ is density, p is the mean pressure, t is time, \mathbf{U} is the flow velocity vector, e is energy and τ denotes the viscous-stress tensor with μ being the dynamic viscosity.

Once simplified, the continuity and momentum equations are then de-coupled from the energy equations requiring no other equations to solve an incompressible flow.

CFD characteristics can be said to rely on three criteria; the modelling features, the numerical methods and the High-Performance Computing (HPC) capability to process the simulations. These three criteria combined, will determine the nature, accuracy and robustness of a simulation. Modelling methods refer to the kind of physics and models involved, whereas the numerical methods indicate the type of discretization schemes and grid types used. On the other hand, the performance in computational power will dictate the ability and potential of the CFD simulation. A critical review is carried out for all three areas with a brief overview of the past, current and future methods, as well as a comparison of any studies carried out and their relation to marine CFD, with particular attention being paid to both the benefits and limitations.

2.2.1.4 CFD Modelling

Fluid Flow Solvers

As previously indicated, marine hydrodynamics involves two working fluids, water and air. In numerical methods, different solvers are used depending on the fluids involved and the requirements from the simulations. As indicated by (Stern et al., 2012), these can be categorised into three; free-surface flow, air flow and two-phase flow solvers.

For the prior single-phase method, only the water phase is simulated, and this is done by applying an atmospheric boundary condition at the free surface. For studies that do not investigate the effects of air and are solely interested in water behaviour, this method is accepted and used by various numerical solvers such as the study carried out by Di Mascio et al. (2007). However, it is considered inappropriate for analysis requiring wave breaking prediction due to its inability to stimulate air behaviour. On the other hand, single phase air flow solvers, as the name suggests, only simulate air fluid. Although not as popular, such solvers are used to understand the aerodynamic behaviour around the body of the vessel without simulating the water fluid for simplicity reasons. Two-phase flows are the most common of the lot and generally used in commercial solvers such as STAR-CCM+ and FLUENT. Both fluids are solved in a coupled manner (Huang et al., 2007) and require a high grid resolution to capture both flows. Such a method is becoming more popular opening new doors for research; wake studies, breaking waves etc. Although, each phase can be separately

solved and later coupled, most solvers opt for a one field formulation that describes the fluid motion for both phases thus saving time.

Air-Water Interface Modelling

In marine applications, air-water interface models are used to compute kinematic and dynamic constraints with the prior ensuring that the water particles remain on the surface and the latter reflecting the continuous stress across the interface. There are two methods to treat free surface effects of viscous flows in RANS simulations. The two approaches are known as free-surface fitting and free-surface capturing, also known as interface tracking or interface capturing respectively.

The prior involves a generated mesh, which solely covers the liquid domain, with one of its boundaries allowed to follow the movement of the free surface motion. The grid adapts and modifies itself with every iteration to conform to the position of the free surface.

On the other hand, the other involves a static computational grid, and the free water surface is captured within the mesh. This approach can be classified into three categories, namely marker and cell, volume of fluid (VOF) and level set technique, as specified in Gallagher et al.'s (2009) report.

Researchers have also carried out various studies to analyse and compare the different methods (Wackers et al., 2011). They compare between surface fitting, level set and volume of fluid methods suggesting that all three methods have their strengths and weaknesses and that the careful selection of a water surface discretisation method should depend on the case study in question. In summary, they claim that all three are able to accurately simulate ship wave patterns. However, surface fitting approaches are not suitable for large motion or complex geometry simulations but are generally robust, accurate, fast and converge easily. On the other hand, capturing methods, being able to address these limitations are applicable to a wider variety of conditions.

Since surface fitting is not ideal for large motion simulations (since the grid has to adapt to the free surface motion) and can also be computationally expensive, the surface capturing approach is generally preferred in the marine industry. This is because it is more suitable for simulating breaking waves, seakeeping, manoeuvring etc. The most common, well-established, free surface, capturing approach used in the marine industry is the 'Volume of Fluid' method proposed by (Hirt and Nichols, 1981).

The VOF model is a fixed model that simulates a number of immiscible fluids (water and air for marine CFD simulations) which share a single set of momentum equations. The volume of fraction of the fluids in each cell is then computed to identify the position of the free surface in the domain. VOF methods are continuously being enhanced, even coupled with other models such as the level set method (Wang et al., 2009) to create further benefits.

Propeller Modelling

There are various ways to model a propeller in CFD. The most common ways in ship hydrodynamics are the body force methods or the fully discretized propeller methods.

As the name implies, body forces are defined using numerical integration to calculate the thrust and torque of the propeller. These can be assigned using polynomial distribution methods that can vary from constant to variable distribution approaches such as radial, transient etc.

More sophisticated methods were developed using propeller performance codes that interact with RANS solvers to analyse hull-propeller interaction (Stern et al., 1994). The code computes the distribution of wake forces according to the blade loading.

A more accurate approach that requires detailed propeller geometry definition and produces a description of the ship- hull interaction is the fully discretized rotating propeller method (Lübke, 2005). Several studies have been carried out using this approach using multi block techniques with a Moving Reference Frame (MRF) or sliding mesh methods (Zhang, 2010). The MRF is a robust and efficient steady-state technique to simulate rotating propellers. The principle behind the techniques is to solve a problem which is unsteady in the stationary frame with respect to the moving frame. It is less expensive than the sliding mesh method but provides sufficient accuracy for most industrial scenarios. The MRF assumes a weak interaction between the moving volume and the surrounding stationary cells. On the other hand, the sliding mesh approach, which is deemed to be more accurate, can predict strong interactions but is a less robust approach. With both of these methods being computationally expensive, studies have also simplified the approach by simulating one propeller blade using periodic boundary conditions (Tahara et al., 2005). The latter technique is becoming a common approach, especially for open water simulations, as they save computational cost and provide reasonable accuracy.

Turbulence Modelling

The working fluids that are mostly considered in the hydrodynamic marine industry, namely water and air, generally result in turbulent flow, especially in large-scale scenarios. Turbulent phenomena change the properties of fluids, thus significantly influencing their flow behaviour such as the flow separation, drag and wakes amongst others. These phenomena have to be accounted for in numerical solvers, and therefore, various turbulence models (Figure 6) have been developed to replicate such behaviour.

Direct Numerical Simulation (DNS) of the Navier Stokes equations, i.e. direct computation of the actual physics, require very dense grids and are computationally expensive (Piomelli and Balaras, 2002). Such simulations would require the generation of significantly large mesh sizes that are way beyond the current state of the art computational capabilities. We therefore make use of turbulence models to predict this behaviour. Various turbulent models have been developed throughout the years, all with their different characteristics and no universal model has been identified.

One of the more popular turbulence models used in the marine industry is the Unsteady Reynolds Average Navier Stokes (URANS) equations that resolve large scales of motion but models the turbulence. URANS equations should be developed to compute the right amount of turbulent dissipation, momentum and energy transfer. Stresses in these equations need to be interpreted in terms of calculated time averaged variables to make them solvable. A turbulence model, involving additional variables for the unknown quantities, is then used to solve the equations simulating certain flow behaviour. Current turbulence models can be classified under different categories, namely Algebraic, Linear Eddy viscosity, One-equation, Two-equation and Stress Transport models.

Algebraic and Linear Eddy viscosity models are both very simple methods with the prior being generally used for simple flows. The one-equation model (Spalart and Allmaras, 1992) is a development of the Algebraic aka zero-equation model by using an eddy viscosity that takes into consideration not only the local flow conditions but also the flow history. An additional transport equation is solved to determine velocity scale hence the name one-equation models. In two-equation models, an additional transport equation is solved to determine the length scales.

Two-equation models are the most popular in the maritime industry, particularly the k - ϵ and k - ω models and will therefore be covered in some depth. For the former model, k represents the kinetic energy and ϵ the rate at which the energy is dissipated by the action of viscosities on the smallest eddies (Launder and Spalding, 1974). This method is applicable to many turbulent low Reynolds number simulations. However, it is generally found to be inadequate for adverse pressure gradients and flow separation. On the other hand, the k - ω model simulates the frequency of large eddies (Wilcox, 1998) and appropriately predicts near-wall regions and boundary flows, particularly in strong adverse pressure gradients. This being said, studies indicated that this turbulence model is sensitive to the value of ω for modelling the free stream (Morgans et al., 1999). One particular limitation for both models is that they are incapable of simulating laminar and transition flow regions since they both assume the flow is fully turbulent. This would lead to inaccuracy of results particularly for model simulations where such flows are found to be significant.

With both turbulent models having their advantages, Menter developed a model known as the Menter Baseline model (BSL) which is based on the k - ω model retaining the desired characteristics in the inner region of the boundary layer but blends to the k - ϵ model in the outer region and free shear regions (Menter, 1994). This makes the model very similar to the k - ω but avoids the associated free stream sensitivity. The same author then further developed this as he took into account the effects of the transport of the turbulent shear stress. Such a model was referred to as the shear-stress transport (SST) model and is deemed most suitable for aerodynamic/hydrodynamic simulations. URANS with anisotropic model simulations are extensively used in marine research and within the industry and are considered desirable to meet benchmark predictions. However, the prediction of vortical and turbulent structures require improvement, and efforts should be focused on considering curvature effects or structure-based non-linear effects (Kassinis et al., 2006) as highlighted by Stern (2012).

Another class of turbulence models are the nonlinear eddy viscosity models or the algebraic stress models (ASM). For these RANS equations, an eddy viscosity coefficient is used to relate the mean turbulence to the mean velocity in a nonlinear relationship providing an implicit anisotropic stress equation. i.e. the turbulent stresses are algebraically related to the rate of strain by the use of higher order quadratic and cubic terms. Some developments of Reynolds stress turbulence models (EARSMS) have been presented by Wallin (2000). Although this method provides a higher level of detail, as it retains features of the Reynolds stress transport equations, it is considered to have similar computational costs to the linear models making it

quite attractive to the marine industry. This being said, they are harder to implement and are less robust, making it difficult for them to grow in popularity.

The two-equation models find it difficult to predict or model complex strain fields because the turbulent stresses are assumed to be linearly related to the rate of strain by means of scalar turbulent viscosity. In addition, it also assumes that the principal strain directions are aligned to the principal stress directions. These are adequate for simple states of strain but not appropriate otherwise. That is why the Reynolds stress transport models (RSM), that are considered to be higher level models, employ a second order closure where the Reynolds stresses are directly computed. These are determined by directly solving a transport equation for each stress component thus requiring the solution of six additional coupled equations together with an additional equation to provide the length scale. The work originates from the Launder's (1975) developments. Such a model is generally considered adequate for complex strain and non-equilibrium flows, making it suitable to predict vortical structures. However, it is computationally expensive and achieving convergence is challenging.

Reynold Stress models (RSM) tend to be better at predicting vortical structures and vortices but are computationally expensive and less robust than the eddy viscosity models, including the two-equation models. Therefore, some efforts were focused on improving the commonly used linear eddy viscosity models to predict the curvature/rotation effects. Spalart and Shur (1997) modified the Spalart-Allmaras one equation model to take into account streamline curvature and system rotation effects by introducing an empirical function that is used as a multiplier of the production term. The associated formulations are provided in Chapter 4. In a similar manner, Smirnov and Menter (2009) have adopted the rotation and curvature correction to the shear stress transport (SST) model by introducing the Spalart-Shur correction term. Using the derived and developed SST-CC model, the authors then investigated and analysed the performance of this new technology for both wall bounded and free shear turbulent flows including wing tip vortex analyses. They concluded that the SST-CC model significantly improved the original model and results proved comparable to the RSM model. The additional expense of computational cost is minimal when compared to RSM models making such technology practical and worthy of further investigation.

Other Authors have followed similar approaches introducing curvature effects to eddy viscosity models (Dhakal and Walters, 2009), (Arolla and Durbin, 2012), (Arolla and Durbin, 2014), (Hellsten, 1998) and (Mani et al., 2004). Studies by Starke et al. (2006) and Rijpkema et al.

(2013) have presented the use of the extended longitudinal vorticity correction (Dacles-Mariani et al., 1995) to one-equation and two-equation models. Various studies have exhibited the use of curvature corrected models by applying them to various applications including impellers flows (Tao et al., 2014), hydroclones (Stephens and Mohanarangam, 2010) and aerodynamic analyses (Arolla and Durbin, 2013a).

A curvature correction approach was also used for marine application (Heinke and Hellwig-Rieck, 2011). However, this was briefly mentioned with no exposure of details. To the best of the author's knowledge, no other studies in the marine industry have made use of such models. This opens an area of further investigation, especially when trying to analyse vortex structures or turbulent flows (e.g. the wake behind a high block coefficient vessel). The use of such models and their feasibility in numerical ship performance prediction require extensive testing with proper V&V procedures and comparison of results. If other industries have adopted the methodology, it would be interesting to see if the technology fares well in the marine industry. It was proven to be a good alternative to RSM and it would be worthwhile understanding, if this is the same in the marine field, as it would help improve practicability and computational cost of design methods.

Other upcoming approaches that are slowly being introduced to the world of CFD are Large Eddy Simulations (LES). These methodologies focus less on modelling and take more of a numerical method approach. They are found to be more accurate, providing a more detailed description of the turbulent flow than URANS methods and are able to simulate eddies appropriately. This is because LES technology resolves turbulent structures and models small-scale quasi-isotropic fluctuations (Stern et al., 2012). Such methods compute the resolution of energy transfer between the coherent and fluctuating scale, which involves the scatter of energy in both directions and requires initial background fluctuation energy to instigate coherent turbulent fluctuations. They demand high computational power, and with the recent increase in computational capability, the use of LES methods in ship hydrodynamics is gradually being applied. Such approaches still require high grid resolution, especially near the wall region (Piomelli, 2008), which is very hard to implement in the near future. A good review of LES turbulence models was carried out by Fureby (2008), who also indicates its evolution and use in engineering applications.

A system that uses the best of both worlds was later developed and is known as Hybrid RANS LES (HRL) modelling. In a brief statement, the only difference between the URANS and LES

models are the definitions of the filter functions. This method is designed to operate in different modes in different areas of the flow field in such a way that it runs with a URANS approach in the boundary layer and LES in the free-shear layer region. HRL models can be described as zonal or non-zonal approaches with the prior specifying the interface to indicate the transition region. The most common non-zonal approach is the Detached Eddy Simulation (DES) method. To accurately capture small detail, hybrid RANS-LES simulations require many, possibly millions or billions of grid points even for model-scale case studies. Such simulations would provide information that could not have been captured or measured with experimental methods or previous numerical procedures. Although their use is becoming popular, these methods are still at the early stages and require verification and validation procedures to ensure the reliability of results.

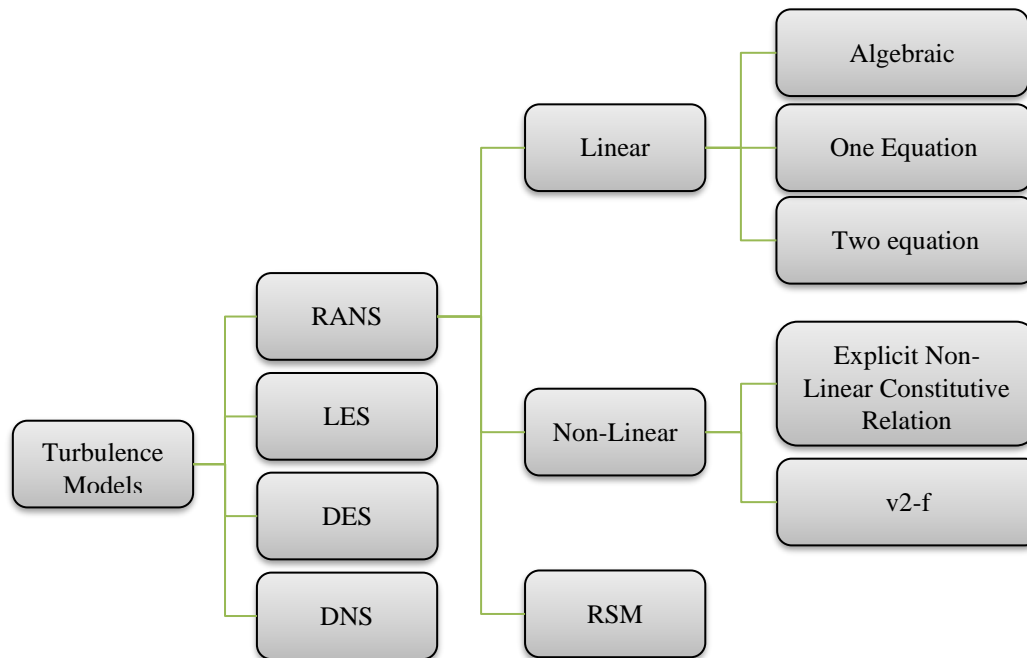


Figure 6. Turbulence Models

Near Wall Modelling

Modelling the flow behaviour near the wall surface/boundary is also of primary concern in computational fluid dynamics. When a fluid flows along a surface, a boundary layer develops due to the inertia and viscous forces producing different turbulent structures from free form flow. The adverse gradients of the flow variables near the wall region are significantly high thus requiring high grid resolution to be resolved (Craft, 2010). In addition, the turbulent fluctuations of the fluid flow nearer the wall are suppressed resulting in dominant viscous effects. Some of the standard turbulence models previously mentioned are inadequate to model

such behaviour requiring specific near wall treatment. Thus, in order to accurately predict near wall flow details, prism layers are generally implemented (Ferziger and Peric, 2002). These are orthogonal cells adjacent that are normal to the ship surface along the geometry. The prism layer characteristics (thickness and number of prism layers) define the cell size closest to the geometry which in turn dictates the wall treatment model to be used.

When possible, the most accurate approach is carried out by fully resolving the flow structure to the wall. This method is known as near wall modelling and requires Y^+ values close to unity meaning the cells adjacent to the geometry need to be considerably small. However, the boundary layer thickness reduces with the increase of the Reynolds number and therefore, in order to maintain Y^+ values around 1, to emulate near wall modelling, fine grid cell requirements are required which in turn, might create grid resolutions issues.

That is why we make use of wall functions (Wilcox, 1998) which avoid the limitations associated with fully resolved near wall modelling that might create computational issues and be computationally expensive. The role of wall functions is to solve the inner boundary layer using flat plate theory with respect to the boundary conditions of the first cells near the wall. The region close to the wall is defined by use of rendered dimensionless variables.

Wall functions are characterised by their ability to be implemented into the numerical solver, their ability to appropriately predict the flow separation point and their ability to account for the varied Y^+ variation on the wall boundary. Most commonly used, is the standard wall function. This was later developed to multi-layer where the boundary conditions change between the sub and log layer profiles depending on the Y^+ value. The cells closest to the boundary wall should be designed to have Y^+ values smaller than 100 but greater than 30 as the wall functions are usually considered invalid under this number. However, new CFD codes are also able to alternate functions if the Y^+ values are smaller than 30 and even change to near wall modelling if numbers are near unity. They also allow the modelling of surface roughness which is generally applied to full-scale simulations but is still an area that requires further attention. Studies that have demonstrated the use of wall functions in marine CFD applications were carried out by Oh and Kang (1992). Although wall functions are good alternatives to near wall modelling, especially for high Re scenarios, they are not as accurate in predicting separated flows. However, they serve as good guides and indicators for flow behaviour prediction.

Numerical Modelling: Velocity-Pressure Coupling

Various coupling methods have been used for different scenarios and requirements; pressure-based methods, density-based methods, projection-based methods etc. In pressure based methods, the continuity and momentum equations can be solved in a fully coupled manner due to the parabolic–elliptic character of the incompressible Navier-Stokes equations (Hoekstra, 1999). This method is found to be computationally expensive due to the large amount of linear equations that require coupling. However, such methods are generally considered robust. For density-based methods, which are generally applicable for compressible flows, a first order time derivative is added to the continuity equation resulting in a hyperbolic behaviour of the continuity and momentum equations that can then be solved in a coupled manner (Rosenfeld et al., 1991). Some studies have used this method for ship hydrodynamic analyses (Hino et al., 2010, Wilson et al., 2008). The most common approach, one that is used in the majority of CFD codes, is the Projection-based method (Larsson et al., 2014). The continuity equation is satisfied through a Poisson equation for pressure correction. SIMPLE algorithms are generally used in steady flow simulations and the SIMPLE-based PISO method for unsteady flows in hydrodynamic solvers. Momentum equations are first solved followed by the computation of the Poisson equation for the new corrected pressure which is then used to calculate the corrected velocity. All the methods mentioned above are mostly suitable for steady flow problems since they are limited in the choice of numerical schemes for discretization. Other ideal methods for unsteady flow have been developed. One in particular is the Fractional-Step method suitable for time dependant solutions and applicable for high fidelity solvers (Dong and Shen, 2010, Dong and Shen, 2012).

Spatial and Temporal Discretization

Spatial discretization can be carried out using Finite Difference (FDM), Finite Element (FEM), Spectral or Finite Volume (FVM) methods with the latter being more popular amongst hydrodynamic solvers.

FDM methods were first developed in 1768 by Euler who used the Taylor series expansions to generate finite difference approximations to the derivatives of the RANS equations. The derivatives in the governing equations were then replaced by the finite difference expressions producing an equation for the flow solutions at each grid point or cell. This can be regarded as a very simple method that requires a regular structured mesh that is somewhat uniform. It also

allows the use of high order schemes resulting in accurate results but at the expense of computational power (Yang and Stern, 2009).

Finite Element methods (FEM), (Chung, 1978, Fletcher, 2012, Girault and Raviart, 2012) are not very common amongst numerical solvers and are generally suitable and applied to structural analyses. This technique uses polynomial functions on the local elements/cells to describe the flow. It approximates functions substituted in the governing equations. Residuals are then introduced to estimate the errors which are minimised by weighting functions and integrated producing algebraic equations. The process requires high computational power producing accurate results.

Spectral methods adopt a similar approach to that adopted by FDM and FEM by replacing the unknowns of the governing equations with the truncated series. However, unlike the others, spectral method approximations are valid throughout the entire domain. Similar to FEM, discrepancies are dealt with weighted functions.

Finite Volume Methods (FVM) were first introduced by McDonald (1971), MacCormack and Paullay (1972) for 2D flows and later extended by Rizzi and Inouye (1973) for 3D simulations. MARNET CFD (Consultants et al., 2002) states that the method discretises the integral form of the conservation laws in physical space producing expressions that abide by the conservation of relevant properties in each finite cell volume. The same approximations carried for the finite difference method are then substituted with the terms of the integrated equations resulting in algebraic equations that are iteratively solved. They can be applied to polyhedral grid volumes (unstructured grids) which are easier to generate than structured grids required by FD methods. One particular limitation of this technology is that they are only suitable for low order schemes.

Temporal Discretization techniques are generally carried out using explicit or implicit time-marching schemes. Most CFD solvers use the latter as it allows larger time steps speeding up simulation processes with large time scales. However, they require solutions of system of coupled non-linear equations, requiring high computational demand. Explicit time-marching schemes use smaller time steps and are rarely used for RANS simulations. For steady cases, time step discretization is achieved by using first-order backward Euler scheme and second-order such as the Crank-Nicolson scheme. Three-level backward schemes are generally used for time-accurate solutions.

Grid Generation

A domain representing the area of interest is made up of a grid of cells that can withhold information to simulate the fluid flow. The shape/size of the domain is defined by the geometrical boundaries. These boundaries are defined with boundary conditions that define the states of the flow at these sides. Grids are made up of assembled cells that can be of various shapes that are able to communicate with each other to exchange information describing the behaviour of the working fluids. Therefore, grids must be fine enough to capture all important geometrical shapes, flow features and information. The smaller the cell size or the more cells within a particular domain, the more accurate the solution.

Various grid types have been developed but the two most common categories are the Structured and Unstructured grid forms. Structured grids, requiring a six-sided domain, were the first to be developed due to their simple configuration with fixed uniform distribution of grid points in all 3D directions. They are generated using hexahedral cells making it rather difficult to model and replicate complex geometries (Thompson et al., 1985). Their capabilities result in quite a few limitations in the CFD industry. However, the use of numerical mapping schemes, which allow the generation of the so-called body fitted meshes, has improved flexibility in such methods. In order to ease the difficulty in generating structured grids with complex geometry, multi-block overset grids are generally applied using overset/overlapping techniques.

Unstructured grids are preferred with most numerical solvers due to their enhanced flexibility when compared to structured grids (Bertram, 2011). Domains can be of arbitrary shapes and assembled without considering continuity of the mesh lines. The grid is generated using tetrahedral cells in the boundary layer and polyhedral cells in the far field (Marcum, 1995, Ferziger and Peric, 2002). It is easy to model complex geometries, however controlling grid quality is difficult (Baker, 1989). Unstructured meshing techniques are also capable of modelling prism layers with structured sub-meshes close to domain boundaries and can also make use of local refinement (control volumes) areas in particular regions of interest. With tools being continuously developed to automate and improve grid generation, the use of unstructured meshes is becoming more popular.

In CFD simulations, grid quality is of critical importance in order to ensure reliability of results. This can be dependant of various criteria that require careful monitoring such as grid density, cell distribution, grid skew, uniformity and cell shapes. These may all have an effect on solution accuracy.

2.2.1.5 Ship Design Optimisation Procedures using Numerical CFD

Optimisation procedures in marine applications have evolved over the years and have been used extensively for various purposes including logistics, operations and design procedures (Papanikolaou, 2010, Parsons, 2009, Pellegrini et al., 2018, de Jongh et al., 2018). The overall system of a ship is relatively complex consisting of many components/areas that might be or might not be dependent on each other. Optimally designing the ship as a complete system introduces numerous design parameters, conflicting objectives and far too many design constraints making the whole procedure complex. The design process is thus broken down into smaller manageable modules. Although the breakdown is generally narrowed down by field and area (e.g. hull design optimisation, route optimisation, etc.), this is still generally considered to be unreasonable and more specific, well defined, optimisation directions (e.g. bulbous bow optimisation) are required. When optimisation methods, take a holistic approach and analyse various areas of a ship system, they generally use lower fidelity methods due to the limitations of computational power and time constraints.

The nature of an optimisation problem or study generally involves, the design variables, parameters, the objective function and the design constraints. Design variables, as the name suggests, are the free variables controlled by the designer that are under investigation to evaluate their output. These can be of continuous, discrete or mixed form. On the other hand, parameters cannot be controlled by the designer and are dictated by the influence of the geometry that can be either known, not known, computed or estimated. These can be labelled as deterministic or stochastic parameters (Yang, 2014). Objectives of a study, i.e. the goals and purpose of this study, can either be singular or multiple and more often than not conflicting thus requiring compromises or user defined weightings. Meanwhile, constraints limit the range of design candidates. They define the boundaries of the design space under investigation.

Optimisation methods for enhancing the hydrodynamics performance of a vessel have also increased in popularity in recent years. Before CFD methods were introduced, scientists also made use of other solvers for hydrodynamic optimisation. Typical examples include the minimization of wave resistance using wave resistance theory (Wigley, 1935) and hull-interaction studies (Nowacki and Sharma, 1971, Huang et al., 1976)). With the increased capability of computational power and improved methods to solve the physics, trends also ventured into hydrodynamic optimisation of hull designs (e.g. bulbous bow optimisation

(Sharma and Sha, 2005)). Developments of hydrodynamics in the 20th century can be referred to in an overview carried out by Nowacki (2001) and Stern (2015).

With great advancements in computational power and numerical codes, CFD methods which predict numerical ship performance became common practice in vessel design procedures together with the application of optimisation methods. Furthermore, V&V procedures are enhancing the reliability and trust of such methods also tempting many to adopt such techniques (Campana et al., 2006). CFD has been used for various applications in the marine industry, but is very popular in the design optimisation of ship hulls (Peri et al., 2001). Local optimisation methods have also been applied to bulbous bow designs (Kim and Yang, 2013) and hull stern forms (Chen and Huang, 2002). Ship design optimisation methods generally include several objectives. However, many studies have been carried out to minimise the resistance/drag of the hull (Huang and Yang, 2016, Kim and Yang, 2013, Huang et al., 2015). Despite the wide range of studies that can be found in the literature, most analysis are carried out at model-scale and in towing conditions. Fast developments are now also venturing into self-propulsion conditions and possibly full-scale environments. That being said, these methods require high computational power and are rarely found to be used in optimisation procedures.

It is good to note that optimization methods have been applied to both the high-fidelity solvers and the more common low fidelity solvers. Sometimes they have even been applied to a combination of both and these are called variable-fidelity solvers. As explained by Huang and Yang (2016), low fidelity solvers are generally potential flow theory methods that are less accurate but are less computationally expensive. On the other hand, high fidelity solvers require higher computational power/capacity but are better at predicting the physics. Common practice is to follow a variable fidelity procedure. This means that variants are investigated using low fidelity methods and if they prove to be promising candidates, high fidelity methods are then used (Kim 2009).

A hull optimization framework using a numerical solver comprises of three main components; the solver, the geometric modeller and the optimisation algorithm (optimiser). The integration of all three modules allows the solver to predict the hydrodynamic performance of the ship geometry provided by the modeller, whose design parameters/variables are controlled by the optimization algorithm. Details of optimization algorithms and computer Aided Geometric Design are not be presented in this review since no novelties were demonstrated in these areas

of study. However, a brief overview is provided. This is detailed to provide a basic understanding of the methods used during this particular study.

As described by Harries (2004), ship geometry modelling techniques (Computer Aided Geometric Design) fall under two main categories namely conventional and parametric methods. The former produces low level definition of the geometry made up of points that define the curves and surfaces. It allows high geometric variations but requires the alteration of many parameters thus introducing many design variables in an optimisation procedure. This means the process is not very feasible. Methods of narrowing down the parameter numbers have also been introduced via radial basis function (RBF) interpolation methods (Kim and Yang, 2010) and modification function methods.

On the other hand, parametric modelling makes use of high-level entities, also known as parameters, that describe the geometry. Parameters are designed to have meaningful relationships that depend on conditions, criteria or sets of equations. These represent geometry surface in higher-level problem-dependent contexts (meaningful surface). Parametric approaches have also been described by Zhang et al. (2008) and Abt et al. (2001). The major advantage of such methods is that small to medium modifications to the surface can be carried out with minimal effort, i.e. less design variables, thus making the whole process feasible and economical. Harries et al. (2004) demonstrate the full and partially parametric approaches that can be utilised in the Friendship Systems modeler known as CAESES. An optimisation study using parametric modelling has been demonstrated by Han et al. (2012).

Optimisation algorithms are generally classified by the methods that are used to control the step size and direction. Algorithms can either be deterministic or stochastic. Stochastic take more of a random approach and direction. A typical method is called the genetic algorithm. Optimisation studies in the marine industry generally make use of deterministic algorithms where the method makes use of an analytical scheme to proceed to the next iteration; i.e. the development of the optimisation direction is based on the information understood and received by the system in the previous steps. Deterministic methods can be categorised into either gradient/ curvature information-based methods or those that rely on objective function (search methods). It is good to note that deterministic procedures generally require less steps to find an optimum (Birk et al., 2004) thus resulting to be computationally cheaper.

Search methods (e.g. pattern search, tangent search), (Hilleary, 1966), tend to be suitable for expensive and noisy objective functions where an approximation of the gradient is too costly.

Their lack of convergence raised concerns and therefore advanced gradient methods have been developed and found to be more reliable. However, they work well in practice and are applicable to various problems, which require minimal user input.

On the other hand, Gradient Methods (e.g. Sequential Quadratic Programming) compute the direction based on the gradient information of the objective function thus enhancing convergence speed considerably. Although these procedures find the optimal candidate more efficiently, they are more complex requiring the accurate evaluation of the objective function. In addition, these derivative based algorithms might lead to the local optimal solution and not the global optimum solution. A typical study that has made use of such a method was carried out by Park et al. (2015a). Meanwhile derivative free optimization algorithms (direct search methods), are more effective in finding the global optimum and have been used in a few studies (Kim and Yang, 2013, Kim et al., 2009, Huang et al., 2015).

Multi-objective optimization workflows are now also being introduced (Tahara et al., 2008, Campana et al., 2006). Typically, multi-objectives result in conflicting interests that require compromises. There are two main approaches that may be adopted in such scenarios; either derive all objectives into a singular parameter or the application of the Pareto Front.

2.2.1.6 Future developments of CFD that would benefit marine applications

Numerical solvers have enhanced significantly over the past few years. This has allowed marine research, and more specifically ship hydrodynamics research, to progress in parallel. The continuous improvement of High Performance Computing (HPC) capabilities and the move towards Exascale computing will allow research methods to be exploited further, opening up new possibilities previously constrained due to computing capabilities. With this in mind, numerical solvers should be further developed taking into consideration the power and capacity of Exascale computing platforms. In time, this will result in more robust, accurate, scaleable, high fidelity, state-of-the art simulations, even when employing optimization procedures.

The development of computer performance to exascale HPC computing will push boundaries in science and research allowing innovative capabilities with current tools as well as newly developed tools to further improve the simulation of real-world problems. Access to much greater computing capacity will allow the use of larger and more refined meshes within CFD simulations, which in turn will lead to more accurate solutions. This capacity will allow for increasingly complex scenarios to be solved, as they will enable more parameters to be

calculated directly rather than be assumed or simplified. Further advances could also be directed towards using LES numerical models for cavitation, simulating cavities and eddies. Although it has been found to be more accurate for certain engineering applications, LES is not currently very common as it is very computationally expensive (Stern et al., 2012). However, the availability of much bigger computational capacity would mean that simulations could be carried out in more realistic conditions with a full-scale self-propelled ship operating in a seaway, which is representative of an actual sea state. An ITTC survey indicated that most institutions do not consider free surface effects and they mostly model the propeller using body force methods. Higher fidelity simulations would enable researchers, and more crucially the industry, to gain a better understanding of the phenomenon in real operational conditions in order to take more informed decisions about the issues that they may encounter. Although optimization methods are widely available, their use with high fidelity solvers is not common practice due to the computational capacity required. Hull and propeller optimization using RANS simulations would greatly benefit the industry allowing the analyses of multiple designs at a reasonable expense when compared to experimental procedures. Looking further into the future there is likely to be a venture into optimization methods in real operational conditions and optimization using LES or DNS numerical models. As explained above, the increase of computational power introduces endless possibilities to the marine industry and research in general (Stern et al., 2015, Gatin, 2019).

However, looking at short term improvements, the ability to create greater mesh sizes with greater elements would increase accuracy, allow more full-scale simulations and make it easier for engineers to satisfy the validation and verification requirements (V&V) of their simulations. This in turn would create more credibility for their work and generate more trust from within industry. An ITTC (2011b) survey indicated that most institutions perform full-scale CFD analyses but only half of them carry out proper V&V studies. One other significant improvement would be to allow more interaction between the HPC and the user i.e. creating a better graphical user interface allowing for interactive simulations. Some CFD engineers find it best to monitor their work while the job is running. This enables them to make sure the simulation is running adequately, and it allows them to make any necessary modifications during the run. This is commonly practiced when carrying out minor jobs on a personal computer. However, when running jobs on a high-performance computer, although some visual elements are allowed, this is somewhat limited. Extending and expanding visual capabilities in HPC would definitely help engineers carry out their work more efficiently. A comprehensive

discussion on the recent advances in CFD, and potential future trends and developments, is presented in (Stern et al., 2015).

2.2.2 Wake Field Analyses

2.2.2.1 Wake Background and Theory

The wake is a region of flow around the vessel (Figure 7) that has been disturbed by the presence of the hull or propeller whereby the uneven flow velocity is usually different to the hull speed. More scientifically, Sampson (2008) outlines that the “Wake is defined as a fraction of ship speed or advance velocity at the propeller plane” and ITTC (2011b) defines it as “The disturbance flow field caused by the relative motion between a hull form and a uniform incident flow parallel to the hull longitudinal center plane”. In real scenarios (self-propelled environment), unlike open water propeller tests, the propeller is installed aft of a hull body, resulting in a retarded non-uniform flow into the propeller.

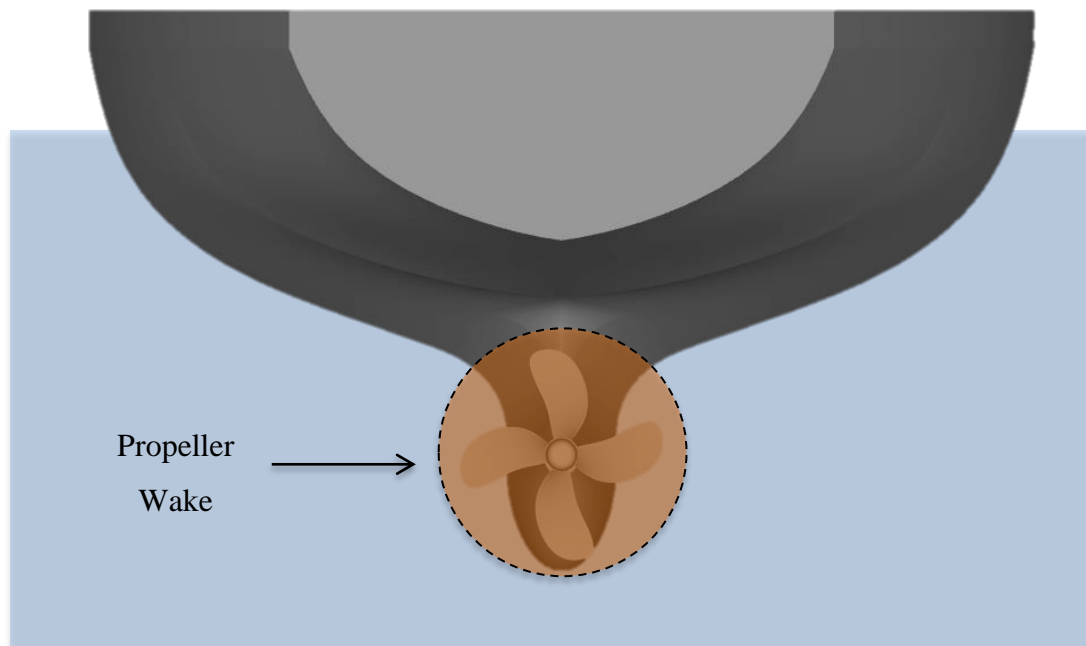


Figure 7. Propeller Wake

The wake field characteristics at the propeller plane arise due to the phenomena listed below:

- The streamline flow along the ship
- Progression of the boundary layer along the ship
- The waves generated by the vessel
- The effect of the propeller (when applicable)

The hull form shape has an influence on all these criteria. This clearly indicates that each vessel design can be considered to have a unique wake field.

When the wake of a vessel is measured in towing conditions, i.e. at the propeller plane without the presence of the propeller, this is known to be the nominal wake. When the wake of a vessel is measured in self-propulsion conditions, with the propeller present aft of the ship, this is known to be the effective wake. The effective wake is the sum of the nominal velocity and the introduced hull-propeller interaction effects. However, as Carlton (2018) points out, the total wake velocity is a combination of the nominal velocity, the hull-propeller interaction effects as well as the propeller-induced velocities. This indicates that the effective velocity is the total wake velocity minus the propeller-induced velocities (Figure 8). It should be highlighted that during propeller design procedures, it is the effective wake that is taken into consideration and therefore various methods have been structured to extract such data from nominal wake measurements. The effective wake can be considered from two standpoints: model tests and numerical computations. From model tests, one can compare self-propulsion tests with propeller open water tests to get an average effective wake that is not spatial-varying but average. From numerical computations, one can derive the total velocities at the propeller plane that are then corrected for the propeller induced velocities. This method provides a spatial-varying effective wake. However, there are some issues with this method. Firstly, it is not possible to extract the information at the propeller plane due to the presence of the propeller geometry. Furthermore, if a coupled potential flow-RANS solver is used (with coupling errors), the accuracy is very code dependent.

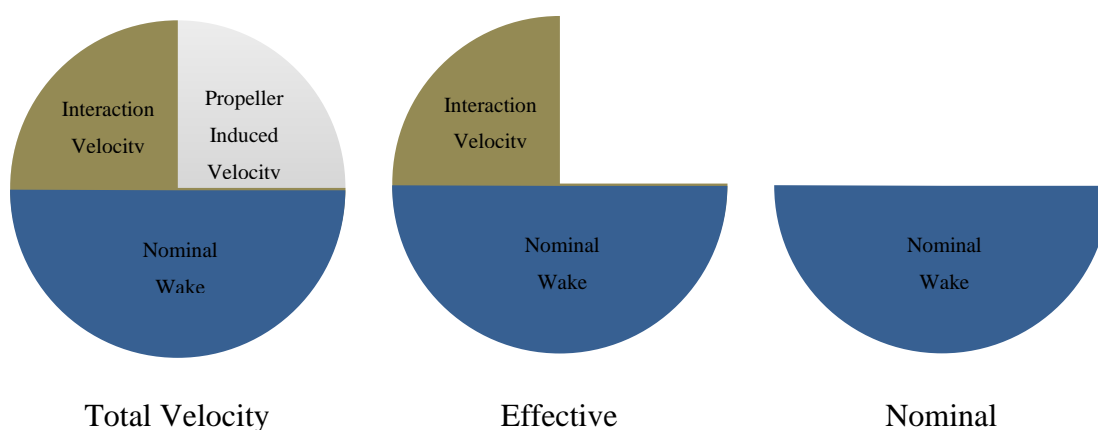


Figure 8. Total Wake Components

Wake field data can be represented in different forms. The two most popular representations are the velocity ratio method and the Taylor method, also known as the wake fraction method.

The prior method is the ratio of the ship speed to the far field water speed and it can be represented using iso-velocity contours. For this form of representation, the velocity is expressed in three components of the 3D environment; axial, tangential and radial and they are all presented as follows

$$\frac{V_A}{V_S}, \frac{V_T}{V_S}, \frac{V_r}{V_S} \quad (13)$$

The other wake fraction method, as the name suggests, considers the loss of velocity at a particular point when compared to the ship speed and is therefore represented using fractions as illustrated below.

$$\omega = \frac{V_S - V_x}{V_S} = 1 - \frac{V_x}{V_S} \quad (14)$$

The mean wake field is another parameter that is used to compare wake fields. Both the velocity and the wake fractions methods can be used to compute what is known as the average mean wake velocity. This is calculated by integrating the wake field on a volumetric basis of the form. Since the wake value at any given radius, varies along the circumferential direction, the wake mean value for each radius is generally computed. The mean value for each radius can then be plotted and computed to identify the average mean nominal wake (Figure 9).

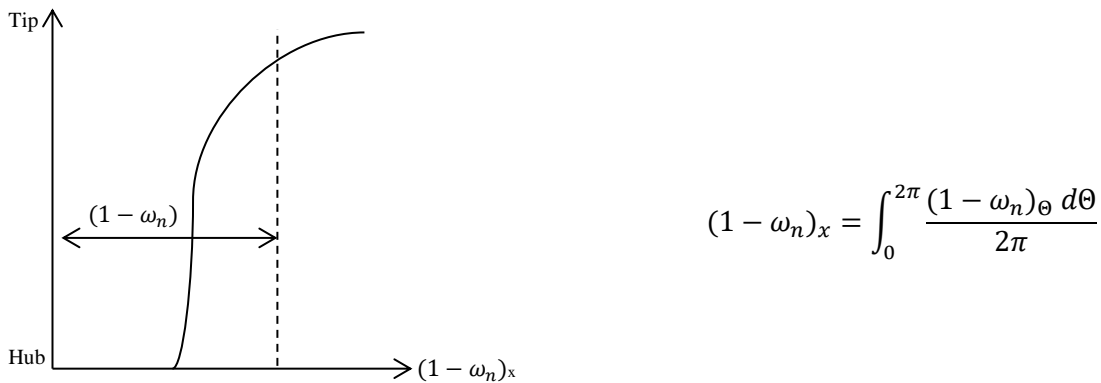


Figure 9. Average Mean Nominal Wake

The generation of the wake is caused by the combination of potential, viscous and wave making effects of the flow (Figure 10). A non-linearity parameter also exists but this is avoided for simplicity reasons.

$$\text{Total Wake} = \text{Potential Wake} + \text{Viscous Wake} + \text{Wavemaking Wake} \quad (15)$$

The wave-making component is generated due to the wave action. This is generated by the movement of the water particles as a result of the gravity action imposed by the ship. The potential wake field contributes to the wake due to the pressure distribution around the vessel, considering the ship is working in an ideal, non-viscous fluid. This is generally considered to be a relatively small component when compared to the total wake (Harvald, 1950). On the other hand, the frictional wake is developed due to the contact between the viscous fluid and the hull surface, which develops the growth of the boundary layer and can be considered to be mostly fully turbulent at full scale.

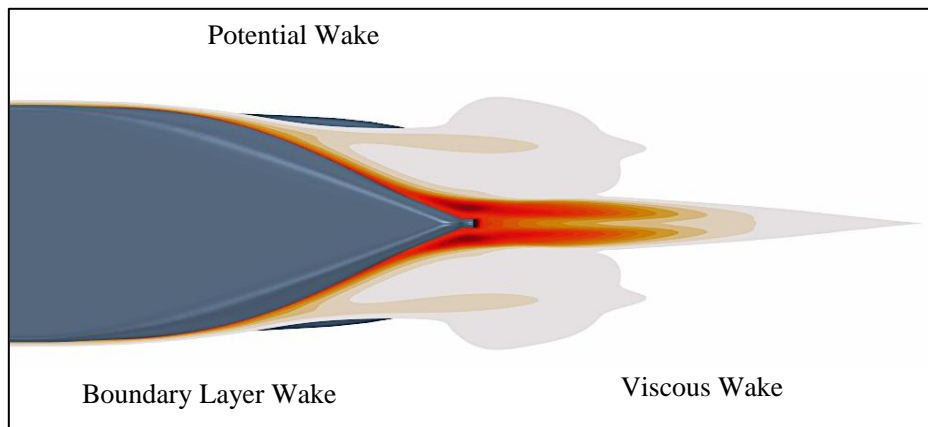


Figure 10. Wake Generation

Since the viscosity of the water generates a boundary layer close to the hull surface, this causes a retardation of the flow. This is more prominent at the stern of the vessel and produces a forward velocity component (Figure 11). As the liquid nearest to the surface progresses along the ship hull, the adverse pressure gradient increases causing the flow to gradually change direction. Once the flow velocity gradient reaches a null value at the surface, flow separation occurs resulting in a region of reversed flow on the hull. All these issues make the prediction of the boundary layer and velocity profile behavior complex.

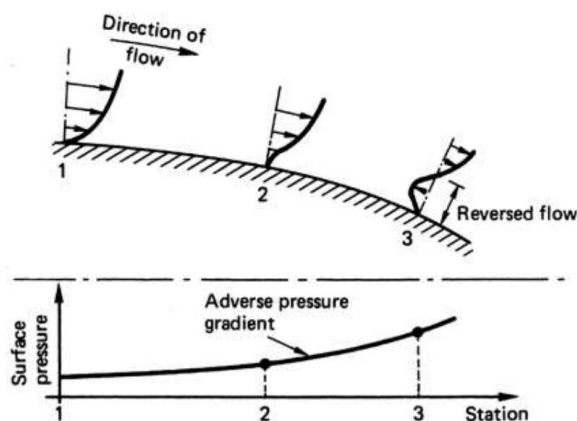


Figure 11. Boundary Layer Development (Carlton, 2007)

2.2.2.2 Wake Prediction and Past Studies

The accurate determination of the wake field characteristics just aft of the vessel where the propeller operates is of utmost importance given that such data is used to determine the right propeller design, improve hull-propeller interaction, enhance propeller performance and understand the impacts of Energy Saving Devices. Wake analyses and the accurate prediction of the ship boundary layer were never an easy task but rather entail a complex procedure. Typical methods for accurate calculation require the analyses of the wake zone, the boundary layer zone as well as the potential flow zone.

Back in the day, before the measurement of experimental wake field data was even possible, designers made use of various limited prediction methods such as regressions equations, formula and historical analyses data. Harvard (1950) outlines the different methods highlighting the merits and limitations of each. Other than being based on certain assumptions, they have been considered adequate for traditional hull forms making them inappropriate for progressive and modern hull form designs. To this day, the most common procedures for determining the total wake fields are experimental model tests. Past experimental investigation of model wakes made use of pitot tubes, hot wire anemometry and tuft strips to measure flow velocity (Carlton, 2018). Today, modern methods make use of non-obtrusive methods such as Particle Image Velocimetry (PIV) (Aktas et al., 2016, Capone et al., 2019) and Laser Doppler Anemometry (Atlar et al., 2007). However, since these investigations are carried out at model-scale, the measured wake data requires scaling, and this is generally not so straightforward. In addition, they are generally carried out in towing condition and neglect the hull-propeller interaction effects that arise due to the presence of the propeller. Wake scaling will be further explained later in this chapter

Continuous effort and developments are being carried out using RANS codes to give accurate predictions for all ship designs and types (Wang et al., 2015). If the wake can be accurately predicted using numerical procedures, CFD methods can prove to be beneficial since simulations can be carried out at full-scale, thereby avoiding scaling effect errors, and a very detailed analysis could be processed at any area of interest extracting any desired parameters (Visonneau, 2005, Queutey et al., 2016). In addition, CFD allows the luxury of setting any kind of environment and condition including different speeds, draft and more. Not to mention the capability of running the simulation in self-propulsion conditions avoiding the necessity of the results to be processed further to provide effective wake data.

2.2.2.3 Numerical Wake Prediction

CFD codes have advanced significantly over the years and the increase in computational power has opened doors to ship numerical simulations both at model and full-scale conditions. This has opened new areas of investigation and exploit details that couldn't be previously studied.

CFD codes and approaches vary in types, turbulence models, grid structure and more. The analyses of interest may also vary in type, with some studies seeking performance parameters such as drag or thrust coefficients and others seeking detailed wake characteristics. With CFD becoming ever more credible and popular within the industry due to its convenience, validation (comparison) with experimental results and verification, approaches have been developed ensuring that the solver is predicting the physics with reasonable accuracy. Since full-scale data is not readily available, a general tendency is to firstly validate CFD simulations at model-scale and then carry out studies at full-scale.

As indicated by Larsson et al. (2003), the type of turbulence model plays a crucial role in wake prediction. The most popular model is the RANS codes, which solves time averaged Navier stokes equations. Visonneau (2005) and Hanninen (2006) continue to explain that it is the turbulence closure that dictates the level of detail in the prediction of wakes. The Gothenburg 2010 workshop on Numerical ship hydrodynamics compared and assessed the different CFD codes. Outcomes from the workshop outlined that significant progress has been made in predicting flow characteristics aft of u-shaped hulls and that most codes compared reasonably well with experimental data. They too indicate that the turbulence models play an important role but continue to add that the grid resolution is also critical to capture certain details. Wang et al. (2010) point out that structured grids are more suitable than unstructured grids and that the RSM is the best model to capture detailed wake characteristics such as the hook.

EFFORT (Visonneau, 2005) is another project worth mentioning as it successfully demonstrated the accuracy of full-scale viscous flow computations that were compared to experimental data. Larsson (2003) indicated that the turbulence model might not be as important for full-scale simulations. However, this was contradicted by Visonneau (2005) who said it still plays a crucial role in full-scale wake analyses. This being said, Visonneau (2014) carried out another study in 2014 stating bilge vortices are not as strong at full-scale and therefore RANS methods can be considered suitable. The EFFORT project focused its efforts on the suitability of the different turbulence models available and highlighted the following outcomes. Although $k-\omega$ and $k-\varepsilon$ turbulence models manage to capture the general flow around

the ship, they fail to accurately predict wake flow characteristics, especially the vortex structures. On the other hand, the SST two equation turbulence models are better suited to wake prediction and serve as a good compromise between $k-\omega$ / $k-\varepsilon$ methods and the EASM or more complex RSM model. The latter are sophisticated models that are able to capture and simulate stronger bilge vortices but are computationally expensive and less robust than the SST $k-\omega$ / $k-\varepsilon$ models.

As previously mentioned, the prediction of the vortical flow using the SST turbulence models require further improvements. A recently introduced novel technology makes use of an implemented curvature corrected SST turbulence model. More details on the subject can be found in the previous section ‘Turbulence Modelling’ (2.2.1.4.5) but the SST-CC was found to improve the model and in particular the vortical structures. It would be interesting to investigate whether such a model would improve the wake characteristic produced by a vessel, especially when trying to analyse vortex structures or turbulent flows (e.g. the wake behind a high block coefficient vessel). To the best of the author’s knowledge, only one study in the marine industry has made use of such a model (Heinke and Hellwig-Rieck, 2011). That being said, not many details regarding the turbulence model were published and validation and verification procedures were not presented. Therefore, it would be worthwhile investigating various studies like, wake prediction, numerical wake scaling, vessel performance in different operational conditions and the use of different retrofitting technologies using this curvature corrected technology.

2.2.2.4 Wake Quality Assessment

Understanding and differentiating a good wake from a bad wake is crucial. Thus, the assessment and judgment criteria of wake quality are very important. Wake quality assessment methods have been investigated for years now, and are generally carried out using two methods; Analytical methods and Heuristic methods (Carlton, 2018). The former makes use of extensive wake field data to investigate the quality in all three direction i.e. axial, radial and tangential vectors. The latter, which is the more common of the two due to its simplicity, utilises the axial velocity component only. Various analytical methods that introduce new criteria, such as vorticity and turbulence, can be referred to in the following studies (Truesdell, 1953, Mockros, 1962).

With regards to the simpler methods, Huse (1974) developed a set of criteria based on the axial fluid flow characteristics in the absence of the propeller. Therefore, this method does not consider issues associated with pressures and vibrations in a hull-propeller configuration system. With this motivation in mind, Odabasi and Fitzsimmons (1978) extended Huse’s work to consider wake quality assessment in this area of interest. Thus, they developed methods, criteria and indicators to satisfy vibrations and hull surface pressures. Although, these parameters are not calculated or simulated, these instructions can be considered as good guidelines or indicators for their avoidance.

2.2.2.5 Wake Scaling

The flow field characteristics around a ship are highly dependent on the Reynolds number as demonstrated by M. Gad-el-Hak and Bandyopadhyay (1989). The concern is that model tests are based on Froude number similarity rather than Reynolds number similarity. The difference in Reynolds number between different scales results in different boundary layer behavior with the thickness decreasing as the Reynolds number increases. This results in different velocity profiles. This has been verified by Lübke and Abdel-Maksoud (2002) and Huang and Groves (1980) who carried out various studies to analyse stern flow fields at different lengths and Reynolds numbers. Lübke and Abdel-Maksoud (2002) continue to indicate that numerical wake results were in agreement with experimental data. Furthermore, model tests tend to have non-fully turbulent behavior due to the size of the model whilst the flow around a ship in full scale is mostly turbulent.

During propeller design procedures, the nominal wake, or even better the effective wake is required at full-scale to ensure accurate modeling. Therefore, wake scaling is a very important issue, one that raises certain concerns within the industry. Generally, scaling procedures take the approach demonstrated in Figure 12 below. This approach first requires the scaling of the nominal wake. The changes are then applied and converted to the effective wake. However, it should be noted that validating the accuracy of scaled wakes is not so easy since this kind of data is not easy to come by.

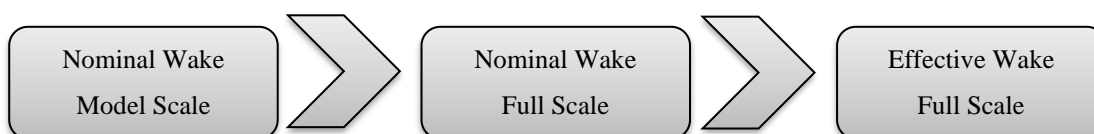


Figure 12. Wake Scaling

Various methods of wake scaling have been developed over the years (Hoekstra, 1975, Sasajima and Tanaka, 1966, Gómez, 1990). There are the so-called ‘Contraction’ methods that are based on semi-empirical formulae with the ‘Sasajima-Tanaka’ method being the most popular of the lot since it has been proven to give reasonable results. These methods, although convenient, have their drawbacks (ITTC, 2011b). All the wake field area is treated equally, and this is unrealistic when taking into consideration certain assumptions. Since their focus is mainly the axial flow, they might not capture certain transverse flow components and fail to predict vortex structures or bilge vortices. In addition, although they might have been proven on certain traditional hulls, they might not perform as well with progressive new generation hulls.

With significant advances in CFD and computational power, new methods of numerical wake scaling have been exploited whereby CFD is used to produce a full-scale wake field that is processed from model test data. These procedures have been overshadowed by the use of more direct approach which simulates full-scale ships in towing or self-propulsion conditions (Visonneau, 2005, Castro et al., 2011).

2.2.2.6 Wake Analyses for Appendages

Improving stern form and propeller designs are not the only ways to reduce propeller induced fluctuations, reduce underwater noise and improve propulsion efficiency. Another approach is to install retrofitting devices aimed at improving the inflow to the propeller. There are different types of Energy Saving Devices with different working principles. For these devices to properly function, one should analyse the stern flow characteristics of the vessel before and after designing the technology. The wake field characteristics should be analysed at full-scale for accurate flow prediction. However, simple wake scaling methods are generally not applicable to ships with installed ESDs due to the difference in the velocity profile. Therefore, accurately predicting wake field characteristics at the propeller plane at full scale is only possible with numerical procedures.

Various authors (Ok, 2004, von der Stein, 1996) have studied wake flows to understand the impact of Wake Equalizing Ducts (WED). They have suggested that WED accelerates the water in the wake peak range resulting in more uniform flow and lower maximum wake fractions. It was also pointed out that the function of a WED is more developed at full scale. Others (Han et al., 2006, Johannsen, 2000), have studied the use of vortex generator fins (VGF).

As the name suggests, the fins generate a vortex which aims to reduce the wake peak. Heinke and Heelwig-Rieck (2011) carried out a similar study analysing both the WED and the VGF using numerical methods and outlined conclusions similar to the previous study. The higher the Reynolds number of a ship, the smaller the boundary layer thickness, the smaller the wake peak range and the smaller the maximum wake fractions. However, the wake gradient is larger and contracted towards the center. These are evident in the results of their study in Figure 13 below.

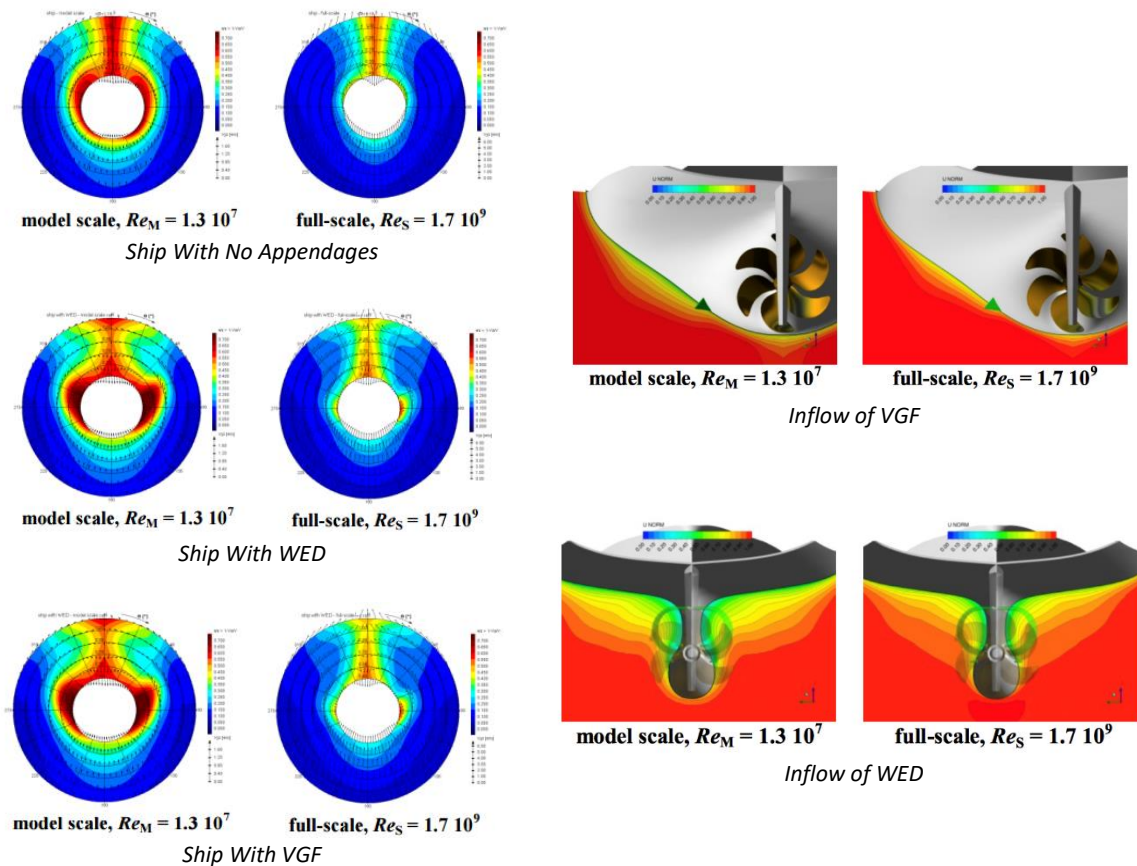


Figure 13. Wake Scaling Effects with Retrofitted ESDs (Heinke and Hellwig-Rieck, 2011)

With the continuous search for a greener environment and more energy efficient ships, the wakes produced by ESD retrofitted hulls are a hot topic in the marine industry with different technologies and solutions still being investigated till this very day. Other motivational factors highlighting the importance of wake field analyses are cavitation and pressure pulses at the aft ship. After carrying out a study, Carlton (2001) indicated that wake irregularity (non-uniformity) has a significant influence on the aft vibrations. One particular wake field region that is susceptible to cavitation is the wake peak inside the wake shadow where the propeller is subject to heavy loads. The wake peak, peak width and non-uniformity are all important parameters that should be investigated when analyzing wakes.

The progressive advancements in CFD methods are continuously enhancing the wake prediction accuracy. Therefore, the need to keep investigating Energy Saving Devices using more novel numerical methods is necessary in order to further understand their function and determine any possible improvements to be made.

2.2.3 Energy Saving devices

2.2.3.1 Introduction to Energy Saving Devices in the Marine Industry

The introduction of regulatory requirements in the marine industry to limit ship emissions has been a major concern in recent years. This has motivated and directed research to improve the energy efficiency of a vessel. One particular area that has been given attention and developed in recent years are Energy Saving Devices (ESDs).

Energy Saving Devices (ESDs), also known as ‘retrofitting devices’, focus on improving the propulsion and hull-propeller interaction efficiencies. They can be installed on optimised new hulls as well as existing vessels by means of refitting (Hansen et al., 2011). Recently a large amount of ESD research has been carried out experimentally and numerically. Studies (Hansen et al., 2011, Atlar and Patience, 1998, Schuiling, 2013, Kawamura et al., 2012) suggest that the installation of ESDs on a ship can result in a significant improvement in energy efficiency. As specified by Hooijmans et al. (2010), ESDs are designed to improve the flow around the hull, improve the wake/propeller inflow and can also be designed to recover energy leaving the ship system. These technologies are installed as a means to improve the hull-propeller interaction and maximize the propulsion efficiency of a vessel. The speed of the vessel, in particular, has a significant impact on the EEDI value and fuel consumption. This is because the parameter is exponentially related to the required propulsive power. In order to meet EEDI requirements and reduce the fuel oil consumption, the installation of ESDs can maximise design speed for a specific power or decrease the power required for a specific speed which in turn would improve the total propulsive efficiency (η_D).

A wide range of ESDs with different features, types and working principles have been developed through the years. Devices to improve propulsive efficiency can generally be classified into three different categories: Pre-swirl, Post-swirl and added features to the propeller (Figure 14). Various authors have reviewed ESDs in the past (Blaurock, 1990). They have outlined the various improvements and gains achieved by the different technologies that

seem quite promising. However, since ESDs tend to produce minor improvements, there is some doubt whether the benefits are achieved during operations. Therefore, reliability and the guarantee of energy savings for such devices remain the principle issue and continuous research is needed in order to support their reliability.

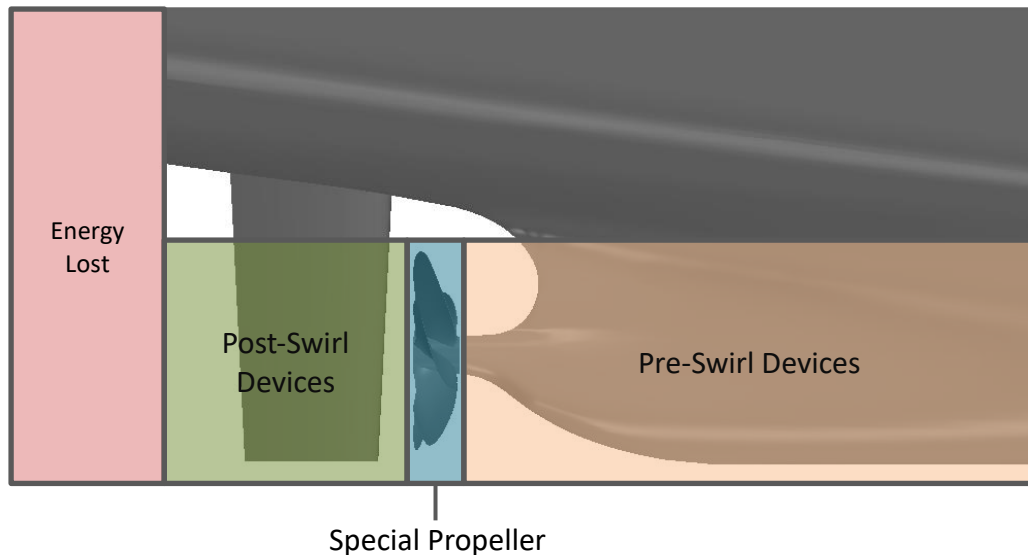


Figure 14. ESD Categories

Ongoing research focuses on maximising the energy efficiency potential of these devices through design improvements. With the increased availability of computational power and advances in numerical tools and modelling software, the use of optimisation procedures are becoming increasingly popular to identify the energy efficiency saving potential of ESDs. Nevertheless, the availability and reliability of many ESDs that can be used to reduce the EEDI value and increase energy efficiency remain uncertain. There is a lack of confidence in their use within the industry because efficiency gains are small and extremely difficult to assess, not only during sea trial measurements but also during model tests.

This section presents a review of the most commonly used energy saving technologies highlighting their benefits and disadvantages. In addition, the various measuring ESD impact methods are outlined and their problematic issues indicated. The key areas are then discussed highlighting and proposing potential areas of investigation

2.2.3.2 Pre-Swirl Devices

Pre-swirl devices are energy saving devices installed upstream of the propeller. These are designed to improve the wake flow into the propeller plane. The flow is either accelerated or directed into the opposite direction to that of the propeller rotation, imposing a better angle of attack on the propeller blades. This helps the flow leaving the propeller plane with less circumferential momentum, thus requiring less kinetic energy to produce forward thrust.

Pre-Swirl Stator

A vessel with a single propeller suffers from significant rotational losses in the slipstream. The function of a pre-swirl stator (Figure 15) is to recover that energy by reducing the rotational losses incurred by the propeller. In general, this ESD consists of four stator blades that are mounted on the stern boss ahead of the propeller in order to re-direct the flow. It generates a swirling flow in the direction opposite to that of the rotating propeller increasing the load through which the delivered thrust per unit of power is increased. Due to the uneven vertical distribution of the wake on either side of the vessel, the number of fins and their orientation are not always symmetrical to the port and starboard sides of the ship thus require a tailored design for each ship. A typical configuration generally involves three fins on the port side and one on the starboard side because reducing the upcoming flow on the port side requires more effort than trying to re-enforce the flow upward on the starboard. The technology itself increases resistance. However, it also improves the propulsion efficiency and hull-aft interaction (Kim et al., 2013). Therefore, systems should be designed in such a way that the gain in propulsion outweighs the added resistance to result in a positive gain. Such technology can offer savings of up to 4.5% (Zondervan et al., 2011) and this is adequate for ships with heavily loaded propellers where no flow acceleration is required but only the re-direction of the flow. These devices can be considered to be simple, robust and cost-effective. It can also be coupled with a duct to accelerate the flow into the propeller.

Ducts

The Wake Equalizing Duct (WED) is made up of two, aerofoil sectioned, half ring designs that are integrated into the stern of the ship hull and positioned in front of the upper region of the propeller. The stern hull form of a vessel generally results in slower flow velocity towards the top of the wake compared to the lower region. The WED is therefore designed to accelerate the flow at the top of the wake, improving uniformity to increase propeller efficiency. The foil

generates a lift that accelerates the flow and increases the duct thrust and decreases the propeller thrust. It also helps reduce the flow separation at the aft end to minimise the thrust reduction factor. This being said, the duct itself creates additional resistance. Thus, the device needs to be optimised to generate a higher thrust than its drag resulting in a beneficial impact. Important design characteristics of the WED are duct angles, longitudinal positions, inner diameters, profile section shapes, lengths and angles of sections. The report (ABS, 2013), identifies that the propeller tip clearance and load, influence the duct efficiency. Accelerated and straightened flow into the rudder also improves steering qualities. In summary, this ESD reduces aft flow separation, generates additional thrust, reduces propeller vibrations and improves manoeuvrability. The Schneekluth duct was installed on over 1500 vessels and has been claimed to produce fuel savings of around 5% and reduce vibration by up to 50% (Lambos Maritime Services Ltd, 2013). The Mewis Duct (Figure 15), developed by Becker Marine systems, consists of an integrated duct with fins configuration. It combines two working ESD principles, that of the contra-rotating propeller and that of the wake equalizing duct, to enhance the propeller inflow and reduce rotational losses. More than 20 Mewis ducts have been installed on different vessels with analyses estimating that the technology results in a mean power reduction of around 6.5% and also reduces vibration excitation and pressure pulses by up to 80% (Mewis and Guiard, 2011). It is most effective for ships that run at lower speeds, generally under 20 knots, and that have high block coefficients (Hollenbach and Reinholz, 2010).

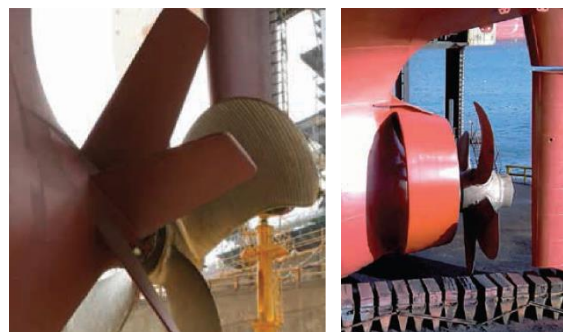


Figure 15. Pre-Swirl Stator (*left*) and Becker Mewis Duct (*right*) (ABS, 2013)

2.2.3.3 Unconventional Propellers

Not many unconventional propellers have been developed over the years. Other than skew and annular profile modification, propellers have been designed through very little innovative development. The most common are the tip propellers, namely Kappel, Contracted and Loaded Tip (CLT), the New Blade Section propellers (NBS) and Contra-Rotating Propellers.

Contracted and Loaded Tip (CLT) Propeller

CLT propellers (Figure 16), which are most effective for slower speed vessels with a higher block coefficient, are installed with end plates at the blade tips located on the pressure side to reduce the tip vortices. The tips are therefore bent sharply towards the rudder. They are designed to enhance propeller open water efficiency by minimising the induced velocities at the propeller disk to reduce the hydrodynamic pitch angle. They have been extensively tested on full-scale trials and results show 5-8% improved efficiency as well as cavitation reduction. They also provide a higher thrust due to their smaller, optimal propeller diameter (Gennaro and Gonzalez-Adalid, 2012).

KAPPEL Propeller

The Kappel propeller was designed with a modified blade tip. It was developed to suppress the tip vortex and generate both lift and thrust to improve the overall efficiency. The tip (Figure 16) is located on the suction side of the propeller featuring a smooth transition between the blade and the tip. The gain in efficiency is reported to be around 6% (Gennaro & Gonzalez-Adalid, 2012).



Figure 16. Kappel (*left*), CLT Propellers (*centre*) (Gennaro and Gonzalez-Adalid, 2012) and CRPP (*right*) (Kluijven et al.)

NBS Propellers

The New Blade Section (NBS) propeller uses a significantly different section profile of the blade allowing the reduction of the optimum diameter without adversely affecting the propulsion efficiency. Studies showed that while the NBS propeller has similar performance to conventional propellers at model-scale, the technology performs better in full scale conditions providing higher efficiency and superior cavitation performance (Sasaki and Patience, 2005).

Contra-Rotating Propeller (CRP)

CRPs come in two different configurations, both of which work with the same principles. One arrangement, commonly known as the Coaxial Contra-Rotating Propeller (CCRP), involves two-contra rotating propellers on a single shaft that is mechanically complex. On the other hand, the Contra Rotating Propeller Pod (CRPP) is a regular conventional propeller with a pod propeller that rotates in the opposite direction. A regular conventional propeller produces a rotational flow aft of the propeller. Other than just producing a forward thrust, the screw generates an undesirable sideways force due to the swirling flow more commonly known as the ‘wheel effect’ and this results in a loss of energy (Kluijven et al.). Therefore, the CRP is used to neutralise this rotation minimising the sideways force to reduce the energy leaving the hydrodynamic system of the ship, causing a higher forward thrust. The CCRP (Figure 16) can reduce cavitation and torque to improve the propulsion efficiency. A study (Rutundi, 1934) comparing CRP with a conventional propeller on a 3500 ton naval training ship claims an 18% improvement in the propulsive performance even though mechanical shaft issues were raised when applied to larger merchant vessels. These mechanical shaft issues were due to the associated higher power (Ghassemi, 2009). IHI has developed a contra-rotating propeller system for large ships and installed it on a 37,000 DWT vessel. Sea trials indicated a 15% power improvement together with less cavitation and noise (Nishiyama et al., 1990). CRPP has drawn attention in recent years due to its beneficial impact, hydrodynamic performance and significant savings. One study (Kluijven et al.) indicated that the CRPP resulted in 8% less fuel consumption. In addition, the POD is able to rotate by 360 degrees improving vessel manoeuvrability.

2.2.3.4 Post-Swirl Devices

Post swirl devices are generally installed downstream of the screw and are used to condition the flow aft of the propeller. They can be designed to recover the rotational flow and use that energy to enhance axial flow. They can also reduce or divert the flow in order to improve rudder efficiency. They are particularly suitable for cases where energy losses in the slipstream are expected to be significant.



Figure 17. PBCF (*left*) (Hansen et al., 2011), Asymmetric Rudder (*centre*) and Rudder Bulb (*right*) (Becker Marine Systems)

Grim Vane Wheel

The Grim Vane wheel is a freely rotating device located behind the propeller, consisting of a number of blades that are larger than the propeller. The inner radii of the vane wheel blades are designed with a pitch such that they act as an impeller and are driven by the wake of the propeller. The extended tips of the blades are designed with a different pitch such that they act as a propeller on rotation thus producing additional thrust. This energy saving device is designed to recover energy from the propeller slipstream and convert it to additional thrust. Ghose and Ghose (2004) have outlined that the vane wheel should be designed with a 25% increase in diameter and have a higher number of blades than the front propeller. They add that the tip clearance to the hull need not be high since the technology is lightly loaded and that it should rotate at an rpm of 30-50% of the propeller in the same direction. It has been claimed that this ESD provides additional thrust and reduces propeller loading to enhance propeller performance by around 5 – 10% (DNV GL, 2015). The reduced propeller load results in smaller propeller diameter requirements and reduced cavitation thus improving the propeller efficiency. Although a few studies focusing on Grim Vane wheels have been carried out in the past, (Kehr, 1986) and (Blaurock, 1983), this technology was not given the attention it deserves because of its failure during sea trials when installed on the QE2 cruise ship (Chen et al., 1989). The results obtained during this trial resulted in a bad first impression which lasted several years.

Stator Fins

These are fins installed aft of the propeller designed to produce an additional thrust and recover rotational energy. They deflect the flow from the propeller and convert the rotational energy to useful axial flow. They tend to be most effective when mounted on the rudder imposing a

horizontal rotation resulting in around 5-8% energy gains (Celik and Guner, 2007). Compared to the pre-swirl stator, the post stator is relatively moderate in size (less than 80% of the propeller diameter) and does not have any effect on propeller cavitation (Hollenbach and Reinholz, 2010).

Propeller Boss Cap Fins (PBCF)

The PBCF (Figure 17) are post-swirl fins that are installed onto the boss cap of the propeller. As water passes through the propeller disc area, it is accelerated and twisted. These effects are prominently dominant near the down-flow just after a blade's trailing edge. The vortices produced at the root of each blade combine together, resulting in a very strong vortex at the end of the boss cap. This phenomenon is known as hub vortex, which reduces the propeller efficiency and may cause rudder corrosion. As explained by Ghassemi et al. (2012), the strength of such phenomena is dependent on the hub geometry as well as the axial load distribution of the propeller. The aim of installing a PBCF is to minimise this hub vortex to reduce rudder cavitation and increase propeller efficiency. With the addition of a PBCF, the rotating fluid flow coming off the propeller hub is rectified, and thus the energy lost from the hub vortex is recovered. Gearhart and McBride (1989) performed a detailed experimental analysis of a PBCF retrofitted model propeller behind a hull-rudder arrangement. The report claimed that out of the total 6% gain in efficiency, 2% was due to a thrust increase, and 4% was due to a decrease in torque. The total gain in efficiency may also be reduced due to the additional frictional drag from the fins. Kawamura et al. (2012), Hansen et al. (2011) and Atlar and Patience (1998) are all in agreement that the beneficial effects of PBCF technology result in a reduction in shaft power and subsequent increase in fuel efficiency.

Hub Vortex Vane (HVV)

The HVV was jointly developed by SVA Potsdam and Schottel. The HVV is a small vane propeller fixed to the tip of a cone shaped boss cap. The vane's diameter is limited to where the tangential velocities due to the hub vortex are greater than those due to the propeller. The small vane propeller diverts the high tangential velocities in the direction of the jet to generate additional thrust. Another effect of the HVV is to divert the torque of the vortex that assists the engine torque and results in power savings. A detailed report by Schulze (1995) claims an increase in propeller efficiency of 3% on full-scale trials.

Asymmetric Rudder

Asymmetric rudder, also known as twisted rudders (Kim et al., 2014), have been used to avoid rudder cavitation such as erosion and gap cavitation. In contrast to the conventional blades, they are designed to reduce low pressure peaks on the rudder blades. Asymmetric rudders (Figure 17) have aerofoil profiles with separate portions of the rudder, above and below the propeller axis, optimised to work in the wake of the propeller. Therefore, they generally feature a twisted leading edge, sometimes merging with a Costa bulb and stators just behind the propeller hub. These types of rudders also take advantage of the rotational flow behind the propeller, but this effect is normally used to improve the rudder efficiency rather than create significant additional thrust. A study (Khorasanchi et al., 2013) indicated 1.25% power savings using numerical simulations.

Rudder Bulb

The rudder bulb (Figure 17) is a streamlined bulb attached to the leading edge of the rudder. The transition between the bulb and the propeller hub can also be bridged by a fairing cap. The rudder bulb attempts to condition the radial distribution of the flow behind the propeller plane at the hub, to reduce losses associated with high rotation and to minimise the generation of a strong hub vortex. The Costa bulb can accelerate the flow past the rudder to improve rudder efficiency. If a Costa bulb is mounted on the rudder rather than on its horn, it is important to take into account the effect of rudder rotation on its efficiency and its interaction with the propeller.

2.2.3.5 Methods to Measure ESD Impact

Although, optimally designed installed ESDs have shown a contribution to the reduction of resistance and improved propulsion efficiency, some aspects of uncertainty, such as scale effects and discrepancies/errors between different methods of measurement, raise concerns and lack of credibility. In this section, the various methodologies used to measure the gains of ESDs are presented, discussed and compared.

Model Tests

Ship performance and hydrodynamics are generally tested and analysed using more popular and traditional methods of experimental fluid dynamics (EFD, model test). These include

resistance and propulsion tests, propeller open water, cavitation and noise/vibration tests, flow line tests, and wake, local and global measurement tests. The basic idea of a model test is to experiment with a smaller model ship of geometrical similarity to extract information which can be scaled to a real ship. Although hull performance has been successfully estimated over the years, full-scale predictions based on model test data tend to result in slight discrepancies when compared to sea trial results. These extrapolation methods are based on the ITTC performance prediction method and correlation factors (ITTC, 1999). An issue with model tests is that they are unable to satisfy both the dynamic similarities of Froude number (Fn) and Reynolds number (Rn) with the prior being related to the ratio between inertia and gravity and the latter related to the ratio between inertia and viscous forces. As shown in equations (16) and (17), the model speeds required to achieve equivalent Rn are too high.

$$\frac{\text{Inertia force}}{\text{Gravity force}} \propto \frac{\rho U^2 L^2}{\rho g L^3} = \frac{U^2}{gL}, \quad Fn = \frac{U_M}{\sqrt{gL_M}} = \frac{U_F}{\sqrt{gL_F}}, \quad U_M = \frac{U_F}{\sqrt{\lambda}} \quad (16)$$

$$\frac{\text{Inertia force}}{\text{Viscous force}} \propto \frac{\rho U^2 L^2}{\mu UL} = \frac{\rho UL}{\mu}, \quad Rn = \frac{\rho_M U_M L_M}{\mu_M} = \frac{\rho_F U_F L_F}{\mu_F}, \quad U_M = U_F \lambda \quad (17)$$

In practice, model speeds according to Froude similarity are applied, which are able to model wave resistance phenomena correctly. For example, for a 7,500TEU container with a length (Lpp) of 286m at 22 kts, Fn is about 0.214 for both model and full-scale ships, whilst Rn values are 9.563×10^6 and 2.712×10^9 respectively, which means that Rn is considerably higher for the ship than it is for the model. The difference in magnitude of the Reynolds number lead to different boundary layer behaviour and velocity profile in the near wall regions resulting in different wake behaviour (Wang et al., 2015).

Generally, ESDs make scaling more difficult because they are operated largely or wholly within the full-scale boundary layer and are strongly affected by viscous effects such as differences in boundary layers, flow separation and vortex formation. The ITTC 1978 performance prediction method has been proven to work properly for hulls without appendages, unconventional propulsors and ESDs. With the availability of computing power and advances in numerical simulation, particularly Computational Fluid Dynamics (CFD), the ITTC 1999 method was proposed to consider ESDs using these technologies. The principal concept of the ITTC 1999 method is that the ratio for the wake fraction of the model to the full-scale ship without ESDs must be the same as that with ESDs, as can be seen in equation (18).

$$\frac{1 - w_{w/o ESD, full scale}}{1 - w_{w/o ESD, model scale}} = \frac{1 - w_{w/ ESD, full scale}}{1 - w_{w/ ESD, model scale}} \quad (18)$$

To apply this method, model tests or computations for the model-scale ship and numerical simulations for the full-scale ship have to be carried out. This does not exclude the fact that further studies, developments of model tests and methods of analysis are needed to measure the exact impact of ESDs for both model and full-scale scenarios. Park et al. (2015b) proposed a propulsive performance prediction method for full-scale ships with ESDs and compared it to the existing extrapolation methods (ITTC 1978 and ITTC 1999). The study predicted the performance of the KVLCC2 with a pre-swirl stator using full-scale CFD computations. The wake predicted by full-scale CFD was similar to that of the proposed method. Therefore, it was confirmed that the proposed method, which takes into consideration the effects of ESDs, could extend the model-scale results to full-scale. The author claims that this approach requires less computational power than full-scale CFD computations.

Sea Trials

After the design and construction of vessels, the official sea trial is conducted to confirm ship performance. Sometimes, a full-scale operation trial is conducted in service at the request of the ship owners. Once the sea trial is carried out, the results, in terms of ship speed, power and propeller shaft speed, are corrected to the calm (no wind and no wave) sea conditions according to certain guidelines, such as the ISO (2015), to verify the satisfactory attainment of the ship speed as stipulated by the EEDI regulations and/or contract. Ideally, sea trials should be carried out in calm water conditions, as far as is practically possible, thereby allowing proper measurements and also noting the current, tide and drift experienced throughout the test.

The impact on efficiencies and fuel oil consumption (FOC) due to ESDs fitted to real ships can be analysed and evaluated from the available data sets of sea trials and ships in service. The first approach is the official sea trial. However, unless the official sea trial is conducted repeatedly before and after fitting the ESDs, the impact can only be confirmed by comparing sea trial results of a vessel installed with ESDs to those of extrapolated model test results of the vessel with no retrofitting technology. This approach cannot be considered very accurate since it includes the errors associated with the extrapolation of the model test results. Another approach would be to measure the performance of the vessel during ship operations allowing the comparison to sister ships with no additional technology. This methodology is conceptually simple and direct, avoiding any scale effect issues such as wake fraction and flow separation.

This can be performed with the close support of engineering staff to evaluate the efficiency improvement of ESDs. That being said, this would incur a considerable cost of ship off-hire not to mention the difficulty of measuring and verifying small improvements. Furthermore, it is extremely difficult to separate and identify the effect of ESDs on fuel consumption from other factors like speed, draft, trim, sea condition, wind, tide or current, etc. Hansen et al. (2011) conducted full-scale trials on an Aframax tanker before and after installing Propeller Boss Cap Fins (PBCF). These are generally considered to be suitable retrofitting devices for existing ships. The technology was fitted on the vessel afloat in the Mediterranean Sea with good weather conditions without the need of dry dock installation. A reduction average of around 3.7% in shaft power and fuel efficiency was confirmed.

CFD

Traditionally, potential flow theory has been used with panel methods to predict ship performance and is still considered to be a popular method for research areas focusing on seakeeping, global wave load and propeller design. This is because potential codes are easy, robust, well developed and require less computational time. These methods assume the flow is inviscid and non-rotational, neglecting any frictional forces and turbulent flows. However, thanks to the rapid development of CFD, which is now capable of simulating viscous flows, the working principles and performance prediction of ESDs is becoming more accurate (Celik and Guner, 2007, Celik, 2007).

Scaling Effects

The introduction of CFD methods are allowing further investigation of scale effects of ESDs (Heinke and Hellwig-Rieck, 2011, Visonneau et al., 2016). Scale effects are a prime concern since the Reynolds number is considerably higher for a ship than it is for a model. Some researchers (Hansen et al., 2011, Kawamura et al., 2012, Prins et al., 2016) have shown that ESDs are more efficient at full-scale than those determined from model tests. Others have indicated that the ESD is no longer effective at full-scale (Visonneau et al., 2016, Khorasanchi et al., 2013). One could question their prediction methods and therefore researchers should discuss whether their design philosophy is reliable. The main scale effects are stated below:

- The boundary layer is relatively thinner in full-scale flows than in model test conditions. Therefore, the wake fraction is larger in model tests than in full scale. ESDs within the boundary layer result in different behaviour between both scales.

– Flow separation is generally delayed in full scale and vortices encounter higher damping. Thus, ship wakes in the propeller plane are significantly changed. Vortices from bilge or struts are much weaker, sometimes vanishing in full-scale simulations.

Dang et al. (2011) investigated three ESDs; the pre-duct with a supporting stator, the pre-swirl stator and the PBCF. They used different techniques to carry out the analyses and measurements, including experimental model tests that took into consideration the local flow measurements using Particle Image Velocimetry (PIV) techniques and the use of CFD simulations. They calculated the nominal wake at the propeller plane as shown in Figure 18 which clearly indicates that the full-scale wake significantly differs from the model scale prediction because of the scale effects. Therefore, CFD simulations and ESDs studies should be performed at full-scale because of the uncertainties associated with the extrapolation of viscous flows from model to full scale

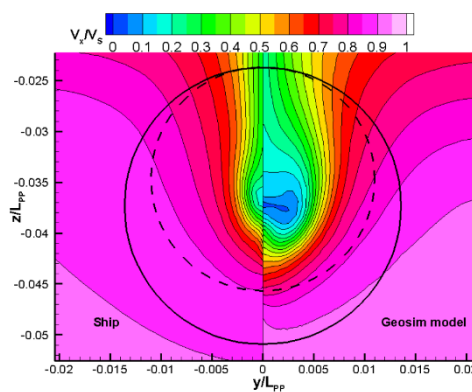


Figure 18. Comparison of Calculated Nominal Wake Field for Model-Scale and Full-Scale (Dang et al., 2011)

Although scaling effects of energy saving devices have been properly studied with the use of Computational Fluid Dynamics, it is hard to analyse the scale effect of the wake behaviour using actual measurements due to the limited resources of measurement during sea trials. As a result of the advancements in CFD and computational power, which provide better wake predictions, these areas need to be re-visited in order to obtain an enhanced and more detailed understanding of the subject. Another area that requires attention within this subject is the performance of retrofitting technologies at different operational profiles. Energy Saving Devices are generally designed and optimised for one particular condition (generally the design or laden condition) at one particular speed and draft. However, it is known that a merchant vessel rarely operates continuously in the same conditions but follows an operational profile. It would be interesting to understand the impact and behaviour of Energy Saving Devices in

different environments and scenarios evaluating whether their functions and benefits are constant throughout.

Multiple ESD Combinations

In more recent events, engineers have started installing a combination of Energy Saving Devices and experimenting with different configurations, also highlighting further benefits (Lee et al., 2017, Jens Ring Nielsen, 2012). The literature review briefly outlined that benefits and efficiency gains are not directly cumulative since some of the technologies affect the flow regimes of others (Terwisga, 2013). The different technologies have different functions and working principles and therefore not all ESDs are compatible (Mizzi et al., 2015). In order to exploit opportunities in combining different technologies, it is vital to understand the impact combinations of ESDs would have on the hull-propeller interaction system. Not just from a performance perspective (end results) but from a detailed analysis such as wake behaviour, energy balance, and velocity contours amongst others. This would provide us with information on which technologies can be successfully combined and indicate their subsequent impact on performance. Although ESDs are well established and thoroughly studied, the development of numerical analyses and computational power open doors to investigate these technologies further with more detail. Combining ESDs seems to be the natural direction this field is taking and although some research has touched on this area, knowledge of the subject is still in its early stages and requires further in-depth analyses for enhanced understanding.

When installing a combination of ESDs for example, a pre-swirl device with a post-swirl device, it should be noted that the total energy efficiency is not cumulative. This is because some ESDs affect the flow regimes of others and can reduce the total effectiveness. The efficiency of one ESD cannot be easily subtracted or added from the total efficiency. However, various ESDs are compatible with each other and can be considered and used to obtain a higher benefit.

Side Effects

Thirdly, it is important to consider the beneficial or detrimental side effects that ESDs can have. These effects should be studied and investigated by model tests and numerical simulations at the design stage to avoid any unwanted deleterious effects, such as the reduction of manoeuvring capability, or in turn, improve and enhance favourable criteria such as the limitation of cavitation and vibration problems. For example, a full-spade asymmetric rudder

could deteriorate seakeeping capabilities. ESDs should be optimised based on the wake field to improve the propeller efficiency but also to limit any cavitation, noise and vibration. The author believes that the studies focusing on side effects of these retrofitting technologies are premature in the industry and literature.

Accuracy

Finally, ESD gains are small and extremely difficult to evaluate not only by model tests but also during sea trial measurements. Improper extrapolation of model tests due to scaling issues together with the correction factors associated with sea trial testing and the disconcertingly great natural variation between the performances of sister ships result in an uncertainty of establishing proper gain figures. With regards to numerical simulations, CFD methods have their own assumptions and simplifications that can produce differences in the results. Thus verification and validation procedures are required in order to justify the accuracy of the method and gains achieved. However, since CFD measurements are consistent and systematic, they allow for a good comparison between different conditions (such as w/o ESD vs w/ESD) providing a good indication of the behaviour of the technology. With the progress in computing power and parallel computing technology, full-scale CFD simulations may reduce the present uncertainty of ESD savings.

2.2.3.6 The Way Forward with Energy Saving Devices

Savings claimed and predicted by ESD developers and manufacturers are very promising, yet the gains achieved from some of the technologies may not be as promising as those published in the literature. In this section, ways to improve analysis methods are discussed.

Initially, at the design stage, the ship's main dimensions are selected, and the hull form is optimized, based on calm water as well as operating conditions, by applying the design spiral focusing on maximizing economic and fuel efficiencies for the given requirements. Regarding propeller design, the number of propeller blades, revolutions per minute (RPM) and propeller diameter are investigated to improve the propulsive efficiency (Hooijmans et al., 2010) whilst considering propeller clearance, cavitation, vibration and the best engine performance. After these basic design procedures, ESDs are selected to further improve ship efficiencies.

Before investigating and designing ESDs, resistance and propulsion power components and ratios have to be considered. The physical phenomenon and reasons for efficiency losses

depending on ship type and size must also be understood. Figure 19 indicates the different resistance component ratios for tankers and containers. It is evident that wave making and air resistance are more prominent for containerships whilst the viscous resistance is more significant for tanker hulls. Therefore, it would be more logical to investigate the impact of ESDs on tanker ships targeting components of resistance and propulsion power.

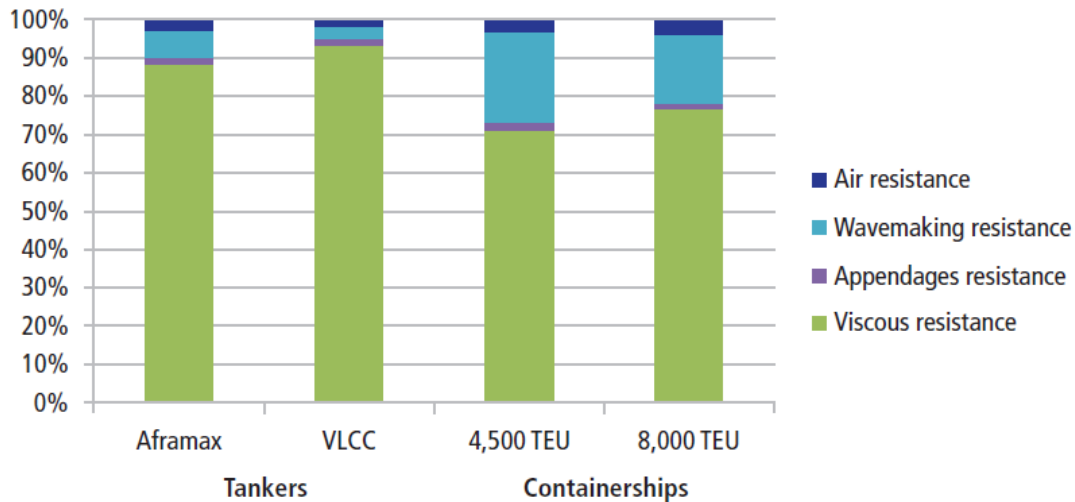


Figure 19. Components of Hull Resistance in Calm Water Conditions at Design Speed (ABS, 2013)

All methodologies to assess the impact of ESDs are interrelated and complementary to each other. Firstly, in the absence of model tests, CFD would not have been developed quantitatively even though there are some minor differences in the results and some challenging problems such as complex breaking waves, fluid-structure interactions of wave impact, slamming and sloshing. Whenever possible, model tests for ESDs analysis are required for CFD validation and verification. If the CFD output shows a good agreement with model test results, there would be no problem in continuing to simulate other cases by CFD and saving extra model test costs. Secondly, with the help of CFD, once the model simulations are verified and validated, more accurate full-scale performances could be predicted, thereby avoiding any associated scaling issues. Data sets or information from sea trials have also proven useful in developing correlation factors to extrapolate model test data to estimate resistance and propulsive coefficients at full scale. Sea trial analysis methods to estimate speed and power performance require further development in order to effectively evaluate ESDs efficiencies and validate the impact of energy efficient technologies in the EEDI formula.

Therefore, the fruitful combination of these analysis tools namely, dedicated model tests, CFD and full-scale sea trials in realistic ship operating conditions, offers a robust and reliable method to successfully apply fuel saving devices on merchant ships.

All these approaches, which have their pros and cons, are interrelated and complementary as previously outlined in this section. Model tests give rise to scaling issues. Full-scale sea trials are carried out in environmental conditions introducing the need of correction factors that might increase the uncertainty of the results, and accurate numerical simulations require state of the art software together with knowledge and expertise to operate. All these inconsistent criteria lead to different sources stating different magnitudes of benefit, even for the same technology. Therefore, a standard procedure for ESD analyses needs to be developed to allow ESD investigations to follow the same approach thereby enabling different sources to compare their devices based on a standard procedure developed through collaborative studies and verifications. Gains between different studies can then be directly compared. In doing so, a better overall picture of these technologies and how they benefit the overall efficiency of a vessel as well as their impact on the EEDI is obtained.

The best controlled environment for experimentation are the model scale tests carried out in model basins avoiding problems with weather conditions and other inconsistent criteria associated with full-scale sea trials. Such methods avoid any numerical prediction discrepancies and any need of special numerical calculations. However, these give rise to scaling issues when extrapolating the results and do not accurately identify the impact of the ESD, not to mention the limited designs that can be studied due to the expensive resources required. With the advancement in computational power and state of the art CFD methods, numerical predictions can produce consistent and accurate results that can be considered satisfactory post validation and verification studies. They can also simulate full-scale conditions in any required environments avoiding any problems with extrapolations and viscous effects in model scale. Therefore, it is proposed that ESDs are analysed using CFD methods due to the consistent procedures, controllable environments and full-scale simulations that can be developed.

2.3 Key Findings & Areas Requiring Investigation

Numerical Ship Performance Prediction

- Advancements in computational power with parallel developments in numerical solvers are allowing better use of higher fidelity CFD models.
- The introduction and availability of High-Performance Computing (HPC) are enabling researchers to push boundaries towards the simulation of full-scale self-propulsion conditions.
- Developments of HPC are permitting the use of high-fidelity solvers in optimisation procedures.
- Validation and Verifications procedures are essential in order to ensure the reliability of the solver and the credibility of the study.
- The most commonly applied turbulence models in the marine hydrodynamic industry are the URANS two-equation k - ϵ / k - ω models and the Shear Stress Transport (SST) model. However, these tools do not predict vortical and turbulent structures very well.
- Another class of higher-level turbulence model known as the Reynolds Stress Models (RSM) are better at predicting vortical structures but are computationally expensive and less robust.
- The recent introduction of the curvature correction technology was applied to the SST model producing comparable results to the RSM model at the minimal expense of computational cost.
- Although curvature correction technology is well established in the aerodynamic industry, it has only been recently introduced to the marine field.
- To the author's knowledge, no validation and verification procedures have been yet published in the marine industry using such turbulence models.
- The development of computational power together with the introduction of improved CFD methods, which are more accurate in predicting vessel performance, should drive research to re-investigate certain issues in greater detail (e.g. Vessel performance at different scales, wake characteristic at different scales etc.)
- While optimisation techniques are developing and using higher level fidelity models, the analyses of many variants using full-scale self-propulsion simulations are not yet feasible. However, there is a need to develop further current optimisation methods towards the highest possible standard, providing a good alternate solution whereby a

compromise to the ideal is sought. The industry consistently needs to take optimisation procedures to the next level.

Wake Fields

- A wake field is a region, aft of the vessel, where the flow is retarded and non-uniform due to the presence of the hull and the propeller.
- Accurate wake prediction is important in order to determine the right propeller design, understand the hull-propeller interaction, improve propeller performance and to identify and avoid any undesired cavitation and pressure pulses. It is also essential to maximise and optimise the function of Energy Saving Devices.
- The most common procedures for determining and analysing wake fields are experimental model tests. However, these are run in unrealistic towing conditions neglecting hull-propeller interaction effects. Moreover, the model test data requires extrapolation and scaling, which introduce further errors.
- Numerical analyses and CFD procedures avoid these errors by predicting wake fields at full-scale and in self-propulsion conditions. Furthermore, CFD is capable of various detailed analyses at any desired area of interest. Hence, continuous effort and developments are being carried out using RANS codes to enhance wake prediction accuracy.
- The recent introduction of the curvature correction to the SST turbulence model improves vortical structure prediction accuracy at the minimal expense of computational cost, thus allowing the analyses of full-scales simulations.
- Therefore, it would be worthwhile to investigate various studies like wake prediction, numerical wake scaling, and the impact of the wake at different operational conditions using this curvature corrected technology.
- When studying the hull-propeller interaction of a vessel, wake quality assessment is of utmost importance as it gives indications on propeller performance, cavitation and hull surface pressures.
- It is computationally expensive to simulate cavitation and pressure pulses; thus it is not a feasible approach when analyzing many wake designs. Wake quality assessment criteria serve as a good compromise providing guidelines or indicators for their avoidance.

ESDs

- Energy Saving Devices (ESDs) can be installed on new ships or existing ships and their aim is to improve the propulsive performance while also limiting cavitation and hull pressure vibrations.
- Most ESDs are not new to the market and different technologies have been developed with different working principles. These can generally be classified into three different categories; Pre-swirl, Post-swirl and Special Propellers.
- Despite being in the market for a while, the energy savings claimed for such retrofitting technologies lack credibility due to the unreliable and inconsistent measuring methods of ESD impact.
- Continuous research should be carried out to support ESDs' reliability.
- Issues with measuring methods of ESD performance:
 - Model tests give rise to scaling issues and improper performance prediction due to different scales of boundary layer behaviour
 - Full-scale sea trials in-service are carried out in different environmental conditions introducing the need for correction factors that might increase uncertainty in the results
 - Accurate numerical simulations require state-of-the-art software, the knowledge and expertise to operate and detailed V&V procedures to ensure the reliability of the solver.
- All these inconsistent criteria lead to different sources stating different magnitudes of benefit, even for the same technology. Therefore, a standard procedure for ESD analyses should be developed to allow ESD investigations to follow the same approach allowing the comparison between different devices and sources.
- The author proposes that ESD impacts should be analysed using validated and verified high fidelity CFD methods allowing consistent procedures, controllable environments and full-scale simulations. This would avoid most of the pre-defined issues but also extends the possibilities of research and detail of analyses/measurements.
- Sources claim that ESDs are more efficient at full-scale than those predicted by model tests researchers (Hansen et al., 2011, Kawamura et al., 2012, Prins et al., 2016).
- When studying ESDs, one should be aware of the beneficial or detrimental side effects they might introduce.

- Wake analyses are critical during ESD design procedures in order to understand, ensure and maximise the functions of the technology.
- Propeller Boss Cap Fins are one of the most widely used ESDs because they are easy to refit and are relatively cheap. Although extensive research has been carried out for PBCF, studies mostly investigated these technologies at model scale. With these devices being so well established in the market, they deserve to be studied in full-scale conditions using newer technology for more detailed performance analyses, understanding, and accuracy.
- With advancements in CFD and computational power, which provide better performance and wake predictions, it would be worthwhile to revert back to certain studies that require further attention such as the prediction of ESD performance at different scales.
- Installing a combination of these technologies does not mean the benefits are cumulative.
- Current trends are leaning towards installing different combinations and configurations of ESDs. Knowledge in this area is still at its early stages and thus requires further in-depth analyses for enhanced understanding.

2.4 Chapter Summary and Conclusion

This chapter has clearly presented the literature on topics that are relevant to this PhD study. These were reviewed in order to outline the basic theory behind the key subjects essential to the thesis as well as to further enhance our understanding of hull-propeller interactions and propeller performance. Furthermore, a review was carried out from a critical perspective outlining the important concepts and key findings together with the research gaps in the literature which require investigation. These research questions could be directly related to the research design, including the aims and objectives, research questions and research strategy outlined in the “Introduction” chapter. These clearly justify the motives behind the research carried out for this PhD study.

3 Study Procedure & Strategy

3.1 Introduction

This chapter demonstrates the approach carried out in this thesis to understand, improve and optimise hull-propeller interactions and stern flow characteristics. The study workflow and procedure are briefly explained identifying the different modules and their contribution to the research. In addition, the ship geometry used in this study are illustrated along with an outline of their respective data. The purpose of this chapter is to help the reader understand the research strategy.

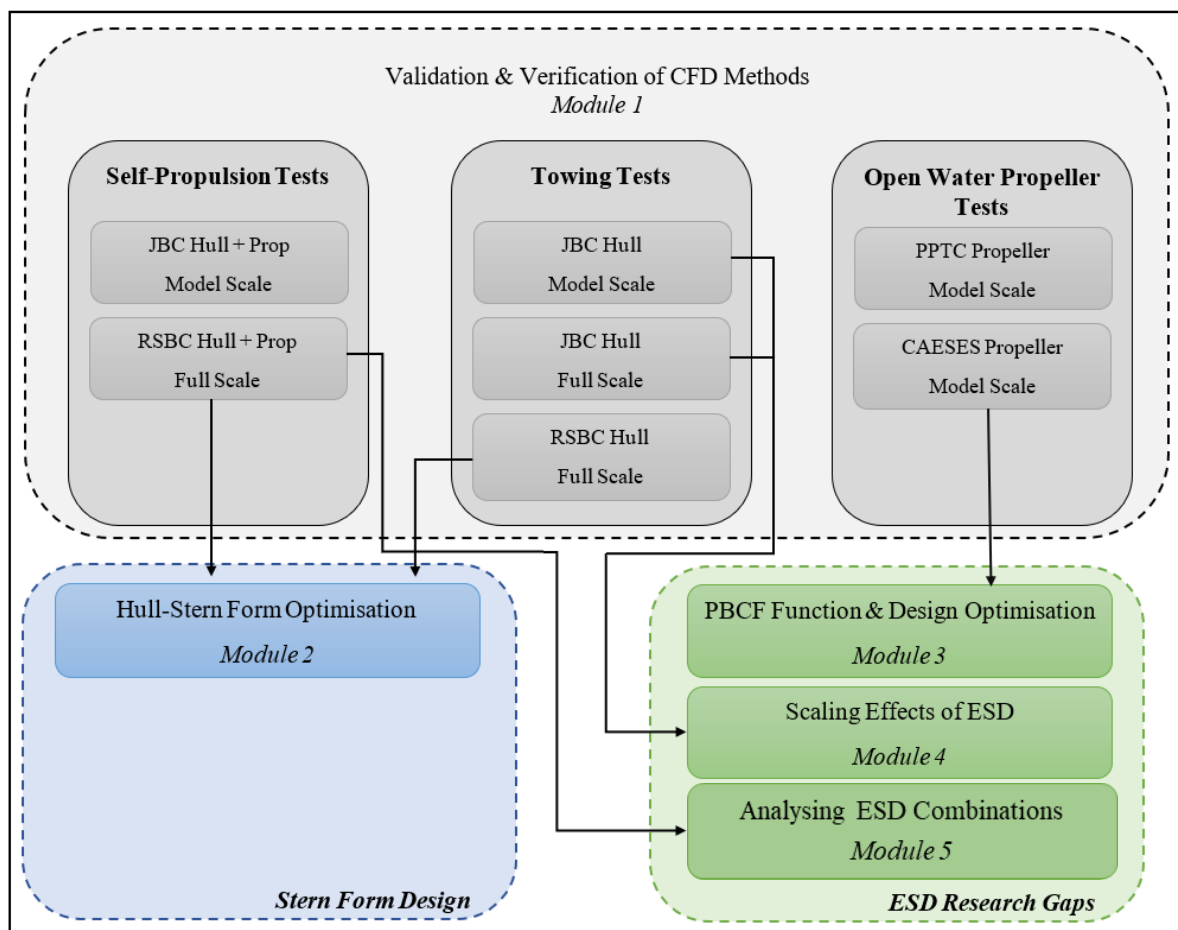


Figure 20. Study Breakdown

3.2 Hull-Propeller Interaction Optimisation Procedure

As previously outlined in the preceding chapters, design methods to improve hull-propeller interaction generally focus on stern form modifications, the installation of retrofitting technologies and propeller design optimization procedures. This study focuses on the former two techniques by developing an advanced stern form optimization procedure but also carrying out numerous analyses that address various research questions associated with the installation of Energy Saving Devices (ESD). The research strategy was designed and devised to accomplish all the pre-defined objectives. The design approach was thus broken down into various modules (subset studies) as presented in Figure 20. It is good to note that distinct modules were investigated using different ship hull and propeller geometries; the Potsdam Propeller Test Case (PPTC), the CAESES propeller, the Japan Bulk Carrier (JBC) vessel and the Real Ship Bulk Carrier (RSBC) ship. These will be further explained throughout the course of this chapter. The research was designed in such a way that all the numerical models used for the study were validated and/or verified to ensure the suitability and accuracy of the CFD methods. Star-CCM+ was the CFD solver used for this study.

Completion of this study will give a thorough insight into hull-propeller interaction effects considering stern form modifications and ESD installations. The contribution of each module to this study is briefly described below.

Module 1 : To demonstrate the reliability of the solvers, verification and validation procedures were carried out for the different CFD methods used in this research in order to predict ship performance. These were applied to the different numerical simulations both at model and full-scale conditions. The techniques in the CFD solvers are exhibited together with the development process. In particular, a curvature corrected turbulence model was demonstrated to produce enhanced prediction of stern wake flow characteristics and behaviour. Details of the methodology and results are described in chapter 4.

Module 2 : A state-of-the-art automated framework was developed to carry out a stern-form optimisation study using a high-fidelity solver. The procedure sought an optimal design candidate with improved hydrodynamic performance

through reduced resistance and improved wake characteristics. The study was carried out to demonstrate whether such advanced CFD Towing optimisation methods are sufficient to improve the performance characteristics of a vessel as opposed to computationally expensive self-propulsion optimisation procedures. The structure of such an automated process required the development of various models that are described in chapter 6 together with all the details of the methodology.

Module 3 : PBCF are one of the most commonly utilised retrofitting technologies that are installed on ships. It was therefore deemed appropriate to carry an advanced study on these devices. The boss cap fins were parametrically designed and installed on the CAESES propeller allowing a design optimisation procedure in open water test conditions. Furthermore, extensive analyses of the physics behind Propeller Boss Cap Fins (PBCF) in full-scale conditions were carried out for better understanding, thus contributing to knowledge. Details of the methodology and results are described in chapter 7.

Module 4 : A detailed study was carried out to investigate the performance of ESDs in different scale conditions. State-of-the-art post-processing capabilities allowed extensive analyses of scaling effects comparing the difference between the model and full-scale results. Module 4 was carried out using the JBC hull both with and without the duct. Details of the methodology and results are described in chapter 8.

Module 5 : The purpose of this study was to look into the effects of installing multiple ESDs on a vessel, understanding the impacts of various configurations, analysing the behaviour characteristics of the flow and outlining the benefits or disadvantages of such procedures. To determine the interaction effects between different ESDs and to predict the net energy-saving performance of a vessel. Several case studies were carried out using the full-scale RSBC self-propulsion model with different ESD combinations. Details of the methodology and results are described in chapter 9.

Figure 20 indicates that the numerical self-propulsion JBC model and the PPTC model-scale propeller simulations were not used for any subsequent studies. However, these were utilised in module 1 to validate the full-scale self-propulsion RSBC and the CAESES open water test models, respectively. This approach was carried out due to the unavailability of experimental data for the RSBC as well as the CAESES models, and to provide a means to ensure the reliability of the methods used.

3.3 Geometry

3.3.1 PPTC Propeller

Table 1. PPTC Parameters

<i>VP1304</i>		
<i>Type</i>	<i>Pitch Propeller</i>	
<i>Diameter (m)</i>	D	0.25
<i>Pitch Ratio</i>	$P_{0.7}/D$	1.635
<i>Area Ratio</i>	A_E/A_O	0.77896
<i>Chord Length</i>	$C_{0.7}$	0.10417
<i>Skew (deg)</i>	θ	18.837
<i>Hub Ratio</i>	D_H/D	0.30
<i>No. of Blades</i>	Z	5
<i>Rotation</i>	<i>Direction</i>	Right
<i>Revs/sec (rps)</i>	n	15

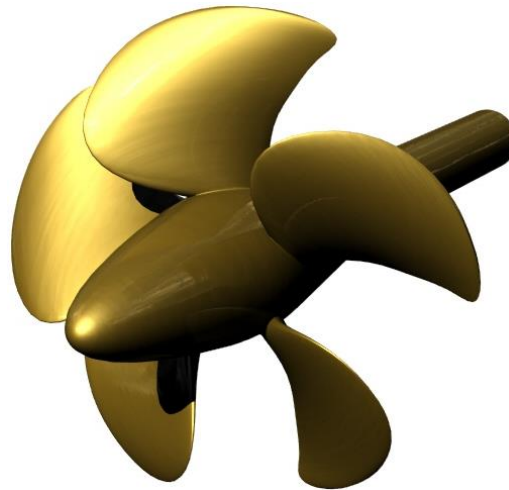


Figure 21. PPTC Propeller

CFD open water test validation studies were carried out using the open source, model-scale, controllable pitch propeller in a pull test configuration, designed by SVA (2011) shown in Figure 21. SVA carried out experimental open water tests using the PPTC hence providing non-dimensional thrust and torque data for an advance ratio range, allowing comparison and validation of our simulation model. The design parameters for this Potsdam Propeller Test Case (PPTC) propeller can be referred to in Table 1.

3.3.2 CAESES Propeller

Table 2. CAESES Parameters

<i>CAESES</i>		
<i>Naca66</i>	<i>Profile</i>	
<i>Rev Per Sec (rps)</i>	<i>n</i>	1.7
<i>Rev Per Minute (rpm)</i>	<i>n</i>	102
<i>Diameter (m)</i>	<i>D</i>	8
<i>Hub Ratio</i>	D_h/D	0.175
<i>Number of Blades</i>	<i>Z</i>	5
<i>Direction</i>	<i>Rotation</i>	Right
<i>Pitch Ratio</i>	$P_{0.7}/D$	1
<i>Rake(m)</i>	$R_{0.7}$	0.2616

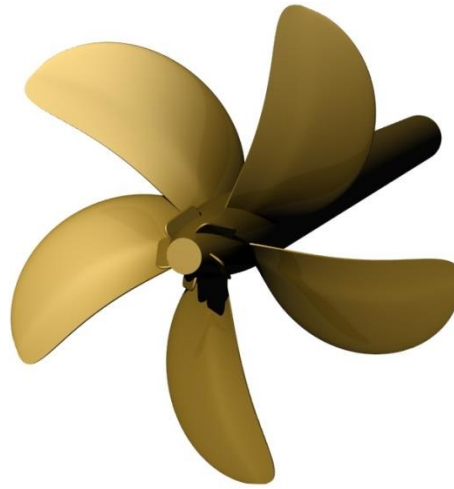


Figure 22. CAESES Propeller

The PPTC propeller was not deemed suitable for the analyses of boss cap fins since these devices are generally installed on more conventional fixed pitch propellers. The PBCF optimisation study was thus carried out using a customised full-scale constant pitch propeller that was designed with the parametric NURBS modeller CAESES provided by Friendship Systems. Since propeller dimensions and parameters were modified and customised according to the requirements of the study, there was no experimental data available for validation procedures. The PPTC propeller was therefore used to validate and verify the CFD open water simulations. For the purposes of this study, the propeller illustrated in Figure 22 will henceforth be referred to as the CAESES propeller. The CAESES Propeller particulars can be found in Table 2.

3.3.3 JBC Ship

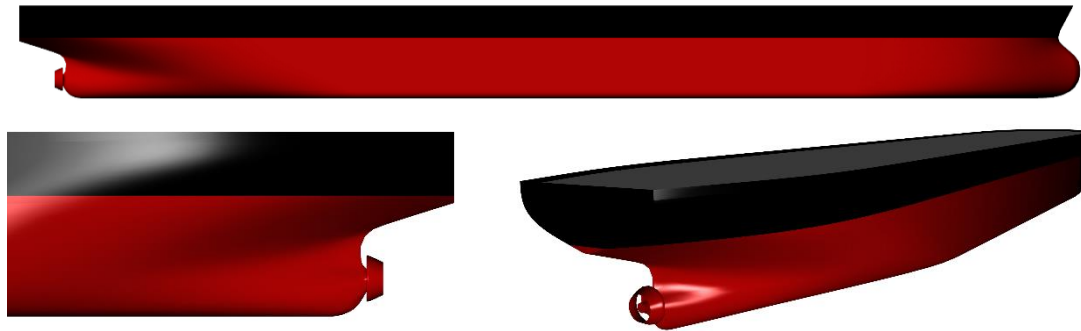


Figure 23. JBC Geometry

The cape size Japan Bulk Carrier (JBC) was used for a workshop focusing on CFD developments in ship hydrodynamics in Tokyo (NMRI, 2015) and is thus provided as open source. The ship geometry is alternatively provided with an installed energy saving device. The JBC hull and its appended circular duct have been designed by the National Maritime Research Institute (NMRI), Yokohama National University and Ship Building Research Centre of Japan (SRC). This high block coefficient vessel was intentionally chosen due to its complex stern flow characteristics making it a suitable candidate for research. Experimental tests of the JBC were purposely built to serve as a benchmark database for detailed flows around a ship with an energy saving device. NMRI carried out experimental tests in their model basin thus measuring and providing relevant data; resistance, self-propulsion parameters, wave profiles, wave cuts as well as detailed velocity distribution around the stern for the JBC with and without the circular duct. A visual representation of the JBC is presented in Figure 23 and its respective particulars in Table 3.

Table 3. JBC Particulars

<i>Japan Bulk Carrier</i>		<i>Full Scale</i>	<i>Model Scale</i>
<i>Length between BP.</i>	<i>LPP (m)</i>	280	7.00
<i>Length of Waterline</i>	<i>LWL (m)</i>	285	7.125
<i>Maximum beam of Waterline</i>	<i>BWL (m)</i>	45	1.125
<i>Depth</i>	<i>D (m)</i>	25	0.625
<i>Draft</i>	<i>T (m)</i>	16.5	0.4125
<i>Displacement Volume</i>	<i>$\nabla(m^3)$</i>	178369.9	2.7870
<i>Wetted Surface area w/o ESD</i>	<i>$S0_{w/o ESD} (m^2)$</i>	19556.1	12.2206
<i>Wetted Surface area with ESD</i>	<i>$S0_w ESD (m^2)$</i>	19633.9	12.2696
<i>Block Coefficient</i>	<i>(CB)</i>	0.858	0.8580

3.3.4 RSBC Ship



Figure 24. RSBC Geometry

The Real Ship Bulk Carrier (RSBC) represents an actual operational 180m vessel that is currently in use and was given this title for the purposes of this research as the actual name cannot be disclosed. The case study vessel is a 35,500 DWT bulk carrier that was built in 2013. Lines plans drawings were provided together with the IGES surface geometry of the vessel. The author made use of this data to accurately parametrically model the ship using CAESES modeller. More details regarding the parametric modelling of the ship can be found in chapter 6. The top picture in Figure 24, presents the RSBC parametric model and its particulars are outlined in Table 4.

Table 4. RSBC Particulars

Hull Particulars			Main Engine Particulars		
<i>Parameter</i>	<i>Units</i>	<i>Value</i>	<i>Parameter</i>	<i>Units</i>	<i>Value</i>
<i>Length Over All (LOA)</i>	(m)	180	<i>M/E Rated Power</i>	(kW)	172
<i>Length P.P.</i>	(m)	172	<i>M/E Rated Speed</i>	(rpm)	30
<i>Breadth</i>	(m)	30	Propeller Particulars		
<i>Depth</i>	(m)	9.5	<i>Parameter</i>	<i>Units</i>	<i>Value</i>
<i>Scantling Draft</i>	(m)	10.1	<i>Pitch</i>		Fixed Pitch
<i>Design Draft</i>	(m)	9.5	<i>No. of Blades</i>		4
<i>Displacement T=10.1m</i>	(m ³)	~43500	<i>Propeller Speed</i>	(rpm)	99
<i>Displacement T=9.5 m</i>	(m ³)	~41500			

When carrying out the studies for module 2 and module 5, using the RSBC vessel, it was essential to define the draft and speed of the vessel. A brief operational analysis was carried out to identify the most popular conditions. The two types of operational data that were provided:

- Satellite data from 02/2015 – 09/2015 and
- Noon reports from 03/2015 – 05/2015.

Various measurements and details were recorded and listed in the reports. However, only the speed, draught and time were considered crucial for this study. Information from both sources (i.e. satellite data and noon reports) that overlapped in time were compared identifying minimal discrepancies indicating the reliability of the results. All the operational data was then processed using statistical analyses in order to identify the most frequent conditions of the vessel highlighting its operational profile. Figure 25 demonstrates the time spent by the vessel underway or moored by share percentage. Figure 26 indicates the frequency (%) of draught and speed when the vessel is in operation. The common speeds and draughts were so far identified independently. After the four most popular speeds were determined, the draught frequency for each speed was computed (Figure 27). A matrix was developed highlighting the most popular operational conditions that are listed in Table 5. The most popular condition, where the vessel is running at 13 knots at 6.2 m draft is when the vessel is in ballast mode. The

second most popular condition, 12.5 knots at 10.1m is when the vessel is laden with cargo. For purposes of this study, the RSBC vessel will be analysed in the laden condition.

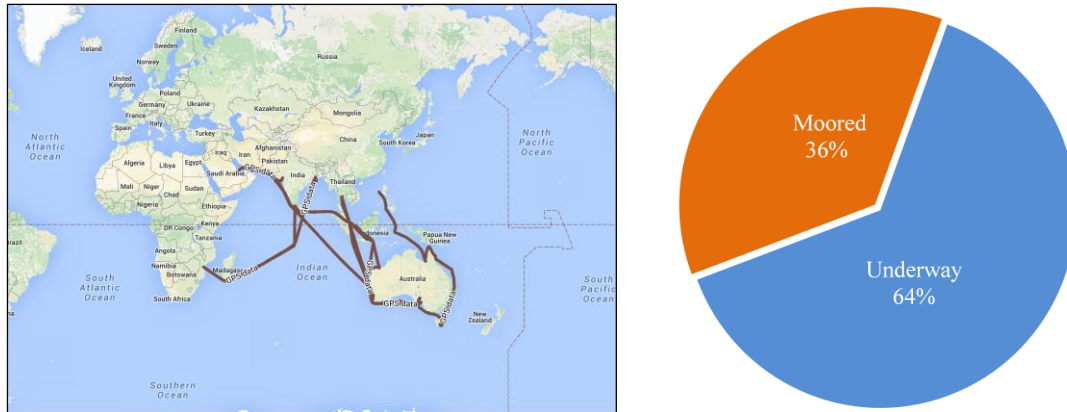


Figure 25. Operational Profile Analyses

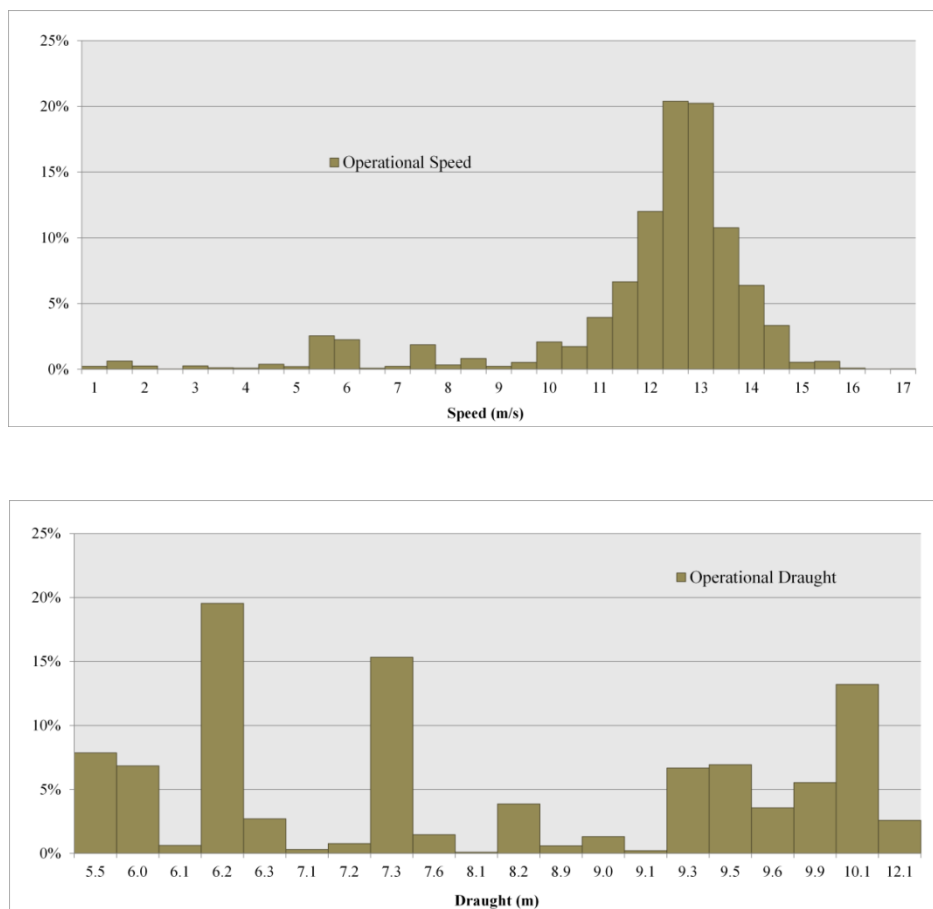
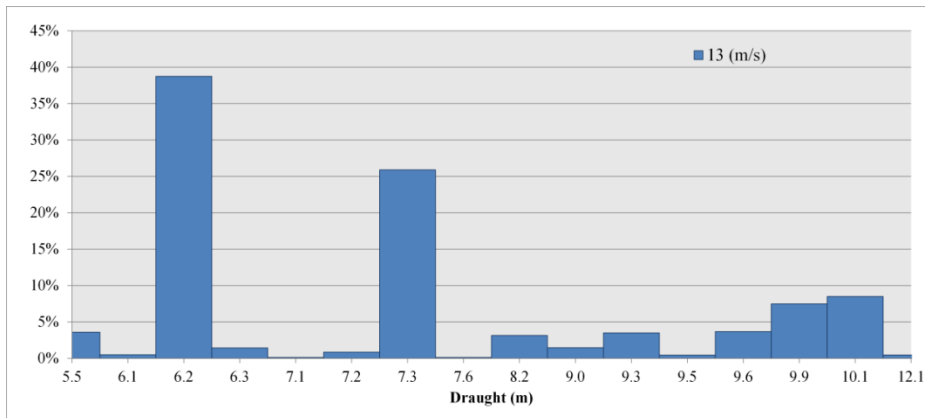
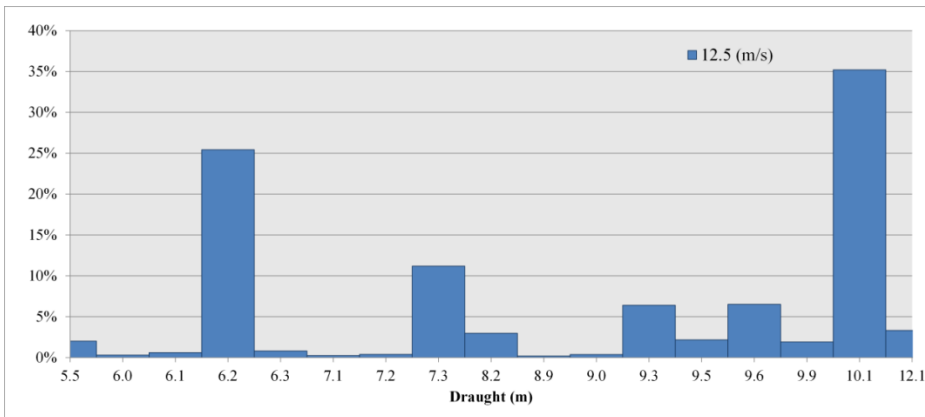
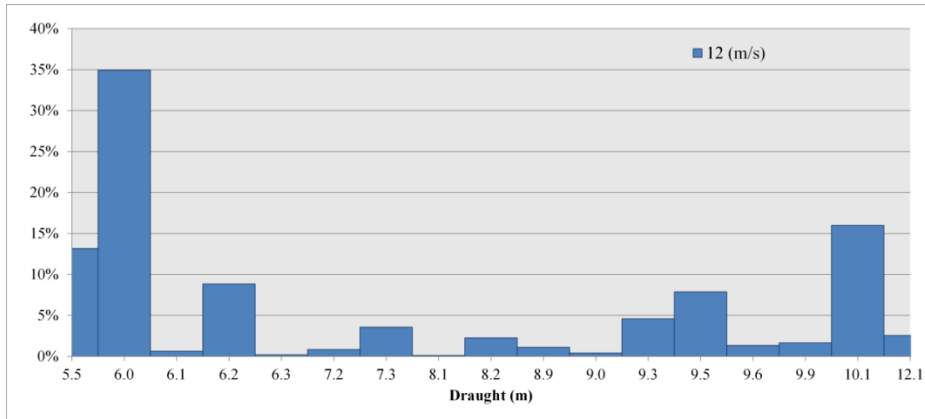


Figure 26. Speed & Draught Frequency

Table 5. Most Frequent Operational Conditions

<i>Conditions</i>	<i>1</i>	<i>2</i>	<i>3</i>	<i>4</i>
<i>V (m/s)</i>	13	12.5	13	12.5
<i>T (m)</i>	6.2	10.1	7.3	6.2
<i>Weight (%)</i>	30.81	28.22	20.60	20.38



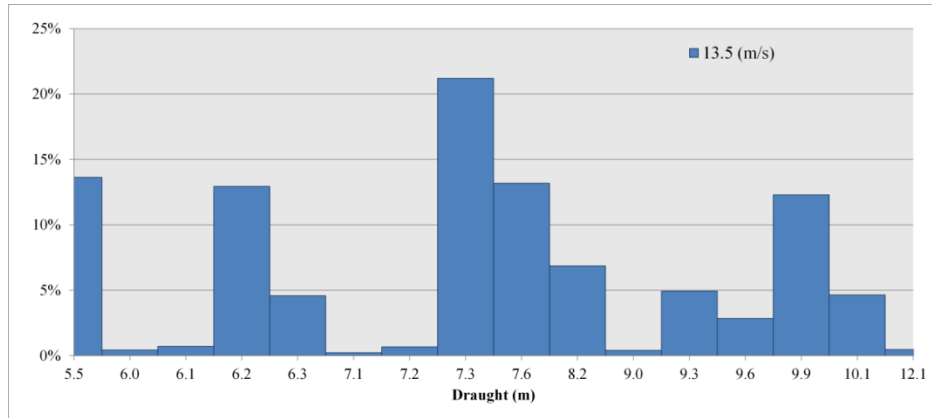


Figure 27. Draught Frequency per Specific Popular Speeds

3.4 Chapter Summary & Conclusion

The study procedure and strategy have been presented in this chapter outlining the various modules and presenting all the geometry that was used for this research. The thesis has been structured in a way that each of the following chapters, excluding the ‘Discussion’ and ‘Conclusion’ sections, describe the different modules depicted in Figure 20. The purpose of this chapter was to outline the contribution of each module along with the strategies used whilst adhering to the principal objectives of the study.

4 CFD Modelling for Hull-Propeller Performance Prediction

4.1 Introduction

Computational Fluid Dynamics (CFD) and High Computational Power (HPC) have shown significant developments in recent years (Stern et al., 2015). Today CFD offers various models and techniques to analyse ship performance, both at model-scale and full-scale, for towing or self-propelled conditions and even providing manoeuvring investigations. Validation and Verification (V&V) procedures for CFD analyses have also been established to ensure the accuracy and consistency of the solvers.

This chapter describes and explains the different CFD methods used to carry out the various case studies in this thesis, together with the validation and/or verification of the models used. All the applied numerical models fall under three categories; Open Water Propeller, Towing and Self-Propulsion simulations. All these methods have been applied to different geometries and case studies, as demonstrated in Figure 4 in Chapter 1.

It was ensured that at least one model from each of the three categories was validated and verified (case 1, 2 & 5). These methods could be then used as a reference to ensure the accuracy and consistency of the solvers. That being said, other numerical approaches used for the various case studies were also verified, as indicated in Table 6 (case 3 & 4). Limited data did not allow for the validation and verification of the full-scale RSBC in self-propulsion conditions. However, in order to ensure the applicability of the CFD method to predict self-propulsion in full-scale, a study was carried out (Case 6) comparing the results from various sources.

Models of the same category follow the same methodology and therefore a common description is presented for each of the three. Each description is therefore subdivided into ‘Physics’ and ‘Mesh’ sections, with the former explaining the physics behind the procedure and the latter describing the grid topology. The techniques in the CFD solvers are exhibited together with the development process and improvement. At the same time, validation and verification procedures were carried out for each of the CFD methods used in this research to predict ship performance.

The prediction of some ship characteristics like drag has been well established. On the other hand, simulating hull-stern interactions using CFD methods has always been challenging. With the availability of more sophisticated methods and computational power, numerical wake analyses and prediction is becoming more accurate and has recently been introduced to state-of-the-art procedures. One particular recent feature that has been introduced to improve wake analyses is the curvature correction of the turbulence model. This chapter also demonstrates how the use of curvature corrected turbulence model enhances the prediction of stern wake flow characteristics and behaviour.

To the best of the author’s knowledge, this novel curvature correction method has been briefly outlined in the literature, but no validation and verification procedures have been carried out using the model on ship simulations. This chapter demonstrates the V&V methods using the curvature corrected turbulence model.

Furthermore, a thorough review of the literature indicated that wake field comparison between CFD methods and experimental results is generally carried out using visual methods. This study also proposes and demonstrates that wake comparison should also make use of quantifiable measures in order to improve the accuracy of wake field validation.

Table 6. Validation and Verification Cases

<i>CASES</i>	<i>Tests</i>	<i>Type</i>	<i>Geometry</i>
1	Open Water	Validation & Verification	PPTC
2	Towing	Validation & Verification	JBC Hull Model-Scale
3	Towing	Verification	JBC Hull Full-Scale
4	Towing	Verification	RSBC Hull Full-Scale
5	Self-Propulsion	Validation & Verification	JBC Hull+ Prop Model-Scale
6	Self-Propulsion	Comparison	JBC Hull+ Prop Full-Scale

4.2 Open Water Propeller Tests

The open water CFD model used for the PBCF study was first validated using the model-scale Potsdam VP1304 propeller in numerical software. In this study, a Reynolds-Averaged Navier-Stokes (RANS) approach was applied using the commercial CFD software Star-CCM+® version 9.0.2, which was developed by CD-ADAPCO (2014). The supercomputer at the University of Strathclyde was utilised to allow faster and more complex simulations. During the validation study, various physics models and meshes were tested to identify the optimal criteria for the simulation that resulted in the most accurate propeller characteristics. Once validated, the same physics, mesh and setup were used to analyse the CAESES propeller in full-scale conditions. This work has been published in a paper (Mizzi et al., 2017).

4.2.1 Numerical Modelling

4.2.1.1 Physics

A Reynolds-Averaged Navier-Stokes (RANS) solver was used to solve governing equations and to simulate a three-dimensional environment using the SST (Shear Stress Transport) $k-\omega$ model assuming a turbulent flow. This turbulence model is a two-equation eddy-viscosity model that enriches the $k-\omega$ model with an additional non-conservative cross-diffusion term that potentially makes the model produce similar results to that of the $k-\epsilon$ model, thus enabling the system to have the best of both worlds. This blends the ϵ approach in the far field and the ω model in the inner field near the solid boundaries, making it suitable for adverse pressure gradients and separating flows (CD-ADAPCO, 2014). Steady state simulations were run for a sufficient number of iterations to ensure proper convergence. For those cases of unsteady sliding mesh simulations during the validation studies, the time step was set to $\text{rps}/200$ as recommended by the ITTC (2011a).

The governing equations were discretised using a Finite Volume Method with the velocity-pressure coupling being handled using a SIMPLE algorithm. A second order convection scheme was used for the momentum equations and a first order temporal discretisation was used. The flow equations were solved in a segregated manner. The continuity and momentum equations were linked with a predictor-corrector approach. The propeller was placed in an immersed incompressible water liquid environment of constant density and segregated flow

represented by the following continuity and momentum flow equations (Ferziger and Peric, 2002) given in tensor notation and Cartesian coordinates by (19) and (20),

$$\frac{\partial(\rho\bar{u}_i)}{\partial x_i} = 0 \quad (19)$$

$$\frac{\partial(\rho\bar{u}_i)}{\partial t} + \frac{\partial}{\partial x_j}(\rho\bar{u}_i\bar{u}_j + \overline{\rho u'_i u'_j}) = -\frac{\partial\bar{p}}{\partial x_i} + \frac{\partial\bar{\tau}_{ij}}{\partial x_j} \quad (20)$$

where ρ is density, \bar{u}_i is the averaged Cartesian components of the velocity vector, $\overline{\rho u'_i u'_j}$ is the Reynolds-stress tensor and \bar{p} is the mean pressure. Finally, $\bar{\tau}_{ij}$ denotes the mean viscous-stress tensor defined below as

$$\bar{\tau}_{ij} = \mu \left(\frac{\partial\bar{u}_i}{\partial x_j} + \frac{\partial\bar{u}_j}{\partial x_i} \right) \quad (21)$$

with μ being the dynamic viscosity.

4.2.1.2 Modelling Variations

In CFD work, a rotating propeller can be simulated using different models, namely the Moving Reference Frame (MRF) method and the Rotating Mesh also known as the Sliding Mesh approach. As the name suggests, for the Rotating Mesh, the domain rotates about an axis yielding transient calculations producing time-accurate results that require high computational power. Meanwhile, with regards to the less computationally intensive MRF approach, the domain remains stationary with an assigned frame of reference rotating about a pre-defined axis with respect to the global co-ordinate system. This type of simulation carries out a steady-state approximation to a transient problem producing time-averaged results. When running unsteady simulations, the MRF approach generally provides a compromise requiring less computational demand at the expense of accuracy (Kellet et al., 2013).

An additional study was carried out using the PPTC model-scale propeller to analyse and compare the difference in results produced by a sliding mesh and moving reference frame domain using unsteady methods for one particular advance coefficient value. Table 7 presents the K_T and K_Q for both simulations, allowing comparison. Results indicated minimal difference in performance between both methods and therefore, being less computationally expensive, the MRF approach was used for all further analyses.

A similar validation study was carried out between steady and unsteady time models for the same propeller, with the latter being typically used for time-dependent simulations or when physical instabilities exist. These models are assigned solvers that control the number of iterations or time step magnitude. As can be seen in Table 8, there are minimal differences between the two and therefore, the optimisation analysis was carried out using the steady model requiring less computational power.

Table 7. MRF vs Sliding Mesh

<i>J = 1</i>	<i>K_r</i>	<i>10 K_Q</i>
<i>MRF</i>	0.38604	0.96894
<i>SM</i>	0.38595	0.96885

Table 8. Steady vs Unsteady

<i>J = 1</i>	<i>K_r</i>	<i>10 K_Q</i>
<i>Steady MRF</i>	0.38623	0.96916
<i>Unsteady MRF</i>	0.38604	0.96895

4.2.1.3 Mesh Generation and Boundary Conditions

The surface mesh was generated using triangulated faces. For proper and accurate simulation, the generation of an accurate representation of the blade geometry was of great importance. Blade tips and sharp edges were captured accurately, indicating feature lines in the modeller. Figure 28 depicts the surface mesh for the VP1304 propeller at model-scale.

The presence of a surface or wall boundary significantly affects the flow behaviour producing different turbulent structures from free turbulent flows. Flows near solid boundaries have a substantial region which is dominated by inertia forces and a thinner region, that closest to the wall, dominated by viscous forces. The latter is made up of three layers known as the ‘linear sub-layer’, the ‘buffer zone’ and the ‘log-law layer’ in order of increasing distance from the wall and are differentiated by the kind of stresses that dominate; The linear sub layer is dominated by viscous stresses, the buffer layer is a balance of viscous and turbulent flow and the log-law layer is dominated by Reynolds (turbulent) stresses.

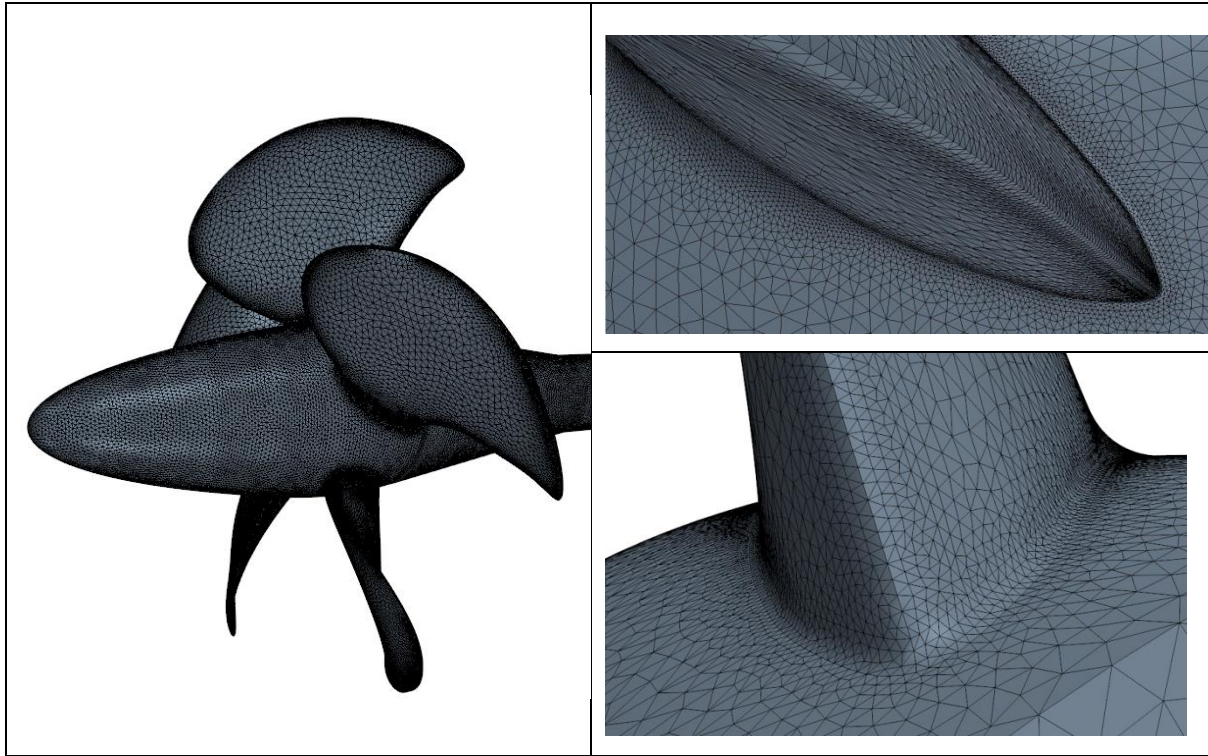


Figure 28. Surface Mesh

Due to the complexities and effects of the boundary layer, the mesh in this region should be refined in order to accurately capture near wall flow details. A prism layer model feature was therefore employed generating refined orthogonal prismatic cells adjacent to the surface with 12 layers. In Star-CCM, the near wall turbulence quantities such as force and velocity are captured using wall treatment models. For this particular study, the All-Y+ treatment approach was used, which is a hybrid that emulates both the Wall Function law approach for Y+ values (Y+ is a non-dimensional wall distance for a wall-bounded flow) greater than thirty and the Near-Wall turbulence for Y+ values lower than one trying to resolve the viscous sub layer.

Since boundary conditions influence the nature of a simulation, their appropriate selection is important. A velocity flow was specified for the inlet boundary condition and an atmospheric pressure field for the outlet. The initial flow velocity at the inlet condition was set to the advanced velocity of the water depending on the advance coefficient (J) in question. The cylindrical boundary of 3 propeller diameter lengths from the axis, was set to a symmetry condition simulating open water with no constraints and the submerged propeller was assigned with a no-slip (wall) condition. The positioning of the boundaries is also an important factor that requires consideration, in particular, the upstream inlet boundary and the downstream outlet boundary. These should be defined in a way to avoid any reflections downstream of the propeller and to ensure uniform incoming flow upstream of the propeller. To model boundary

independent solutions and to avoid any fluid reflection effects/interactions, the inlet was placed 2 propeller diameter lengths upstream of the propeller and 5 propeller diameter lengths for the outlet. This configuration and arrangement were used for both the validation and optimisation study. Figure 29 demonstrates the domain configuration and associated boundary conditions.

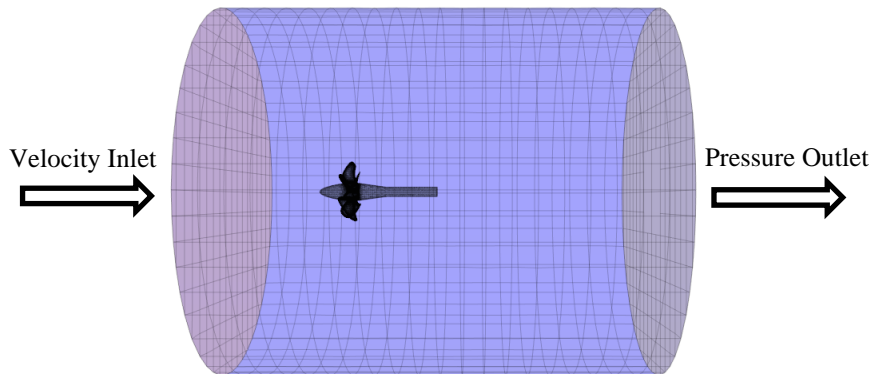


Figure 29. Boundary Conditions Configuration

4.2.2 Validation and Verification

Figure 30 presents a graph that demonstrates the comparison between experimental and numerical results for the PPTC propeller characteristics. Results yielded satisfactory open water efficiency accuracy of 3% between the advance coefficients (J) from 0.6 to 1; with the accuracy decreasing significantly outside this range. This corresponds well to other authors' outcomes indicating that this behaviour is a result of the lack of the transition model in the simulation. The RANS simulation model was set to assume a fully turbulent flow which failed to predict the transition behaviour in the boundary layer.

The accuracy can be improved by either employing a transition model into the simulation or by carrying out open water tests at full scale. The transition region within the boundary layer of a full-scale model is less significant compared to that for a model-scale, thus improving accuracy. Although full-scale simulations minimise errors, as Bhushan et al. (2009) indicate, these require a high grid density near the wall which might prove to be computationally expensive and might cause high grid spacing aspect ratios near the wall. This increases errors in the mass, momentum and flux calculations (governing equations), thus requiring the use of wall functions.

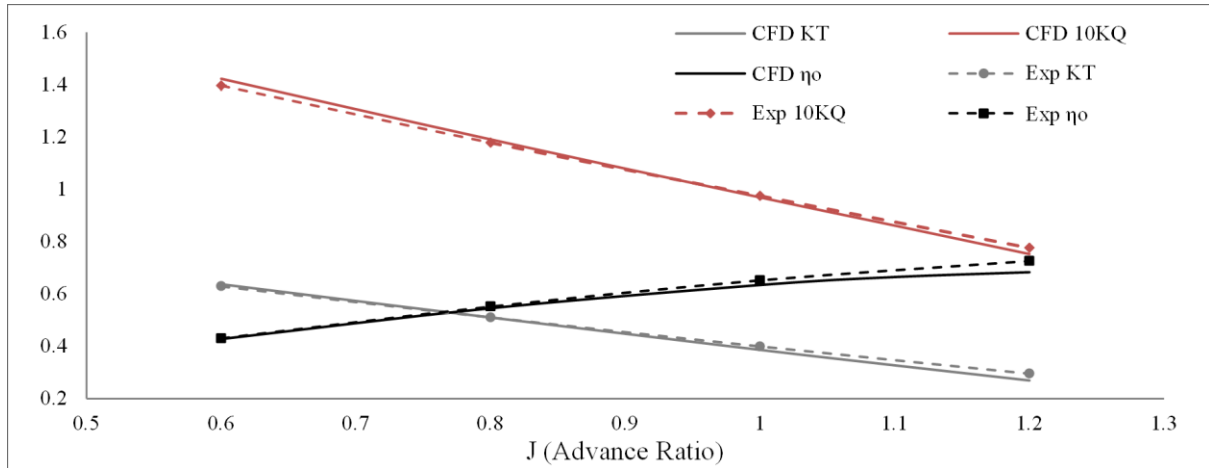


Figure 30. PPTC Open Water Characteristics

During the validation stages, three different types of mesh grid refinements were also investigated, classifying them as coarse, medium and fine. Refining the mesh resulted in insignificant differences in the efficiency values. Although the three models produced similar results, the fine mesh (Table 9), was deemed most reasonable approach as it is able to capture local flow quantities accurately. A mesh of around 9 million hexahedral cells was generated, selecting a reasonable cell size growth-rate from the inner to the outer field while also specifying local area refinements in critical regions.

Table 9. Mesh Size Comparison for PPTC Model-Scale Propeller

	<i>Coarse</i>			<i>Medium</i>			<i>Fine</i>		
<i>Cell Number</i>	4.59 M			6.5 M			9.2 M		
<i>J = 1</i>	KT	KQ	η₀	KT	KQ	η₀	KT	KQ	η₀
<i>Results</i>	0.3798	0.0960	0.6297	0.3843	0.0967	0.6324	0.3862	0.0969	0.6343
<i>Accuracy (%)</i>	95.09	98.47	96.57	96.22	99.20	97.00	96.70	99.41	97.28

* Accuracy (%) represents the difference between the numerical results and the experimental values.

A verification study was carried out on the PPTC propeller to demonstrate and ensure the capability of the model and solver using the Grid Convergence Index (CGI). This method is based on the Richardson extrapolation (Richardson, 1911, Richardson and Gant, 1927) and is used in this study to calculate the discretisation error estimation as described by Celik et al (2008). It is good to point out that this method makes use of an unstructured mesh. This is not strictly, a rigorous procedure for determining the grid-size uncertainty on the entire computational domain. However, it gives indications on uncertainty levels on a large part of the computational domain.

The apparent order of the method, p , is calculated by

$$p = \frac{1}{\ln(r_{21})} |\ln|\varepsilon_{32}/\varepsilon_{21}| + q(p)| \quad (22)$$

$$q(p) = \ln\left(\frac{r_{21}^p - s}{r_{32}^p - s}\right) \quad (23)$$

$$s = 1 \cdot \text{sign}(\varepsilon_{32}/\varepsilon_{21}) \quad (24)$$

where r_{21} and r_{32} are refinement factors, i.e. $\sqrt{2}$ in this study, and $\varepsilon_{32}=\phi_3-\phi_2$, $\varepsilon_{21}=\phi_2-\phi_1$, ϕ_k is the key variable, i.e. KT and KQ in this case, on the k^{th} grid.

The extrapolated values are obtained by

$$\phi_{ext}^{21} = (r_{21}^p \phi_1 - \phi_2)/(r_{21}^p - 1) \quad (25)$$

The approximate and extrapolated relative errors are calculated using the following equations, respectively.

$$e_a^{21} = \left| \frac{\phi_1 - \phi_2}{\phi_1} \right| \quad (26)$$

$$e_{ext}^{21} = \left| \frac{\phi_{ext}^{12} - \phi_1}{\phi_{ext}^{12}} \right| \quad (27)$$

The fine-grid convergence index is calculated by

$$GCI_{fine}^{21} = \frac{1.25 e_a^{21}}{r_{21}^p - 1} \quad (28)$$

These parameters were calculated for KT and KQ values and are presented in Table 10.

Table 10. Calculation of the Discretisation Error for KT and KQ Values (with monotonic convergence)

	KT	KQ
r_{21}, r_{32}	$\sqrt{2}$	$\sqrt{2}$
ϕ_1	0.3862	0.0969
ϕ_2	0.3843	0.0967
ϕ_3	0.3798	0.0960
p	2.4789	3.6147
ϕ_{ext}^{21}	0.3876	0.0970
e_a^{21}	0.4920 %	0.2064 %
e_{ext}^{21}	0.3582 %	0.0825 %
GCI_{fine}^{21}	0.4494 %	0.1032 %

As can be seen from Table 10, insignificant numerical uncertainties (0.4494% for KT and 0.1032% for KQ) are estimated for the computed values.

4.3 Virtual Towing Hull Tests

This section outlines the numerical modelling for the developed towing test simulations both for model-scale and full-scale conditions with and without the appended retrofitting technologies. Since they follow the same methodology, the figures presented in this section interchange between base hull geometries and ESD appended ships. In order to carry out such procedures, the commercial CFD software Star-CCM+® version 9.0.2, which was developed by CD-ADAPCO (2014) and the High-Performance Computer (ARCHIE-WeSt) were utilised. The same methodology (physics and grid topology) has been applied to carry out modules 2, 4 and 5 (Please refer to Figure 20 in chapter 3). That being said, these case studies make use of different geometries and therefore, validation and/or verification studies have been presented for the different cases (2, 3, and 4) as outlined in Table 6. Please note that although no case study required a model-scale towing simulation, this was still carried out to replicate the JBC experimental towing tests (NMRI, 2015) for validation of the results. Furthermore, this section outlines the development and improvements carried out to enhance the accuracy of the towing tests simulations with particular emphasis on the use of the curvature corrected turbulence model to enhance wake prediction capabilities. It also proposes and demonstrates that wake field velocities should also be compared using quantified values and not solely by means of visual comparison. This methodology has been published in a journal (Maasch et al., 2019).

4.3.1 Numerical Modelling

4.3.1.1 Physics

The commercial CFD solver, STAR-CCM+, was used to model the multiphase flow using Unsteady Reynold Averaged Navier-Stokes (URANS) equations to simulate a three-dimensional environment using a two-equation eddy viscosity model. In particular, the SST (Shear Stress Transport) $k-\omega$ model with the novel Curvature Correction (CC) was used. This CC feature was implemented post the modelling variations study producing enhanced wake accuracy. The continuity and momentum governing equations (Ferziger and Peric, 2002) for incompressible flows can be represented in tensor notation and Cartesian coordinates as follows:

$$\frac{\partial(\rho\bar{u}_i)}{\partial x_i} = 0 \quad (29)$$

$$\frac{\partial(\rho\bar{u}_i)}{\partial t} + \frac{\partial}{\partial x_j} (\rho\bar{u}_i\bar{u}_j + \overline{\rho u_i' u_j'}) = -\frac{\partial \bar{p}}{\partial x_i} + \frac{\partial \bar{\tau}_{ij}}{\partial x_j} \quad (30)$$

$$\bar{\tau}_{ij} = \mu \left(\frac{\partial \bar{u}_i}{\partial x_j} + \frac{\partial \bar{u}_j}{\partial x_i} \right) \quad (31)$$

With regards to the air-water interface capturing scheme, a Volume of Fluid (VOF) method was used to model the free surface effects using a second order upwind convection scheme. The VOF method computed the volume fraction of the immiscible fluids (air and water) to predict the motion of the free surface. The VOF model assumes that the same basic governing equations used for a single-phase problem can be similarly applied to all the fluid phases present within the simulation. The equations are therefore solved for a “single” phase that represents the different fluids by use of volume fractions. The inlet velocity and pressure outlet boundaries make use of volume fraction functions to simulate the free surface interface which for this study is a flat wave. Significant refinements at the free surface allow for the accurate prediction of sharp interfaces i.e. volume fraction change representing the free surface. The modelling variations study (4.3.1.2) indicated that finer elements at the free surface produced better wave cut analyses when compared to the experimental results. Refinements at the free surface are also crucial for predicting the wave profile on the vessel by minimising the VOF change for a sharper interface which is desirable. Figure 31 demonstrates the wave profile of the model-scale JBC hull as previously suggested. A value of 0.5 indicates the phase is 50% water and 50% air representing the free surface.

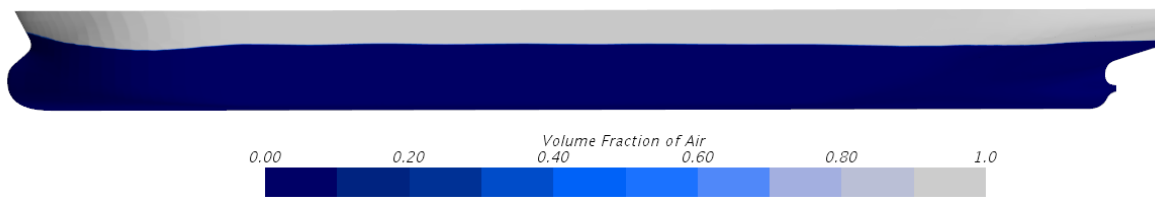


Figure 31. Model-Scale JBC Wave Profile

The velocity-pressure coupling was computed using a projection-based method making use of a SIMPLE type algorithm. All the case studies were carried out in calm water conditions. For the model-scale and full-scale JBC simulations (cases 2 & 3), the motion of the vessel was allowed to pitch and heave using the Dynamic Fluid Body Interaction (DFBI) feature that computed the forces and moments on the vessel solving the governing equations of rigid body motion. However, for the full-scale RSBC simulation (case 4), the vessel was fixed at level trim. This was due to the extensive computational requirement, as explained later in this section. For all the models, wall functions were used accordingly to model the wall treatment with the appropriate blending of the prism layer cells to the near domain cells.

An implicit unsteady time marching scheme together with a Finite Volume Method (FVM) approach was carried out to treat temporal and spatial discretization. The time step for the model-scale simulations (case 2) were set to be $\Delta t = 0.025s$ and for the full-scale simulations (case 3 & 4) to be 0.01s. These values were selected as to give Courants numbers (CFL) $CFL \approx 1$ in the zones of interest as recommended by CD-ADAPCO (2014) for enhanced numerical stability. Figure 32 demonstrates the Courant number for a typical case. The time step should also be kept small enough to capture the desired flow details particularly in the area of interest, which for this study, was considered to be the stern region.

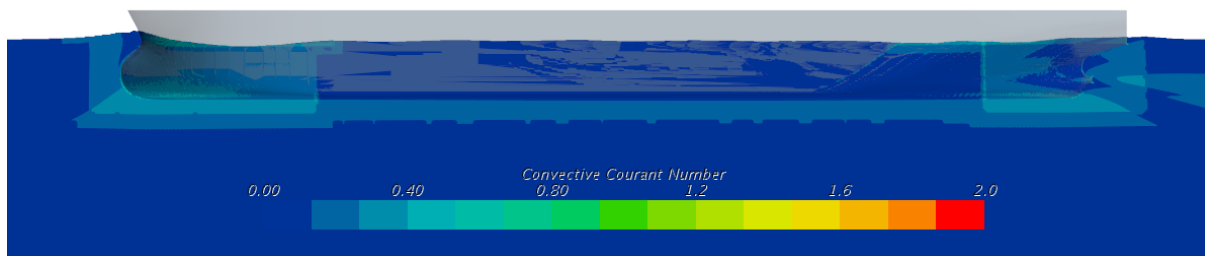


Figure 32. Convective Courant Number

4.3.1.2 Modelling Variations

Prior to outlining the virtual towing test CFD model utilised for the case investigations (modules) and the one used to carry out the validation and verification procedures, a series of studies was carried out to improve and fine tune the results. These were mostly investigations focusing on turbulence models, grid development and physics criteria. These were judged based on the suitability of the residuals, the Courant number and agreement with experimental results (NMRI, 2015). Although quite a few variations and parametric studies were carried out, it is valid to highlight those with the most prominent and significant impact.

Curvature Correction Turbulence Model

The improved towing CFD model, i.e. the one that was ultimately used for all the case studies, features a recently adopted curvature corrected turbulence model.

Standard Eddy Viscosity Models (EVM) tend to over or under predict the generation or dissipation of turbulence when subject to streamline curvature with concave streamlines tending to increase the turbulence and convex the reduction. Therefore, since the rotation of flow characterises high gradients of curvature, it experiences similar impacts to the turbulence. The EVM do not incorporate any terms to consider the effects of curvature, thus making the transport equation for the turbulent kinetic energy insensitive to effects associated with curvature streamlines.

CD-ADAPCO have recently adopted and implement a curvature correction (CC) feature whereby a factor is introduced to modify the turbulent kinetic energy production term according to the local rotation and vorticity rates. To the best of the author's knowledge, this novel curvature correction method has not been yet implemented or used for ship simulations. This study, therefore, investigates the use of this method for numerical ship prediction, also demonstrating the validation and verification of the results. The curvature correction formulation is adopted from Arolla and Durbin (2012), and CD-ADAPCO (2014) define the curvature correction as follows:

$$f_c = \min \left(C_{max} \frac{1}{C_{r1}(|\eta| - \eta) + \sqrt{1 - \min(C_{r2}, 0.99)}} \right) \quad (32)$$

$$\eta = T^2(S:S - W:W) \quad (33)$$

Where T represents the time-scale, S the Strain-Rate Tensor, W, the absolute rotation rate tensor and C_{max} , C_{r1} , C_{r2} are model coefficients. The curvature correction factor modifies the turbulent kinetic energy production term of the transport equation according to the local rotation and vorticity rates. Please refer to (Arolla and Durbin, 2013b) for more details regarding the formulation of the curvature correction.

A study was carried out to investigate the differences and the results output between the older model and the improved simulation that features a curvature corrected k- ω model. Figure 33 presents the difference in the wake field characteristics with regards to axial velocity (V_x) at different planes along the hull (without Duct).

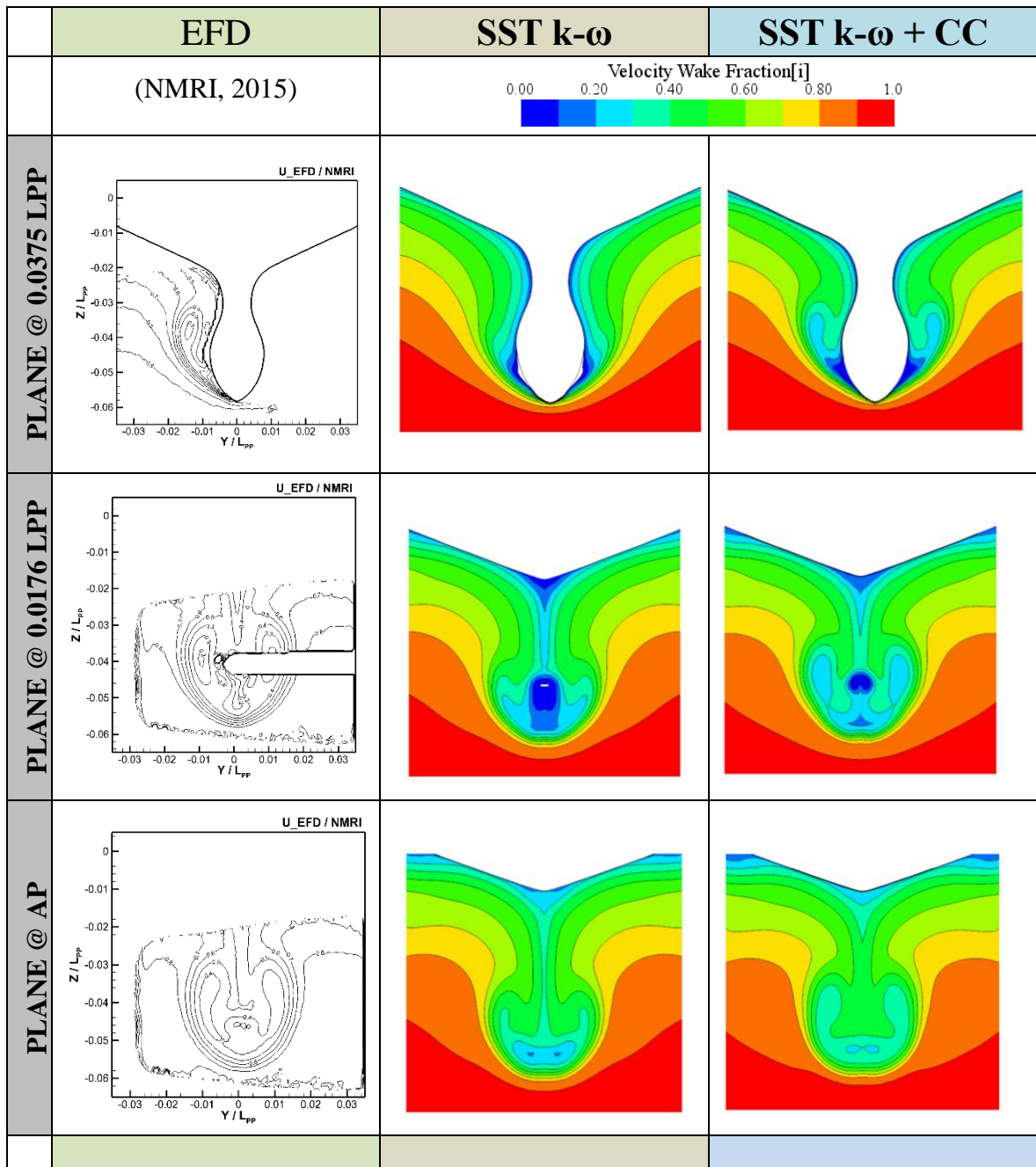


Figure 33. Wake Field CC Model Study

When comparing the CFD results to the EFD experimental JBC model scale data (NMRI, 2015), in Figure 33 it is evident that the standard SST k- ω turbulence model fails to capture the circulation of the vortices. The curvature corrected model SST k- ω model exhibits a significant improvement in the region of recirculation. It is therefore concluded that the CC turbulence model better simulates the wake field of a vessel which is very important for this study since the thesis focuses on hull-propeller interaction. Improvements in the other direction velocity vectors (V_y & V_z) are also noticeable. Furthermore, the CC model significantly improves the Sinkage accuracy as indicated in Table 11.

Table 11. Sinkage & Trim CFD Model Comparison

	EFD	SST k-ω	SST k-ω + CC
<i>Sinkage(mm)</i>	6	5.5	6.1
<i>Sinkage error %</i>	-	9.1	-2.5
<i>Trim (deg)</i>	0.1	0.1061	0.1062
<i>Trim error%</i>	-	-3.54	-2.45

Free Surface Refinement

Another study was carried out to investigate the resultant impact of refining the free surface grid in the vertical direction. The newly improved model featured cell sizes of 0.05% Lpp at the free surface as opposed to 0.2% Lpp. This variation had a significant impact on the wave cut accuracy. Figure 34 presents wave cuts at different planes offset from the ship centreline with the orange line representing the experimental results (NMRI, 2015) and the black line representing the CFD results. Results clearly indicate that the finer free surface provides a better representation of the wave behaviour when compared to the experimental data, especially past the stern where higher damping of waves is evident.

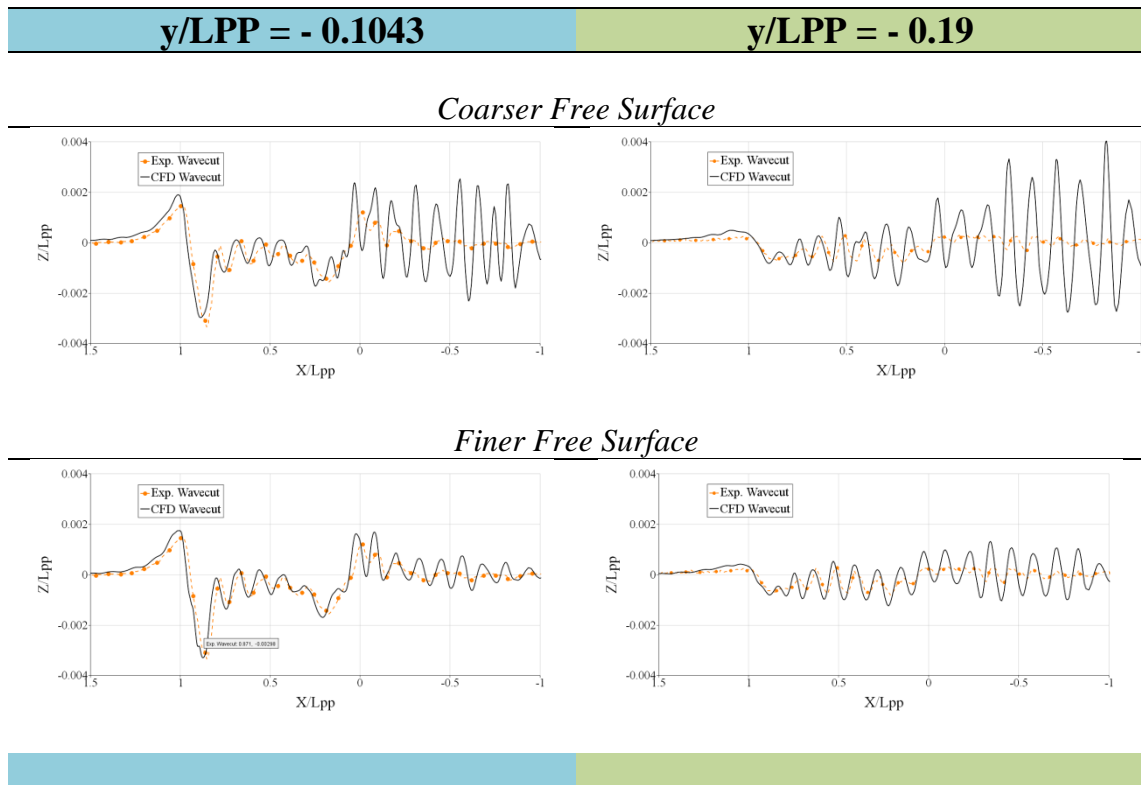


Figure 34. Wave Cut Comparison

STATIC vs DFBI

In contrast to module 2 and 3 studies, whereby only half the domain was required to be simulated due to the symmetry about the centre plane, module 4 required a full-domain CFD towing simulation. This module involved the investigation of an ESD in different operational conditions. With the ESD not being symmetrical about the centre plane, the half-domain simulation was no longer considered suitable and appropriate, thus requiring a full-domain simulation at full-scale. The same physics and grid topology were applied in a similar manner. However, in order to maintain a high level of detail and fidelity, the respective generated mesh sizes were very large as indicated in the following section. It is computationally expensive to run such a simulation with Dynamic Fluid Body Interaction (DFBI), i.e. the vessel being allowed to sink and trim. This was not considered feasible and an investigation was carried to analyse the impact on results between a static vessel and one that is allowed to sink and trim in a full-scale environment. Figure 35 presents the resistance and wake field differences between:

- Half - Domain with DFBI enabled
- Half - Domain no DFBI
- Full - Domain no DFBI

The results indicate a maximum variation of 2.6% in the resistance and insignificantly minor differences in the wake field behaviour. With the discrepancies being relatively small, the static full-domain simulation was thus considered appropriate to carry out this module, especially since the trends in impact and results are more important than the actual values. Furthermore, simulations not computing DFBI, are less computationally expensive since the motion of the vessel does not need to be calculated. It is important to note that the greatest distinction in the resistance was due to the DFBI de-activation and not because the model was run in a full-domain environment.

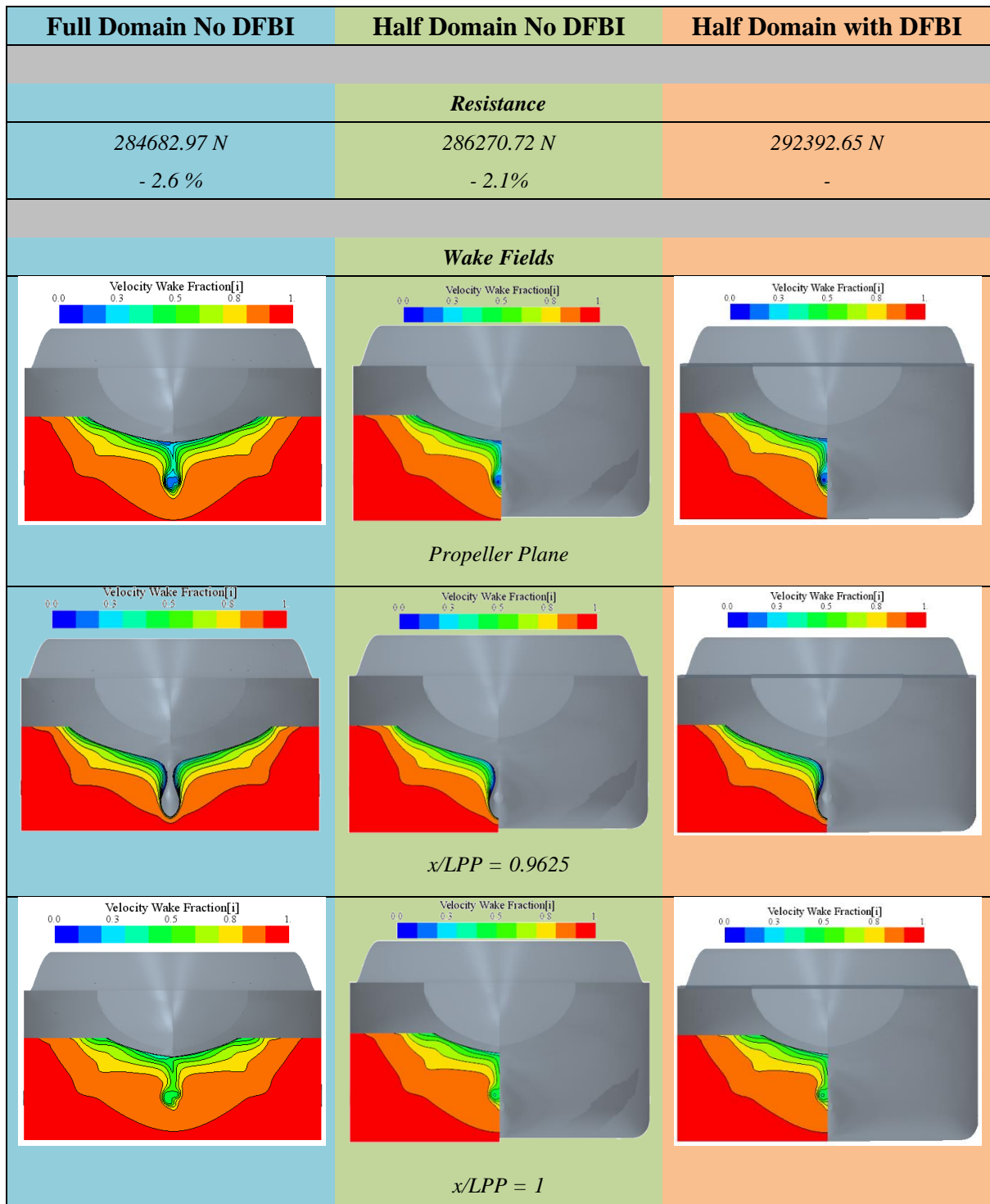


Figure 35. Static vs DFBI Impact Study

4.3.1.3 Mesh Generation and Boundary Conditions

The computational domains and grid topology explained below are common to all the different conditions and cases unless stated otherwise. Variations are outlined in reference to their respective case number, as indicated in Table 6.

The accurate representation of ship geometry is very important as this dictates the flow behaviour and characteristics around the vessel. The surface mesh was generated using fine triangulated faces producing detailed geometry definition for each of the three cases.



Figure 36. Surface Mesh (*side view*)

The volume mesh was developed using the STAR-CCM+ automatic grid generation tool that makes use of a Cartesian cut-cell method, also known as the Trimmer producing an unstructured grid. All three meshes were generated following the same topology and refinement structure amounting to the number of elements specified in Table 12. The significant difference in mesh size for case 4 is due to the fact that the full domain had to be simulated as opposed to half the grid as previously indicated in section ‘Modelling Variations’ (4.3.1.2).

Table 12. PL No. & Mesh Size

<i>Case</i>	<i>Prism Layer No.</i>	<i>Mesh Size No.</i>
<i>2: Model-Scale JBC</i>	5	6.8 M
<i>3: Full-Scale JBC</i>	12	7.8 M
<i>4: Full-Scale RSBC</i>	11	21.5 m

Table 13. Refinement Details

<i>Refinements Region</i>	<i>Element Size: %LPP</i>
<i>Bow</i>	0.1
<i>Free Surface</i>	0.05
<i>Near Hull</i>	0.2
<i>Stern</i>	0.1
<i>Wake</i>	0.2
<i>ESD</i>	0.01-0.05

Mesh refinements were specified in designated areas of interest, particularly the stern region for accurate prediction of stern flow behaviour (see Figure 37). Despite the variations in the grid due to mesh refinements, the domain was designed in a way to allow for a reasonable uniform growth between cells avoiding high skew developments. Refinement details and respective element sizes are outlined in Table 13. Figure 37 presents a top view of the free surface mesh showing the typical refinement shape that follows the Kelvin angle, with a dense mesh near the hull that gets coarser with increasing distance from the vessel.

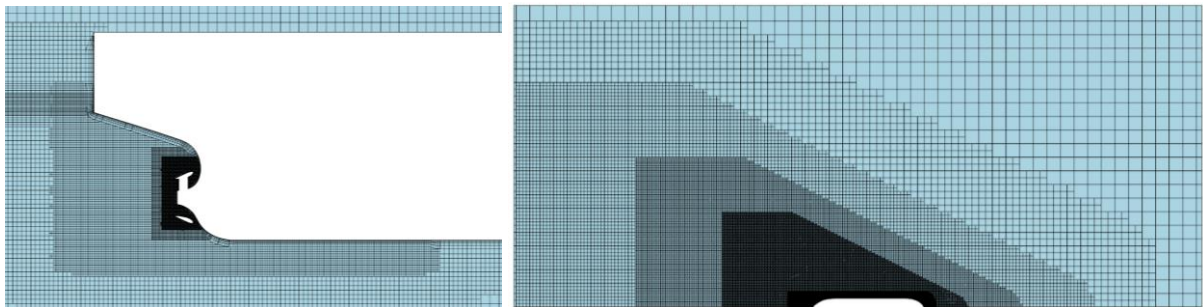


Figure 37. Mesh Refinements: Side (*left*) & Top (*right*)

In computational fluid dynamics, the cells near the surface/wall boundaries are of prime concern. Fluid flow passing along a surface generates a boundary layer that develops due to the inertia and viscous forces producing different turbulent structures from free form flow. In order to accurately predict near wall flow details, a prism layer (PL) feature was employed, generating a number of orthogonal prismatic cells adjacent to the surface along the ship hull. The number of layers and their thicknesses were designed and computed to achieve the desired Y^+ requirements. Since the CFD towing studies (module: 2,4 & 5) involved in this thesis are carried out in full-scale conditions (model-scale simulations are used for validation purposes), it was deemed feasible to carry out the near-wall treatment using the wall function approach where the wall shear stress, turbulent production and turbulent dissipation are all derived from equilibrium turbulent boundary layer theory. As specified by CD-ADAPCO (2014), such a methodology requires Y^+ values greater than 35. On the other hand, resolving the viscous sub-layer by the mesh requires very fine cells that produce Y^+ values lower than 1 that were considered to be computationally expensive for full-scale scenarios. Therefore, although the All Y^+ Wall Treatment model was selected for the simulation, the prism layer was designed as to give Y^+ values around or greater than 35 ensuring appropriate treatment of the wall function. Figure 39 demonstrates the Y^+ values for the model-scale JBC and the full-scale JBC simulations. It is appropriate to note that the PL thickness was varied along the hull,

constructing a nice blend (Figure 38) to the nearest core cells that resulted due to different mesh refinements. Since the different cases involved different size of geometries, that produced different Reynolds numbers, prism layers (number and thicknesses) were custom designed for each condition. The details of the number of prism layers used for the different cases are presented in Table 12.

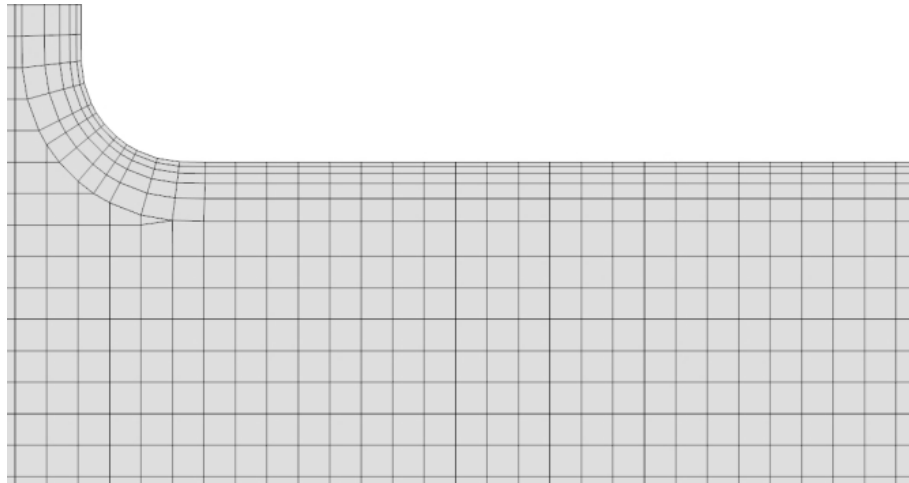


Figure 38. Prism Layer Blending

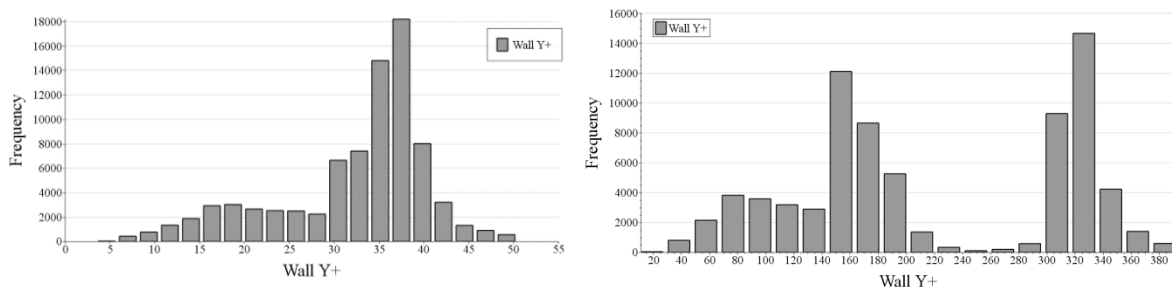


Figure 39. Wall Y+ for Case 2 (left) & 3 (right)

The selection of boundary conditions and initial conditions in CFD is of critical importance to ensure the right methodology and approach of simulation. Suitable initial and boundary conditions have an influence on time convergence and can save on computational cost (Date and Turnock, 1999). Date and Turnock (1999) also maintain that the distance and positioning of the boundary conditions are equally important. These should be defined in such a way that the boundaries have no influence on the flow characteristics/behaviour under investigation resulting in boundary independent solutions.

For all three cases, a velocity flow field condition was specified at the inlet boundary located 2.5 ship lengths upstream of the vessel, and a pressure field for the outlet boundary placed 2.8 L_{pp} downstream. Since the conditions for case 2 & 3 (Module 2 & 4) of a towing test simulation are symmetrical about the centre plane, it was therefore deemed feasible to model half of the domain saving computational cost and time. A symmetry plane was thus set along the x-axis. However, as previously explained in section ‘Modelling Variations’ (3.3.1.2), half the domain was not suitable for case 4 (Module 5) since the respective ESD was not symmetrical about the centreline. For this case, the symmetry plane was removed and the domain was extended in such a way that the sides were 2.5 L_{pp} lengths on either side of the vessel and specified to be velocity inlet boundaries. The rest of the boundary conditions were designed similarly to the half-domain settings.

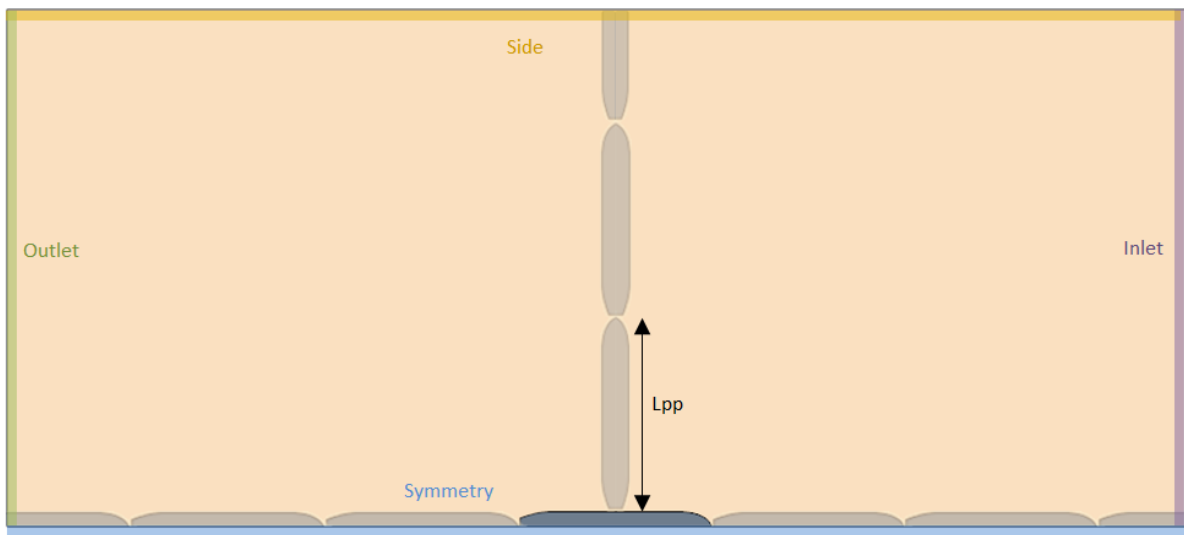


Figure 40. Dimensions of Free Surface

The hull geometry was specified with a non-slip wall boundary allowing boundary layer developments. On the other hand, remaining boundaries were set to velocity inlet conditions featuring slip wall characteristics, thus preventing the development of velocity gradients between the wall and fluid. The bottom boundary was placed far enough below water level to avoid any shallow water effects. VOF wave damping was also applied to the inlet, outlet and side boundaries preventing wave reflections that might interfere with the results. Figure 41 demonstrates the configuration that was used for the validation & verifications procedures of case 2 and 3.

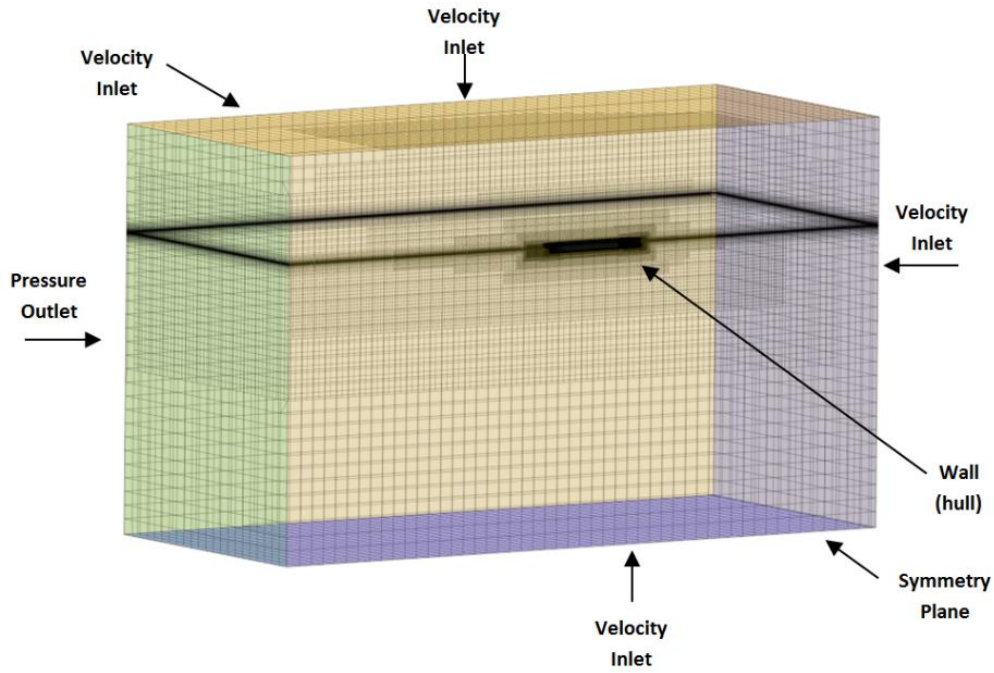


Figure 41. Domain Boundary Conditions

4.3.2 Validation and Verification

Validation and verification (V&V) procedures for the virtual towing tests were carried out using the JBC (model and full-scale) and the RSBC hull geometry. The V&V procedures for these cases followed the methodology indicated by Stern et al. (2006). Simulation error δ_S is a combination of modelling and numerical errors. In a similar manner, simulation uncertainty is also a combination of modelling and numerical uncertainties. The validation process provided the modelling uncertainty U_{SM} and error δ_{SM} whereas the verification procedure identified the numerical uncertainty U_{SN} and numerical errors δ_{SN} demonstrating the capability of the solver. It is good to indicate that the experimental results (EFD) utilised for the “True” values of the V&V procedures, were published by NMRI (2015) as open source data.

A grid convergence study for most cases was carried out to investigate the influence of an increasing mesh resolution on the solver solution. Such a study requires at least three solutions by varying the numerical mesh size. For the purpose of this study, three grids were systematically generated varying by a factor of $\sqrt{2}$. Convergence analyses require grids of similar structure and while this is challenging to achieve with unstructured grids, efforts were made to keep the mesh development similar. This was accomplished by varying each cell size in the domain by a specific factor ($\sqrt{2}$) in each spatial direction. That being said, the prism layers were retained constant across all meshes preventing any changes of the wall treatment

of the turbulence model. All three grids (Fine, Medium and Coarse) were computed producing three solutions S_1 , S_2 , S_3 respectively, allowing the derivation of the convergence ratio. Figure 42 shows the results of the grid convergence study by plotting the error of the total drag coefficient, the dynamic sinkage and the dynamic trim over the grid base size.

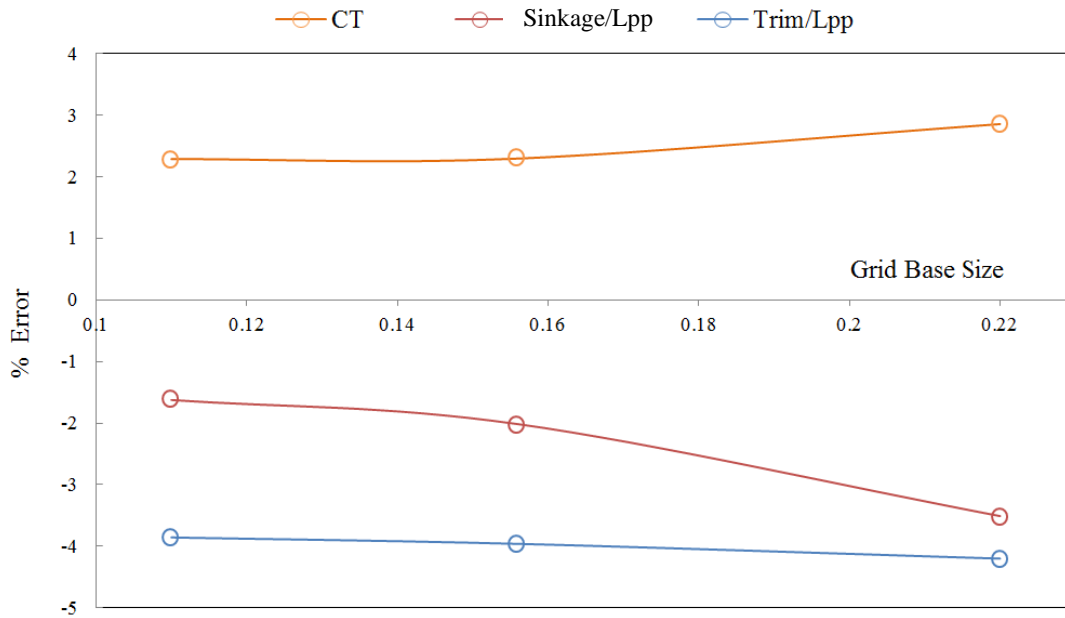


Figure 42. Grid Dependency Study

The refinement ratio for the grid dependency study exhibited monotonic convergence according to the criteria specified by Stern et al. (2006). The numerical errors and uncertainties were then computed using the Generalised Richardson Extrapolation (RE) methods (Richardson, 1910). Table 14 outlines the different solutions achieved for the grid densities indicating minor and comparable error percentages. The verification of the drag coefficient for the grid convergence study yielded insignificant uncertainties as presented in Table 15 for the different methods indicating that the results are not sensitive or dependent on the grid size when using the fine mesh.

Table 14. Grid Dependency Study

	<i>Coarse</i>	<i>Medium</i>	<i>Fine</i>
<i>Base Size (m)</i>	0.22	0.156	0.11
<i>Mesh Size (M)</i>	1.36	2.7	6.87
<i>C_T Error %</i>	2.85	2.29	2.28
<i>Sink/Lpp error %</i>	-3.51	-2.02	-1.62
<i>Trim/Lpp error%</i>	-4.20	-3.96	-3.86

The numerical uncertainties were estimated using Roaches' (1998) Grid Convergence Index GCI with factor of safety as recommended by Celik et al. (2008). Alternatively, RE with the concept of correction factors was also used to estimate the errors and uncertainties (Stern et al., 2001). The extended correction factor to the Richards extrapolation is a means to determine the proximity of solution to the asymptotic range.

Table 15. Case2: Grid Convergence Study for C_T

<i>Parameter</i> r	EFD	S_C	r_G	<i>Solutions</i>			R_G	$\delta_G(\%S_1)$	$U_G(\%S_1)$		$U_{GC}(\%S_1)$	
				S_1	S_2	S_3			CF	GCI	CF	GCI
C_T	4.289	4.192	$\sqrt{2}$	4.1914	4.1901	4.1657	0.0167	-0.0095	0.0189	0.0002	0.0094	0.00004

Table 16. Case 2: Validation for C_T

<i>Parameter</i>	<i>Uncorrected</i>		U_D	<i>Corrected</i>		$E(\%)$
	U_{SN}	U_v		U_{SN}	U_v	
C_T	0.0185	1.0002	1.0	0.0092	1.0	2.2733

In the respective validation approach, the Comparison Error (E) is considered to be the difference between the Solver Output (S) and the True Value (T). Deducting the experimental error estimate δ_D from the Data (D) gives the truth. E is generally compared to the validation uncertainty U_v in order to determine whether the numerical model complies. For this case study, the solver output is C_T (drag coefficient) with D being the experimental value as outlined by NMRI (2015) and the experimental uncertainty given as 1%. The comparison Error E shows a simulation accuracy of 2.27% for the total drag coefficient C_T being higher than the experimental uncertainty (see Table 16). For further understanding and detailed information on the above analyses, reference can be made to Stern et al. (2006).

The same validation and/or verification procedures were applied to cases 3 and 4. Since the aforementioned cases involved full-scale conditions with no experimental or sea trial data for comparison, validation could not be carried out. However, CFD results for the full-scale JBC hull in towing conditions were also stated by Visonneau et al. (2016). These values were therefore referred to for comparison in order to carry out validation for case 3. Results for the respective cases are as follows:

Table 17. Case3: Grid Convergence Study for C_T

<i>Parameter</i>	<i>EFD</i>	<i>S_C</i>	<i>r_G</i>	<i>Solutions (N)</i>			<i>R_G</i>	<i>δ_G</i>	<i>U_G(%S₁)</i>		<i>U_{GC}(%S₁)</i>	
				<i>S₁</i>	<i>S₂</i>	<i>S₃</i>			(%S ₁)	<i>CF</i>	<i>GCI</i>	<i>CF</i>
	$\times 10^3$	$\times 10^3$		$\times 10^3$	$\times 10^3$	$\times 10^3$						
<i>Drag</i>	1075.6	1073.8	$\sqrt{2}$	1080.6	1087.4	1109.5	0.3091	0.6311	0.9799	0.3529	0.3488	0.0706

Table 18. Case 3: Validation for C_T

<i>Parameter</i>	<i>Uncorrected</i>		<i>U_D</i>	<i>Corrected</i>		<i>E</i> (%)
	<i>U_{SN}</i>	<i>U_v</i>		<i>U_{SN}</i>	<i>U_v</i>	
<i>Drag</i>	0.9845	2.6868	2.5	0.3504	2.5244	0.1664

Table 19. Case4: Grid Convergence Study for C_T

<i>Parameter</i>	<i>EFD</i>	<i>S_C</i>	<i>r_G</i>	<i>Solutions (N)</i>			<i>R_G</i>	<i>δ_G</i>	<i>U_G(%S₁)</i>		<i>U_{GC}(%S₁)</i>	
				<i>S₁</i>	<i>S₂</i>	<i>S₃</i>			(%S ₁)	<i>CF</i>	<i>GCI</i>	<i>CF</i>
	$\times 10^3$	$\times 10^3$		$\times 10^3$	$\times 10^3$	$\times 10^3$						
<i>Drag</i>		284.33	$\sqrt{2}$	284.68	285.03	288.23	0.1085	0.122	0.2291	0.0186	0.0037	0.1071

Table 17 and Table 19 demonstrate that both cases exhibited monotonic convergence outlining insignificant uncertainties and indicating that the results for the finest grid are insensitive to the mesh density. In a similar manner to the validation of Case 2, Table 18 indicates an insignificant comparison error *E* of 0.17% for the simulation model of case 3. As previously mentioned, due to the unavailability of experimental data for full-scale conditions, the full-scale simulations were validated with results from another institute that were also using CFD methods. This could be the reason for the high accuracy.

Due to the availability of experimental data (NMRI, 2015) for the JBC model, further validation was carried out by analysing and comparing sinkage and trim magnitudes, the wave profile along the vessel, wave cuts and wake contours. The validation of sinkage and trim values, together with the wave cuts and some of the wake contours have been previously demonstrated in the ‘Modelling Variations’ section (4.3.1.2).

In order to further demonstrate the accuracy of the CFD model with regards to wake prediction, Figure 43 shows a wake contour plot overlay of the baseline JBC hull describing the axial

velocities at a transverse plane located at $0.0157 L_{PP}$ (from aft peak forward). The illustration compares the coloured numerical wake distribution with the experimentally measured flow field represented by the black wake isolines. The comparison shows that the numerical simulation is able to capture the detailed structure of the ship wake field, not only in contour but also in magnitude demonstrating the enhanced accuracy achieved with the implementation of the curvature corrected (CC) turbulence model.

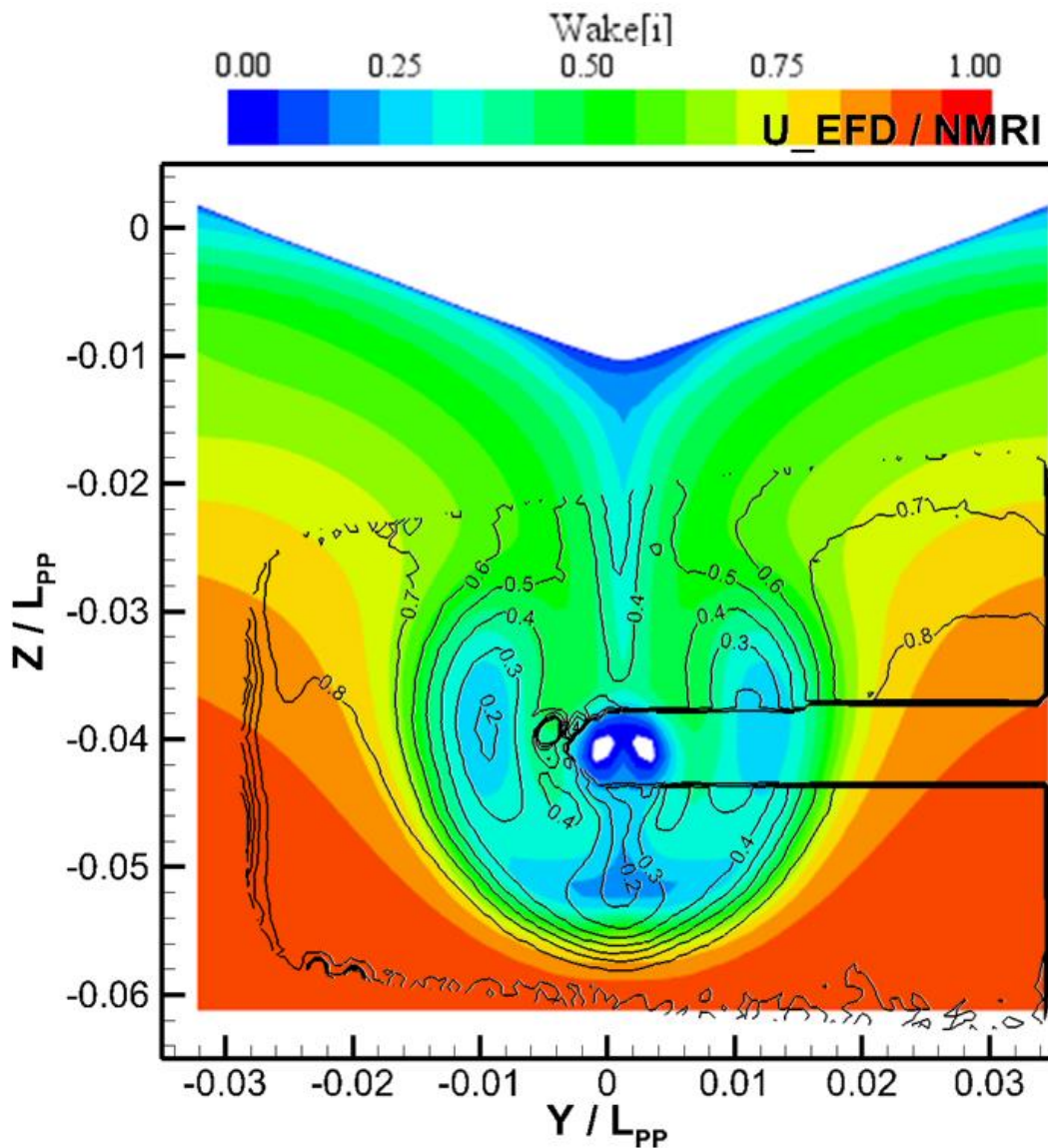


Figure 43. Comparison of Experimental Results (*black contour lines*) and Numerical Results (*contour plot*)

Furthermore, Figure 44 demonstrates the accuracy of the CFD solver in predicting the wave profile along the vessel with the orange line representing the experimental values and the black line the numerical output.

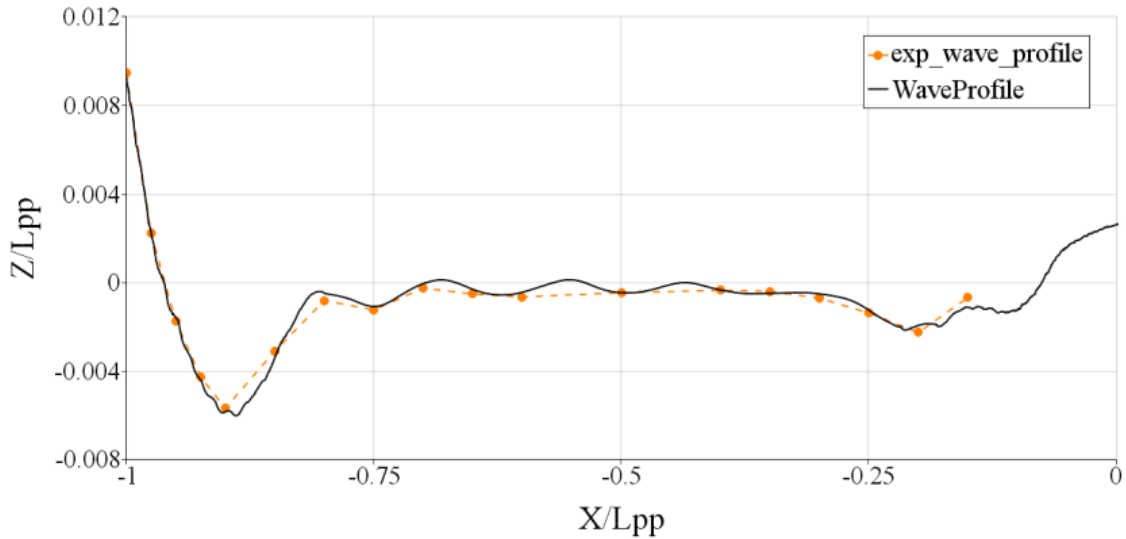


Figure 44. Wave Profile Comparison

Since the validation and verification procedures of the CFD model demonstrate the accuracy and capability of the solver, the numerical procedure was thus considered appropriate to be used for the study.

It should be noted that validation and verification studies were not carried out for geometries (JBC & RSBC) with retrofitted ESDs. Carrying out the validation and verification procedures for ESD retrofitted geometries would double the number of computations required making it too expensive and time consuming within the available time frame. However, some additional cases (computations) with appended retrofitted devices were run and results were compared to experimental data (NMRI, 2015). Table 20 exhibits the validation of drag for the model scale JBC hull with retrofitted JBC duct, also confirming good agreement with the experimental data.

Table 20. Case 2 with Duct Validation

	<i>EFD</i>	<i>SST k-ω + CC</i>
C_T	4.263	4.173
C_T error %		2.1

In addition, wake contours and velocities (in all three directions) for the JBC with the installed Duct have also been compared. Wake contours for the axial velocities between the experimental (NMRI, 2015) and the numerical results are presented in Table 21, showing good agreement between both sets of data with similar behaviour and fluid flow characteristics. As

can be seen at the plane @ $0.0375L_{pp}$, the vorticity is somewhat predicted. With regards to the plane @ $0.0176L_{pp}$, retardation of the flow in the wake field is also predicted. However, it seems that the CFD approach overestimates the retardation of the flow.

Table 21. JBC w/Duct Wake Contour Comparison

	EFD	SST $k-\omega$ + CC
	(NMRI, 2015)	Velocity Wake Fraction[i]
		0.00 0.20 0.40 0.60 0.80 1.0
PLANE @ 0.0375 LPP		
PLANE @ 0.0176 LPP		
PLANE @ AP		

4.4 Self-Propulsion Tests

This section describes the numerical modelling used to carry out the self-propulsion test simulations for the model-scale as well as the full-scale conditions. The methodology follows the lines of the towing simulations with some minor differences. In order to avoid unnecessary repetition, the differences are highlighted. The development of these simulations was also carried out using the commercial CFD software Star-CCM+® version 9.0.2, which was developed by CD-Adapco (CD-ADAPCO, 2014) and the High-Performance Computer (ARCHIE-WeSt). The methodology presented in this section was used for the module 4 study (Please refer to 20 in chapter 3) in this thesis but was also used to validate and verify the self-propulsion simulation at model scale due to available experimental results. Hence in reference to Table 6, this methodology has been used to carry out the validation and/or verification studies for cases 5 and 6.

4.4.1 Numerical Modelling

As previously mentioned, the physics of the self-propulsion model follows a similar methodology to that of the towing simulations. The same CFD solver is used to compute the multiphase flow to simulate the three-dimensional environment using the (Shear Stress Transport) $k-\omega$ model with the recently implemented Curvature Correction (CC). The VOF method was also used to calculate the volume fraction of the two different fluids in order to predict the free surface and all the simulations were run in calm water conditions

The differences are the following; The DFBI was de-activated and the simulations were run at a static level trim. Self-propulsion simulations are computationally expensive and predicting the dynamic sink and trim increases the complexity of the simulation and hence the computational power required. Similar to the towing CFD simulations, the hull was treated with a wall function approach requiring Y^+ values greater than 30. However, the propeller was modelled in a way in order to accurately predict the complex flow that was produced by the propeller hence requiring Y^+ values lower than 5. The prism layer numbers and respective thicknesses were selected accordingly in order to ensure appropriate wall treatment and smooth blending of the near-wall cells to the domain elements. Figure 45 demonstrates the computed Y^+ values on the hull and the propeller presenting their difference in magnitude.

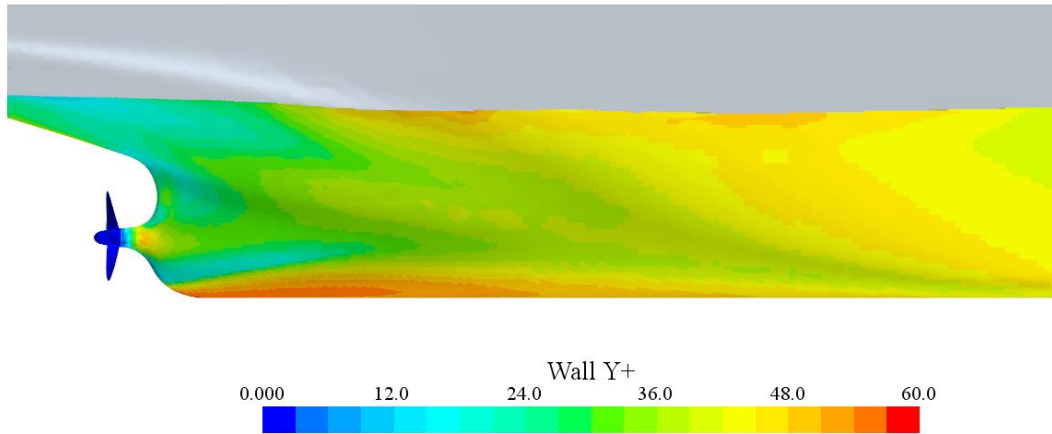


Figure 45. Visual Y+ of Propeller and Hull

An implicit unsteady time marching scheme was again used to treat temporal and spatial discretization. Time step values were selected to give Courants numbers (CFL) around the value of 1 in the zones of interest as recommended by CD-ADAPCO (2014) for enhanced numerical stability. Figure 46 demonstrates that CFL values in the regions of interest are around one accurately capturing the required flow details. A higher Courant number (still below two) can be identified in the propeller region. This is due to the fast rotation rate of the propeller thus requiring a very small-time step to reach low CFL numbers. Reaching convergence with such a low time step would require significant time and computational power. Therefore, the simulation is initiated with a large time step and after convergence is achieved, the time step is progressively reduced until the desired value is around $(1/rps)/200$ as suggested by the ITTC (2011a). The time step for the model-scale simulations (case 5) was initiated with a value of $\Delta t=0.01s$ and reduced to $\Delta t=6.25 \times 10^{-4}s$. Meanwhile, values for the full-scale simulations were set to be 0.01s and reduced to 0.0025s.

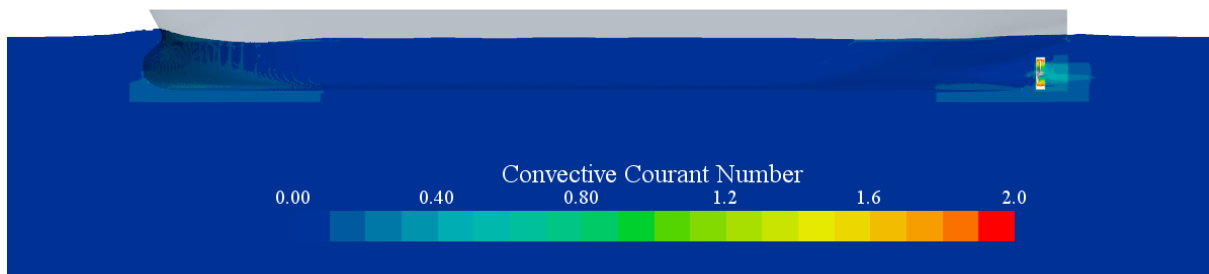


Figure 46. Convective Courant Numbers (Case5)

4.4.2 Mesh Generation and Boundary Conditions

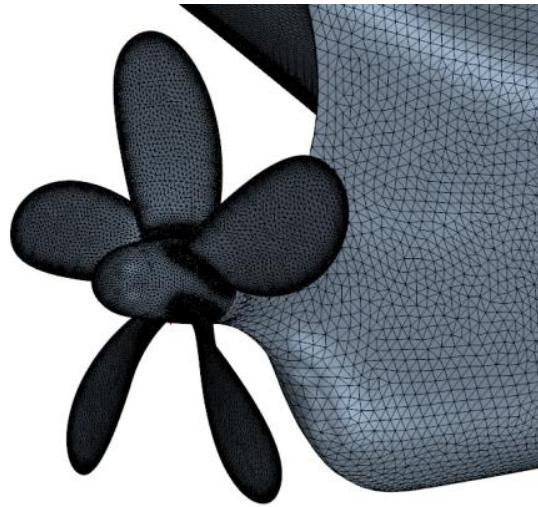


Figure 47. Propeller Surface Mesh

For the self-propulsion simulations, the propeller was included and considered using actual blade surface representation as opposed to the more simplified actuator disk, thus taking into consideration the viscous effects of the propeller. The geometric surface of the propeller was also represented using triangulated faces. However, as demonstrated in Figure 47, the sizes were significantly reduced to capture sharp edges such as the trailing edge.

The inclusion of the propeller introduced a new cylindrical rotating region inside the existing block domain, as depicted in Figure 48. The block domain follows a similar grid topology to the one presented for the towing simulations. That being said, after having gained more experience and knowledge in the field, some minor changes were applied to avoid refinement in unnecessary regions and reduce the number of elements at no expense of accuracy.

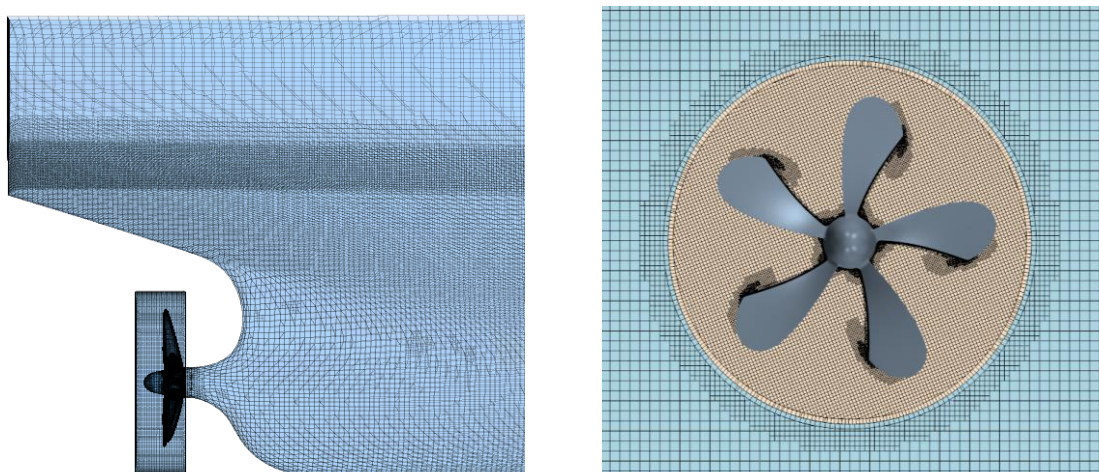


Figure 48. Rotating Region

The cylindrical region, which was designed to be slightly bigger than the extents of the propeller (Figure 48), was rotated using a sliding grid approach and made to interact with the block domain using interface boundaries. The sliding grid or sliding mesh physics was previously introduced in the ‘4.2.1.2 Modelling Variations’ section of the open water test case methodology in this chapter. For the model scale simulations (Case 5), the rotation rate of the rotating region was specifically set to particular values as highlighted by the experimental data. On the other hand, for the full-scale conditions, the RPM was adjusted accordingly until the self-propulsion point was met i.e. the thrust and the resistance have the same magnitude resulting in a null net force indicating that the vessel is moving forward at a constant speed with no acceleration.

Due to the rotating propeller, a full (as opposed to half) domain was simulated. Hence there was no symmetry boundary about the centre plane but a full extended domain with 2 sides. The boundary conditions for the block domain were similar to the ones specified for the towing simulations, more specifically Case 5, due to the full domain conditions. With regards to the boundary conditions for the rotating region, the propeller was set to be a non-slip surface, and the boundaries of the cylinder were set to be interface boundaries that interact and allow the transfer of data between the block domain and the rotating region.

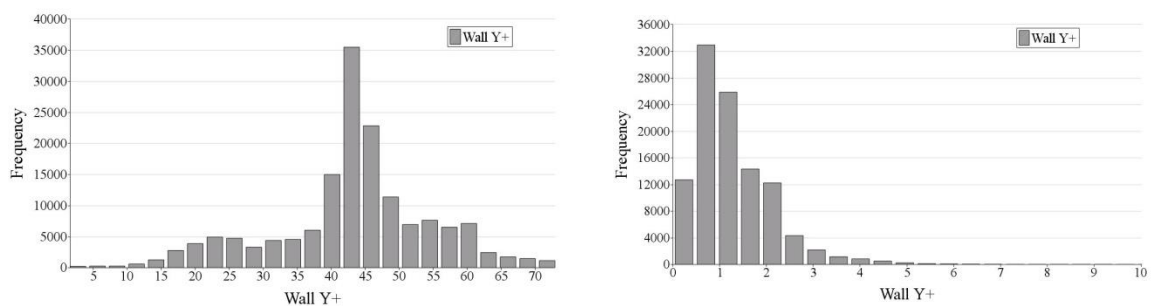


Figure 49. Y+ Values of Hull (Left) and Propeller (Right)

In relation to the orthogonal prismatic cells adjacent to the hull or propeller surface, i.e. the prism layer, the number of layers and the respective thickness were developed to achieve the desired Y+ requirements. As previously mentioned, it was deemed appropriate to treat the hull with the wall function approach thus requiring Y+ values on the hull to be greater than 35 and the propeller to be wall resolved requiring Y+ values to be less than 5. Figure 49 presents the Y+ values achieved for the numerical model used in Case 5. The prism layer settings were thus adjusted differently for the hull and the propeller always producing smooth transitions and adequate cell growth between the orthogonal cells and the nearest core cells (Figure 50). Once again, the different cases involved different scale conditions producing different Reynold

numbers and thus, the prism layer settings were modified accordingly. Furthermore, one prism layer of constant thickness was applied to each side of the interface boundaries between the stationary and rotating region, as depicted in Figure 48. This allows for accurate interaction, interpolation and ease of transfer of data between both regions.

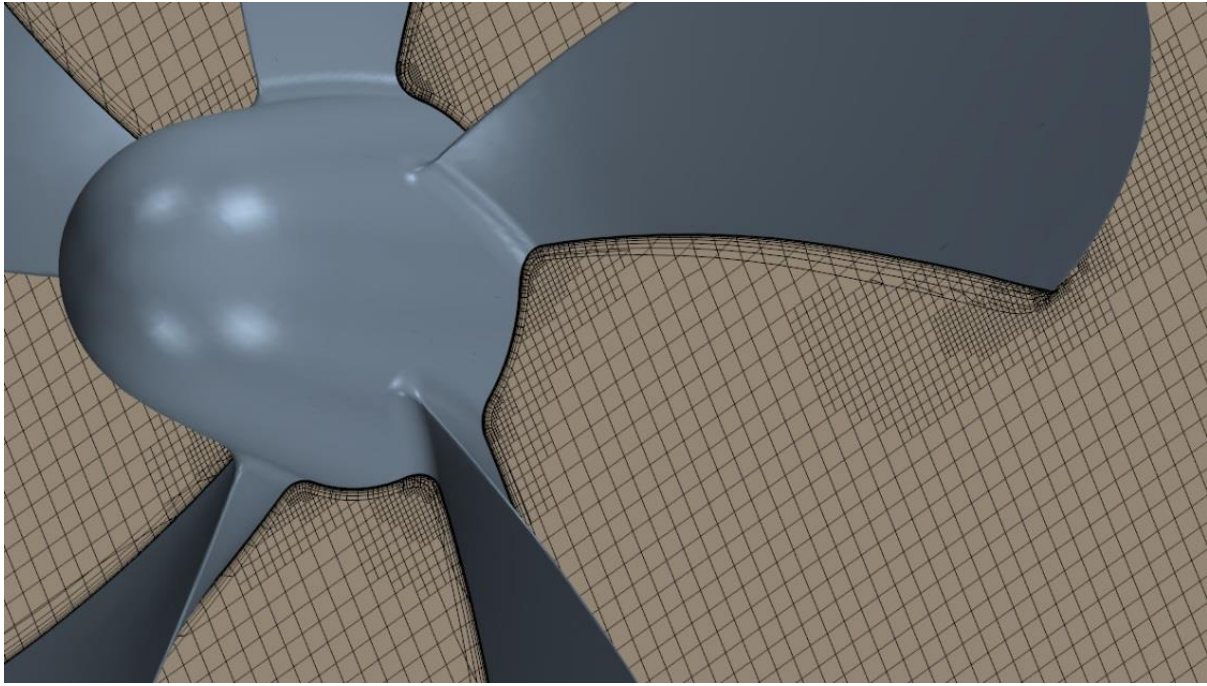


Figure 50. Propeller Prism Layer

Further details of the prism layer settings and the cell size number of the different self-propulsion cases are outlined in Table 22.

Table 22. PL. No & Mesh Size (*Self-Propulsion*)

<i>Case</i>	<i>Prism Layer No.</i>	<i>Mesh Size No.</i>
<i>5: Model-Scale JBC</i>		10.8 M
- <i>Region: Stationary</i>	4	9.3 M
- <i>Region: Rotating</i>	8	1.5 M
<i>6: Full-Scale RSBC</i>		16.8 M
- <i>Region: Stationary</i>	5	13.8 M
- <i>Region: Rotating</i>	9	3 M

4.4.3 Validation and Verification

Validation and verification procedures for self-propulsion case 5 was also carried out using the methodology indicated by Stern et al. (2006) identifying modelling together with numerical errors and uncertainties. The grid convergence study was carried out in a similar manner by varying the cell sizes in the grid by a factor of $\sqrt{2}$ in all three directions and keeping the prism layer details constant. Validation & verification studies were not carried out for geometries with retrofitted ESDs. Carrying out the validation and verification procedures for ESD retrofitted geometries would double the number of computations required making it too expensive and time consuming given the available time frame. It is good to indicate that the experimental results (EFD) utilised for the “True” values of the V&V procedures, were published by NMRI (2015) as open source data. Table 23 outlines the different solutions achieved for the grid densities indicating minor and comparable error percentages.

Table 23. Self-Propulsion Grid Dependency Study

	<i>Coarse</i>	<i>Medium</i>	<i>Fine</i>
<i>Base Size (m)</i>	0.22	0.156	0.11
<i>KT Error %</i>	-0.13	-2.34	-3.12
<i>KQ Error %</i>	-1.30	-3.07	-3.63
<i>C_T Error %</i>	1.98	1.85	1.16

Validation and verification results for the self-propulsion model are demonstrated in Tables 24 – 29 below. It is understood that although resistance simulations exhibit higher accuracy (as expected), self-propulsion simulations are still able to provide accuracies (E) less than 5% with C_T resulting in 0.46%, KT 3.92% and KQ 4.1%. It is evident that advanced CFD procedures are very good at predicting drag performance, such as the C_T parameter outlined above. Self-propulsion models are more sophisticated than resistance models, but the accuracy is constantly improving and heading in the right direction.

While the V & V results indicate reasonable accuracy, not all parameters meet the experimental error defined at 2.5%. This might have been a relatively optimistic target to start with. Furthermore, while the convergence ratio for the KT and KQ indicated monotonic convergence, the C_T did not exhibit such behaviour. The reason being that with the finer meshes, the results did not reach asymptotic behaviour, thus probably requiring further refinement. That being said, the results are considered satisfactory in order to carry out the case studies for this thesis.

Table 24. Case5: Grid Convergence Study for K_T

<i>Parameter</i>	<i>EFD</i>	S_C	r_G	<i>Solutions</i>			R_G	$\delta_G(\%S_1)$	$U_G(\%S_1)$		$U_{GC}(\%S_1)$	
				S_1	S_2	S_3			<i>CF</i>	<i>GCI</i>	<i>CF</i>	<i>GCI</i>
K_T	0.217	0.2255	$\sqrt{2}$	0.2238	0.2221	0.2173	0.3542	-0.7596	1.1027	0.5207	0.3431	0.1041

Table 25. Case 5: Validation for K_T

<i>Parameter</i>	<i>Uncorrected</i>		U_D	<i>Corrected</i>		<i>E</i> (%)
	U_{SN}	U_v		U_{SN}	U_v	
K_T	1.1372	2.7465	2.5	0.3538	2.5249	-3.9171

Table 26. Case 5: Grid Convergence Study for K_Q

<i>Parameter</i>	<i>EFD</i>	S_C	r_G	<i>Solutions</i>			R_G	$\delta_G(\%S_1)$	$U_G(\%S_1)$		$U_{GC}(\%S_1)$	
				S_1	S_2	S_3			<i>CF</i>	<i>GCI</i>	<i>CF</i>	<i>GCI</i>
K_Q	0.0279	0.02906	$\sqrt{2}$	0.02891	0.02876	0.02826	0.3	-0.51885	0.81534	0.27796	0.29649	0.055591

Table 27. Case 5: Validation for K_Q

<i>Parameter</i>	<i>Uncorrected</i>		U_D	<i>Corrected</i>		<i>E</i> (%)
	U_{SN}	U_v		U_{SN}	U_v	
K_Q	0.84485	2.6389	2.5	0.30722	2.5188	-4.1577

Table 28. Case 5: Grid Convergence Study for C_T

<i>Parameter</i>	<i>EFD</i>	S_C	r_G	<i>Solutions</i>			R_G	$\delta_G(\%S_1)$	$U_G(\%S_1)$		$U_{GC}(\%S_1)$	
				S_1	S_2	S_3			<i>CF</i>	<i>GCI</i>	<i>CF</i>	<i>GCI</i>
C_T	4.811	4.7885	$\sqrt{2}$	4.7553	4.7221	4.7156	5.1077	-0.69817	4.0007	1.0852	1.5663	0.21703

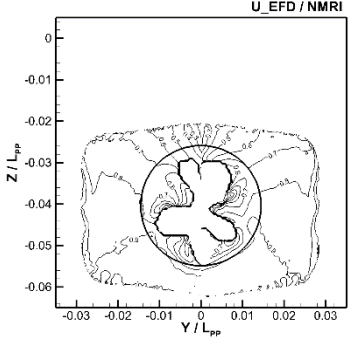
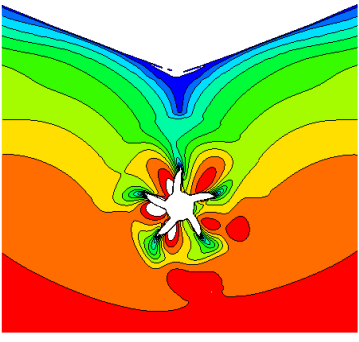
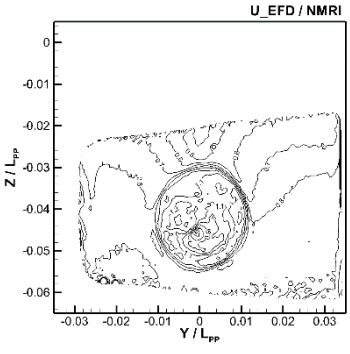
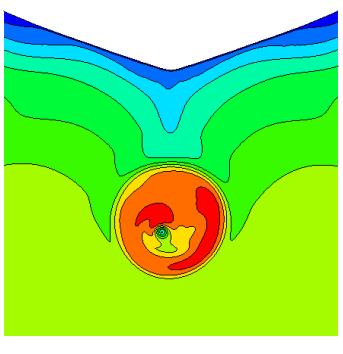
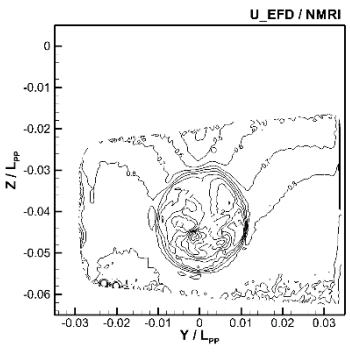
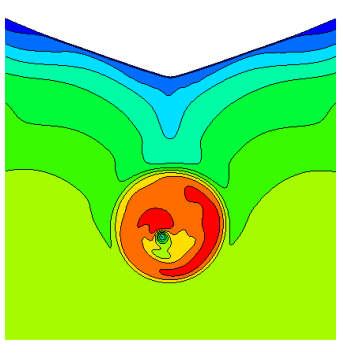
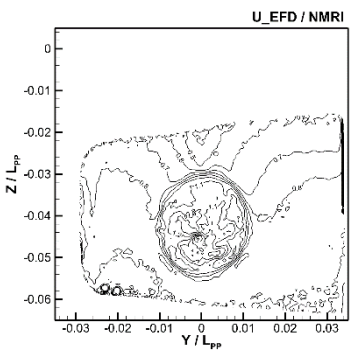
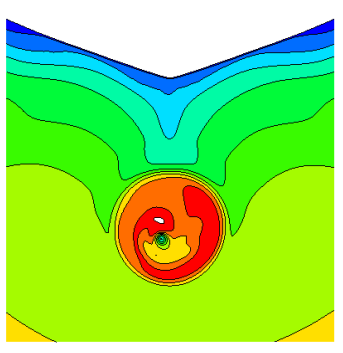
Table 29. Case 5: Validation for C_T

<i>Parameter</i>	<i>Uncorrected</i>		U_D	<i>Corrected</i>		<i>E</i> (%)
	U_{SN}	U_v		U_{SN}	U_v	
C_T	3.9544	4.6784		1.5482	2.9405	0.46768

Further validation was carried out by visually comparing wake contours (Table 30). As can be seen at the plane @ $0.0375L_{pp}$, the vortical structure, although not outlining the exact shape, is somewhat predicted. The wake contours seem to be well in agreement. Flow velocities near the hull surface are under predicted using CFD, especially at the AP plane. With regards to the planes to follow, comparison is not so easy due to the highly turbulent flow generated by the propeller itself.

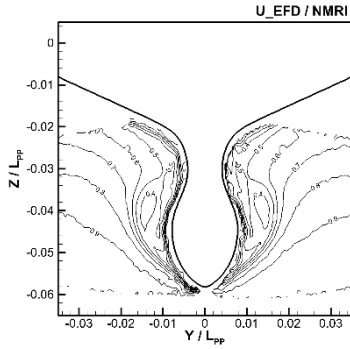
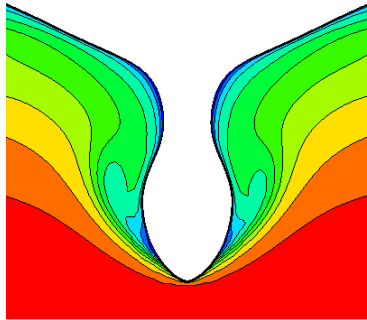
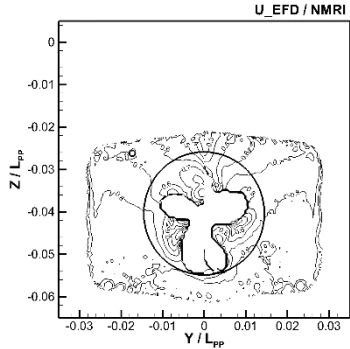
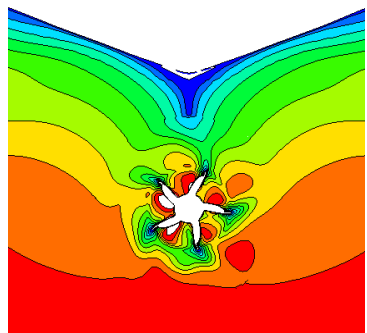
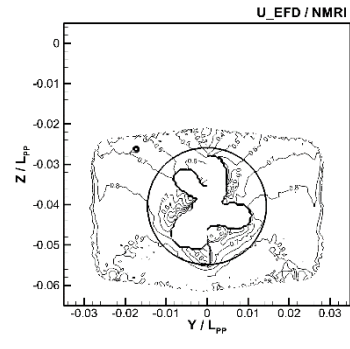
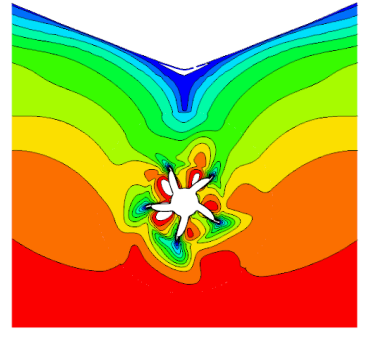
Table 30. JBC No Duct Wake Contour Comparison (*Self-Propulsion*)

		EFD	SST $k-\omega$ + CC
		(NMRI, 2015)	Velocity Wake Fraction[i] 0.00 0.20 0.40 0.60 0.80 1.0
PLANE @ 0.0375 LPP			
PLANE @ 0.0176 LPP	Blade Angle : 0 Deg		
PLANE @ 0.0176 LPP	Blade Angle : 24 Deg		

<p>PLANE @ 0.0176 LPP</p>	<p>Blade Angle : 48 Deg</p>		
<p>PLANE @ AP</p>	<p>Blade Angle : 0 Deg</p>		
<p>PLANE @ AP</p>	<p>Blade Angle : 24 Deg</p>		
<p>PLANE @ AP</p>	<p>Blade Angle : 48 Deg</p>		

This process was also carried out for the JBC with Duct at self-propulsion (Table 31). Similarly, at plane @ $0.0375L_{pp}$, the wake contours seem to be well in agreement. Once again, the separation or stagnation of flow at the hull surface is under predicted using CFD. Comparing at the other plans is not easy due to the highly turbulent flow. With regards to the wake contours; it is good to note that only the axial velocities at the three different planes have so far been presented. However, radial and transversal velocities have also been compared successfully. This was just a matter of presenting too much data.

Table 31. JBC w/Duct Wake Contour Comparison (Self-Propulsion)

		EFD	SST k- ω + CC
		(NMRI, 2015)	Velocity Wake Fraction[i] 0.00 0.20 0.40 0.60 0.80 1.0
PLANE @ 0.0375 LPP			
PLANE @ 0.0176 LPP	Blade Angle : 0 Deg		
PLANE @ 0.0176 LPP	Blade Angle : 24 Deg		

<p>PLANE @ 0.0176 LPP</p>	<p>Blade Angle : 48 Deg</p>		
<p>PLANE @ AP</p>	<p>Blade Angle : 0 Deg</p>		
<p>PLANE @ AP</p>	<p>Blade Angle : 24 Deg</p>		
<p>PLANE @ AP</p>	<p>Blade Angle : 48 Deg</p>		

4.5 Full-Scale Accuracy Comparison

With most of the case studies (modules) for this PhD work, which are being carried out in full scale scenarios, it would be useful to indicate that CFD is capable of predicting hydrodynamic performance at full scale conditions. However, full-scale validation of CFD is not so easy to carry out due to the lack of available or inaccurate full-scale data.

Although sea trial data gives a good indication on the powering performance, the processing of such data involves many assumptions and corrections leading to estimated result. An alternative approach to predict full-scale performance is the extrapolation of model scale experimental data (NMRI, 2015). There are various types of extrapolation methods with different organizations or institutes following different approaches as explained in (Suzuki et al., 2017). In a similar manner, these procedures involve many assumptions and empirical formulae such that the tweaking of a single parameter might slightly alter the results. That being said, such approaches have improved with knowledge and experience over the years and are well established within the marine industry. They are regarded as useful performance indicators.

Since the Japan Bulk Carrier (JBC) is a hull form that was developed for research purposes, there is no full-scale data available. Therefore, it was deemed appropriate to extrapolate the model scale data (NMRI, 2015) and compare them to two full-scale CFD predictions; one of the analyses was carried by the author of this thesis for the purposes of this research ('CFD Direct') and the other results ('Other Study') derived from an external study (Visonneau et al., 2016). The direct full-scale CFD approach developed by this study makes use of the RANSE SST k-w with Curvature Correction turbulence model whilst that of Visonneau et al. (2016) make use of a slightly different approach (AVLSMART scheme). Please refer to the respective publication for more details on the differences. For purposes of proper investigation, it was decided to compare four different data sets:

- Extrapolation or Powering of model-scale EFD data (NMRI, 2015)
- Extrapolation or Powering of model-scale CFD Results
- Full-Scale CFD Analyses (Direct)
- Full-Scale CFD Results from an external study (Visonneau et al., 2016).

Such analysis was able to provide an insight into the accuracy of full-scale numerical performance predictions and identify their limitations in general. Although the results from the

‘Other Study’ produced minor differences to ‘CFD Direct’, this provided additional insight and reliability into the capabilities of CFD solvers. Having more than one sample re-confirms the outcomes of the study.

The extrapolation procedures were carried out using the ITTC 1978 guidelines (ITTC, 1999) and a clear explanation of the process can be found in (Suzuki et al., 2017) . Without going into too much detail, the process follows ‘Hughes’ methods whereby a form factor was taken into consideration. Since the JBC is a slow speed high block coefficient vessel, the wave resistance was considered insignificant and excluded from the formulae. Furthermore, due to simplicity reasons, the form factor was assumed to be the fraction of the total resistance coefficient to the frictional resistance coefficient as stated in ITTC 1957. Since no roughness was simulated for any of the surfaces in the numerical computations, the roughness allowance (ΔC_f) was also assigned with a null value excluding any contribution of resistance due to surface roughness. With regards to the powering procedure, in order to compute the propulsive performance and respective parameters, the open water model scale data (i.e. propeller characteristics) were firstly extrapolated and corrected for scale effects according to the 1978 ITTC performance prediction method (ITTC, 1999). The extrapolated full-scale propeller open water propeller characteristics ‘(s)’ are presented and compared to the computed open water test results at full scale (Figure 51). Therefore, the extrapolated OWT results were used to compute the propulsive performance of the “CFD Model Powering” and the other for the “CFD Direct” respectively.

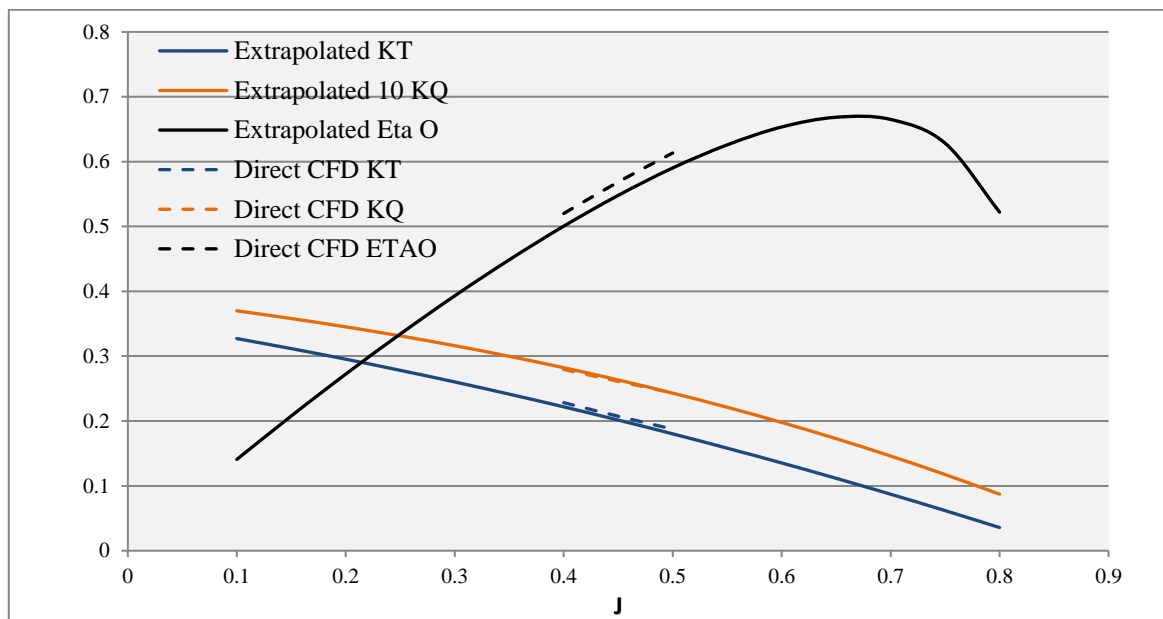


Figure 51. Full-Scale Propeller Open Water Characteristics

The correlation of the full-scale ship wake fraction was also computed using the ITTC method as demonstrated in (Suzuki et al., 2017). The end results were tabulated as follows. Table 32 presents the propulsive performance parameters at full scale for all four datasets whilst Table 33 compares the percentage differences of the power (DHP), thrust deduction term (1-t), mean velocity ratio (1-w) and propulsive efficiency (η_D) between the four. Please note that a positive % difference indicates overestimation whilst a negative implies the opposite.

Table 32. Powering Performance (No Duct)

<i>Parameter</i>	<i>Units</i>	<i>EFD Powering</i>	<i>CFD (Model) Powering</i>	<i>CFD DIRECT</i>	<i>Other Study</i>
V_s	<i>m/s</i>	7.46	7.46	7.46	7.46
Fn		0.141	0.141	0.141	0.141
Ct_m		0.004289	0.0041911	-	-
Cw		0	0	-	-
Cf_m		0.00314916	0.00314916	-	-
K		0.361	0.361	-	-
CT_s		0.001941	0.001941	0.001939	0.001928
R_t	<i>N</i>	1082386	1082386	1081514	1075600
EHP	<i>kW</i>	8071	8071	8064	8020
R_{sp}	<i>N</i>	-	-	1428975.0	1289100
t		0.196	0.202	0.24	0.17
$1-t$		0.804	0.798	0.758	0.834
T	<i>N</i>	1346251	1355615	1427610	1289163
CT		2.04	2.06	2.17	2.10
w_m		0.448	0.443	-	-
$1-w_m$		0.552	0.557	-	-
w_t		0.332	0.333	0.332	0.355
$1-w_t$		0.668	0.667	0.668	0.645
V_a	<i>m/s</i>	4.98	4.98	4.98	4.807
J		0.49	0.49	0.48	0.48
KT		0.1888	0.1946	0.1957	0.1892
KQ_{ow}		0.0249	0.0251	0.0251	0.0252
KQ_{bh}		0.0245	0.0258	0.0243	0.0252
η_o		0.5855	0.605	0.596	0.573
η_R		1.014	0.974	1.03	0.996
η_H		1.204	1.196	1.134	1.294
η_D		0.715	0.704	0.698	0.739
Q	<i>N-m</i>	1421083	1459008	1436940	1394254
P	<i>W</i>	11290231.02	11457008.02	11547528.62	10829242
N	<i>rps</i>	1.26	1.25	1.28	1.24
DHP	<i>kW</i>	11290.23	11457.01	11547.53	10855.04

Table 33. Propulsive Performance Comparison (No Duct)

<i>% Difference</i>	<i>EFD Powering</i>	<i>CFD (Model) Powering</i>	<i>CFD Direct</i>	<i>Other Study</i>
<i>EHP</i>	Base	0.00	-0.08	-0.63
<i>1-t</i>	Base	0.69	5.77	-3.77
<i>1-w_t</i>	Base	-0.10	-0.03	-3.49
<i>η_o</i>	Base	3.29	1.74	-2.10
<i>η_D</i>	Base	-1.46	-2.31	3.36
<i>DHP</i>	Base	1.48	2.28	-3.85

During this analysis, ‘EFD Powering’ was considered to be the base reference assuming that this approach is the most accurate since it is a commonly used and well-established method for performance prediction. That being said, many assumptions are involved, and the results are subject to minor tolerances. At first glance, it is demonstrated that ‘CFD Direct’ is overestimated by 2.28% whilst ‘CFD (model) Powering’ and ‘CFD Other Study’ are underestimated by 1.48% and -3.85% respectively. This gives us a general indication that CFD prediction at full scale is relatively accurate, on track and is heading in the right direction. However, it is unfair to base the performance just on the DHP value. As we know, this parameter is based and depends on other factors where percentage differences do not behave in a similar manner. Looking into this with greater detail will provide better insight to what extent this CFD method (‘CFD direct’) is able to predict the various parameters independently.

It is shown that the EHP is predicted very accurately at full scale by both direct CFD methods (0.08 % and 0.63%). This indicates that the numerical solvers are very good at predicting the resistance of slow speed bulk carriers without the presence of the propeller.

When introducing the action of the propeller there is an augment in resistance and this is represented by the ‘Thrust Deduction Term’ (1-t). Results indicated that the prediction error of the 1-t using CFD direct methods increased slightly. Considering that the vessel is moving at a constant speed with no acceleration, the thrust of the propeller has the same value as the resistance of the hull (with propeller action). This error therefore arises from the thrust difference between the data sets. Similarly, the mean velocity ratio (1-w_t), open water efficiency (η_o) and the propulsive efficiency (η_D) are fairly accurate. As can be seen from Table 33, the predictions of most propulsive parameters are within 5.5% error and can be considered fairly accurate.

Looking into further details, the discrepancy in the open water efficiency was further investigated. One can only compare the propeller efficiencies (possibly even at different loading conditions), if the propeller is producing the same characteristics i.e. comparing the same propeller geometry. We therefore investigated whether CFD is predicting the same propeller characteristics as the powering methods. Making use of ‘Momentum theory’, the ideal open water efficiency (blue line) was analysed and plotted on a graph (Figure 52). This line was corrected (due to losses not considered in momentum theory) to fit in line with the open water parameters of the powering methods. This line (blue line), therefore represented the open water curve for the propeller used in the powering methods. Similarly, another ideal efficiency curve (black line) was corrected to fit the open water parameters of the “Direct CFD” method. It was noted that the CFD powering open water performance (green bullet), was almost aligned with this black line thus indicating similar propeller behaviour between the CFD models at different scales. It turned out that different correction factors were used for both line fitting procedures and a discrepancy is evident between the two. This indicated that the propeller characteristics derived from the powering procedure are slightly different from those predicted using direct CFD methods. To be more precise, there is a 3% difference between the correction factors.

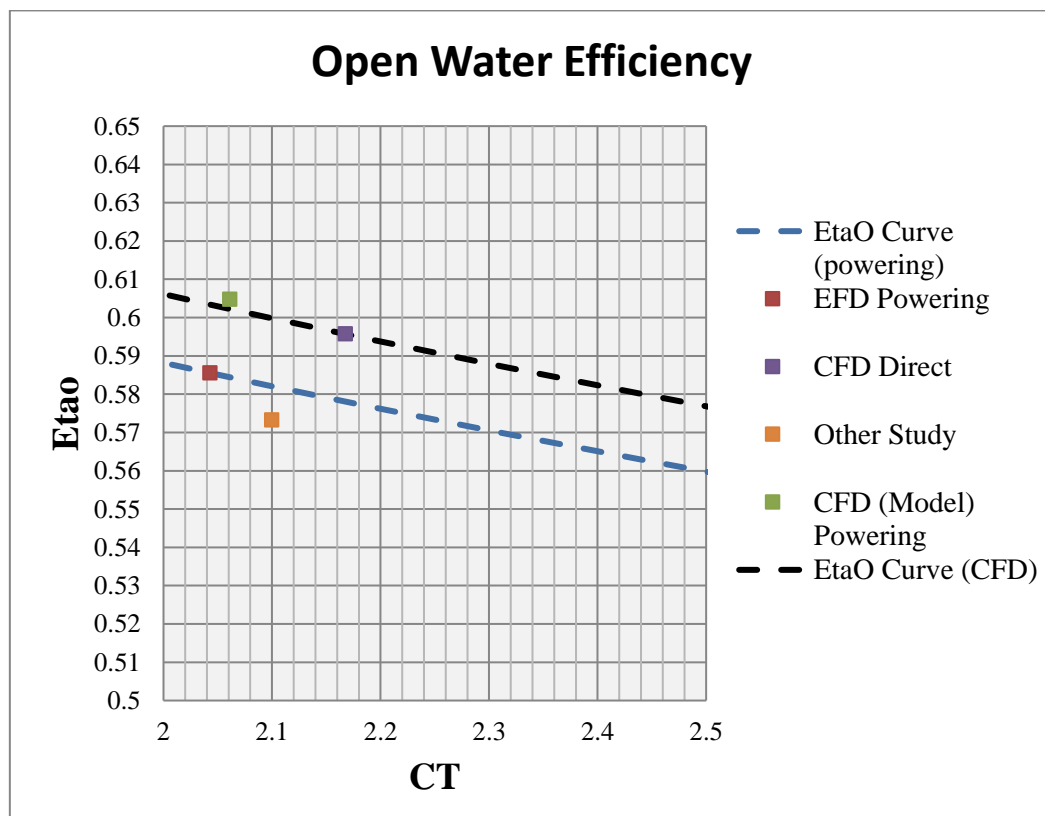


Figure 52. Difference in Propeller Characteristics

At this point, it was interesting to investigate the outcome of the performance if common propeller characteristics were used. The open water efficiencies for the direct CFD simulations were thus corrected to fit the Eta O powering curve as demonstrated in the Figure 53.

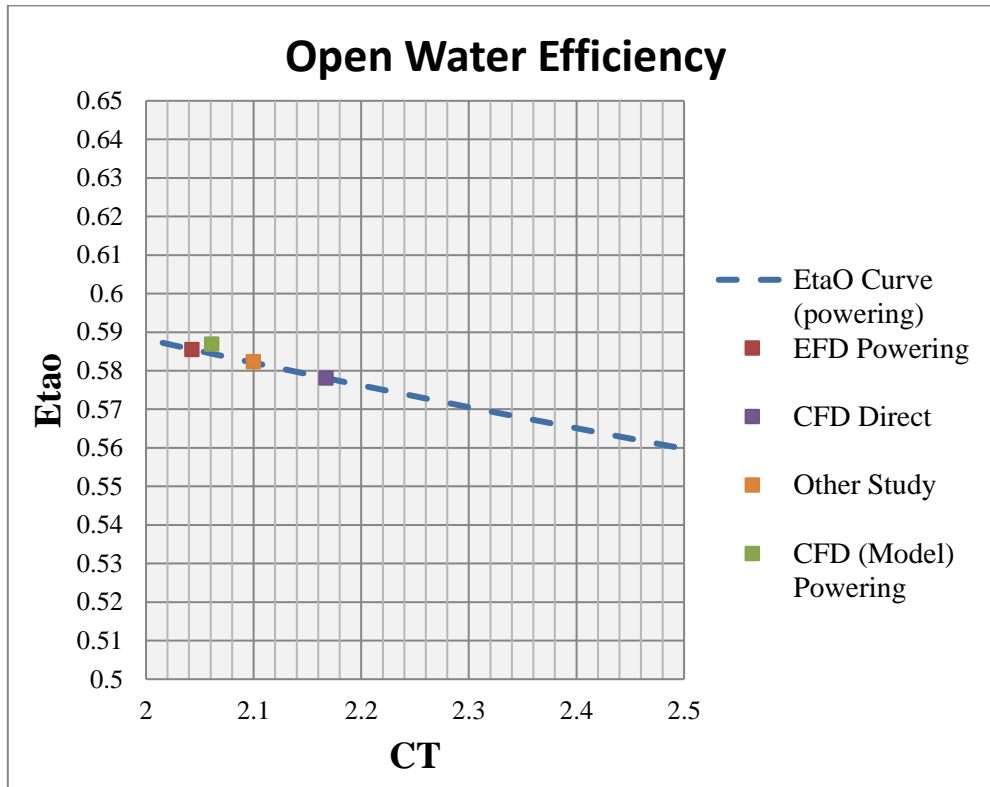


Figure 53. Common Propeller Characteristics

Table 34. Propulsive Performance Comparison Considering Common Propeller Characteristics (No Duct)

<i>% Difference</i>	<i>EFD Powering</i>	<i>CFD (Model) Powering</i>	<i>CFD Direct</i>	<i>Other Study</i>
<i>η_o</i>	Base	0.24	-1.27	-0.55
<i>DHP</i>	Base	-1.53	-0.75	-2.34

As presented in Table 34, if common propeller characteristics were to be utilised, performance prediction with ‘Direct CFD’ methods would improve. This resulted in a reduced open water efficiency (η_o) percentage difference and improved power prediction (DHP) accuracy (-1.53%, -0.75% and -2.34% respectively). For identical power performance, the conditions would ideally have the same CT and EtaO values. The difference in CT reflects the difference in hull efficiency i.e. thrust deduction fraction and wake fraction.

Similar analyses were carried out for the full-scale simulation with duct and the results and figures are tabulated as follows:

Table 35. Powering Performance (With Duct)

<i>Parameter</i>	<i>Units</i>	<i>EFD Powering</i>	<i>CFD (Model) Powering</i>	<i>CFD DIRECT</i>	<i>Other Study</i>
V_s	<i>m/s</i>	7.46	7.46	7.46	7.46
Fn		0.141	0.141	0.141	0.141
Ct_m		0.004263	0.0041716	-	-
Cw		0	0	-	-
Cf_m		0.00314916	0.00314916	-	-
K		0.383	0.383	-	-
CT_s		0.001972	0.001972	0.001980	0.001980
R_t	<i>N</i>	1104258	1104258	1104598	1104700
EHP	<i>kW</i>	8234	8234	8237	8237
R_{sp}	<i>N</i>	-	-	1477476.0	1384000.0
t		0.189	0.202	0.25	0.20
$1-t$		0.811	0.798	0.747	0.798
T	<i>N</i>	1361600	1383410	1479500	1384016
CT		2.49	2.45	2.60	2.86
w_m		0.501	0.530	-	-
$1-w_m$		0.499	0.470	-	-
w_t		0.391	0.381	0.380	0.428
$1-w_t$		0.609	0.619	0.620	0.572
V_a	<i>m/s</i>	4.54	4.61	4.62	4.268
J		0.45	0.46	0.45	0.43
KT		0.2007	0.2060	0.2073	0.2096
KQ_{ow}		0.0262	0.0261	0.0261	0.0271
KQ_{bh}		0.0260	0.0264	0.0253	0.0272
η_o		0.5527	0.581	0.569	0.533
η_R		1.009	0.992	1.03	0.995
η_H		1.332	1.290	1.204	1.394
η_D		0.743	0.743	0.708	0.739
Q	<i>N-m</i>	1430106	1437193	1464060	1394254
P	<i>W</i>	11083125.3	11080088.23	11636684.76	10829241.99
N	<i>rps</i>	1.23	1.23	1.27	1.22
DHP	<i>kW</i>	11083.13	11080.09	11636.68	11142.63

Table 36. Propulsive Performance Comparison (With Duct)

<i>% Difference</i>	<i>EFD Powering</i>	<i>CFD (Model) Powering</i>	<i>CFD Direct</i>	<i>Other Study</i>
EHP	Base	0.00	0.03	0.04
$1-t$	Base	1.58	7.94	1.58
$1-w_t$	Base	1.65	1.86	-5.98
η_o	Base	5.12	2.90	-3.64
η_D	Base	0.03	-4.73	-0.49
DHP	Base	-0.03	4.99	0.54

Table 37. Propulsive Performance Comparison Considering Common Propeller Characteristics (With Duct)

<i>% Difference</i>	<i>EFD Powering</i>	<i>CFD (Model) Powering</i>	<i>CFD Direct</i>	<i>Other Study</i>
<i>η_o</i>	Base	1.04	-1.09	-3.27
<i>DHP</i>	Base	-3.90	0.92	0.92

Therefore, in conclusion, the study indicates that CFD prediction of full-scale hydrodynamic performance is fairly accurate. Future investigation should focus on improving numerical propeller performance in full-scale environments. The author believes that significantly refining the mesh in the propeller region will contribute to the task.

Despite all this, the direct full scale CFD prediction method can be regarded as a good approach to analyse different hull designs and identify best design candidates. One must keep in mind that absolute values can have a slight discrepancy as demonstrated in this chapter. However, considering that the same CFD approach is used, this prediction error is consistent throughout all the simulations and therefore behaviour in trends with regards to vessel performance between different designs can be clearly identified.

With this in mind, this CFD method ('CFD Direct') will be used to carry out various case studies such as the investigation of ESD function at different scales and the analyses of various ESD combinations. With regards to the former, the JBC hull with an installed duct will be analysed at full-scale. Furthermore, various ESD combinations are to be installed on a different bulk carrier (RSBC) and investigated. What automatically comes to mind, is why not investigate the various ESD devices at model scale and extrapolate the performance just like the approach demonstrated in this study? Although this is a good solution for traditional hull forms and designs, extrapolation of the results (or powering) when retrofitting technologies (ESD) are involved is not so straightforward. Although correlation procedures that take ESD into consideration have been developed (ITTC, 2011b), these were not found to be accurate and reliable thus requiring the actual investigation of the performance at full scale, such as the 'CFD Direct' approach.

4.6 Chapter Summary and Conclusion

This chapter presents the high-fidelity numerical simulations used to carry out the different case studies for this thesis outlining the physics, grid topology and validation and/or verification results for:

- Open Water Test Simulations
- Towing Test Simulations and
- Self-Propulsion Simulations

All three methodologies have been used to carry out the investigations required in the different modules of this study. Advanced and well-established validation and verification procedures have been carried out on baseline geometries exhibiting monotonic convergence with good accuracy. Geometries with retrofitted technologies were additionally validated and compared to experimental data also indicating satisfactory agreement.

Furthermore, this chapter highlights the weaknesses of traditional eddy-viscosity models (EVM) which are unable to accurately capture wake characteristics. It also demonstrates the benefits of the recently introduced novel curvature corrected (CC) turbulence models. The CC feature is shown to improve the wake characteristics significantly.

To the best of the author's knowledge, there is currently no published literature demonstrating validation and verification procedures with the use of the curvature corrected turbulence model in the marine industry. This chapter contributes to knowledge in the shipping industry by carrying out well established validation and verification procedures with the use of the CC $k-\omega$ turbulence model. This feature has been widely used in the aeronautical industry but has not yet been properly introduced and implemented in marine applications.

Following the satisfactory validation and verification results, together with the improved flow prediction characteristics, it is clear that the implementation of the curvature correction turbulence model is a step in the right direction for wake prediction at no significant expense. This model is a good compromise compared to the higher fidelity solver that requires higher computational power, the Explicit Algebraic Reynolds Stress Model (EARSM), that has also been demonstrated for wake prediction by Visonneau et al. (2016). The model allows greater flexibility for CFD engineers who can use the CC model to analyse flow at both model and full-scales scenarios for many design variants.

Wake flow prediction improvements have been clearly identified and compared with experimental data at different planes and locations. The use of the CC model had no adverse effect on the resistance results but improved the accuracy of trim and sinkage magnitudes. Additionally, the refinement of the free surface resulted in enhanced accuracy of wave cuts at different positions from the centreline.

In terms of recommendations for future research, it is clear that the application of the verification and validation procedures for the ESD retrofitted hulls would provide further insight into the accuracy of the solver when studying Energy Saving Devices. However, this would require running double the number of simulations that was not possible within the available time frame. Moreover, refining the mesh for the full-scale test cases should improve flow prediction characteristics and this requires further investigation. For the development of the full-scale simulations, the model-scale grids were scaled uniformly in accordance with the scale ratio. Hence the size of the mesh elements was increased respectively. However, it should be noted that fluid characteristics cannot be scaled and therefore the elements might be too big to capture all the required flow details. This would in turn require the same element sizes for the model-scale simulations to be applied to the full-scale domains generating significantly large grids that are too computationally expensive, impractical and not feasible with the available computational power. With advancements in high performance computing in due time, this could be less of an issue and should also be investigated.

In summary, this chapter successfully presents the methodology for the numerical models used to carry out the different case studies and investigations outlined in the following chapters. It also demonstrates the beneficial use of a modified turbulence model, as opposed to the traditional methods, to provide improved wake prediction capabilities.

5 Hull-Propeller Performance Analysis

Techniques

5.1 Introduction

A list of techniques and methods for analysing the hull-propeller interaction of a vessel was developed. Some of the methods investigate the overall performance while others analyse the flow interaction providing the engineer with a detailed understanding of the science. Other than just predicting the overall beneficial or detrimental impact, justifications and explanations behind such outcomes are equally important. The aim of this chapter is to enhance the understanding of flow interaction and what brings about the benefits. Therefore, this chapter outlines detailed and in-depth techniques to analyse hull-propeller interaction. One that was designed and developed through personal experience and methods from the literature that were deemed to be appropriate, relevant and advanced. Some or most of the techniques/methods outlined in this chapter will be used in the case studies presented in the chapters to follow. The selection of analyses would depend on the nature of the study in question.

5.2 Hull-Propeller Performance Analysis Techniques

The various methods are listed and outlined in Table 38. Each section is briefly described and explained.

Table 38. Hull-Propeller Analysis Techniques

1.	Overall Performance Analyses
2.	Force Components Breakdown (Drag, Lift between Different Components)
3.	Wake Analyses (Before and After Propeller)
4.	Criteria: BSRA + PEV Criteria
4.	Local Flow Analyses: Pressure distribution, Streamlines, Separation
5.	Energy Balance

1. Overall Performance Analyses

Initially, the net performance is analysed by comparing the thrust, torque, rpm and other global parameters together with the resultant delivered power. As shown in Eq. (34), this is broken down into various components of the propulsive efficiency (η_D) in order to identify where the impact is originating from.

$$\eta_D = \eta_H \times \eta_O \times \eta_R \quad (34)$$

Where, η_H represents the hull efficiency, η_O the open water efficiency and η_R the relative rotative efficiency.

2. Force Components Breakdown

The forces and moments between the different parts of the vessel, (e.g. hull, propeller, duct, PBCF) are also identified individually. This gives an indication to how different components are performing and how they contribute to the performance of the vessel.

3. Wake Analyses

A wake analyses tool (WAT) (Maasch et al., 2019) is used to visualise, analyse and extract wake values before and aft of the propeller. The Taylor wake fraction and the wake non-uniformity are both computed at the different planes. The differences in the wake properties can be then discussed between the different variants. Please refer to the work carried out by Maasch et al. (2019) for more details regarding the WAT tool.

4. BSRA Criteria

The hull-propeller interaction was then analysed to investigate the quality of the wake together. This was carried out using the well-established BSRA (The British Ship Research Association) criteria developed by Odabasi and Fitzsimmons (1978).

The WAT is made available for open access allowing further developments from any third-party user. The author has contributed in extending the functionality of the WAT tool to evaluate the wake quality by using the well-established BSRA criteria. These criteria give an insight into the wake quality indicating whether it can be considered satisfactory to meet certain standards. Such empirical methods provide good wake assessment making them ideal during ship design procedures. The BSRA (The British Ship Research Association) criteria, were developed by Odabasi and Fitzsimmons (1978) who extended Huse (1974) work to develop criteria to assess for any potential propulsion or vibrations problems. Odabasi and Fitzsimmons outline five wake quality criteria which have all been implemented into the WAT tool. The criteria have also been published by Maasch et al. (2019) who presented the criteria from Odabasi and Fitzsimmons (1978) as follows:

1. The first criterion states that within the angular interval φ_B and in the range of dimensionless propeller radii $\frac{r}{R} = 0.4 - 1.15$, the maximum measured wake w_{max} should be smaller than either 0.75 or the ship block coefficient c_B , whichever is smaller (35).

$$w_{max} < (0.75, c_B)_{min} \quad (35)$$

2. The second criterion states, that the maximum acceptable wake peak on the measured wake disc should not exceed 170% of the measured mean wake at the effective non-dimensional propeller radius $\frac{r}{R} = 0.7$ (36).

$$w_{max} < 1.7 \bar{w}_{0.7} \quad (36)$$

3. The third criterion analyses the width of the wake peak and relates it to the width of the wake shadow area. The wake shadow area (see Figure 54), also known as the wake shadow angle (φ_B), is a particular area of interest in the wake field that is susceptible to cavitation where a wake peak is likely to occur and the propeller is subject to heavy

loads. This wake shadow area range is defined as a function of the propeller blade number and lies about the top dead centre. For more details please refer to the article by Odabasi and Fitzsimmons (1978). After analysing whether the measured wake distribution at the non-dimensional propeller radius $\frac{r}{R} = 1.0$ consists of a single wake peak with its maximum at $\varphi = 0^\circ$ or of a double weak peak (see Figure 55) the width of the peak gets measured by finding the intersection of the wake minimum and the maximum absolute wake gradients before and after the peak. Hereby the width of the measured peak should be larger than the wake shadow area to avoid high gradients within the wake shadow area (37).

$$\varphi_B > (\varphi_{max})_{1.0} \quad (37)$$

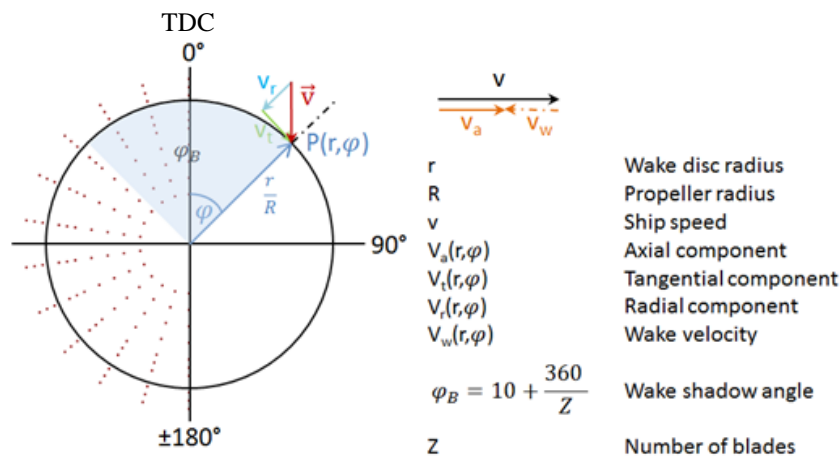


Figure 54. Wake Shadow Area (Maasch et al., 2019)

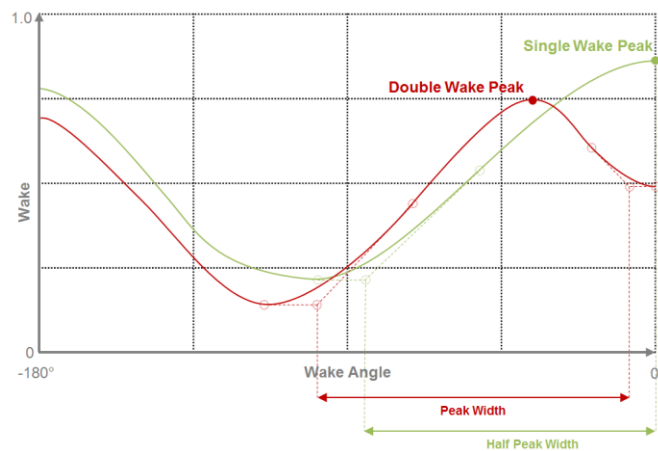


Figure 55. – Single and Double Wake Peak Width Definition

4. The fourth criterion estimates the excitation forces on the hull by relating the tip cavitation number (38) and the wake non-uniformity at the non-dimensional propeller radius $\frac{r}{R} = 1.0$.

$$(\sigma_{nl})_{1.0} = \frac{P_a - P_v + P_I}{0.5 \rho (\pi ND)^2} \quad (38)$$

$$P_I = \rho g H_i \quad (39) \quad H_i = T_A - \left(\frac{D}{2} + Z_p \right) \quad (40)$$

The corresponding intersection point of the wake non-uniformity $(w_\Delta)_{1.0}$ and the cavitation number $(\sigma_{nl})_{1.0}$ should lie above the dividing band in Figure 56, originally provided by Odabasi and Fitzsimmons. The non-dimensional averaged wake non-uniformity $(w_\Delta)_r$ (41) gives a measure for the extent of the velocity variation on each radius.

$$(w_\Delta)_r = \frac{\Delta(w)_r}{1 - (\bar{w})_r} \quad (41)$$

The maximum wake variation Δw (42) and the average wake \bar{w} on each radius (43) are defined as follows.

$$\Delta(w)_r = \left(1 - \frac{v_a}{v} \right)_{r,max} - \left(1 - \frac{v_a}{v} \right)_{r,min} \quad (42)$$

$$(\bar{w})_r = \left(1 - \frac{\bar{v}_a}{v} \right)_r \quad (43)$$

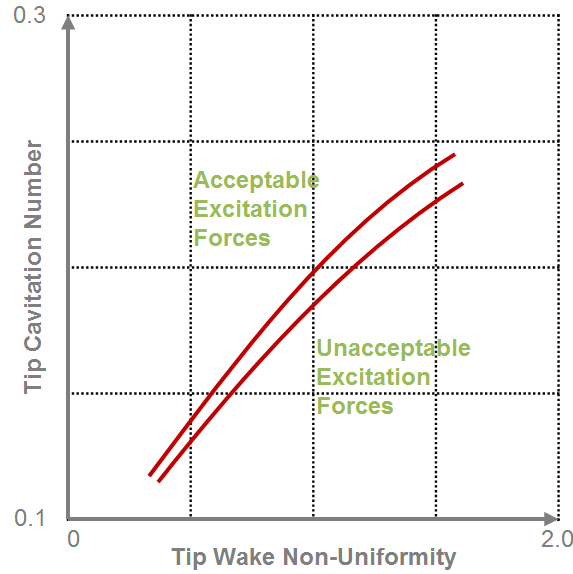


Figure 56. - Wake Non-Uniformity Criterion reproduced by (Carlton, 2007) with Permission of (A Yucei Odabasi and Fitzsimmons, 1978)

5. The fifth criteria only needs to be checked if the fourth criterion returns an intersection point that falls within the dividing band of Figure 56. This would indicate that the propeller is susceptible to cavitation. In this case the local wake gradient per unit axial velocity for all measured radii $\frac{r}{R}$ inside the angular interval φ_B in the range of $\frac{r}{R} = 0.7 - 1.15$ (44) should be less than unity.

$$\frac{1}{r/R} \left| \frac{dw/d\varphi}{(1-w)} \right| < 1.0 \quad (44)$$

The WAT interface has also been extended to allow the user to input the properties required for computation of the criteria and to display the results by stating whether the criteria was fulfilled or not as depicted in Figure 57. The WAT tool is now able to evaluate the wake properties but also the wake quality which is a very useful in hull-propeller interaction studies

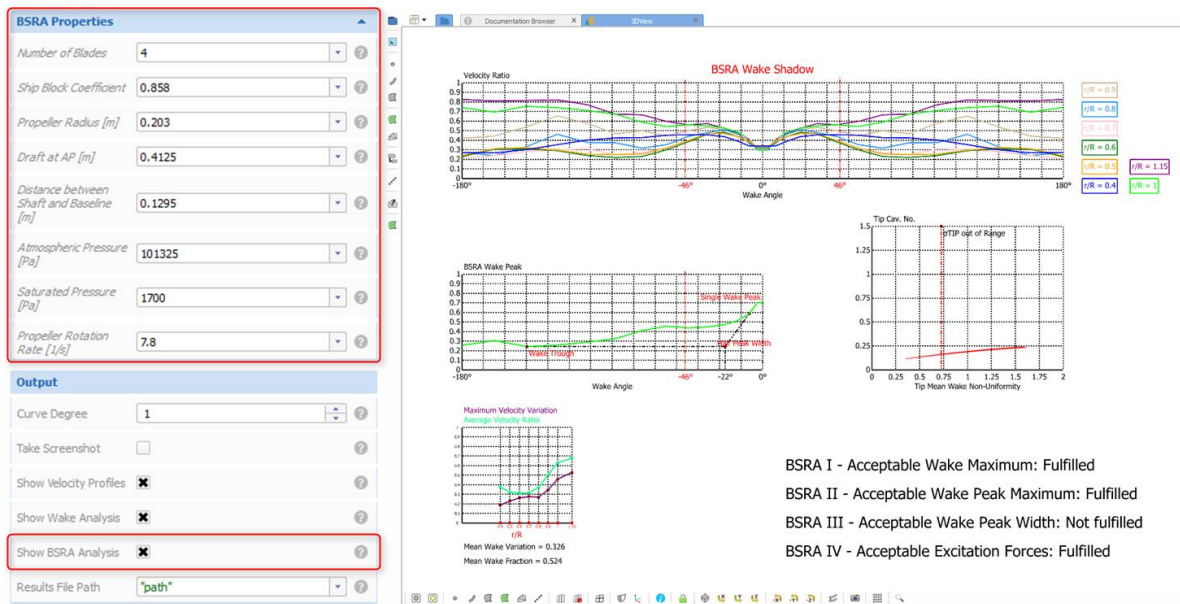


Figure 57. BSRA Output

5. Local Flow Analyses

Post-processing measures were also carried out to assess and visualise different criteria on the different parts of the vessel (e.g. propeller, hull etc.). Pressure distribution analyses over the geometry parts identified regions of pressure drops giving indications of force directions. In addition, streamlines were computed to simulate the flow action and interaction with the components giving a better understanding of the flow behaviour. Wall shear stress and skin friction parameters were used to identify any separation of flow on the hull or Energy Saving Device (ESD). These criteria and analysis will be demonstrated using visual figures and discussed accordingly shedding light into the understanding of propeller–hull interaction flow behaviour.

6. Energy Balance

When investigating the performance of a vessel or its efficiency, it is vital to understand where the losses are originating from. Schuiling and Terwisga (2016) demonstrate a procedure for identifying marine energy loss components in a propulsion system. Such a method is also very useful to identify the function and working principles of energy saving devices (ESD) by identifying the source of the energy recovery within a control volume. The concept is based on the principles of conservation of energy outlining that the propeller has three main losses; namely axial, rotational and viscous. This idea was introduced by Dyne (1995) and later

adopted by Lee et al. (2012) and Terwisga (2013) by making use of energy analyses to investigate the working principles of Energy Saving Devices. Full details of the method can be referred to in the work carried out by Terwisga (2013). This approach can be used to investigate the energy loss components of the hull-propeller interaction system in accordance with equation (45) and the results displayed in a pie chart format as depicted in Figure 58, where the energy losses between different variants can be compared and identified in a user friendly output.

$$\eta_o = \frac{P_{useful}}{P_{delivered}} = 1 - \frac{Losses}{P_{delivered}} = 1 - \frac{AXL}{P_{delivered}} - \frac{ROTL}{P_{delivered}} - \frac{VISL}{P_{delivered}} \quad (45)$$

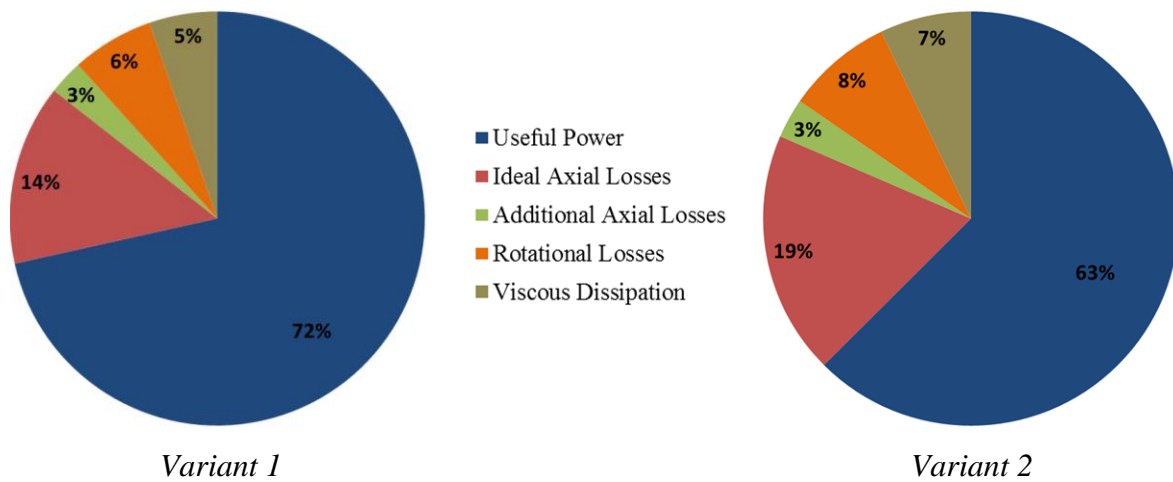


Figure 58. Energy Components Results Format

A simplified approach based on the above methodology was further outlined by Dang et al. (2015). In contrast to measuring the energy within a control volume, the energy was measured across a plane aft of the propeller. This can provide an indirect but easy assessment on the propulsive efficiency and velocity fields. All the theory and details can be referred to in the article by Dang et al. (2015), who simplify the total kinetic energy losses into axial and transverse losses. Comparing the kinetic energy losses between different variants aft of the propeller, may provide an indication or information on the energy saving. This methodology was thus adopted and carried out to investigate the energy loss components of the hull-propeller interaction system by highlighting the axial and transverse losses.

5.3 Chapter Summary and Conclusions

This chapter describes and outlines the necessary procedures and methodologies to analyse the performance of a hull-propeller system and interaction of flow. For the purpose of this thesis, these methods will be used for the various case studies presented in the chapters to follow. Most of the methods will be utilised to analyse the performance of vessel designs and ESD configurations.

6 Hull-Stern Optimisation

6.1 Introduction

This chapter demonstrates a developed state-of-the-art hull stern form optimisation procedure providing valuable insight into the hull –propeller interaction of a vessel. More specifically, a multi-objective optimisation procedure of a vessel in towing test conditions is carried out to investigate the relations between drag and wake quality parameters. Shortlisted optimal candidates are further analysed in self-propulsion conditions providing valuable information into whether the towing simulations can provide any sort of insight into propulsive performance behaviour when taking into consideration the wake quality.

This study contributes to the body of knowledge of hull-propeller interaction by understanding whether such a process can provide a feasible alternative to computationally expensive optimisation of full-scale vessels in self-propulsion conditions. Furthermore, it investigates whether the quality of the nominal wake can give any indication on the respective propulsive performance.

In view of the impractical and demanding full-scale numerical optimisation procedures, it was deemed necessary to find an alternative solution that can provide a reasonable compromise. With the available current methods, optimisation processes are generally carried out in model-scale environments. These methods, however, fall short of accurately predicting the actual performance and impact at full-scale. With the expansion in computational power and advancements in CFD techniques (now also allowing enhanced wake prediction as demonstrated in chapter 4), the next natural step would be to venture into numerically analysing vessels in full-scale environments and in self-propulsion conditions providing more realistic and meaningful information.

As previously mentioned, such sophisticated methods require significant computational power, making optimisation procedures very expensive and impractical. There is a need to develop a smart and feasible process to optimise the performance of a vessel using less demanding full-scale towing simulations.

It is generally understood that towing tests are only able to provide information on the drag of the vessel giving no indication on the propulsive performance. Consequently, towing ship

optimisation procedures generally aim to reduce the resistance without aiming to improve the wake quality in the process. It is known that the wake characteristics before a propeller have a big influence on the propulsive performance (η_D) of a vessel and related parameters appear as the hull efficiency (η_H), relative rotative efficiency (η_R) as well as the open water efficiency (η_O). Therefore, it would be interesting to investigate whether the nominal wake can give any indication/relation to the propulsive performance and if so, the extent of the impact. It was therefore decided to carry out a multi-objective optimisation procedure in full-scale towing conditions to improve the drag but to also improve the wake characteristics. Variants with different drag and wake parameters would be then further analysed in self-propulsion tests and their performance compared to each other.

This chapter describes and outlines all the necessary procedures and methodologies to carry out the different phases of the case study in Module 5, presenting the different components of the optimisation framework and analyses methods. Results are then discussed, and findings are clearly outlined.

6.2 Optimisation Procedure Outline & Methodology

6.2.1 Procedure Process Outline

The overall study involves two parts, whereby the process is initiated with an optimisation procedure to improve the performance in towing conditions. This is followed by analysing a few of the best candidates in self-propulsion conditions. The initial study demonstrates a state-of-the-art multi-objective stern form optimisation of a full-scale bulk carrier in towing conditions with the aim of improving the hydrodynamic performance of the vessel (primary objective) but also reducing propeller excited vibrations (secondary objective). The process was carried out using a coupled framework (Figure 59) on a High-Performance Computer (HPC) integrating the parametric modeller to generate the design variants, a CFD solver to evaluate the performance and an optimisation algorithm that optimised the design candidates. The RSBC vessel was parametrically modelled and developed using (CAESES®) software. This set up allows the automatic generation of various design candidates that were then solved in full-scale towing conditions using Reynolds-Averaged Navier-Stokes (RANS) equations to simulate the hydrodynamic flow. The optimiser then processed the results and generated the next set of parameters for the new design candidate.

The study was initiated by carrying out a multi-objective optimisation designed to reduce the resistance of the vessel, reduce the wake non-uniformity and increase the wake fraction of the vessel. It is commonly known that seeking to increase the wake fraction is not necessarily beneficial to the propulsive efficiency. Since this parameter, wake fraction, forms part of the hull efficiency as well as the open water efficiency, a compromise should be sought. However, since we are solely dealing with towing test cases for the optimisation process, hence dealing with hull efficiency, it would be best to try and increase the wake fraction. Furthermore, lower energy consumption is a priority at this stage and when dealing with slow speed ships, such as the RSBC, pressure excited vibrations are considered as a secondary issue.

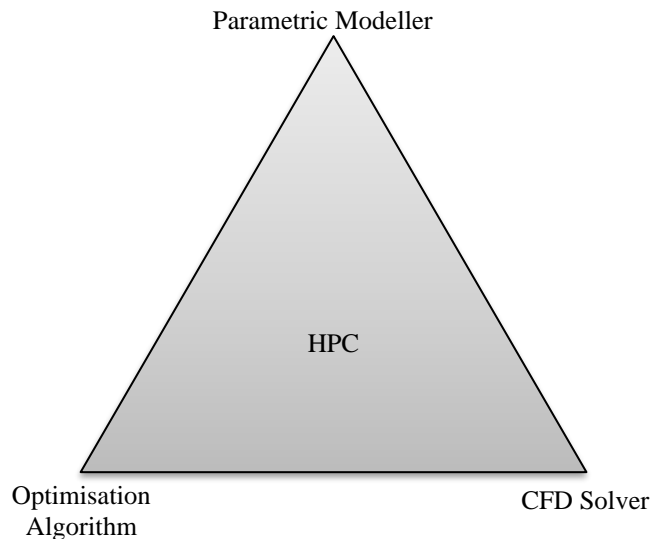


Figure 59. Coupled Optimisation Framework

Parametric Modeller

An optimisation process requires a meaningful model that is defined by the use of parameters in order to allow the automatic generation of the geometry. Parameters of interest, ones that are generally associated with the area under investigation, are then assigned as design variables. These are controlled and automatically altered by the optimisation algorithm to generate new variants. The RSBC was thus parametrically developed and designed from scratch, enabling the surface geometry to be implemented in the framework. With this study seeking to improve the performance of the vessel by optimising the stern form, relevant design variables were selected accordingly. Details of parametrically designing the ship together with the selection of design variables can be found in section 5.2.2.

CFD Solver

The generated surface geometry from the parametric modelled is then evaluated in a towing test numerical model representing a full-scale environment. The CFD simulation and methodology, together with the validation and verification of the process, has been demonstrated in Chapter 4. The absence of the propeller resulted in a symmetrical environment about the ship centreline, thus only requiring the simulation of half the domain. This led to savings on computation power and time, allowing the analyses of more design variants. Each candidate was analysed using the CFD model to solve the physics and fluid flow until the results converged.

Analyses

Once each simulation run is complete, the procedure is set to automatically carry out the analyses and read the results. The drag is directly read from a report that is outputted from the CFD solver. However, the wake velocities that are read from a report are then processed using the WAT tool in order to compute the wake fraction and wake non-uniformity. More details on the WAT tool are explained in section 5.2.3. The results are then fed into the optimiser for evaluation and a new design variant is generated based on the results.

The Optimisation Process

The optimisation process for this study follows an approach outlined by Harries (2015) that constitutes of two consecutive phases; exploration and exploitation. The former involves the examination of the design space identifying promising design candidates. This is followed by exploitation, where those candidates are then optimised to further improve their performance or meet their subsequent objectives.

A sobol sequence was used to carry out the exploration of the design space using a quasi-random approach. This is a deterministic algorithm of a quasi-random low-discrepancy sequence that produces a random but somewhat deterministic pattern over the design space. Further details regarding this methodology can be found in Chapter 6 where the sobol sequence was also utilised for the optimisation process.

The optimisation algorithm used for this study was based on a response-surface based method by using the Dakota toolkit developed by Sandia National Laboratories (Adams et al., 2017). This plug-in is readily implemented in the CAESES software providing a wide variety of state-of-the-art numerical methods. The Dakota model was developed to provide a systematic and efficient way of identifying optimal designs.

This method makes use of response surfaces that are surrogate models that represent a real engineering problem saving significant computational time. Surrogate models are considered to be an effective and efficient compromise to the more expensive high-fidelity models where the process involves data fits, multi-fidelity procedures and reduced order model surrogates.

The numerical optimisation method for this study was carried out using the surrogate-based global minimisation or the global optimisation using the response surface. A Multi-Objective Genetic Algorithm (MOGA) approach is used on a response surface that is generated from

several design candidates. This is then updated with every iteration based on the new designs producing a new response surface. The surrogate model is used to exploit the variations in performance response of design variants via a surface fitting method over a design space.

The initial response surface, as was used in this study, could be extracted from a previous run to generate the first surrogate model. For our case study, the designs that were previously evaluated from the Sobol sequence were then used to build the first response surface. After each iteration, the designs produced from the MOGA run were then added to the pool of candidates and a new surface response is developed based on the new list. The tool processes the data and makes use of relevant data fits and interpolation to identify promising design candidates, thus reducing the number of expensive simulations required.

The Sobol engine was used to generate a total of 40 independent variants producing a quasi-random scatter over the design space. Each design was run in the pre-defined CFD environment to predict the drag, wake fraction and wake non-uniformity. This process was followed by a multi-objective optimisation procedure using the Dakota tool to utilise the surrogate-based global minimisation numerical model. Results from the Sobol sequence (40 Designs) were used to create the initial response surface of this method. The surrogate model was then iterated 5 times producing 3 new design candidates per iteration. An additional 15 variants were thus generated for this phase of the study. In summary, a total number of 55 Ship designs were tested at full-scale in towing conditions.

The results from the optimisation process were analysed and discussed. Three of the design candidates were shortlisted and analysed in self-propulsion conditions to predict their actual performance. The selection was based on their different characteristics in towing conditions. The CFD model used at this stage was also presented in Chapter 4 of this thesis (RSBC full-scale self-propulsion). Their performance was analysed using some of the pre-defined 'Hull-Propeller Interaction Analyses'.

6.2.2 Parametric Ship Modelling

When dealing with optimisation procedures for CFD, we require models that are defined by means of descriptors or meaningful information. These so-called parametric models would allow for the generation of different variants that are defined by a number of parameters.

As described by Harries et al. (2015)), these models can either be fully-parametric or partially-parametric. As the name suggests, full-parametric modelling allows full flexibility when it comes to the modification of the model. The entire geometry is defined by parameters that describe the model that can be altered to generate variations.

On the other hand, partial parametric modelling does not allow such freedom. The methodology is based on the modification of an existing shape or surface that has no meaningful information to describe it. The outcome is a series of variants that are evolved from the baseline model and reflect the parent design to some degree. Shift transforming a surface is a typical partial-parametric modelling method that is used in the marine industry.

In order to allow thorough variation of the bulk carrier, the RSBC ship was fully parametrically modelled using Friendship Systems software, CAESES (Friendship Systems). The ship was modelled following directions, methodologies and best practices as highlighted by Friendship Systems. This means that RSBC model was developed from scratch with the use of meaningful parameters in order to replicate the form of the actual vessel.

The ship geometry was developed using the MetaSurface approach (Harries et al., 2015). The concept is based on a surface that is defined by a curve definition in one direction. The other direction of the surface is then controlled by varying the input parameters of the curve definition, thus varying the form of the curve definition along that direction.

A parametrically modelled simple case foil followed by basic ship geometry will be explained for ease of understanding. Figure 60 demonstrates a foil surface that is defined by a curve definition, as indicated in the diagram. This curve definition represents the cross-section shape of the foil and is controlled by parameter P1 (chord length) that varies along the length of the foil accordingly. This implies that the curve definition form changes along the length of the geometry. The parameter distribution indicates that the chord length (P1) of the foil reduces as it moves towards the tip. The end result is a generated metasurface in the shape of a fin.

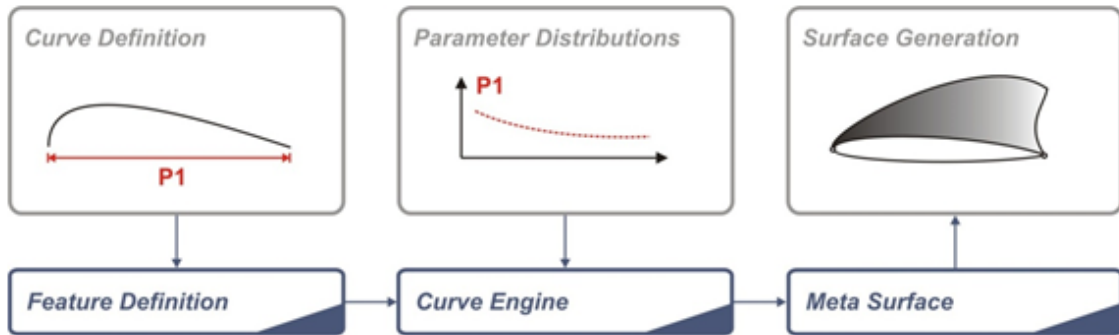


Figure 60. Parametric Foil

In a similar manner, if we take into consideration the modelling of a simple hull ship geometry. The midsection of the vessel can be easily defined using three curves as indicated in Figure 61. The start and end of each curve is defined by parameters whereby X_{pos} is the unit length of the vessel, $DeckZ$ and B are the height and width of the vessel respectively while FOB_Y is the width of the flat of bottom and FOS_Z is the height where the flat of side surface starts. Some of these parameters are considered to be constant along the length of the vessel such as $DeckZ$ whereas other parameters (e.g. $DeckY$) are a function of x_{pos} and vary along the vessels length as indicated in Figure 61. Taking $DeckY$ into consideration, the parameter is reduced at the stern reaching maximum width towards the middle section and reduces to 0 at the bow making surface ends met.

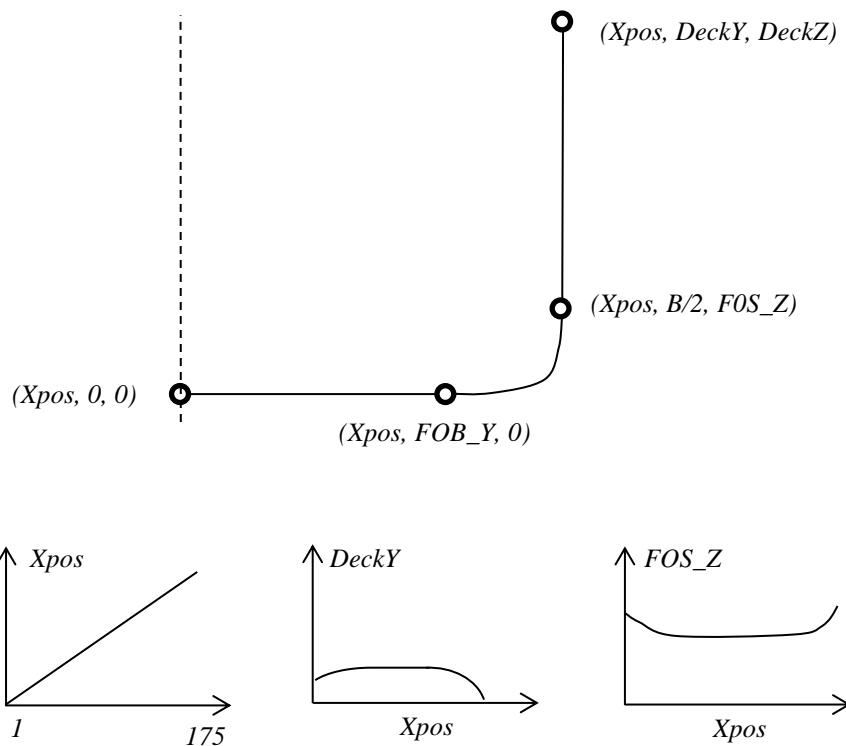


Figure 61. Basic Ship Curve Definition & Parameter Distribution

The Real Ship Bulk Carrier was developed using a similar approach with more detail and sophistication providing more parameters and design variations. The complex geometry of the vessel did not allow the model to compromise of one metasurface, but of various connecting surfaces producing a watertight geometry. Quite a few parameter distributions and curve definitions were required. Figure 62 demonstrates the schematic diagrams that represent the parameter distributions and the different number of metasurfaces that are represented by the different colours. Since the ship is modelled using numerous metasurfaces, that might not share information with one another, it was made sure that the surfaces were designed in a way to produce the best possible seamless and smooth connection.

The availability of ship form data, such as lines plans and IGES geometry provided a base reference to map and trace curve definitions and parameter distributions. Some parameters were modelled to control the endpoints of the curves in the x, y, z co-ordinates while others were developed to control the area under the curve allowing shape or form modifications within the same ship particulars.

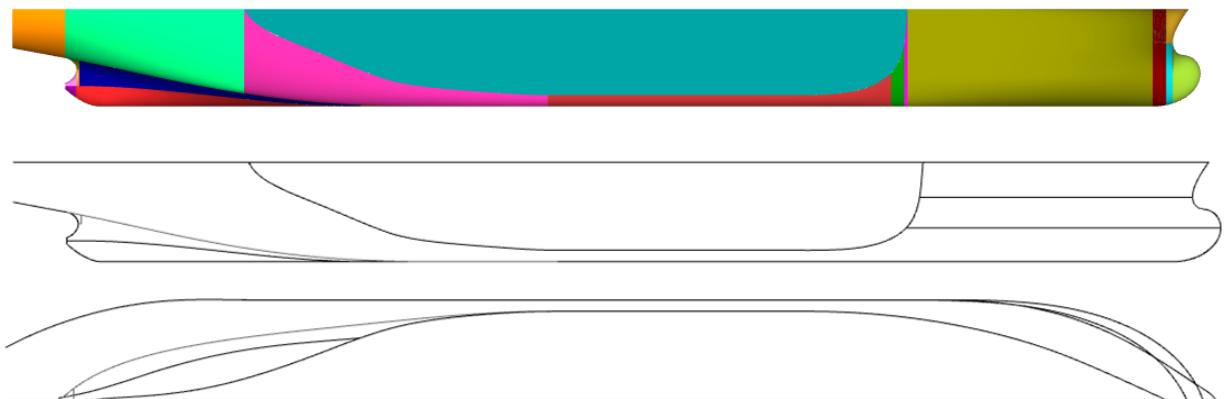


Figure 62. RSBC Parametric Hull

With the use of the provided data as reference, parameters were then tweaked in order to replicate the original hull form as much as possible. The parametric model was compared to the original hull form using Section Area Curve (SAC) Analyses and displacement value comparison. Figure 63 exhibits the SAC difference between the fully-parametric model (orange line) and the original hull (Blue). It is quite evident that it is hard to differentiate between the two curves indicating that the lines are very similar to each other. Furthermore, the difference in volume displacement between both models was optimised to be 0.027% making the ships near to identical.

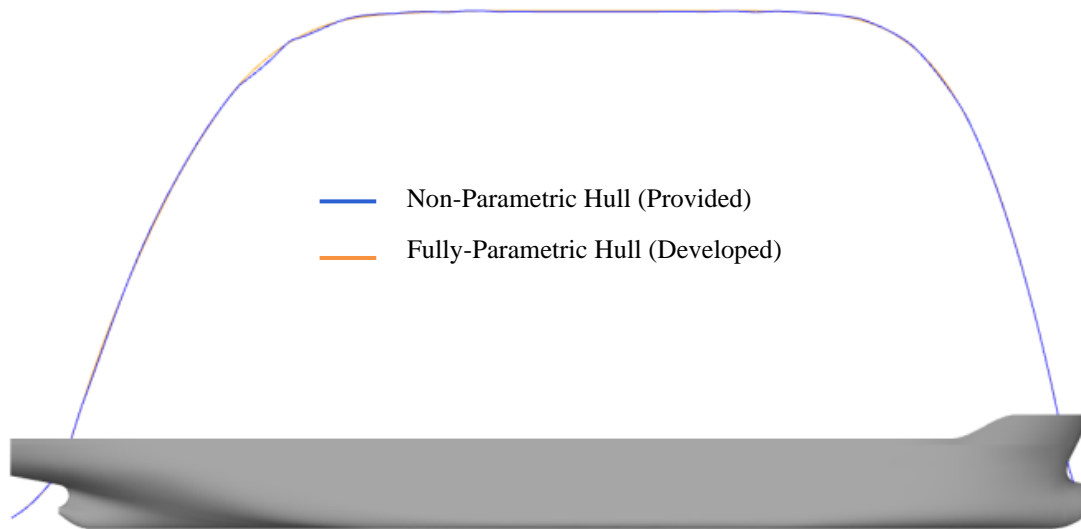


Figure 63. RSBC SAC Analyses

The objective of this module is to carry out a stern form optimisation procedure, thus generating variations in the aft part of the hull altering the wake flow into the propeller. The selection of the design variables (DV) for the multi-objective optimisation was shortlisted to the stern of the vessel totalling to a number of 6 varying parameters that are demonstrated in Figure 64.

1. CPCSideProjectedYPlane_AreaFactor
2. CPCSideProjectedZPlane_AreaFactor
3. Keel_Area Factor
4. BilgetoMidboss_Ycurve_AreaFactor
5. BilgetoMidboss_Zcurve_AreaFactor
6. zTransom

As depicted in the diagram, variables 1&2 and 3&4 control their respective lines in the y and z direction by modifying the area under the curve. In a similar manner, DV 3 is used to control the area under the curve of the boss keel, thus altering its gradient and slope accordingly. On the other hand, zTransom controls the endpoint of the indicated line to alter the height of the transom. These variables were designed with pre-defined ranges to allow variations within these extents. Limiting bounds were chosen based on experience but also to make sure that the ship geometry is intact and free of errors. It is good to note that the displacement volume of the vessel was only allowed to vary by 1% and any variants that exceeded such constraints were highlighted with a red triangle.

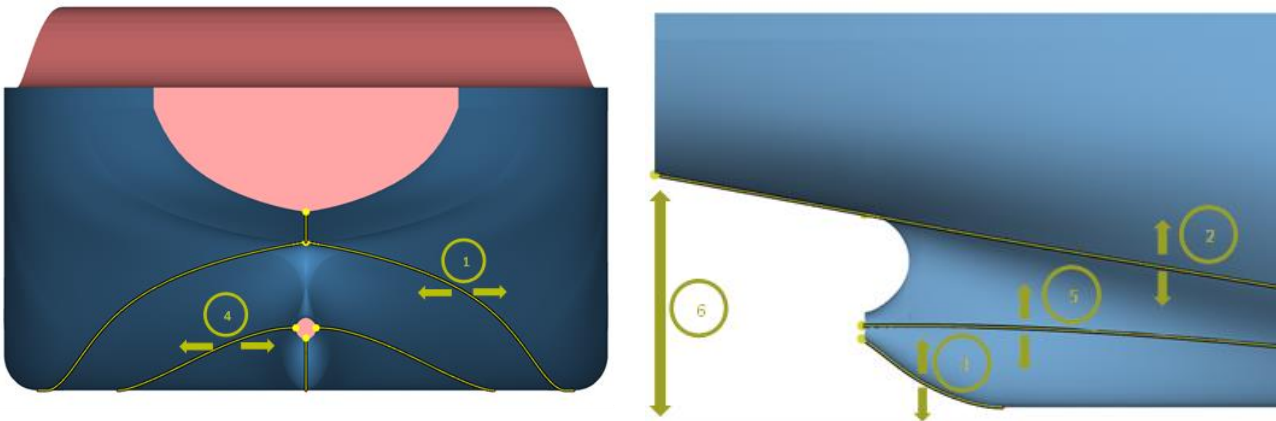


Figure 64. Design Variables

6.2.3 Automation: WAT Tool

To allow for the automatic calculation of the wake fraction and the wake non-uniformity, the WAT developed by Maasch et al. (2019), was utilised and implemented in the optimisation framework. The WAT tool is a wake analyses code that was developed using the CAESES software to process the flow data of an external flow solver.

The WAT was designed to read flow information that is exported from the flow solver and imported into the code via an automatic process giving the user various options for parameter computations and visualisation through the user friendly WAT graphical user interface (Figure 65).

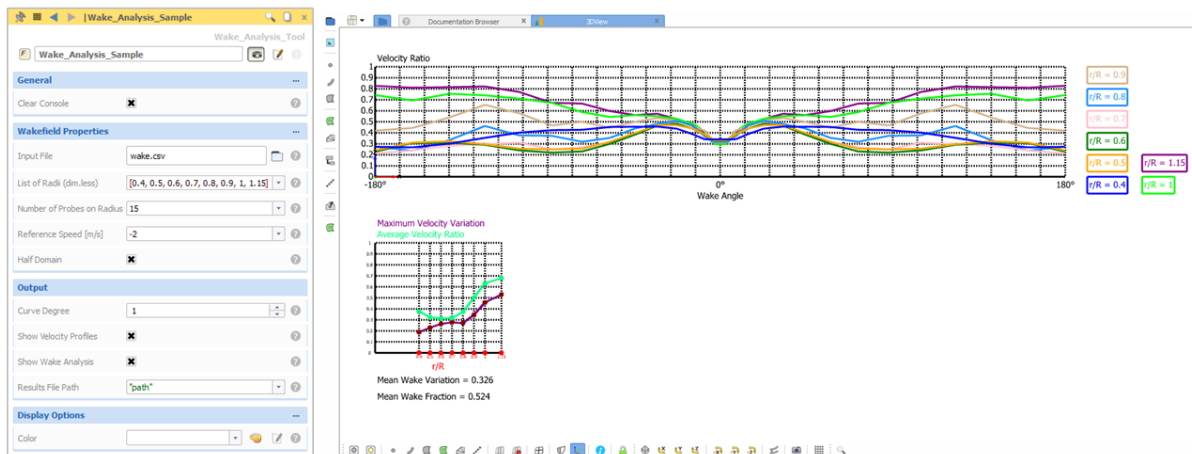


Figure 65. WAT Graphical User Interface (Maasch et al., 2019)

The wake quality assessment follows a standard method that is able to consider axial, tangential or radial velocity depending on the requirements of the user. Other than presenting the axial velocity ratios at different radii of the disc over a distributed range of angles, the code is designed to compute the mean wake fraction (w) and wake variation (Δw). These are accessible as parameter outputs that can be therefore used in an optimisation study. The paper explains that these criteria were evaluated using formulations (46) and (47):

$$\Delta w = \frac{1}{(r_{max} - r_{min})} \int_{r_{min}}^{r_{max}} \Delta \left(1 - \frac{v_a}{v}\right)_r dr \quad (46)$$

$$w = \frac{1}{\Delta\varphi(r_{max}^2 - r_{min}^2)} \int_{r_{min}}^{r_{max}} r \int_{\varphi_{min}}^{\varphi_{max}} \left(1 - \frac{v_a}{v}\right)_r d\varphi dr \quad (47)$$

The code is also able to deal with half-domain wake fields (due to half domain simulations) by mirroring the wake characteristics about the centreline of the wake disc. Which is why the angular integration limits are either $[0, 2\pi]$ or $[0, \pi]$, depending if one uses the full or half (symmetric) domain.

The WAT tool has the benefit of coupling with the STAR-CCM+, thus allowing automatic integration for optimisation procedures. An additional feature code was developed using Java Script to carry out the whole process from generating the necessary objects in STAR-CCM+, reading the results and exporting them back to the WAT tool. The script can be easily modified using the Wake Probe Code interface that gives the user the options to specify propeller position, propeller diameter, number of points, number of radii etc. The file output from this script is then used by the WAT to process the data and carry out the necessary computation.

Figure 66 demonstrates the workflow of such a process, where the Wake Probe Code is defined in CAESES, via a graphical user interface, outlining the necessary parameters and dimensions. This will automatically generate the required java script. Once the script is activated inside the CFD solver, it automatically generates probe points according to the parameters specified in the Wake Probe Code, extracts the necessary flow data (wake velocities and probe point positions) and writes it in a CSV file. This information is then fed back to the WAT tool that processes the data into meaningful parameters and visual outputs.

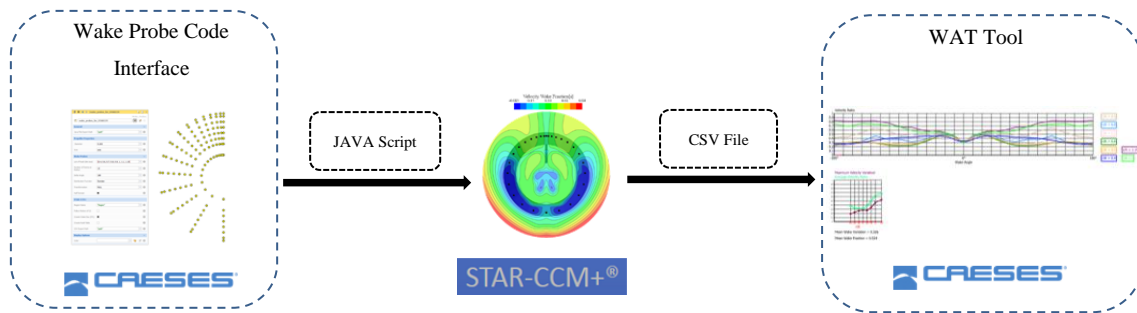


Figure 66. Wake Probe Evaluation Workflow

6.3 Results and Discussion

As previously indicated in the procedure process (5.2.1), the optimisation study involved both an exploration phase and an exploitation phase producing a total of 55 variants. Three of the design candidates were later run in self-propulsion conditions and analysed using some of the hull-propeller interaction analyses methods. Results for each of the phases were thus presented respectively in the following sections and discussed accordingly.

Exploration (Sobol Sequence)

For the exploration part of the study, 40 different hull designs were simulated in full-scale towing conditions. The sobol sequence algorithm that generated the different variants produced a quasi-random spread over the design space. The limiting bounds of the design area were defined by the ranges of the six different specified design variables. The drag, wake fraction and wake non-uniformity were evaluated for each of the designs that produced a distributed and varied output of results as depicted in Figure 67.

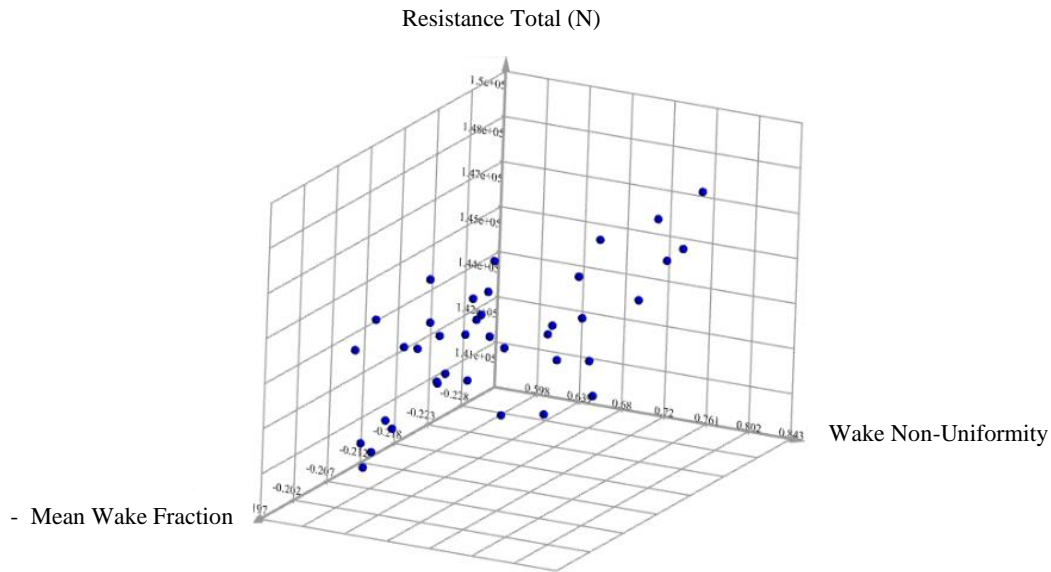


Figure 67. Exploration Output

The correlations between the design variables and the objectives were then analysed in order to understand or identify any common trends in behaviour. This provided insight on how the shape of the stern affects any of the three objectives. The parametric modeller as well as the optimisation framework tool, CAESES, provides a feature that easily allows you carry out such analyses producing a range of graphs comparing the design variables with the objectives as presented in Figure 68. Please refer to the Parametric Modelling (Section 6.2.2) in order to understand the name of the design variables and which areas of the stern they control or represent. Any clear correlations were deduced as follows:

- Increasing the area of the CPC line in the z direction increased the resistance. This indicated that pushing the CPC line upwards in the z direction, thus moving the bulkiness in that region higher up increased the resistance of the vessel.
- Increasing the height of the Z Transom decreased the resistance. This indicates that the area of the submerged overhang stern is reduced thus leading to a lower resistance which follows logical behaviour.
- Having a less bulky keel, (more slender shape with reduced gradient change) resulted in a reduction of the wake fraction.
- A less bulky BilgetoMidboss curve (smaller area factor in y direction) reduced the resistance but increased the non-uniformity of the wake and reduced the mean wake fraction. Increasing the height of this curve has reduced the resistance and wake-non-uniformity and has also reduced the mean wake fraction.

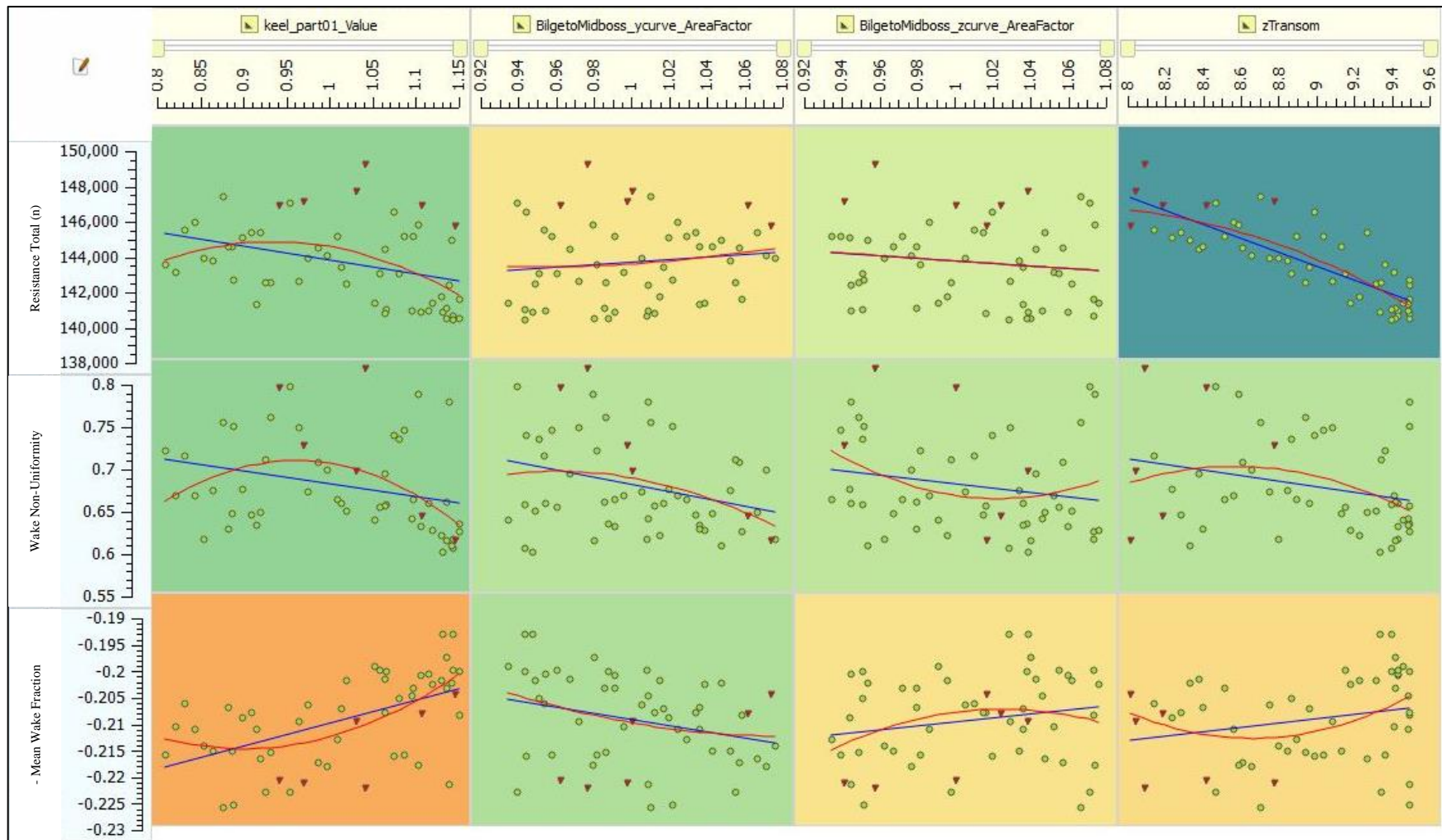


Figure 68. Design Variables Correlations

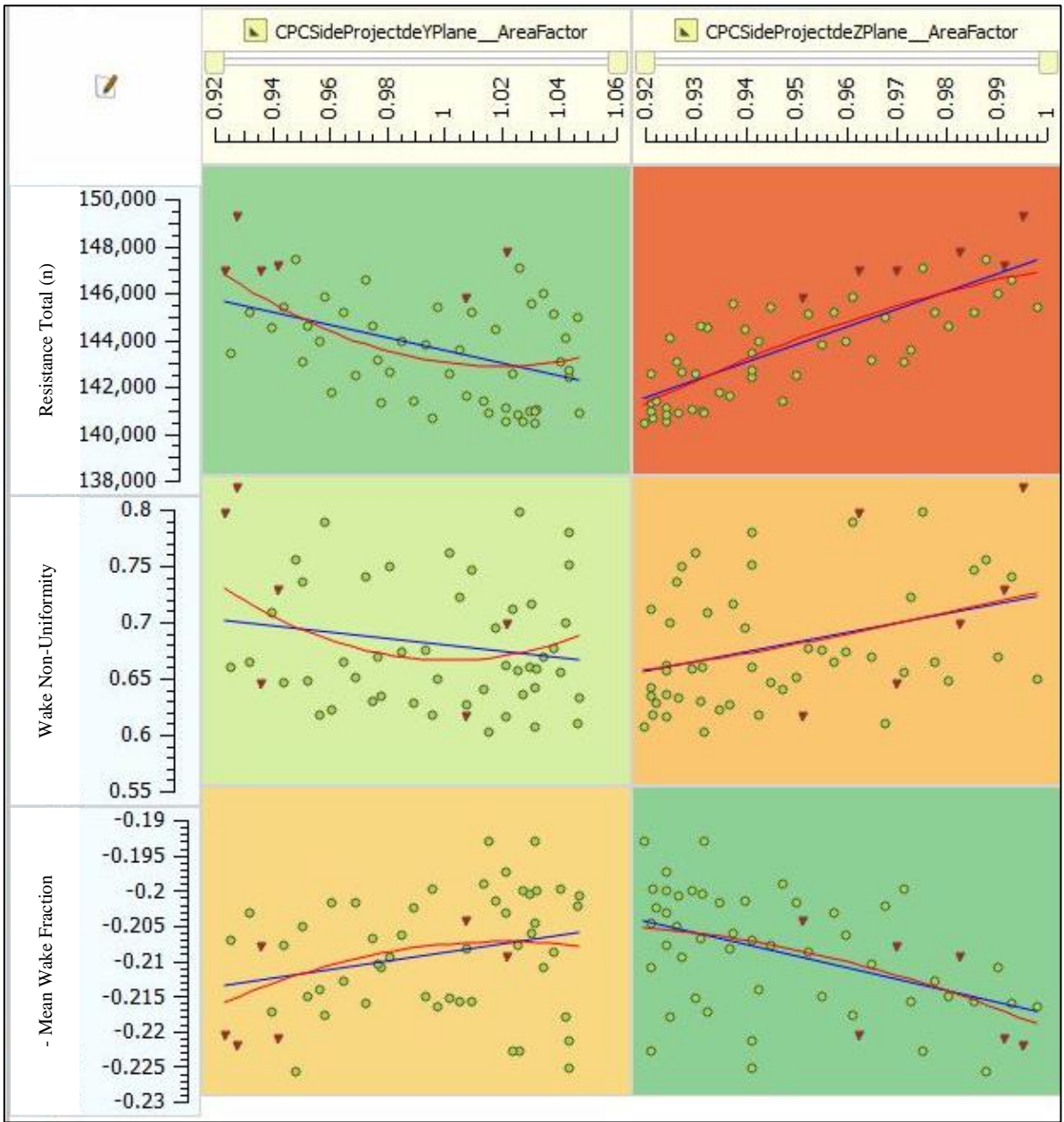


Figure 68. Design Variables Correlations

Exploitation (Dakota Tool)

For the optimisation part of the study, an additional 15 designs were generated within the design space using the Dakota tool that made use of a multi-objective genetic algorithm (MOGA) approach. These were also simulated in full-scale towing conditions but were not however randomly designed. The surrogate based model identifies beneficial designs in the design space and seeks to optimise the designs generating new variants. A total of 55 designs were thus generated with 40 being generated using the Sobol generator and another 15 using the Dakota tool.

It was also considered important to understand how the objectives behave with one another and to acknowledge whether improving one objective will have an adverse or beneficial on the other. Can the objectives be improved simultaneously, creating a pareto front or are they conflicting, thus requiring a compromise?

The figures below, Figure 69, Figure 70 and Figure 71, present the comparisons between the objectives for all the evaluated variants (56) including the baseline design. The blue dots represent the design variants generated from the Sobol, and the coloured designs represent those generated using the Dakota tool. The point that is identified with the blue lines is the baseline design. This was displayed as such in order to be able to distinguish between improved or worse performing hulls in comparison to the original.

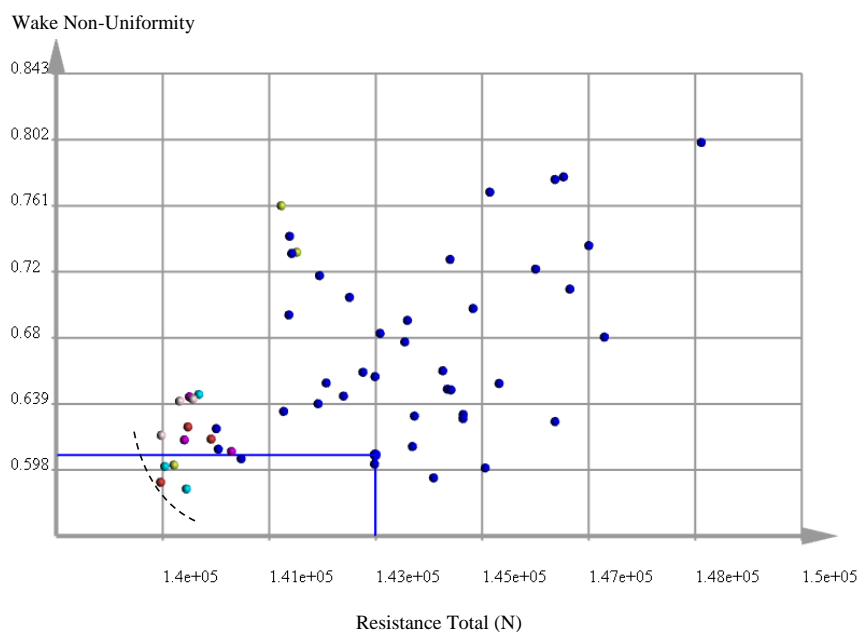


Figure 69. Wake Non-Uniformity vs Resistance

When comparing the Wake Non-Uniformity objective with the Resistance Total objective (Figure 69), it was noted that most of the designs that were generated by the batch system (Sobol generator), produced worse results. This indicated that the baseline ship had been properly designed through experience in the marine industry. That being said, the Dakota tool successfully produced improved designs. These are demonstrated below and to the left of the blue lines depicted in Figure 69.

The best design candidates produced wake non-uniformity and resistance improvements of 3.5% and 2.4% respectively. Reduced wake non-uniformity should result in better open water efficiency. Whether such a slight variation would have an impact is yet to be investigated. On the other hand, 2.4% reduction in Resistance is significant and this could save significant energy. That being said, it should be noted that the design variant with the optimal resistance has 1% less displacement. It was also understood that the reduction of the wake non-uniformity together with the resistance is possible. The best variants are identified at the bottom left corner of Figure 69, almost demonstrating Pareto front behaviour (black dotted line).

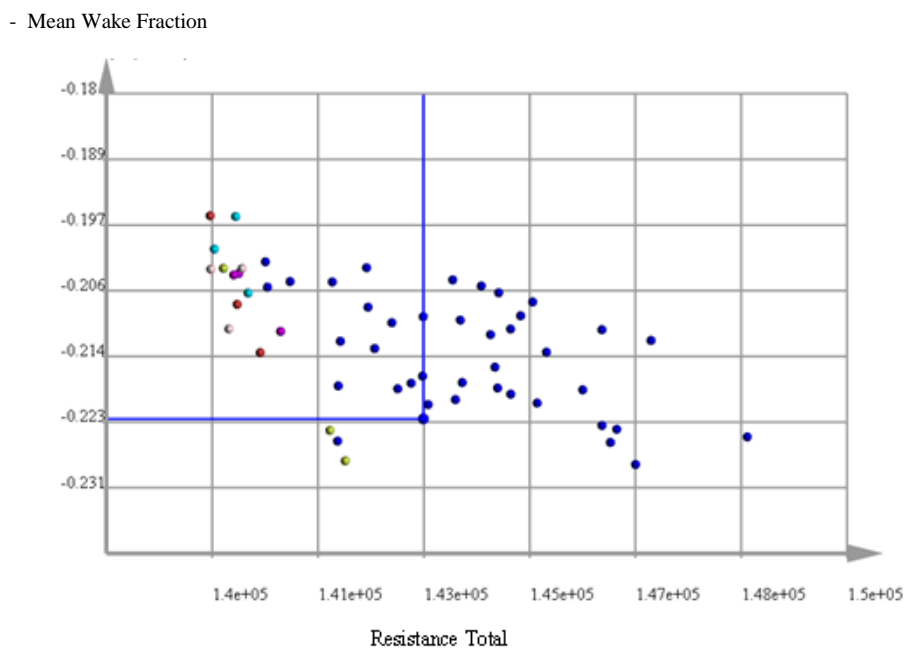


Figure 70. Wake Fraction vs Resistance

On the other hand, when comparing the wake fraction with the resistance (Figure 70), it was deduced that these two objectives conflict and oppose in trend with lower resistance hulls producing reduced mean wake fractions. Please note that the negative sign of the wake fraction was introduced due to the optimisation framework functionality where each value was

multiplied by -1. The system would then seek to minimise the wake fraction, which is in actual fact maximising the value once the negative sign is removed. It is evident that all the generated designs have not produced any significant range of variation for the wake fraction outputs. It can therefore be deduced that it is hard to considerably alter this parameter unless substantial changes to the vessel form are carried out (e.g. changing ship type).

The Dakota system seems to have figured out the minimal impact on the wake fraction objective, thus focusing its efforts more on the other two objectives (resistance and wake non-uniformity). That being said, the optimization tool has also tried to enhance the wake fraction by generating a couple of improved designs represented by the yellow dots.

The variants with wake fraction values at both extents of the range were later investigated using self-propulsion methods in order to understand the impact or sensitivity the parameter has on the performance of the vessel.

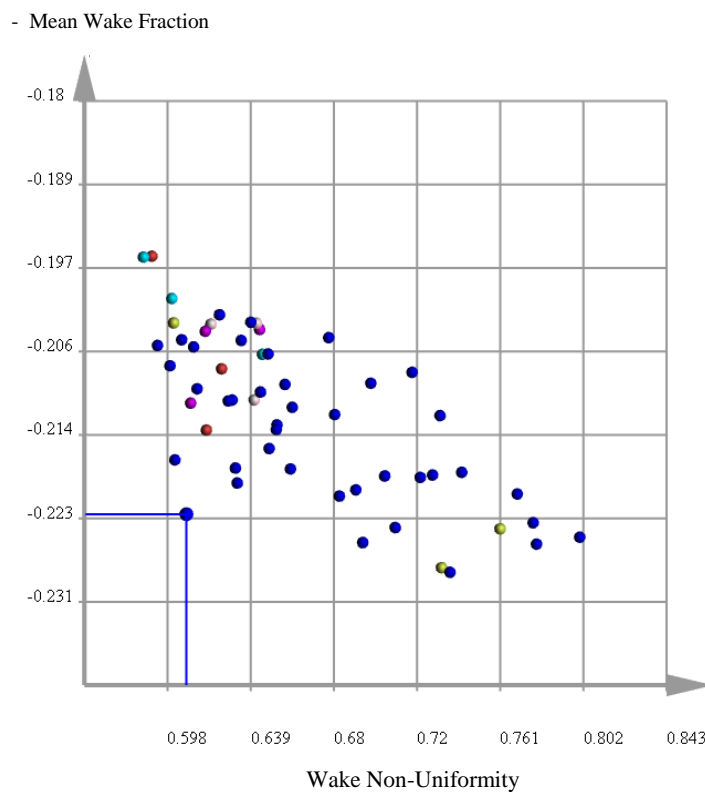


Figure 71. Wake Fraction vs Wake Non-Uniformity

Figure 71 demonstrates that the wake fraction and wake non-uniformity have a linear trend and that the increase of one of the mean wake fraction resulted in an undesired increase in the wake non-uniformity. When not taking into consideration the resistance, the baseline design provided the best compromise between the two.

Self-Propulsion

Three design candidates were then shortlisted and identified to be simulated in full-scale self-propulsion conditions using the validated and verified methodology outlined in Chapter 4. The three designs were selected as follows:

- Dakota07 Des01
- Sobol02Des33
- Dakota 04 Des 02

These were then compared to the performance of the baseline design in self-propulsion conditions.

The selection of these three designs was based on their performance characteristics in the optimisation process. These have been identified according to the optimal designs on the pareto fronts of the various performance parameters. Namely, wake non-uniformity, mean wake fraction and resistance. As previously explained, some of these parameters might oppose in trend. Therefore, an optimal parameter might negatively affect another parameter. The designs were therefore selected to understand the parameter (in towing condition) that can provide the most benefit in self-propulsion conditions.

Pareto Front: Wake Non-Uniformity vs Resistance

Best Design: **Dakota 07 Des01**

This design offers the best performance on the Pareto front in subject, offering the optimal wake non-uniformity and the least resistance. However, this design also produced the worst wake fraction as depicted in the figure below.

- Lowest Mean Wake Fraction
- Lowest Wake Non-Uniformity
- Lowest Resistance

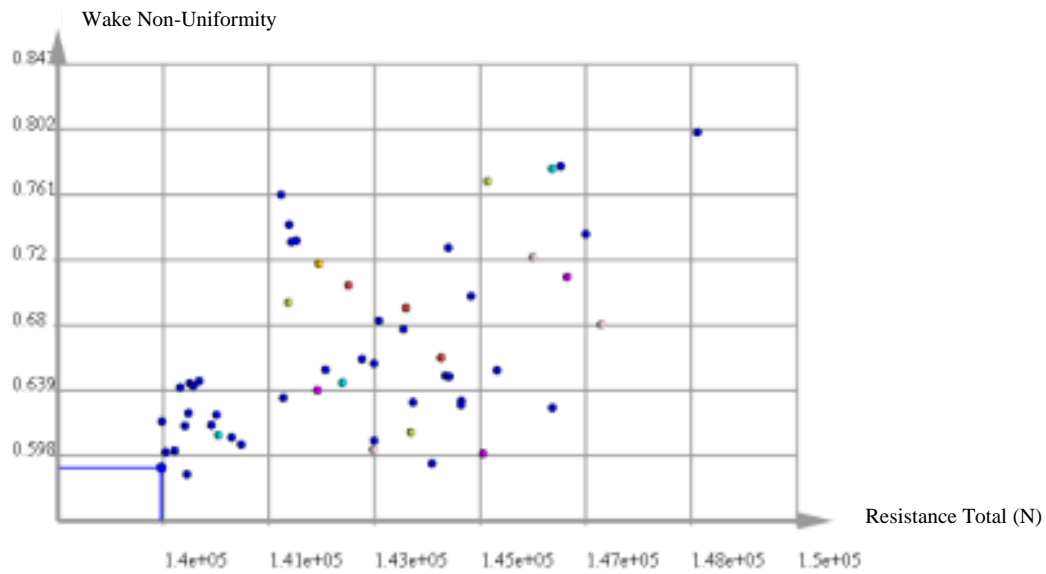


Figure 72. Wake Non-Uniformity vs Total Resistance: *Dakota07 Des01*

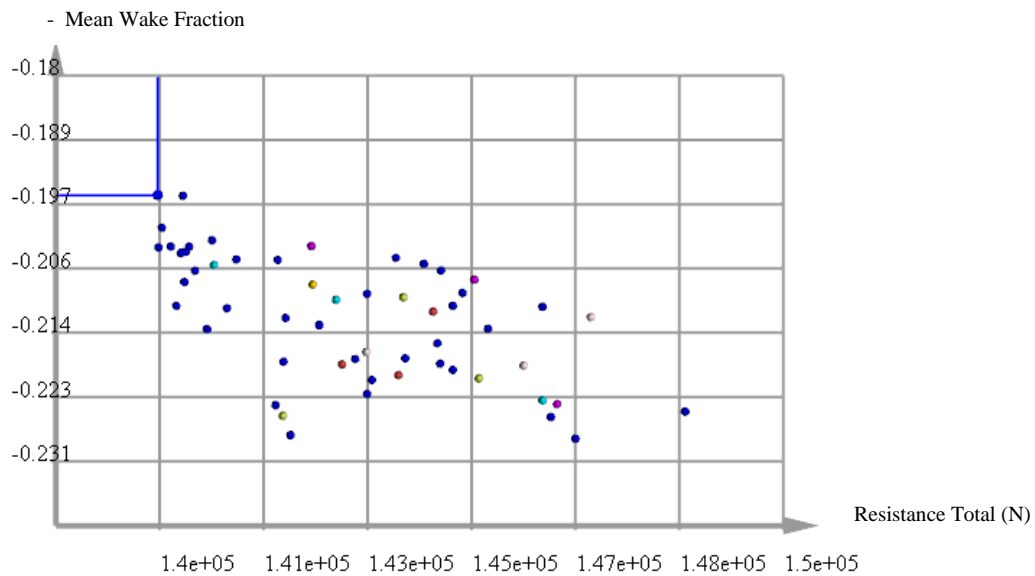


Figure 73. Mean Wake Fraction vs Total Resistance: *Dakota07 Des01*

Pareto Front: Wake Fraction vs Resistance

Best Design: **Sobol02 Des33**

When analysing the design pool, this design produced one of the highest wake fractions and generated an average total resistance. Furthermore, the wake non-uniformity produced by Sobol02Des33, was neither on the higher or lower end but provided a compromise sitting in mid-range of the result pool.

- High Mean Wake Fraction
- Average Wake Non-Uniformity
- Average Resistance

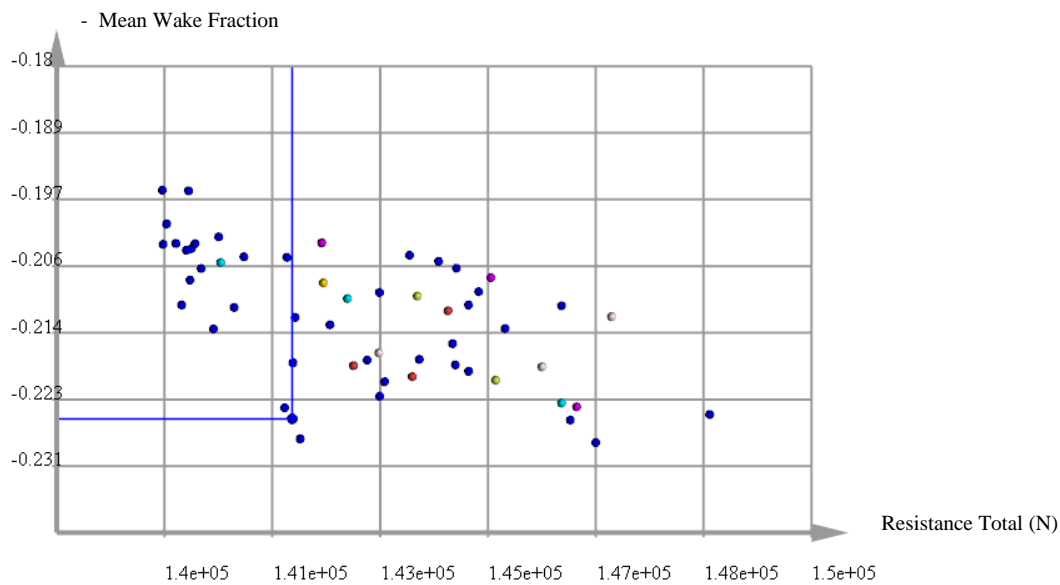


Figure 74. Mean Wake Fraction vs Total Resistance: *Sobol02 Des33*

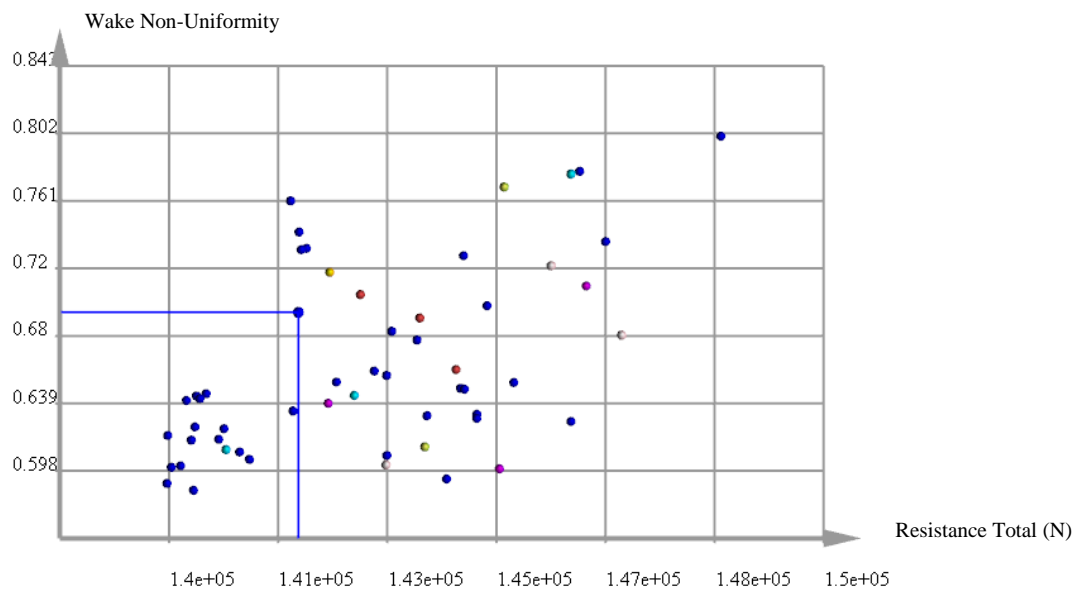


Figure 75. Wake Non-Uniformity vs Total Resistance: *Sobol02 Des33*

Pareto Front: Wake Fraction vs Resistance

Best Design: **Dakota04 Des02**

This design produced a similar performance to design Sobol02Des33 with the exception that it produces higher wake non-uniformity.

- High Mean Wake Fraction
- High Wake Non-Uniformity
- Average Resistance

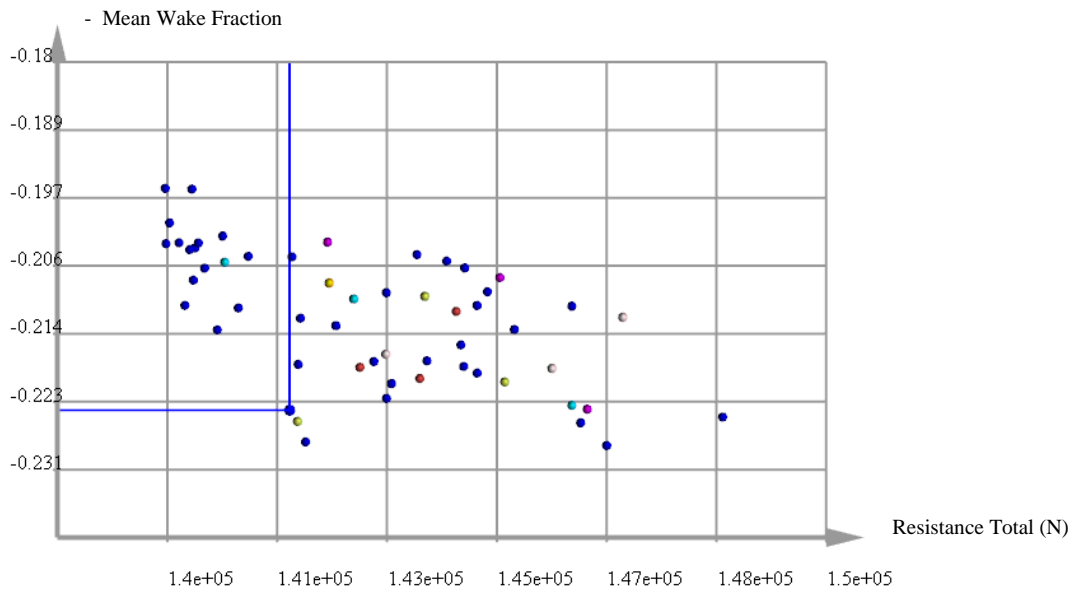


Figure 76. Mean Wake Fraction vs Total Resistance: *Dakota04 Des02*

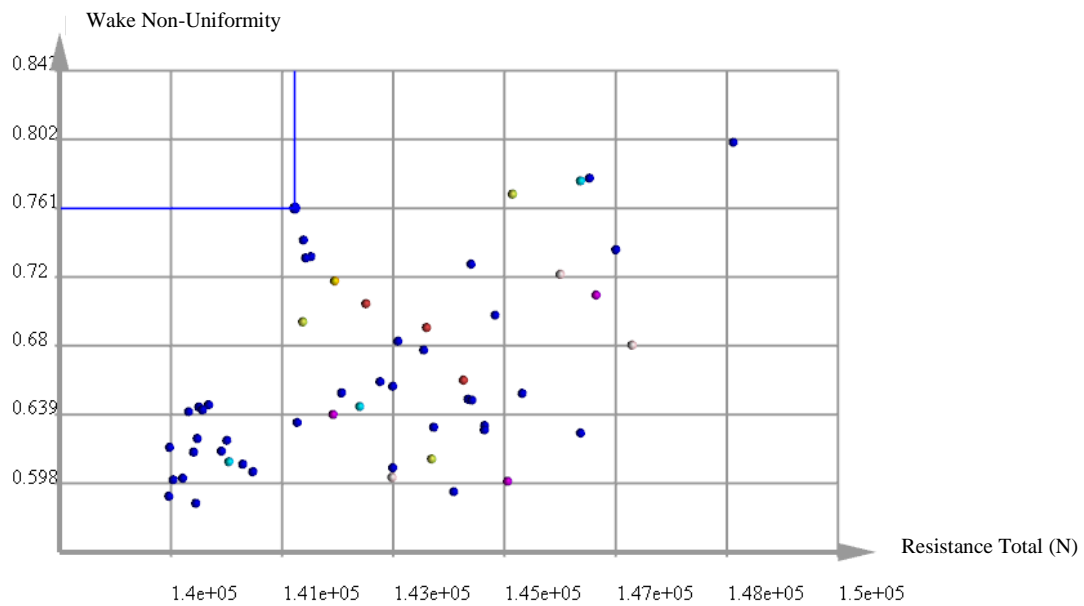


Figure 77. Wake Non-Uniformity vs Total Resistance: *Dakota04 Des02*

Pareto Front: Wake Fraction vs Wake Non-Uniformity

Best Design: **Baseline Design**

This design produces similar performance to design Sobol02Des33 with the exception that it produces a lower wake non-uniformity.

- Low Mean Wake Fraction
- Low Wake Non-Uniformity
- Average Resistance

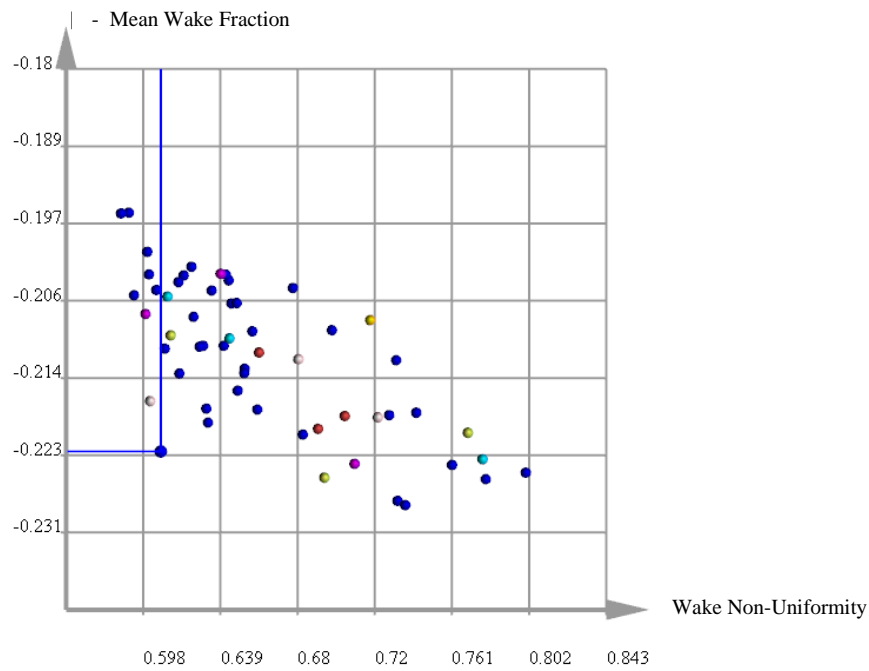


Figure 78. Mean Wake Fraction vs Total Resistance: *Dakota04 Des02*

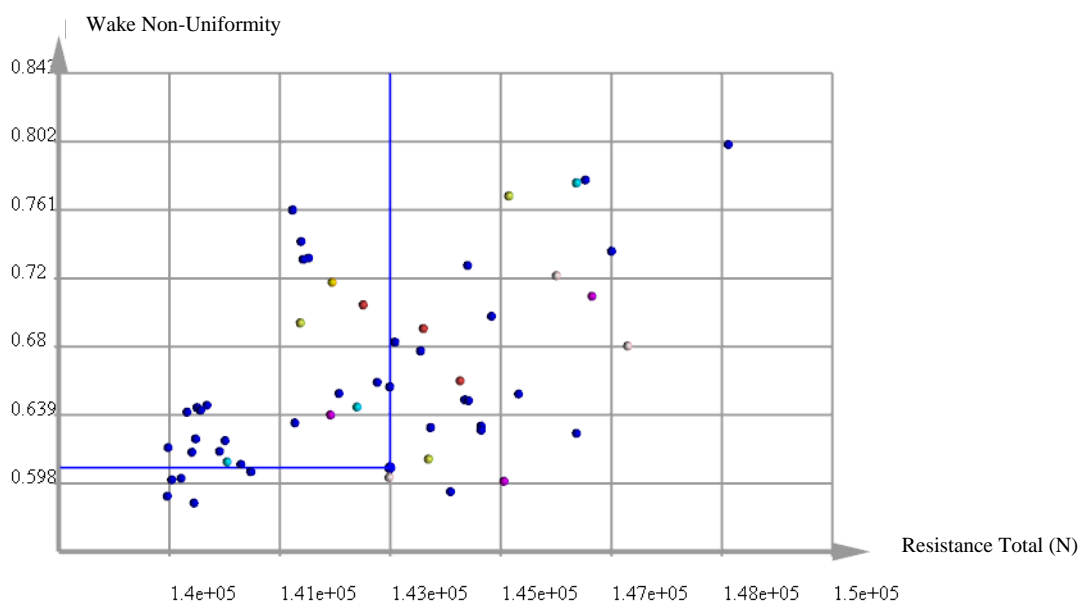


Figure 79. Wake Non-Uniformity vs Total Resistance: *Dakota04 Des02*

Table 39. Self-Propulsion Comparison Analyses

	<i>Hull Design</i>			
	<i>Baseline</i>	<i>Dakota04 Des02</i>	<i>Dakota07 Des01</i>	<i>Sobol02Des33</i>
<i>Ship Speed (m/s)</i>	6.43	6.43	6.43	6.43
<i>Towing Resistance (N)</i>	284682.97	283248.78	279363.92	283491.82
<i>>Difference</i>	--	- 1.06 %	- 2.41 %	- 0.97 %
<i>SP Resistance (N)</i>	399475.50	389625.00	385023.00	390205.00
<i>>Difference</i>	--	- 2.47 %	- 3.62 %	-2.32 %
<i>Thrust Deduction Term</i>	0.71	0.73	0.72	0.73
<i>Thrust (N)</i>	400350.65	389333.00	389121.50	390615.00
<i>Torque (N-m)</i>	357209.00	343411.00	343710.00	348227.00
<i>Thrust Coefficient</i>	0.1865	0.1801	0.1808	0.1822
<i>Torque Coefficient</i>	0.0291	0.0278	0.0279	0.0284
<i>Propeller Rev. (rps)</i>	1.40	1.40	1.40	1.40
<i>Advance Ratio</i>	0.59	0.60	0.60	0.60
<i>Average Velocity Ratio</i>	0.73	0.75	0.75	0.74
<i>Open water efficiency</i>	0.65	0.66	0.66	0.66
<i>Relative Rotative efficiency</i>	0.92	0.93	0.93	0.92
<i>Hull Efficiency</i>	0.97	0.97	0.96	0.98
<i>Propulsive Efficiency</i>	0.59	0.60	0.59	0.60
<i>Power (W)</i>	3137685.66	3027274.07	3023431.07	3056600.75
<i>Power (kW)</i>	3137.69	3027.27	3023.43	3056.60
<i>>Difference</i>	--	- 3.52%	- 3.64%	- 2.58%

One immediate observation is that all three designs produced better performance requiring less power. It would be useful to understand where this benefit is originating from.

As previously explained, when analysing the towing resistance in Table 39, all designs generated lower drag with Dakota 07 Des01 resulting in the lowest value that is 2.4% lower than the baseline. However, when analysing these designs in self-propulsion it is evident that greater benefits have been achieved with power requirements reaching a maximum of around 3.64% reductions. This indicates that optimising these designs have also achieved further benefits when placed in front of a propeller. Design Candidates Sobol02Des33 as well as Dakota04Des02 improved propulsive efficiency by 1%.

The increment in propulsive efficiency for Sobol02Des33 came from the enhanced hull efficiency and open water efficiency. The augment in hull efficiency stemmed from an increased thrust deduction term (1-t) that outweighed the increase in the velocity ratio (1-w). It is good to remember that this design was selected due to its high wake mean wake fraction (w)

characteristics. Therefore, this indicates that an increased wake fraction in towing conditions does not necessarily correlate to an increased wake fraction in propelled conditions. In actual fact, quite the contrary, the wake fraction was reduced also resulting in an enhanced open water efficiency due to the higher advance velocity.

With regards to Dakota04Des02, the enhanced propulsive efficiency was due to improved open water efficiency and relative rotative efficiency. The hull efficiency did not alter, with the benefit in the thrust deduction term $(1-t)$ cancelling the increase in the velocity ratio. It is good to note that this design was shortlisted due to its high mean wake fraction (w) characteristics (i.e. low velocity ratio $(1-w)$) and high wake non-uniformity in towing conditions. Therefore, this also indicated that the wake fraction and wake non-uniformity could not give any insight or trend toward the performance in self-propulsion. The higher open water efficiency was also a result of a higher advance velocity.

When looking into design candidate Dakota07Des01. This design was selected for having low resistance, low wake non-uniformity and an undesired low mean wake fraction in towing conditions. This design also resulted in a lower resistance or thrust in propeller conditions providing a substantial benefit. It produced a slightly higher open water efficiency and higher relative rotative efficiency but a lower hull efficiency. The increment in the thrust deduction term $(1-t)$ did not outweigh the increase in the mean velocity ratio $(1-w)$, thus reducing the efficiency of the hull.

Unfortunately, the wake fraction and wake non-uniformity did not provide any insight or trend into the self-propelled behaviour. It can be deduced that these parameters were not necessary for the optimisation process during the towing conditions. On the other hand, the towing resistance parameters contributed most to the improvement in general. It can be said that the effective wake is more important than the nominal wake in design procedures. Therefore, with regards to future work, this study could be replicated using an actuator disc for propeller performance.

6.4 Chapter Summary and Conclusions

This chapter has successfully demonstrated a developed state-of-the-art multi-objective stern form optimisation procedure analysing a total of 55 full-scale hulls in towing conditions, with 3 of those candidates being also investigated in self-propulsion. Forty of the designs were generated using a quasi-random batch method and an additional fifteen variants were developed using the Dakota tool. The latter code makes use of recently introduced surrogate-based global minimisation methods using response surfaces in order to save significant computational time.

Furthermore, this section investigates whether such a process can serve to be a good compromise to the computationally intensive optimisation procedures that make use of numerical full-scale self-propulsion methods, which are currently considered unfeasible. The study has also indicated whether optimisation techniques, seeking to improve hull performance, are enhanced when taking wake quality into consideration. The research also helped in developing a better understanding of hull-propeller interaction by investigating relations between drag and wake quality parameters together with the impact of different stern form designs on the objectives. Moreover, whether the optimisation of nominal wakes can give any insight into the propulsive performance was investigated, thus contributing to the knowledge and understanding of efficient hull-propeller optimisation procedures.

Unfortunately, considering wake fraction and wake non-uniformity parameters in the optimisation process of ship performance in towing conditions did not provide any insight or benefit for self-propelled behaviour. A clear trend could not be identified between wake fraction in towing conditions and in self-propelled conditions. That being said, optimisation of the towing resistance rendered significant benefits in propelled conditions. Therefore, it can be deduced that the optimisation of resistance in towing conditions as outlined in this chapter is a beneficial process in hull design. Furthermore, in the availability of enhanced computational power, it is recommended that further optimisation is carried out for the wake fraction and wake non-uniformity parameters in self-propelled conditions. Since these parameters, in towing conditions, could not provide insight for propelled environments, it would be ideal to analyse and optimise their performance directly in propelled simulations.

This study indicated that these nominal wake characteristics did not provide any indication/relation to the propulsive performance. This study contributes to the body of knowledge by outlining a particular hull-optimisation process and by deducing that taking the wake parameters into consideration for the towing performance optimisation, did not provide a feasible alternative to computationally expensive optimisation of full-scale vessels in self-propulsion conditions. That being said, this requires further study and verification.

This chapter describes and outlines all the necessary procedures and methodologies to carry out the different phases of the case study in Module 2 (Chapter 1, Figure 4), presenting the different components of the optimisation framework and analyses methods. Results are then discussed, and the findings are clearly outlined.

7 Full-Scale Design Optimisation of PBCF

7.1 Introduction

As previously explained in chapter 2, ESD research and investigations were generally carried out at model scale, giving unrealistic performance predictions. Studies show that ESDs are more efficient in full-scale environments than in model-scale conditions (Kawamura et al., 2012, Hansen et al., 2011). ESD investigations, optimisations and analyses should therefore be performed at full scale to minimise uncertainties and error (Mizzi et al., 2015). That being said, sea trials are not considered to be accurate methods for investigating the performance of the installed technologies due to the various associate uncertainties and assumptions. The small savings that are achieved with the use of ESD are hard to capture in sea trial environments. The author considers full-scale CFD analyses to be the preferred methods for analysing Energy Saving Devices due to the relatively accurate results obtained in recent years and their systematic approach towards performance prediction. In addition, their consistent format allows a useful comparison of trends and behaviour.

Propeller Boss Cap Fins (PBCF) are one of the most commonly installed retrofitting technologies as they are cheap and easy to install and remove. As the name implies, a PBCF is a post – swirl fin that is installed onto the boss cap of the propeller. It is well known that a propeller produces a hub vortex which reduces the propeller efficiency and may cause rudder corrosion. As Ghassemi (2012) explains, the strength of such phenomena is dependent on the hub geometry as well as the axial load distribution of the propeller. The aim of installing a PBCF is to minimise this hub vortex, increase propeller efficiency and reduce fuel costs. To the best of the authors' knowledge, no study has yet:

- Focused on analysing the physics of PBCF in full-scale environments
- Carried out full-scale PBCF optimisation procedures using high fidelity numerical methods.

Thus, A PBCF design optimisation process using RANS CFD methods was developed. Its sole purpose, is to improve propeller efficiency whilst taking into consideration a number of parameters that might be dependent on each other.

This chapter describes the study carried out for module 3 whereby a state of the art full-scale PBCF design optimisation procedure is proposed and demonstrated. All the methodologies and results are outlined and presented accordingly. Furthermore, an in-depth analysis of the physics behind the PBCF is explained and discussed. This study has also been published as an article (Mizzi et al., 2017).

7.2 Optimisation Framework

This study demonstrates an advanced full-scale PBCF design optimisation approach using a coupled optimiser-CFD framework with the aim to improve the propulsion efficiency of a propeller system. The structure of the optimisation process made use of a parametric modeller, a CFD solver and an optimisation algorithm, all of which were integrated on a high-performance computer (HPC) system as presented in Figure 80.

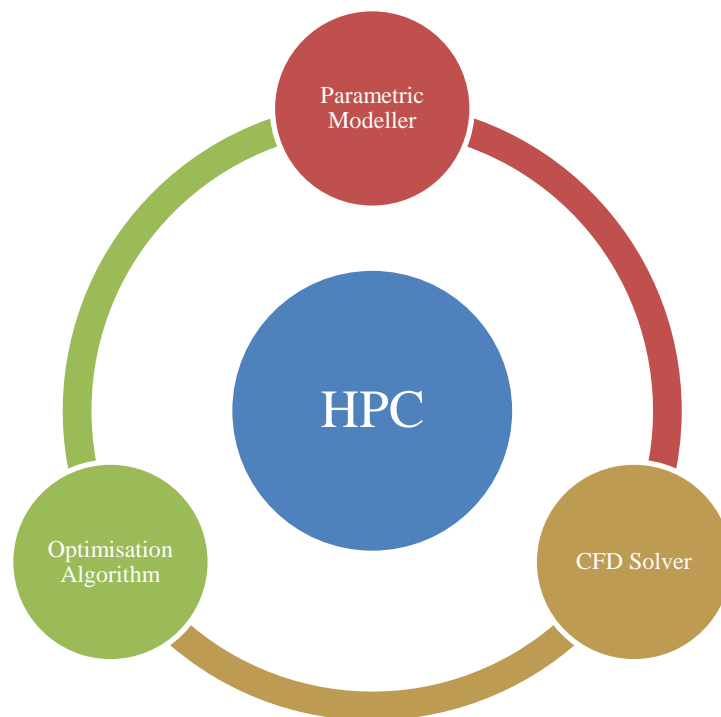


Figure 80. Optimisation Framework

Once the PBCF parametric model had been developed using (CAESES[®]) software, various geometric design candidates were generated and solved in submerged water conditions of uniform flow using Reynolds-Averaged Navier-Stokes (RANS) equations to simulate open water tests. These were then analysed to predict the ESD impact on propulsive efficiency. The CFD solver was then coupled to an optimisation algorithm (also in CAESES[®]) that processed the results and generated the next set of parameters for the new design candidate.

7.3 Parametric Model



Figure 81. PBCF Geometry

The PBCF as shown in Figure 81 was designed in such a way to produce a parametric model which incorporated appropriate design variables; namely fin length, angular fin position, fin thickness, fin pitch angle and fin height. The educated selection of these parameters was based on the literature; (Kawamura et al., 2012, Atlar and Patience, 1998, Hsin et al., 2009, Ghassemi et al., 2012, Hansen et al., 2011). The limiting bounds and range of the design variables were defined according to the validity of the parametric model as depicted in Table 40.

Table 40. Design Variables

<i>Parameter</i>	<i>Lower Limit</i>	<i>Upper Limit</i>
<i>Length (m)</i>	0.42	0.84
<i>Height (m)</i>	0.062	0.41
<i>Maximum Thickness (m)</i>	0.004	0.08
<i>Pitch (deg)</i>	-50	50
<i>Angular Fin Position (deg)</i>	0	71

7.4 Optimisation

7.4.1 Optimisation Background

Shape optimisation helps give a better insight into the study and enables the design and manufacture of superior products that might offer superior performance and/or save costs. Optimisation methods can be carried out in various ways: using different algorithms and approaches; defining one or more constraints; or/and seeking a single or multi-objective approach. Processes might also be computationally expensive and time-consuming, and therefore careful selection for a robust and efficient system is of utmost importance.

There is no general consensus regarding optimal optimisation methods. Each procedure depends on the design task at hand as well as the time and computational power available. Harries (2015) outlines the optimisation approach in 2 consecutive phases; exploration and exploitation. The prior indicates the exploration of the design space, thereby identifying areas of interest. Once promising candidates have been identified, they are then fine-tuned to produce the best possible result - exploitation.

Exploration identifies the regions of interest in the design space as well as promising variants. This allows for the understanding of design trends whilst evaluating any possible sensitivity. For full potential benefits of design exploration in a 3D space environment, x number of design variables would require 3x number of variants to be investigated that can accumulate to a high number of required simulations. Since this can be very time consuming, other strategies have been developed that exclude unnecessary points in the design space. Such an algorithm is called the Sobol Sequence (Press et al., 2007), which is used in this study.

Post the exploration process, optimisation strategies are then used to modify and fine tune the variables with the aim of advancing towards optima. Ideally, the search would yield the finding of a global optimum; however, resources generally limit the detail required in the optimisation process to do so. Therefore, there is a possibility of not managing to exploit a global optimum. This being said, a local optimum, one that represents a better candidate than the baseline design, is generally determined. The exploitation method used in this study is the Tangent Search Method (Hilleary, 1966).

7.4.2 Optimisation Algorithm

CAESES is a powerful and flexible 3D parametric modeller that can be integrated with a CFD solver to enable design optimisation with post-processing capabilities. For this particular study, CAESES was integrated with Star-CCM+ ensuring proper interaction and file transfer. CAESES has a choice of different algorithms and optimisers built-into the software, but only the Sobol and the T-search methods were used for this particular study. These two engines generally complement each other with the Sobol examining a design space (batch design approach) to identify the best candidates and the T-Search analysing those candidates further and modifying them to meet certain goals within specified constraints (optimisation).

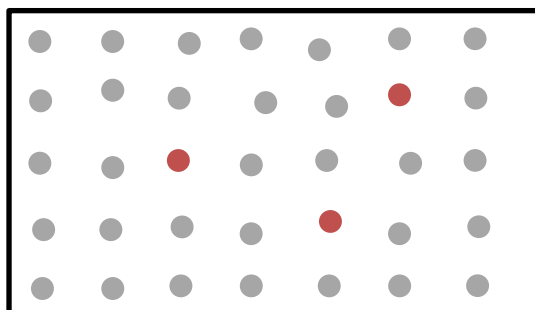


Figure 82. Quasi-Random Sequence

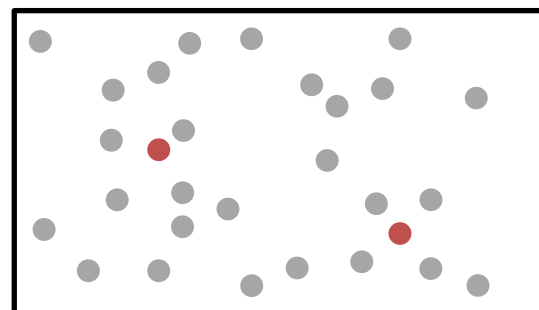


Figure 83. Local Optimum

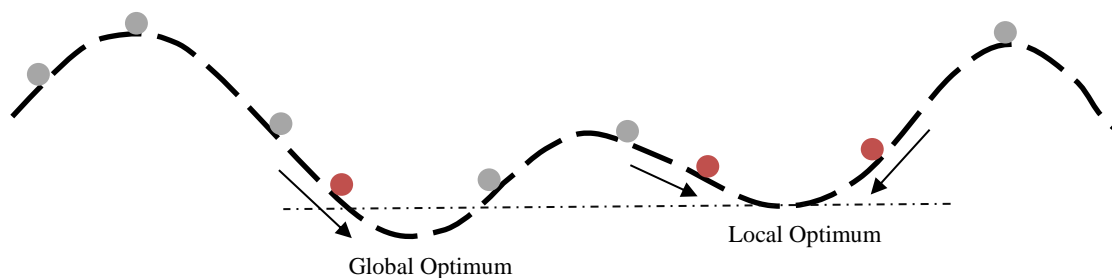


Figure 84. Optimisation Algorithm

The Sobol sequence is a deterministic algorithm of a quasi-random low-discrepancy sequence (Figure 82) that produces a pattern in the design space that seems random but is somewhat deterministic. It is designed to generate uniform sampling over a design space by generating candidates in regions that are less populated, thus avoiding the repetition of the same geometry (Press et al., 2007). On the other hand, random sequences (Figure 83) tend to produce busy areas as well as voids in the sample space. Quasi-random or low discrepancy sequences are less random than pseudorandom number sequences because they tend to sample space smartly and more uniformly making them more effective for global optimisation. The quasi-random approach generates a more efficient variation than the random sequence over a design space leaving no clusters or voids, resulting in better analysis for design exploration (Friendship Systems).

The Tangent Search Method, originally proposed by Hilleary (1966), is a gradient-free method that features moves similar to those of gradient directions. The T-search method is a reliable optimisation algorithm (Figure 84) with a single objective goal which is to consider inequality constraints. The algorithm detects a descent search direction in the solution space towards a goal whilst restricting itself to a feasible domain. It applies a direct search method within the pre-defined constraints. The method is based on exploratory moves to find promising search directions in the design space and global moves making steps along with the identified directions towards superior designs. Such a method is capable of identifying the local minimum in a solution space (Friendship Systems).

7.4.3 Optimisation Procedure

With this study only requiring one objective i.e. improving the propeller efficiency, the following optimisation process was carried out. The Sobol engine was used to generate a total of 45 variations producing a sufficient spread of designs over the design space. For each design, the K_T , K_Q and propeller efficiency were computed to identify the best designs while also ensuring the validity of the y^+ range. The best three design candidates were then assigned to be parent designs requiring further optimisation using the T-search method for 25 iterations each. The reason for not simply carrying out the optimisation analyses using only the best design is due to the room for improvement that can be achieved for each of the three. Prior to optimisation, a parent design might produce less favourable characteristics than another, but it might turn out to provide better results after the optimisation process has been carried out, reaching the global min/max. It is for this reason that three designs were selected for analysis.

After taking into consideration the computational time, power and resources available, a selection of three designs seemed most appropriate. These were then compared, and the global optimum deduced.

7.4.4 CFD Solver

In this study, a Reynolds-Averaged Navier-Stokes (RANS) method was applied to simulate open water tests in submerged conditions of uniform flow to analyse propeller performance characteristics using the MRF approach. Since the CAESES propeller is a customised design, no experimental data was available to proceed with the validation procedure of the numerical solver. Therefore, the open water CFD model used for this PBCF study was firstly validated and verified using the model-scale Potsdam VP1304 propeller, which is an open source geometry with available experimental data. Details of the numerical model together with the V&V procedure, can be found in Chapter 4, which entails all the methodology, validation and verification of all the numerical models. During the validation study, various physics models and meshes were tested, identifying the optimal criteria for the simulation that resulted in the most accurate propeller characteristics. Once validated, the same physics, mesh and setup were used to analyse the CAESES propeller in full-scale conditions. The surface mesh (Figure 85) was generated using triangulated faces making sure to capture blade tips and sharp edges for accurate representation. With regards to the full-scale numerical model, a mesh of around 10 million hexahedral cells was generated selecting a reasonable cell size growth-rate from the inner to the outer field while also specifying local area refinement (Figure 9). Figure 89 demonstrates the domain configuration and associated boundary conditions of the CFD solver.

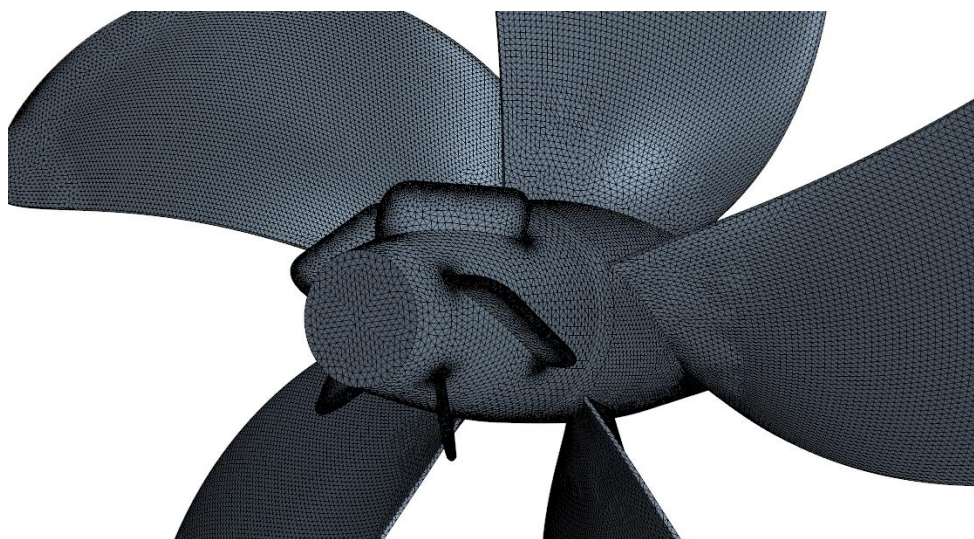


Figure 85. Surface Mesh for CAESES Propeller with PBCF

For this particular study, the All- Y^+ treatment approach was used, which is a hybrid approach that emulates both the Wall Function law approach for Y^+ values (Y^+ is a non-dimensional wall distance for a wall-bounded flow) greater than thirty and the Near-Wall turbulence for Y^+ values lower than one trying to resolve the viscous sub layer. Since the validation study was carried out at model scale, the simulation was modelled in such a way as to avoid Y^+ values greater than 1 for enhanced accuracy. This being said, in order to achieve such small Y^+ values in full-scale conditions, a high cell number is required, and this was not deemed feasible for this study. Therefore, with regards to the full-scale CAESES propeller, it was necessary to have the smallest Y^+ values but preferably greater than 30 in order to avoid the buffer region. It was therefore deemed appropriate to run model-scale simulations with both high and low Y^+ values in order to validate simulations using both the Wall Function and Near-Wall approaches. As can be seen in Table 41, the two methods produced similar results with the lower Y^+ simulation, giving slightly enhanced accuracy as was expected. It was decided that the validation would run at model scale using lower Y^+ values (<1) and at full-scale using higher Y^+ values (>30). Figure 86 and Figure 87 below indicate the wall Y^+ frequency distribution range for the propeller simulations post-completion.

Table 41. Wall Y^+ Study

	$Y^+ < 1$			$Y^+ > 30$		
$J = 1$	KT	KQ	η_0	KT	KQ	η_0
<i>Error (%)</i>	3.30	0.59	2.72	4.19	-0.62	4.78

* Error (%) represents the difference between the numerical results and the experimental values.

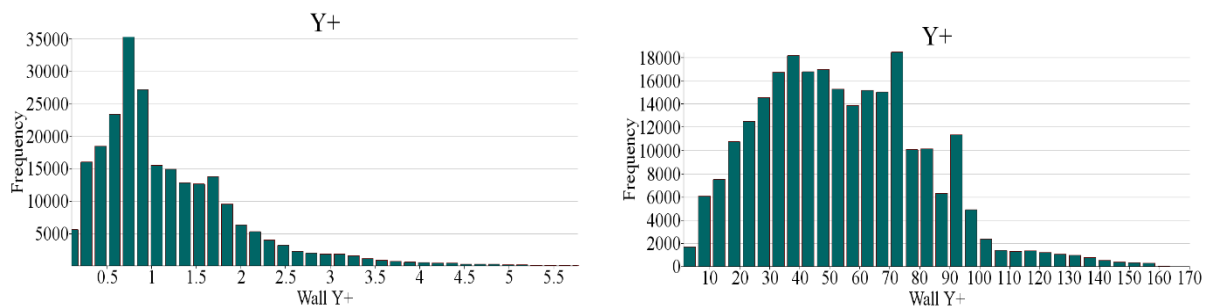


Figure 86. Y^+ Histogram (Model and Full Scale Respectively)

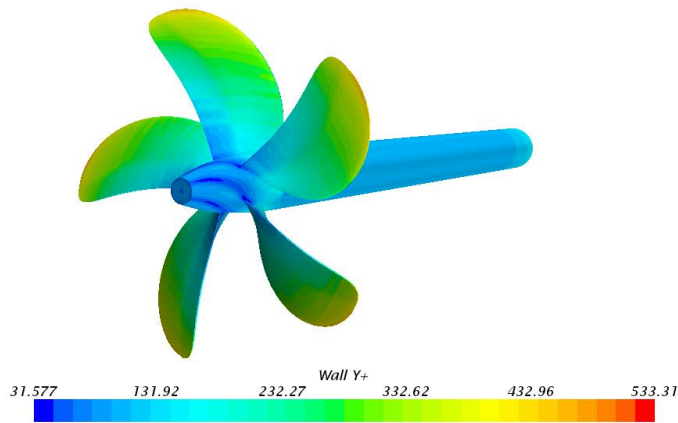


Figure 87. Y⁺ Values (Full-Scale CAESES)

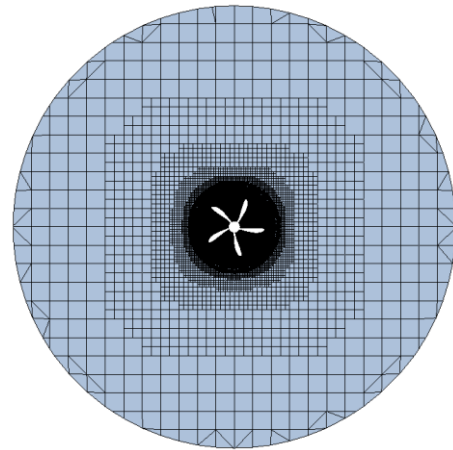


Figure 88. Mesh Refinement

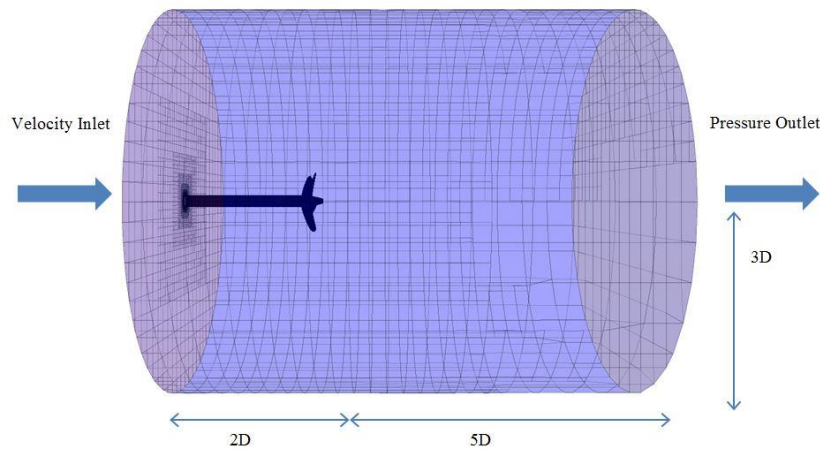


Figure 89. Boundary Conditions

7.5 Results & Discussion

7.5.1 Full-Scale Propeller Analyses

Although validation was carried out at model-scale with the Potsdam propeller geometry, the CAESES propeller was analysed in full-scale conditions in order to produce more accurate results. As seen in Figure 30, the CAESES propeller was first numerically analysed without any PBCF over a range of J values in order to analyse the propeller performance and identify a propeller operating point for the PBCF optimisation. A suitable condition was found to be at $J=0.8$, which is in between the accurate range of the simulation as previously indicated in the validation study. Various PBCF designs were then installed on the CAESES propeller, simulated at the operation point ($J=0.8$) and compared with the no fins condition.

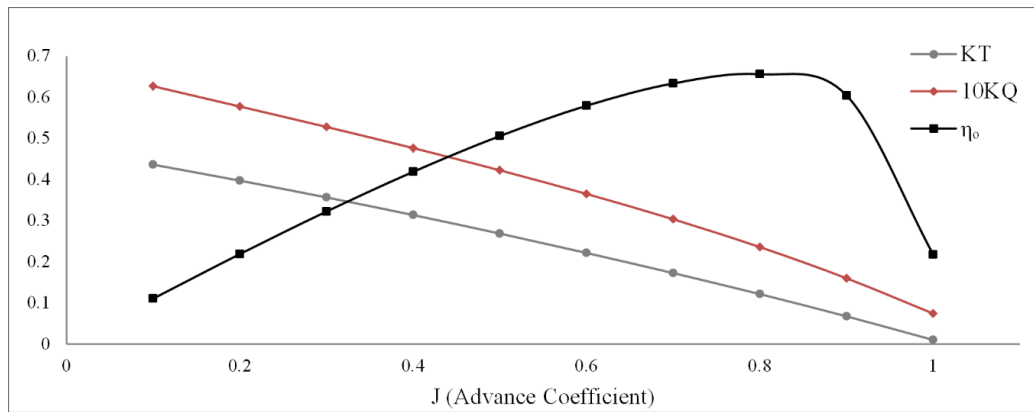


Figure 90. CAESES Open Water Characteristics

7.5.2 Optimisation Results

Figure 91 indicates the results of the 45 installed fins generated by the Sobol engine with respect to the no-fin propeller condition at the operating speed. For the ease of visual purposes, the graph only indicates from 0.75 to 0.95 η_0 , representing the peak of the open water efficiency curve in order to be able to identify the better designs. Most of the designs were detrimental to the open water efficiency, with only a few of them providing beneficial results. Promising candidates indicated a potential propulsion efficiency benefit of up to 1%. Table 42 presents a few selected cases of the analysed designs showcasing the parameter values and the associated results. It can be seen in Figure 92 that the best design candidate produces the highest thrust. However, it is noted in Figure 93 that this design does not feature the lowest torque. Thus, this indicates that the 2.5% gain in KT outweighs the expense of 1.4% increase in KQ, resulting in a 1% net efficiency gain. These outcomes are not in agreement with other authors' works (Kawamura et al., 2012, Ouchi et al., 1990) who state that the enhanced efficiency is a result of an increased KT and a decrease in KQ. This could be due to a number of reasons such as different geometry configuration, scale effects and also behind- propeller conditions. Results from this study have however indicated that the best design candidate in full-scale open water conditions produced a significant gain in KT outweighing the increase in KQ. This could be due to the fact that the thrust produced is larger at full-scale Reynolds number (Kawamura et al., 2012). These results and outcomes would be interesting to investigate further.

A deduction that was concluded from the better designs was that the fin pitch angle was of the same orientation and similar value to that of the propeller blades. In addition, the circumferential angular position of each fin was best suited to be like that of the blades. Three optimal candidates were then identified for further analyses using an optimisation algorithm.

Table 42. Sample of Sobol Design Results

<i>Sobol Designs Number</i>	<i>Fin Height (m)</i>	<i>Fin Length (m)</i>	<i>Max. Thickness (m)</i>	<i>Pitch (°)</i>	<i>Start Angle (°)</i>	<i>KQ</i>	<i>KT</i>	<i>η0</i>
1	0.32	0.53	0.0610	25.0	53.3	0.0239	0.1244	0.6617
3	0.19	0.58	0.0515	37.5	62.1	0.0239	0.1246	0.6628
17	0.35	0.51	0.0111	34.4	37.7	0.0239	0.1247	0.6637
19	0.22	0.46	0.0396	21.9	46.6	0.0239	0.1244	0.6616
30	0.08	0.64	0.0349	28.1	33.3	0.0239	0.1240	0.6616

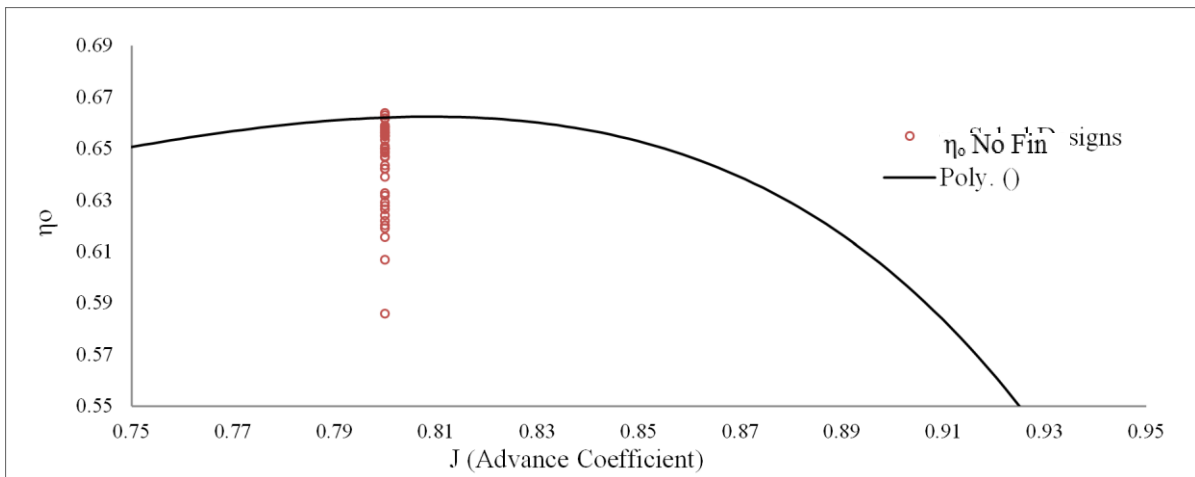


Figure 91. Quasi Random Designs

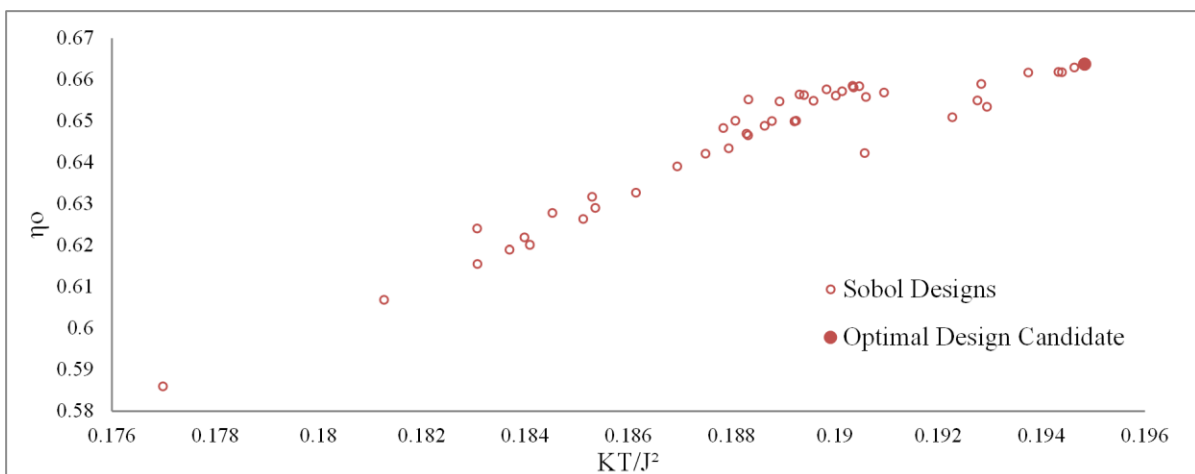


Figure 92. KT Optimal Design Candidate

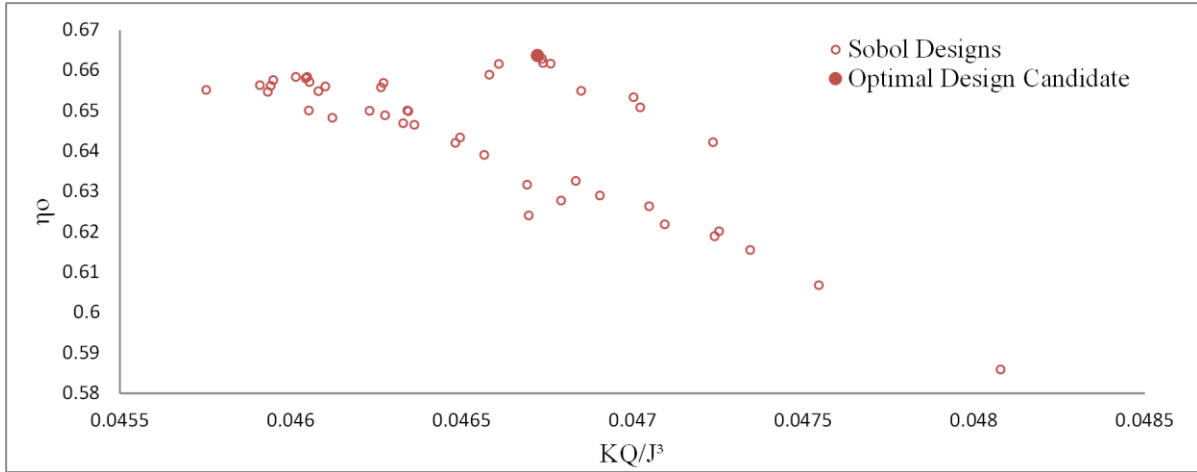


Figure 93. KQ Optimal Design Candidate

These candidates were named A, B and C in descending order of favourable open water characteristics. They were optimised further for 25 iterations using the T-search method. After the optimisation process, design A proved to be the best design. Results indicated that optimising the candidates resulted in only fine tuning the angular fin position as can be seen in Figure 94. The optimiser also varied the other parameters independently, which did not produce any better results. This can be seen in Figure 94, where the angular fin position remained constant. Table 43 demonstrates the optimal open water efficiency gained by the three designs post the T-search analysis when compared to the no PBCF condition. Therefore, after analysing 120 PBCF designs, the maximum energy efficiency gained by using such a process resulted in being 1.30%. It should be noted that 1% of the net gain was achieved using the quasi-random batch design analyses (Sobol) and the other 0.3% by using the optimisation algorithm (T-search). Table 44 represents the design parameters for the optimal PBCF (A).

Table 43. Energy Efficiency Gain

<i>Design</i>	<i>KT</i>		<i>KQ</i>		η_o		<i>Increase in η_o (%)</i>
	<i>Sobol</i>	<i>T-search</i>	<i>Sobol</i>	<i>T-search</i>	<i>Sobol</i>	<i>T-search</i>	
<i>No Fin</i>	0.1216		0.0236		0.6563		-
<i>A</i>	0.12470	0.12468	0.02392	0.02388	0.6637	0.6648	1.30
<i>B</i>	0.12457	0.12461	0.02393	0.02392	0.6628	0.6632	1.06
<i>C</i>	0.12437	0.12455	0.02393	0.02394	0.6617	0.6625	0.95

Table 44. Optimal Design Parameters

<i>Design A</i>				
<i>Height (m)</i>	<i>Length (m)</i>	<i>Thickness (m)</i>	<i>Pitch (deg)</i>	<i>Angular Fin Position (deg)</i>
0.352	0.512	0.0111	34.38	37.06

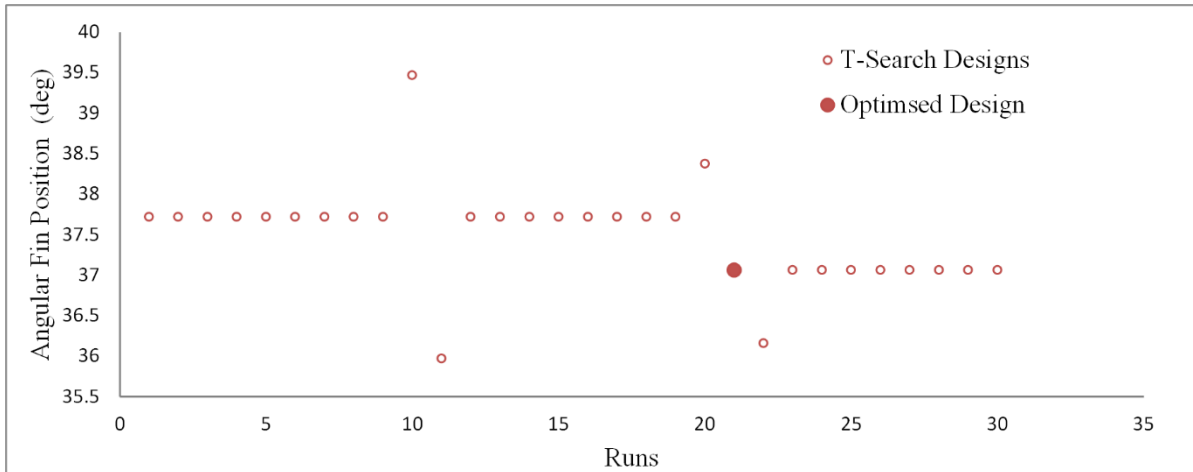


Figure 94. Angular Fin Position Variations

7.6 Physics of PBCF

7.6.1 Pressure Distribution

The propulsion system has also been analysed for pressure distribution, as can be seen from Figure 95. The figures show a pressure drop on the suction side (right) of the boss cap fins indicating that they are actually producing a lift force in the opposite direction to that of the propeller thrust, hence generating a drag. Simultaneously, such a force results in the PBCF generating a torque in the opposite direction to the propeller torque, which contributes to the cancellation of the propeller hub vortex. An additional interaction effect results from the optimum angular position of the PBCF relative to the blades. As shown in Fig. 95, the optimum position of the fins coincides with the angular position of the blade root section. The high-pressure side of the fin is more affected than its low pressure side by the lower pressures present at the propeller blade root. Similarly, the pressure side of the propeller blade root is more affected than the suction side of the blade root due to the high pressures generated by the fins. Such interaction effects would modify the magnitude of the negative thrust of the fins, and that

of the positive thrust at the blade root sections. The propeller efficiency improvement of the system can therefore be assumed to be coming from the interaction effects of the propeller with the PBCF. It was deemed necessary to look into the performance breakdown of the propulsion system in order to understand the changes in the system behaviour with and without the fins.

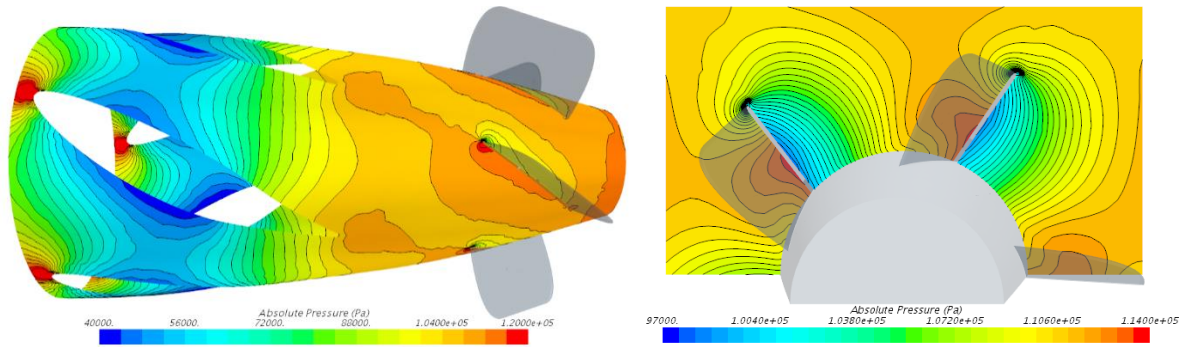


Figure 95. Pressure Distribution

7.6.2 Propulsion System Performance Breakdown

Table 45 presents the performance breakdown, in terms of Thrust and Torque, of each component in the propulsion system as a percentage, outlining their contributions to the system before and after the fins were installed. A positive value indicates a force/moment in the same direction of the propulsion systems' thrust or torque, and a negative percentage subsequently indicates the opposite. For example, if one looks at the thrust ($1.435 \times 10^6 N$) of No PBCF condition, it is understood that the blades are generating a higher thrust ($100.72\% \times 1.435 \times 10^6 N$) than that net force produced by the propulsion system that is subsequently reduced due to the resulting drag of hub and boss cap. As expected for both the PBCF and No PBCF conditions, the blades produced most of the thrust and torque with the hub generating a negative thrust (drag) and a negligible torque. However, at the No PBCF condition, the boss cap produced minimal drag, which was then converted to thrust once the fins were installed.

Table 45. Performance Breakdown

	No PBCF		PBCF	
	Thrust (N)	Torque (Nm)	Thrust (N)	Torque (Nm)
<i>Propulsion System</i>	1.435×10^6	2.228×10^6	1.471×10^6	2.259×10^6
<i>Blades %</i>	100.72	99.99	100.67	100.29
<i>Hub %</i>	-0.67	0.01	-0.64	0.01
<i>Boss Cap %</i>	-0.05	0.00	0.52	0.00
<i>PBCF %</i>			0.55	-0.3

Table 46. Performance Difference after PBCF Installation

Propulsion Components	Performance Difference	
	<i>Thrust (%)</i>	<i>Torque (%)</i>
<i>Propulsion System</i>	2.50	1.39
<i>Blades</i>	2.47	1.69
<i>Hub</i>	0.01	0.00
<i>Boss Cap</i>	0.58	0.00
<i>PBCF</i>	-0.57	-0.30

Table 46 outlines the change in performance of each propulsive component after PBCF installation as percentages of thrust and torque values of the baseline propulsion system (No PBCF condition). Once the fins were installed, the total propulsion system produced net values of 2.5% additional thrust and 1.39% more torque than the corresponding NO PBCF condition. In order to further understand where these increments came from, the performance of each component was analysed individually and compared to its own performance prior to the installation of the fins. The following deductions were identified:

- The significant differences come from the blades themselves generating +2.47% and +1.69% higher thrust and torque respectively.
- The installation of the fins introduced a drag (-0.57%) as depicted in Figure 95. They are however reducing the torque (-0.30%) of the system.
- The boss cap goes from creating drag to producing a thrust (+0.58%).

The difference in behaviour of the boss cap was considered interesting. This could only be justified by the disappearing low-pressure gradient at the tip of the boss cap once the fins were installed (Figure 96). This pressure drop occurs at the same location where the hub vortex is generated and could be the cause for a generated lift in the opposite direction of the thrust. An additional outcome from this study has indicated, that the propeller efficiency improvements do not come from the fins themselves but from the interaction effects, thereby resulting in performance differences of the blades and boss cap. This statement, however, requires further investigation and justification.

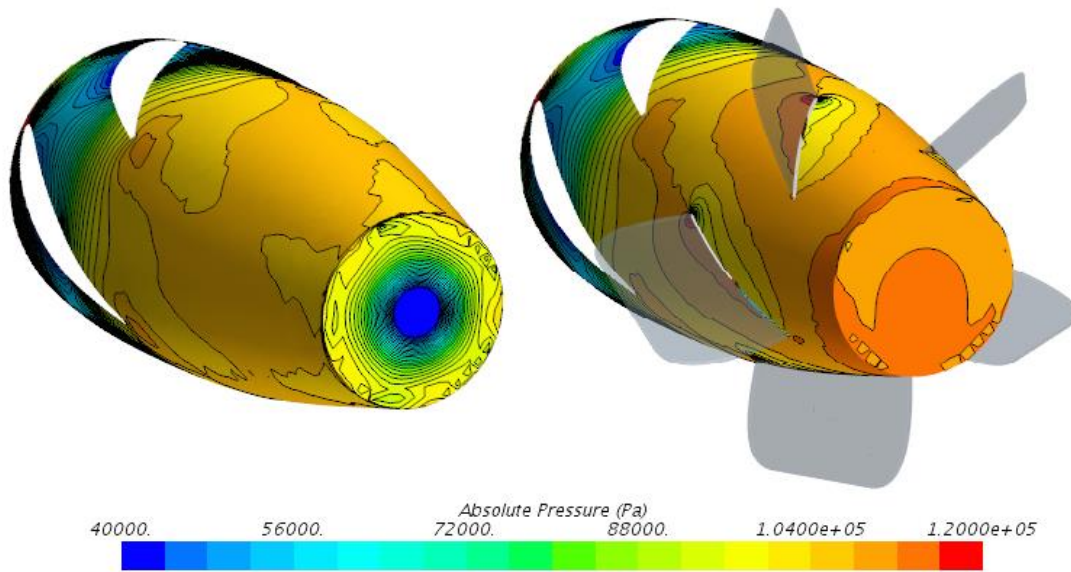
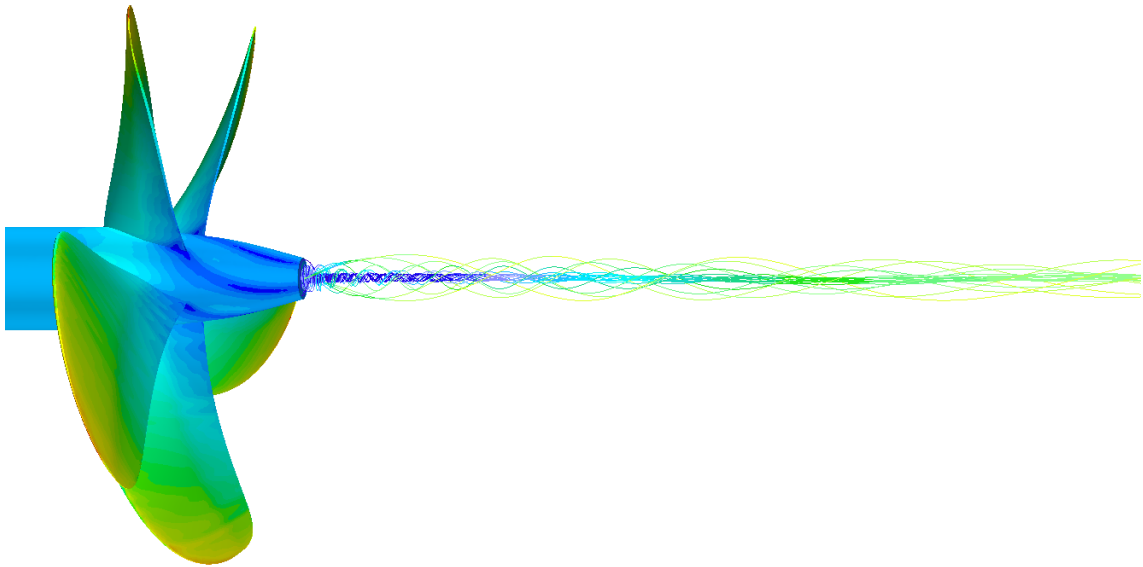


Figure 96. Boss Cap Tip Pressure Drop

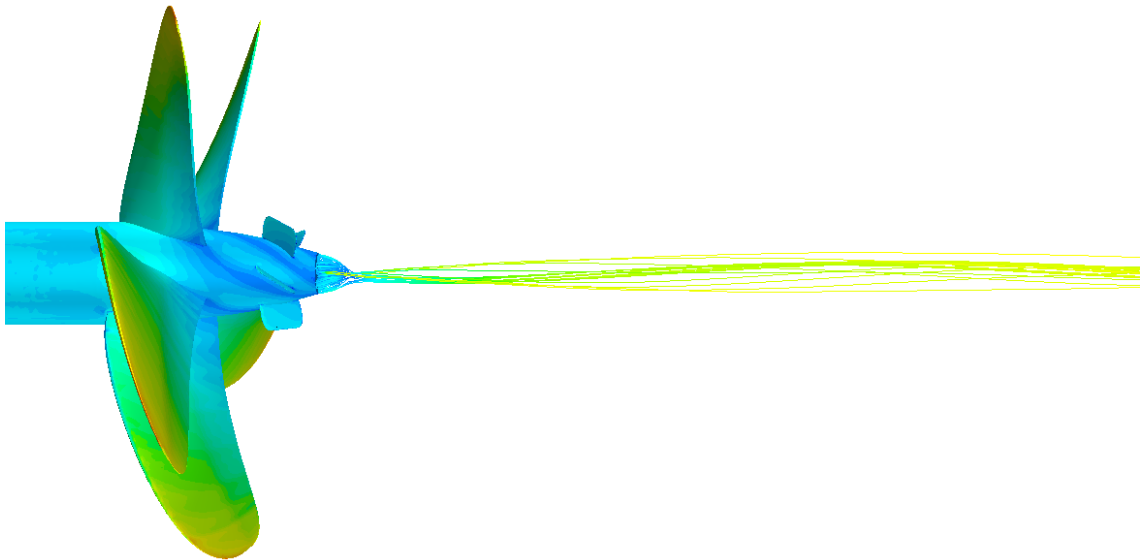
7.6.3 Hub Vortex

Other than just providing favourable open water characteristics, a PBCF can also help reduce the hub vortex. As explained by Atlar et al. (1998), this wastes a lot of energy as it introduces an adverse, strong swirl into the propeller slipstream. In addition, a hub vortex can also lead to rudder cavitation and cause undesirable vibration and noise. Figure 98 demonstrates the beneficial effect of the PBCF (optimised A) by reducing the hub vortex downstream of the hub.

Atlar et al. (1998) explain the formation of this vortex by breaking it down into two types of flow i.e. primary and secondary. The former is caused by the inversely magnified values of tangential water velocities around the hub, and the latter is generated as a result of the moving flow on each side of the blade creating differences in pressure thus generating a vortex element at each blade root. The latter can be clearly seen in Figure 97a. In addition, it was indicated that the viscous boundary layer caused by the frictional drag also contributed to the secondary flow and hence the vortex. Further to this, Funeno (2002) points out that the shape or form of the boss cap also has an effect on the performance characteristics of a propeller. He carries out a study to analyse the flow around a boss cap and hub vortex using CFD techniques, by comparing a truncated boss cap with a cone type geometry. The truncated shape produced a smaller maximum vorticity hub vortex with a lower minimum pressure, leading to a weaker vortex and better propeller efficiency.



a) Without PBCF



b) With PBCF

Figure 97. Hub Vortex

7.7 Additional Comments

Previous studies have shown that PBCF are capable of producing higher efficiency gains than that indicated in this study, especially with regards to controllable pitch propellers (Wang and Department, 1985). This could be due to a number of factors. It should be noted that most of the experimental tests and numerical simulations have been carried out at model scale. As

previously discussed, the laminar flow plays a significant part in model scale conditions while full-scale scenarios generate fully turbulent flow with insignificant laminar regions. Generally, the scale effect is accounted for by making use of empirical formulae which can prove to be unreasonable or inaccurate as indicated by Funeno (2002). For more accurate simulations, all the analyses for this study were carried out at full-scale, which might explain the differences in the outcomes. That being said, this statement requires further verification. In addition, this study did not take into account any cavitation modelling that might influence the propulsion efficiency characteristics of a propeller; this could be another valid reason for the discrepancy.

By considering the factors mentioned above, it might be worthwhile to extend this study by adding more design variables, such as boss cap design parameters together with its shape. Furthermore, as previously mentioned, outcomes from this study indicated that the benefits of PBCF did not come from the fins themselves but from the interaction effects resulting in performance differences. This area requires further investigation and justification. Additionally, a multi-objective optimisation approach could be used to seek a geometry providing maximum energy efficiency and a reduction in hub vortex cavitation; which might result in different optimal fin geometry altogether. Further to this, studies (Ouchi et al., 1990) demonstrated that the presence of the rudder behind the propeller significantly affects the results. The incoming flow in open water tests is uniform in contrast to the case for hull-stern conditions, which might result in different optimal PBCF designs. Therefore, the installation of PBCF on the stern of a ship in self-propulsion condition was later analysed in Chapter 9 to better understand their function in these conditions. Since cavitation adversely affects propeller characteristics, future work should put more effort into implementing a cavitation model into the open water simulation. As evidenced by Tezdogan et al. (2015), ship motions could also be effectively modelled using CFD. Therefore, another sophisticated study would be to carry out the optimisation of PBCF on the stern of a ship under wave conditions. Furthermore, to what extent is the hub vortex cancelled, and to what extent is the original propeller designed to have a large circulation at the root (resulting in hub vortex), are both key factors that should be taken into account into the design philosophy of PBCF.

7.8 Chapter Summary and Conclusion

This study has demonstrated the benefits of the developed automated optimisation technique which is able to deliver the best designs and maximise results from a system in an easy, quick and effective manner. The proposed methodology can be applied to different case studies and modified to suit different scenarios. This chapter exhibits the capability and process for designing PBCF using numerical methods and optimisation procedures, enabling the identification of optimal designs for different case studies and situations. After analysing 120 different PBCF designs, using a quasi-random batch method together with an optimisation algorithm approach, a particular PBCF design was identified to produce an open water efficiency improvement of 1.3% at full scale compared to that of a propeller without PBCF. This does not imply that this particular design would be optimal for all case scenarios; each ship form and propeller results in different ship flow patterns, thus requiring tailored optimal models. Although this study focused on the optimisation of PBCF, the same process and methodology can be applied to different energy-saving devices or case studies to suit different requirements.

Furthermore, this study successfully contributed to the knowledge and understanding of the physics behind PBCF in full-scale conditions by looking into the pressure distributions, performance breakdown of different components and hub vortex phenomena. This technology (PBCF) is later analysed behind a ship in Chapter 9.

8 ESD Performance Impact in Different Scale Environments

8.1 Introduction

As previously highlighted in the Literature Review, different magnitudes of Reynolds Numbers lead to different fluid flow behaviour at different scales. This implies that wake characteristics, together with vessel performance, differ in different scale environments. Although well-established extrapolation methods have demonstrated they successfully identify the performance of full-scale vessels (with no retrofitting technology) through correlated data and model basin experience, it is very hard to measure and study the flow behaviour on a real ship that is under operation. This phenomenon, also known as scaling effects, becomes even more complicated when considering Energy Saving Devices (ESD) in ship design. Due to the change in boundary layer behaviour at different lengths or sizes, the performance of ESD alters and the impact of technology is not straightforward. ESD function is highly dependent on the wake of a vessel, which is also determined from the boundary layer. In other words, the measured performance of these retrofitting technologies will change between model scale and full-scale scenarios. This makes it challenging to identify the impact of ESD in full-scale environments through model test experiments. This is a popular topic in the marine industry with different sources claiming they have different impacts and behave differently to full-scale ESDs.

With these issues being the motivational drivers behind this part of the study, the analyses will focus on analysing the following areas using the validated and verified state of the art CFD methods highlighted in Chapter 4:

1. Fluid Flow Analyses at different scales
2. ESD impact at model scale
3. ESD impact at full scale

This chapter is divided into three main sections with each tackling a respective study, highlighted above, by using the geometry presented in Chapter 3. Furthermore, these studies correspond to module 4 presented in Figure 4 (Study Procedure). With regards to the first study, the JBC geometry (with no duct) is analysed in both model and full-scale conditions and

compared, focusing particular attention on the wake flow characteristics. This is followed by another study, whereby the JBC geometry (with duct) is analysed in model and full-scale conditions and the impact of the ESD in each environment is analysed and compared. The differences between the two scales are also highlighted. These studies are analysed in great detail, investigating performance breakdown, wake flow characteristics, propeller excited vibrations and more.

In summary, this chapter addresses a key issue in the marine industry, scaling effects. The studies have been devised into three segments, with each focusing on a particular investigation. The research behind each module is presented and discussed together with any concluding remarks, and findings are outlined.

8.2 Performance and Fluid Flow Behaviour at Different Scales

This section compares the performance of the JBC vessel at two different scales. It is not new knowledge that a particular hull-propeller system performs differently in different scale scenarios. One of the main drivers behind such issues is the different flow behaviour that develops at different ship lengths due to the difference in Reynolds number, thus generating different flow fields.

These effects have been well accounted for in traditional designs where well-established methods (ITTC, 1999) have been developed to extrapolate the model scale data that was measured from towing tank procedures. These methods or empirical formulae have matured over the years through cumulative experience, extensive data and advanced knowledge. However, when it comes to unconventional designs, such as newer hull forms and/or the installation of Energy Saving Devices, maintaining performance prediction accuracy at full scale is rather challenging. With extrapolation methods being refined according to data sets of conventional hull forms, these approaches are no longer applicable to the progressive hull – propeller interaction systems. Hence, the current need to analyse these types of designs using computational fluid dynamics to simulate the performance at full-scale and predict realistic parameters. These issues were demonstrated in Chapter 4, where the powering (extrapolation) of the model scale data of the hull with no duct agreed fairly-well with the full scale CFD analyses. However, the powering methods indicated that the installation of the duct improved the performance, whereas the CFD methods indicated a detrimental performance with duct inclusion. As previously indicated, extrapolation procedures for such designs are not yet mature

enough to ensure reliability. CFD procedures are considered to be more trustworthy due to their systematic measurement methods. Always taking into consideration the measurement uncertainty of CFD methods, these methods give a good indication of performance trends if approaches are carried out systematically providing valuable insight into the function of ESD at full scale.

Section 8.2 will focus on analysing the impact on the propulsive performance at different scales of the baseline hull with no duct. An investigation was carried out to analyse the performance of the baseline Japan Bulk Carrier with no duct both at model-scale and full-scale conditions. Results were compared and key findings/outcomes are outlined and presented in this chapter. All the simulations were carried out using the state of the art CFD procedure outlined in Chapter 4. Since scaling effects of ‘conventional designs’ have been studied extensively over the years, these criteria will be briefly analysed outlining key issues and findings, especially those related to wake field development and flow field behaviour. The purpose of this section is to re-confirm the difference in ship performance at different Reynolds numbers.

As demonstrated in Table 47, the full-scale JBC hull-propeller system produced a smaller propulsive efficiency (0.698) than the corresponding model scale configuration, (0.740) recording a reduction of about 5.7%. Although the relative rotative efficiency (η_R) and the open water efficiency (η_{ow}) increased in ship scale conditions, the significant reduction in hull efficiency, from 1.517 to 1.172, reduced the overall propulsive performance.

The hull efficiency was then further analysed in order to understand the science behind the contrasting performance. With the hull efficiency being a function of the thrust deduction fraction and the wake fraction, these parameters were further investigated. The thrust deduction term (1-t) resulted in minor changes between both scales with the discrepancy in the wake fraction (w_t) being more significant. Thus, it can be considered to be the primary parameter behind the hull efficiency variation. The mean velocity ratio (1-w) has increased from 0.5264 at model scale to 0.649 in full scale conditions. If this parameter had to be represented in terms of wake fraction values, it could be outlined that the mean wake fraction decreases at larger scales. This is not new knowledge and re-confirms the outcomes and findings from the literature, whereby the difference in Reynolds numbers alters the fluid flow behaviour. This results in a reduced boundary layer thickness ratio which produces a reduced wake fraction, thereby indicating a higher velocity flow field in the wake.

Table 47. Propulsion Performance Scaling

Parameter		Model Scale	Full Scale
U	[ms] : Ship Speed	1.179	7.4566
n	[rps] : Propeller Revolution Rate	7.72	1.28
K_T	: Thrust Coefficient	0.22295	0.1947
K_Q	: Torque Coefficient	0.028793	0.0243
$I-t$: Thrust Deduction Term	0.798	0.761
J	: Advance Ratio	0.396	0.47
$K_{Q,ow}$: Torque Coefficients Open Water	0.02884	0.0257
$I-w_t$: Mean Velocity Ratio	0.5264	0.649
η_{ow}	: Open Water Efficiency	0.487	0.562
η_R	: Relative Rotative Efficiency	1.00163	1.06
η_H	: Hull Efficiency	1.517	1.172
η_D	: Propeller Efficiency	0.740	0.698

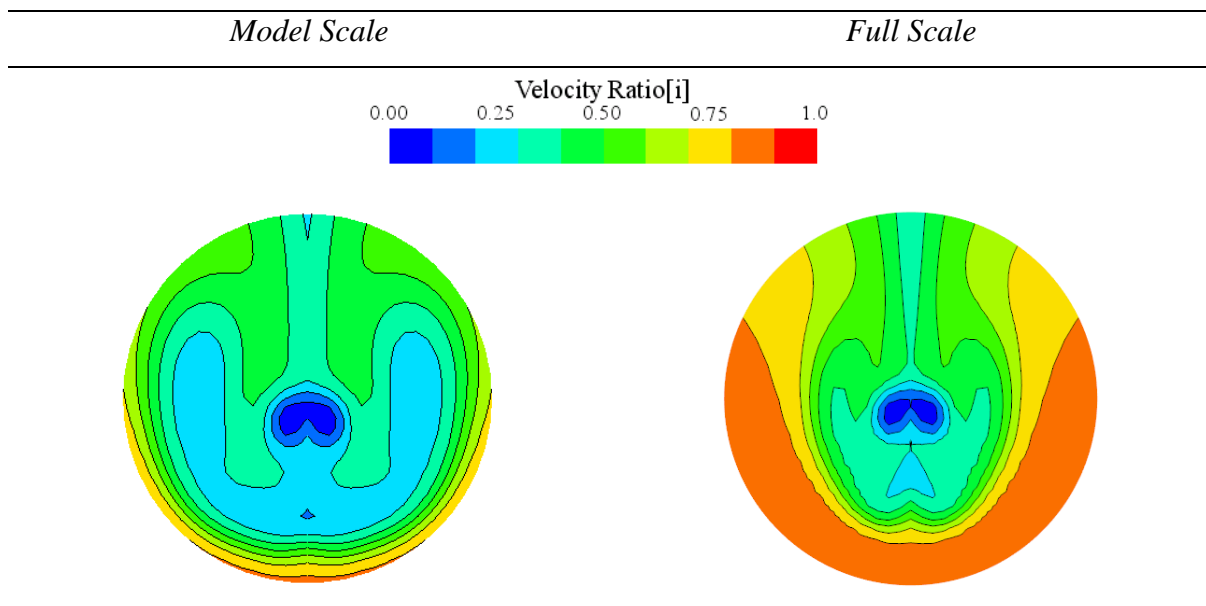
Such changes in the wake fraction cause the hull efficiency to decrease but also bring about an increase in the open water efficiency due to the higher advance ratio (J). That being said, the hull efficiency parameter has a greater weight on the propulsive efficiency thus reducing the overall value. This analysis clearly indicates that the propulsive behaviour differs at different scales.

Post-processing analyses was further carried out to analyse the axial wake velocities at different locations/ planes in the longitudinal direction. The previously defined WAT tool was utilised to quantify the wake characteristics. As demonstrated in Table 48, wake analyses at the propeller plane in towing conditions indicated a significantly smaller wake fraction at full scale with contrasting values of 0.524 (model) and 0.296 (full). However, the non-uniformity of the wake increases in ship scale scenarios (from 0.324 to 0.448), resulting in a higher risk of pressure excited vibrations. This fluid flow behaviour was further demonstrated via visual representations as presented in Table 49. The increased change in velocity near the top dead centre position is evident in the full-scale condition. Furthermore, the vortical structures (vortices) are less pronounced and flow stagnation region areas decreased due to less separation of the flow.

Table 48. Wake Scaling Analyses @ Propeller Plane (Towing)

Parameter	Model Scale	Full Scale
<i>Taylor Wake Fraction</i> $[w_t]$	0.524	0.296
<i>Non- Wake Uniformity</i> $[\Delta w]$	0.326	0.448

Table 49. Wake Scaling @ Propeller Plane (Towing)



Similarly, wake analyses in self-propulsion conditions at $0.0168L_{pp}$ and $0.0375L_{pp}$ in the longitudinal direction exhibited similar behaviour. The furthest, upstream, wake plane at $0.0375L_{pp}$ demonstrates that the vortices are no longer present in full-scale conditions and that flow stagnation is less pronounced around the hull.

It is worth highlighting that although the wake fraction reduced at $0.0168L_{pp}$ at full scale, the overall wake non-uniformity was barely affected as demonstrated in Table 51. That being said, it is evident from Table 52, that at the lower radii, the velocity variation over the whole radius is greater and at the higher radii, velocity variation is lower. This probably evened out the overall value explaining why the results are similar in magnitude. However, as presented in Table 52, wake characteristics are significantly different, with the full-scale scenario indicating high wake non-uniformity around the top dead centre once again.

Table 50. Wake Scaling @ 0.0375Lpp (Self-Propulsion)

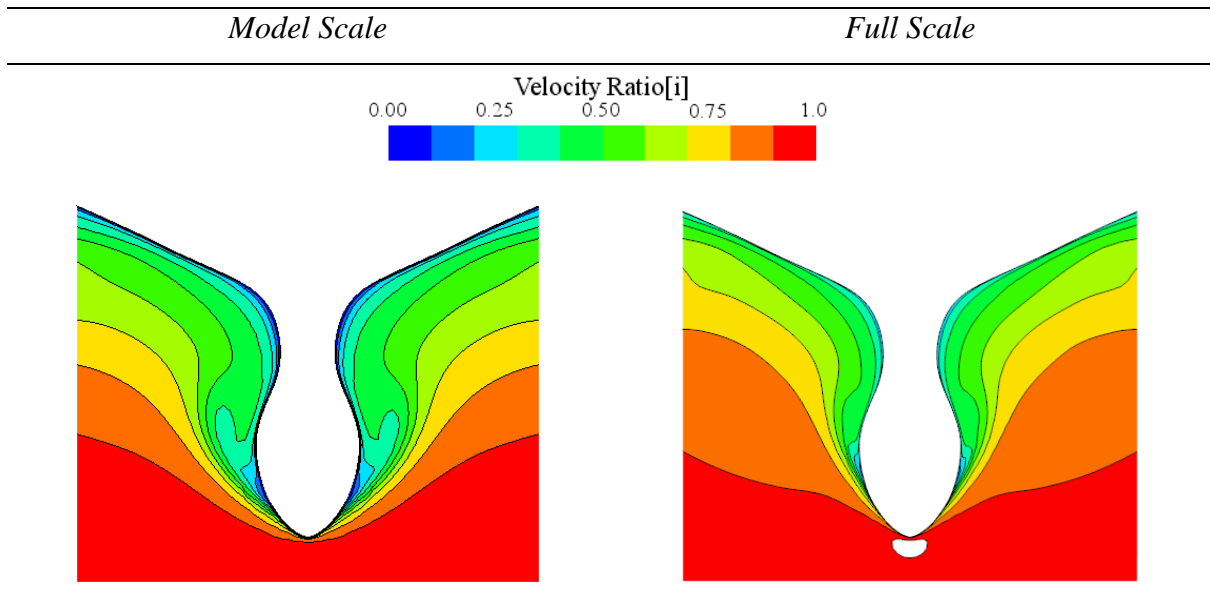
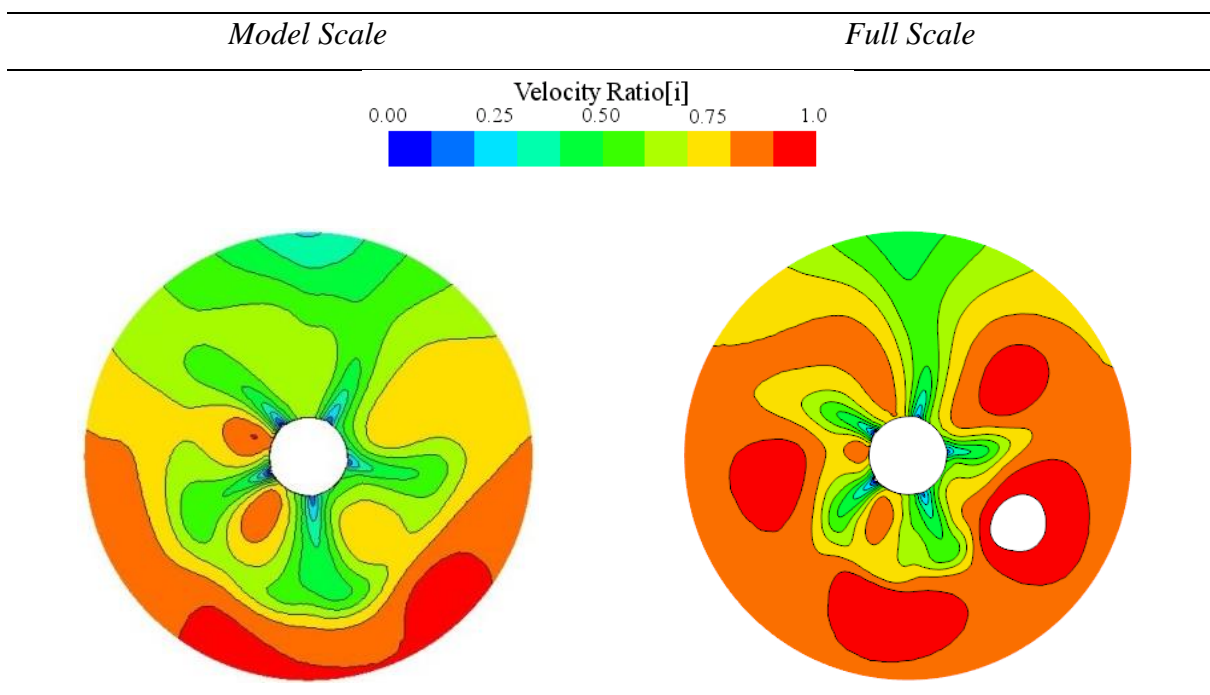


Table 51. Wake Scaling Analyses @ 0.0168Lpp (Self-Propulsion)

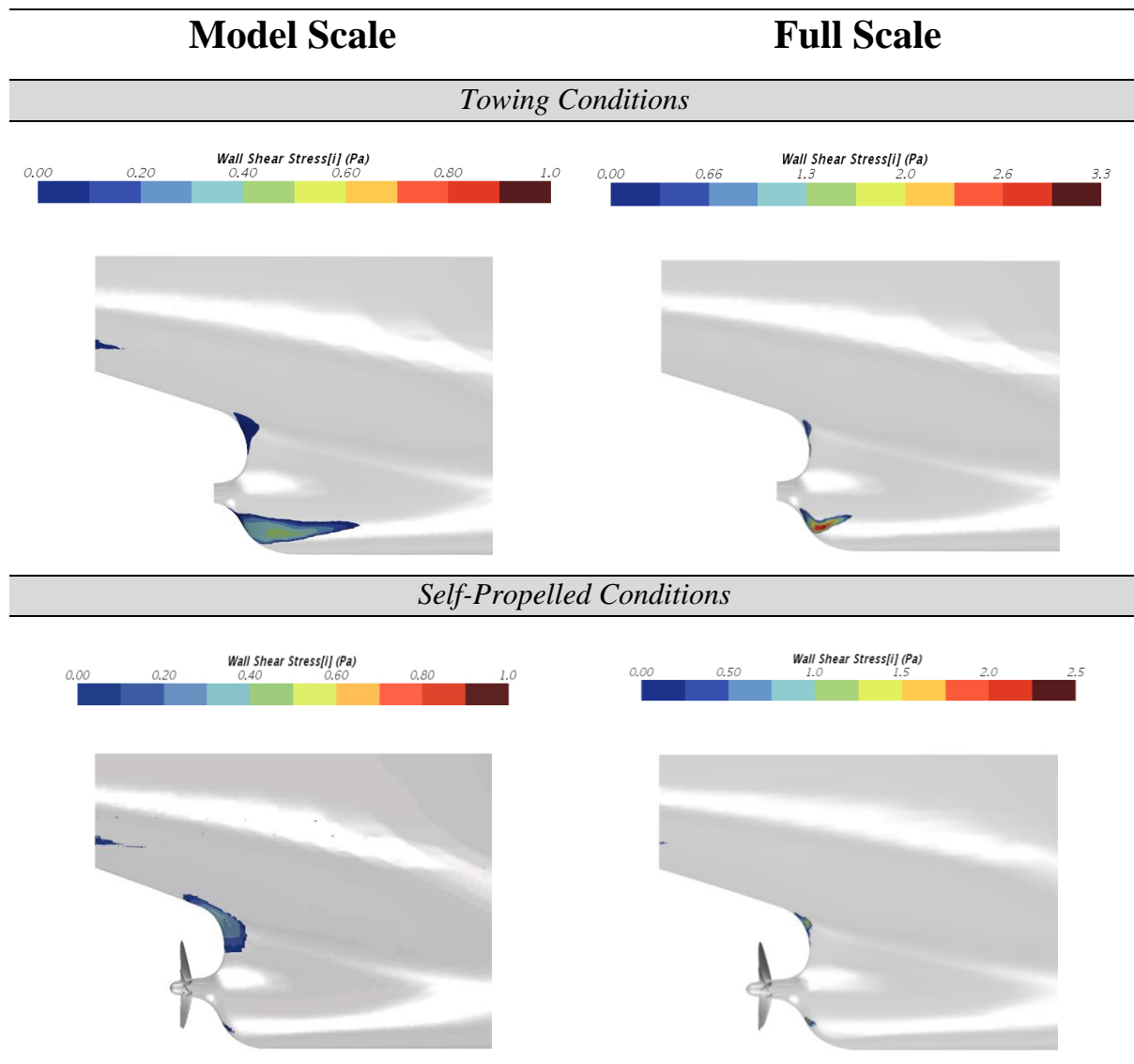
Parameter	Model Scale	Full Scale
<i>Taylor Wake Fraction</i> $[w_t]$	0.304	0.213
<i>Non- Wake Uniformity</i> $[\Delta w]$	0.468	0.463

Table 52. Wake Scaling @ 0.0168Lpp (Self-Propulsion)



The figures presented in Table 53 illustrate the wall shear stress analyses at both scales, where a null value indicates flow separation and a positive value indicates recirculation of the flow. It is noticeable that the towing ship experiences less separation both at the underside of the hull below the boss cap, as well as in the stern valley region. However, although the area of positive wall shear stress is diminished, the maximum value for the full-scale conditions is greater, indicating that the ship experiences stronger reversed flow for that particular region. It also shows that the presence of the propeller further reduces these effects in both scenarios.

Table 53. Wall Shear Stress Analyses Scaling effects



8.3 ESD Impact at Different Scales

This section analyses the impact of the duct on the vessel performance both in model and full-scale conditions using CFD analyses. The ESD analyses checklist is processed for both scales independently and the section concludes by comparing the differences and investigating the change in duct performance at different lengths. A comprehensive analysis is done in order to understand the physics behind such impacts and behaviours.

8.3.1 ESD Investigation at Model Scale

This case study investigates the performance of the JBC vessel at model scale with and without duct by going through most of the pre-defined ESD analyses checklist and the major findings/outcomes are presented. All the simulations were carried out using the state of the art CFD procedure outlined in Chapter 4.

Table 54. Performance: Towing

Parameter			Without ESD	With ESD
U	[ms]	: Ship Speed	1.179	1.179
R_T	[N]	: Towing Resistance	35.533	35.52
CT	[m]	: Total Resistance Coefficient	4.191	4.171

Table 55. Performance: Self-Propulsion

Parameter			Without ESD	With ESD
U	[ms]	: Ship Speed	1.179	1.179
R_{TSP}	[N]	: Self-Propulsion Resistance	40.073	40.037
D	[m]	: Propeller Diameter	0.203	0.203
n	[rps]	: Propeller Revolution Rate	7.72	7.5
T	[N]	: Propeller Thrust	22.524	22.4
Q	[Nm]	: Propeller Torque	0.5905	0.575
K_T		: Thrust Coefficient	0.22295	0.23492
K_Q		: Torque Coefficient	0.02879	0.02970
$I-t$: Thrust Deduction Term	0.798	0.798
J		: Advance Ratio	0.396	0.3655
$K_{Q,ow}$: Torque Coefficients Open Water	0.02884	0.0299
V_a	[ms]	: Advance Velocity	0.6206	0.5565
$I-w_i$: Mean Velocity Ratio	0.5264	0.4720
η_{ow}		: Open Water Efficiency	0.487	0.456
η_R		: Relative Rotative Efficiency	1.0016	1.0065
η_H		: Hull Efficiency	1.517	1.691
η_D		: Propeller Efficiency	0.740	0.776
P_d	[W]	: Delivered Power	28.64	27.1

Table 56. Resistance Breakdown: Towing

	Baseline Resistance			Retrofitted ESD/s		
	<i>Shear (N)</i>	<i>Pressure(N)</i>	<i>Total(N)</i>	<i>Shear (N)</i>	<i>Pressure(N)</i>	<i>Total(N)</i>
<i>Bare Hull</i>	27.01	8.52	35.53	27.005	8.17	35.177
<i>Duct</i>	-	-	-	0.045	0.288	0.333
<i>Total</i>	27.01	8.52	35.53	27.05	8.458	35.51

The impact of the duct on the performance of the bulk carrier is analysed in both towing and self-propulsion conditions. We will primarily look into the breakdown of forces (resistance) without the action or presence of the propeller and move on to study the performance and forces in self-propulsion environments (resistance, thrust and torque).

As demonstrated in Table 56, the introduction of the duct to the vessel geometry resulted in an insignificant reduction in the total resistance (please note that the experimental tests indicated a higher reduction in resistance). However, when taking the wetted surface area into account, one can see a noticeable reduction in the resistance coefficient (Table 54). This indicates that although the wetted surface area has increased (due to duct contribution), the total resistance value has minimally decreased from 35.53 N to 35.51N by 0.06%. As a general indication, this reveals that some kind of benefit is being produced. Although this magnitude of reduction lies within the simulation uncertainty, which raises some concern, experimental results exhibited similar behaviour with a higher reduction in resistance. It was therefore deemed appropriate to further analyse the force components.

If we solely focus on the hull resistance i.e. the drag produced by hull form, analyses indicate that the introduction of the ESD reduced the resistance of the hull by around 1% (from 35.53 N to 35.18N. More specifically, the benefits are originating from a reduction in pressure resistance, i.e. 8.52N to 8.17N (3.4%). Therefore, it can be said that although the duct, in towing condition, is producing a drag, this detrimental effect is being outweighed by the benefit the duct has on the bare hull resistance. More particularly, a reduced bare hull pressure resistance indicates a reduction in flow separation and less energy lost to the slipstream due to the generation of vortices. This was further justified by comparing the Wall Shear Stress values between the geometries as presented in Figure 100 with values higher than 0, indicating regions of flow separation. Although a significant area of separation is evident on the JBC hull with duct, the magnitude of separation was higher on the JBC without duct. It is clear that the baseline hull without duct experiences stronger separation of flow. This was further confirmed

when analysing the wake at different planes upstream of the duct, highlighting reduced extents of separation around the ship hull (Figure 101). Visonneau et al. (2016), who also carry out the same study using a CFD approach, outline that this drag reduction is due to the suction effect of the duct that minimises the unsteadiness at the stern while Terwisga (2013) explains that a pre-duct reduces the flow separation at the aft resulting in a reduction of viscous pressure resistance. These comments reconfirm the outcomes of this study.

Table 57. Resistance Breakdown: Self-Propulsion

	Baseline Resistance			Retrofitted ESD/s		
	Shear (N)	Pressure(N)	Total(N)	Shear (N)	Pressure(N)	Total(N)
Bare Hull	26.9925	15.572	42.564	26.9	14.957	41.857
Duct	-	-	-	0.107	0.543	0.65
Boss Cap	0.0255	-2.517	-2.491	0.0205	-2.492	-2.47
Total	27.018	13.055	40.073	27.0275	13.008	40.037

Table 58. Thrust and Torque Breakdown: Self-Propulsion

	Baseline		Baseline with ESDs	
	Thrust (N)	Torque (Nm)	Thrust (N)	Torque (Nm)
Propulsion System				
Blades	22.52	0.5905	22.4	0.575
Total	22.52	0.5905	22.4	0.575

Shifting our attention to the self-propulsion simulations, the performance parameters in Table 55 are discussed first. This is followed by an analysis of the resistance, thrust and torque breakdown by the different components (Table 57 & Table 58). Before going any further, it is good to point out that although the hub is producing thrust, this was taken into consideration when calculating the resistance value. This was done because during experimental tests, due to thrust identity procedures, the thrust is only measured for the blades and therefore the propeller hub is considered to be part of the ‘hull’ system. The hub component still produces thrust and this is reflected in the net value of the resistance. The torque of the hub is negligible, around $2.5e-5$ Nm, so it was not taken into consideration.

The results show that the introduction of the duct improved the delivered power from 28.64W to 27.1W as a result of the reduced torque and rpm. Therefore, this suggests that the duct is having a beneficial impact. Further examination shows that the installation of the duct barely altered the relative rotative efficiency, reduced open water efficiency and significantly

improved hull efficiency (from 1.517 to 1.691); and this is the main attribute contributing to the overall increase in propulsive efficiency. The unaffected value of the thrust deduction fraction reveals that there is no difference in the self-propelled resistance between the two design configurations. This reflects the same drag behaviour output from the towing simulations. Although the thrust deduction fraction is uniform in both conditions, the ESD design configuration produced a higher wake fraction, thus providing an improved hull efficiency which is defined as shown in Equation 48. Since hull efficiency is defined as the ratio of the effective power to the trust power delivered by the propeller, a reduced $1-w_t$ indicates that less work is done by the propeller in delivering the required thrust thus indicating that the propeller performance has improved.

$$\eta_H = \frac{1-t}{1-w_t} \quad (48)$$

Generally, the optimisation and compromises involved in the ESD game is to increase w whilst ensuring that the expense of η_o does not outweigh the benefits of η_H . It is also important to point out that the influence of hull efficiency has more weighting than the open water efficiency on the propulsive efficiency.

Drawing attention to the resistance breakdown in Table 57, the shear resistance of the baseline hull (no duct) between towing and self-propulsion conditions varied insignificantly. However, the introduction of the propeller significantly increased the pressure resistance. This is normal since the augment in drag is due to the propeller action that is represented by the thrust deduction factor.

The hull with the duct in self-propulsion produced a slight increase in total shear resistance which exhibits similar behaviour to the towing test results in Table 56. This is logical due to the higher wetted surface area that the duct introduces. On the other hand, the duct reduced the total pressure resistance from 13.05 N to 13.00 N compared to the hull with no ESD. More specifically, despite the duct introducing an increase in shear and pressure resistance, the duct has a beneficial impact on the viscous pressure resistance of the bare hull (from 15.57 N to 14.96 N) which outweighs the resistance introduced by the duct. This indicates a reduction in the flow separation at the aft, as explained by Terwisga (2013). This resulted in an overall minimally reduced total resistance for the hull with the duct. At this point, it is also good to point out that experimental results indicated a bigger decrease in resistance than CFD predictions. Simulation results outlined that the resistance of the duct doubles when operating

in front of a propeller and this increment seems to be reflected in both the shear and pressure resistance of the duct.

With regards to concluding remarks regarding the function of the duct at model scale, it seems that the duct itself is producing a drag both in towing and self-propulsion conditions. However, its presence has a beneficial effect on the bare hull resistance (both in shear and pressure). Whilst CFD indicates that the difference in total resistance is minimal, the highest benefit is achieved through the enhanced propeller performance that is reflected in the hull efficiency.

As can be seen in Table 58, the thrust and torque produced by the propeller blades have decreased with the inclusion of the duct. These values, however, cannot be compared since the propeller is working under different conditions (e.g. rpm).

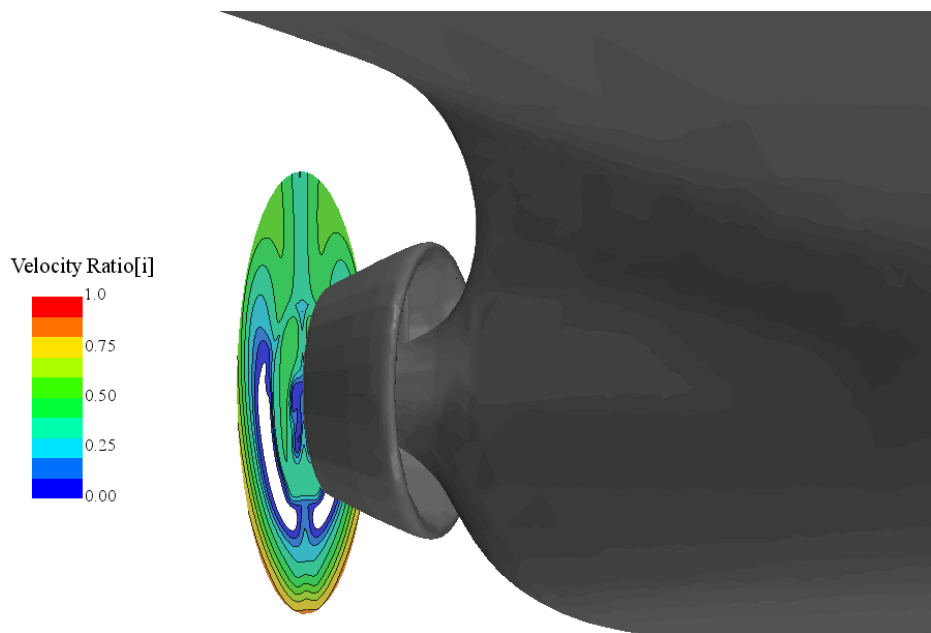


Figure 98. Wake Analyses

It has been demonstrated in the previous chapters that the CFD methods outlined in this study are capable of predicting wake behaviour. Therefore, the wake analyses in different conditions using this CFD procedure provides good insight into the physics of the fluid flow behaviour. The wake field data is analysed by using the previously mentioned WAT tool that quantifies the velocity field with meaningful information such as the wake fraction and non-wake

uniformity parameters. Furthermore, essential graphs exhibiting the velocity ratio distribution as well as the velocity variation along the radii are plotted for enhanced understanding of the flow behaviour. With the axial velocity being the most prominent component, the following wake analyses and figures are based in the axial direction.

Table 59. Wake Analyses @ Propeller Plane (Towing)

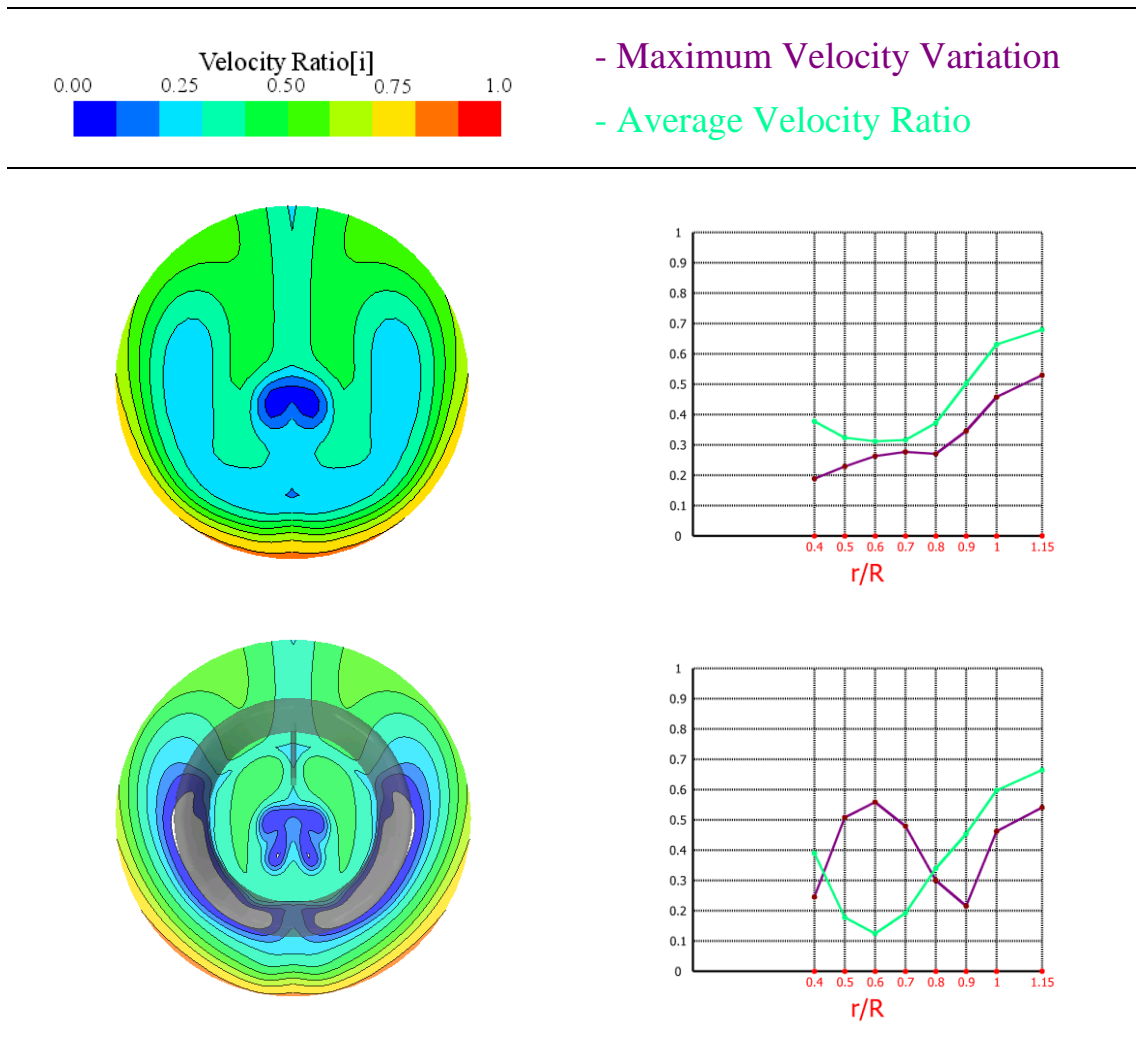
Parameter		Without ESD	With ESD
<i>Taylor Wake Fraction</i>	$[w_t]$	0.524	0.591
<i>Non- Wake Uniformity</i>	$[\Delta w]$	0.326	0.422

Analysis of the nominal wake gives an initial assessment of the duct effectiveness and impact. Introduction of the duct has increased the wake fraction and also increased the wake non-uniformity. Therefore, at first glance, it indicates that the duct will increase the hull efficiency at the expense of reduced uniformity with the latter outcome being undesirable when looking into vibrations etc.

As can be seen in Table 60, the duct introduces a sudden decrease in the axial velocity along radius $r/R=0.6$ also reflecting some areas of reversed flow as depicted in the figure. Meanwhile, at the same radius, the maximum velocity variation was increased. However, the influence of the duct decreased the velocity variation on the outer radii and this could be desirable for the reduction of vibration and cavitation risk. Furthermore, the maximum velocity variation plot indicates that this spike of reversed flow also influenced the neighbouring radii, $r/R=0.5$ and $r/R=0.7$, which led to an overall increased mean wake variation and mean wake fraction.

Flow behaviour analysis indicated that the nominal wake field quality reduced with the installation of the energy-saving duct. However, no conclusions can be identified from solely analysing the wake flow in the absence of the propeller. The same analysis should also be carried out in self-propulsion conditions to fully comprehend the performance of the Energy Saving Device. This is the next natural step and direction of the study.

Table 60. Flow Field Behaviour @ Propeller Plane (Towing)



Therefore, the wake was also analysed using the WAT tool in self-propulsion conditions. Due to the presence of the propeller and the duct, the data was extracted at a location of 0.0168 Lpp. This plane location was specifically selected as it does not interfere with any geometry.

Table 62, indicates that the presence of the propeller reduced the wake fraction and this implies that the advance velocity increased for both conditions. This is logical due to the propeller induced velocities. The propeller creates a suction effect increasing the velocity of the flow. The analysis was carried out at different planes (Propeller plane and 0.0168Lpp) and cannot be directly comparable, but the difference is significant and clearly evident especially since the difference in plane location is fairly small.

This behaviour is also explained by Carlton (2007) who outlines and defines the differences between nominal velocity, effective velocity and total velocity, as demonstrated in Figure 99. He explains that when a propeller operates behind the stern of a vessel, the velocity of the flow inside the wake increases due to propeller induced effects as well as interaction effects. The latter is not generally taken into account in propeller theories due to irrotational and unbounded flow assumptions. However, such phenomena give rise to significant impacts on propeller performance, giving rise to the Total velocity. Despite all this, it is this effective velocity that is required for propeller design procedures. Trying to identify the effective velocity of a hull-propeller interaction system remains a challenge till this very day.

As exhibited in Figure 99, using CFD procedures, we can identify the nominal wake field using towing simulations as well as the total wake field using self-propulsion tests. The wake fraction that is identified using thrust identity procedures in power performance analyses relates to the effective velocity that should lie between both of the above. Always keeping in mind the definition of wake ($1 - V_A/V_S$), this is clearly evident in our results where the computed wake fraction from the propulsion performance analyses (Table 55) is lower than nominal wake fraction (Table 59) but higher than the total wake fraction (Table 62). These results have been represented in the form of advance velocities in Table 61 for ease of understanding. These have been presented in order to outline that the effective and total velocities are not directly comparable due to their different definitions. However, these parameters can be studied independently, and the impact of the duct investigated for each.

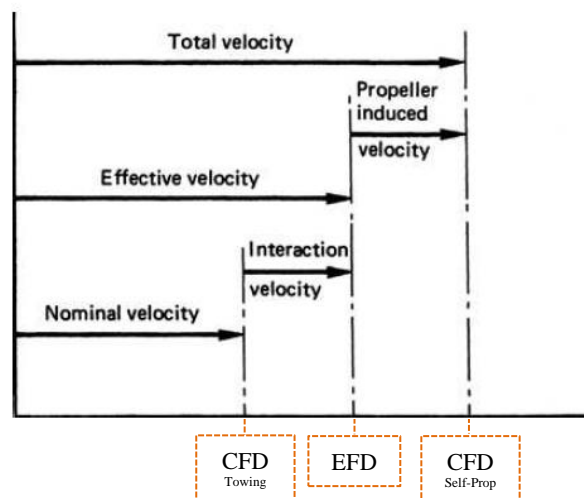


Figure 99. Velocity Definitions

Table 61. Velocity Comparisons

	Velocities		
	<i>Nominal</i> (m/s)	<i>Effective</i> (m/s)	<i>Total</i> (m/s)
<i>Baseline Hull</i>	0.561	0.621	0.821
<i>Hull with Duct</i>	0.482	0.557	0.748

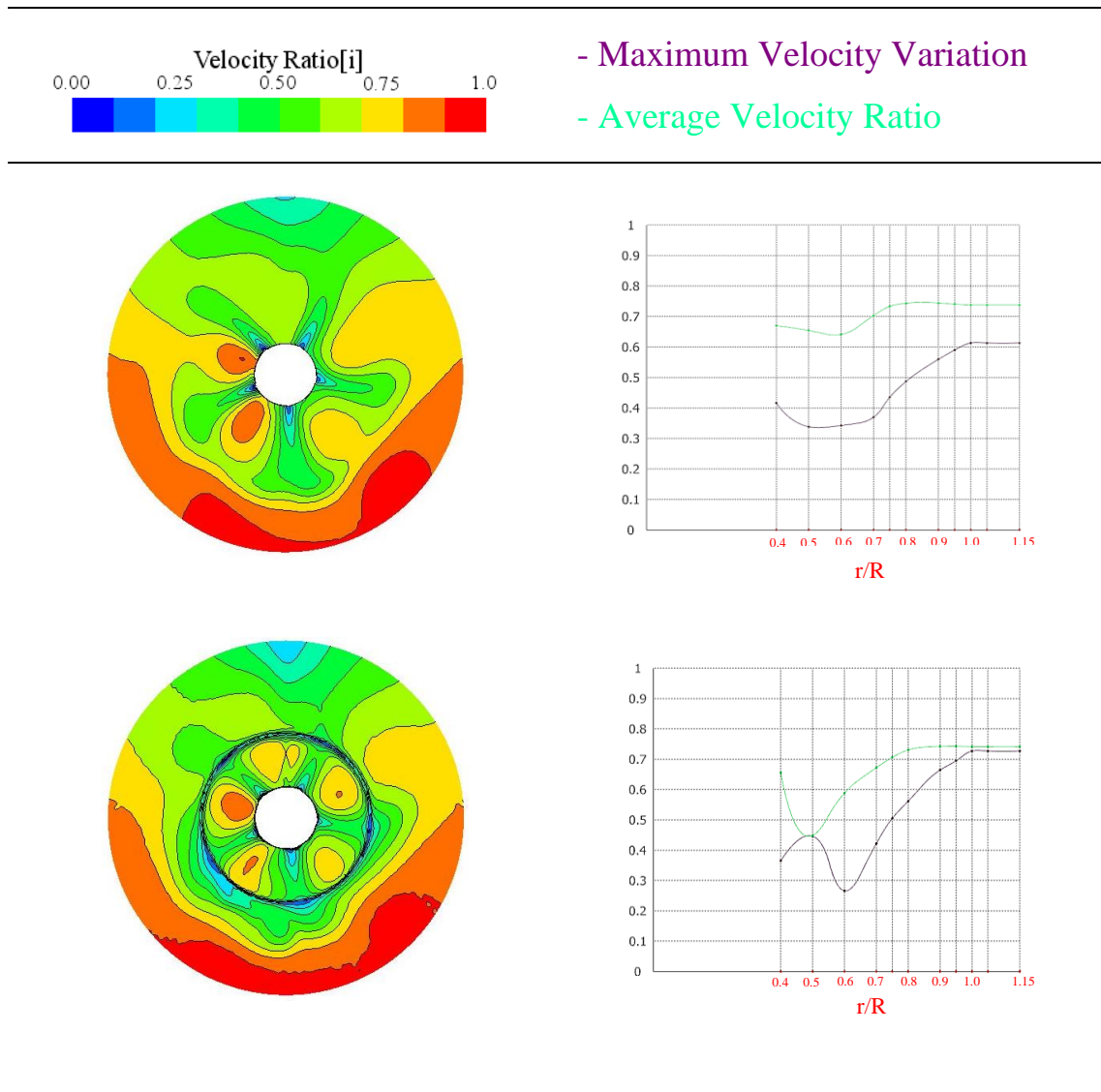
As demonstrated in Table 62, the introduction of the duct in self-propulsion conditions increases the overall wake fraction from 0.304 to 0.336 (+10.5%), implying an improvement in the hull efficiency. This behaviour is also reflected in the effective wake fraction and subsequent hull efficiency values in Table 55. However, installation of the duct increased the wake non-uniformity. This might increase the risk of propeller excited vibrations or propeller cavitation and is probably worth looking into in full-scale scenarios where such studies are more meaningful. A higher wake fraction also implies that the advance velocity into the propeller is reduced. The smaller advance ratio resulted in a decrease in the open water propeller efficiency. That being said, the gains achieved from the enhanced hull efficiency outweighed the detrimental effects on the open water efficiency.

Studying the details of the flow field behaviour further in Table 63, the plots indicate that the duct introduced a sudden decrease in velocity at $r/R=0.5$. This sudden spike also influenced a reduction in velocity flow in the neighbouring radii, which produced an overall increase in wake fraction. On the other hand, this velocity change at 0.5 r/R increased the non-uniformity at this radius but significantly decreased this parameter at 0.6 r/R . However, as represented in Table 63, the duct produces a higher wake non-uniformity for the remaining higher radii. It is worthwhile mentioning that this imprint at 0.5 r/R is a result of the trailing edge of the duct.

Table 62. Wake Analyses @ 0.0168Lpp (Self-Propulsion)

Parameter		Without ESD	With ESD
<i>Taylor Wake Fraction</i>	$[w_t]$	0.304	0.336
<i>Non- Wake Uniformity</i>	$[\Delta w]$	0.468	0.535

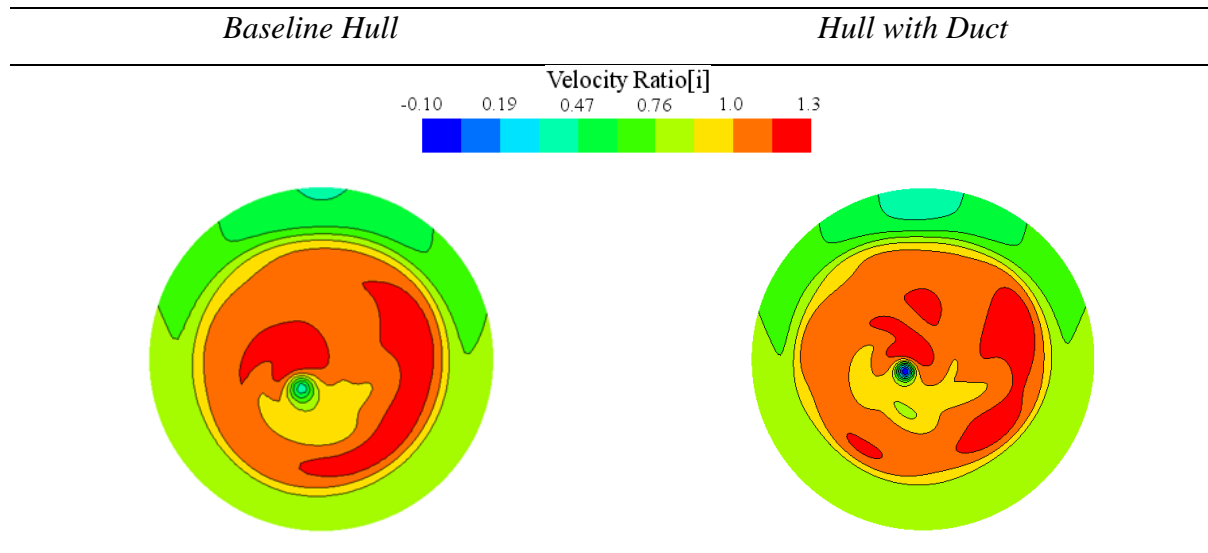
Table 63. Flow Filed behaviour @ 0.0168Lpp (Self-Propulsion)



It was also interesting to analyse the wake post the propeller, once the flow or energy leaves the system. The general idea is to try and minimise the energy leaving the system to minimise energy losses. The wake was therefore analysed at $x=App$. This plane location was selected because in the far field wake, numerical dissipation might be too strong and although the static pressure behind the propeller might not be completely recovered, it is assumed that the pressure between both hull geometries will not be significant allowing comparison analyses. The fluid flow behaviour just behind the propeller, is presented in Table 64. The WAT tool indicated that the wake fractions between both wake discs are very similar, but the ducted hull produced lower wake non-uniformity. Although this might indicate less energy leaving the system, no conclusion can be made just yet as these analyses were only carried out for the axial velocities

and are not meaningful. The energy balance at the post-propeller plane is later investigated giving better indications for these criteria.

Table 64. Flow Field behaviour Post-Propeller (*Self-Propulsion*)



The resistance breakdown analyses (Table 56 & Table 57) demonstrated that the duct reduced the resistance of the bare hull. More specifically, this beneficial decrease was determined due to a noticeable decrease in the bare hull pressure resistance both in towing and self-propulsion conditions. This would indicate a reduction in flow separation and less energy lost to the generated vortices. It was thus deemed appropriate to analyse the Wall Shear Stress values between the geometries as presented in Figure 100 and Figure 103.

Shear stress is caused by the viscosity/friction of the near fluid on the wall. The continuous retardation of the flow along the wall surface reduces the shear stress to a point 0 where flow separation occurs (generally due to high-pressure gradients). Negative values of the wall shear stress indicate re-circulation of the flow, indicating that flow is moving in the opposite direction. The shear stress was thus analysed along the ship hull in the x-direction. Due to the co-ordinate system of the CFD model, the sign value is opposite in trend where the motion of the vessel reflected a positive x-direction and the motion of the fluid a negative x-direction. Therefore, a null value indicates flow separation and a positive value indicates recirculation of the flow. A higher positive value indicates that the flow is reversed at a higher velocity, thus reflecting more loss of energy.

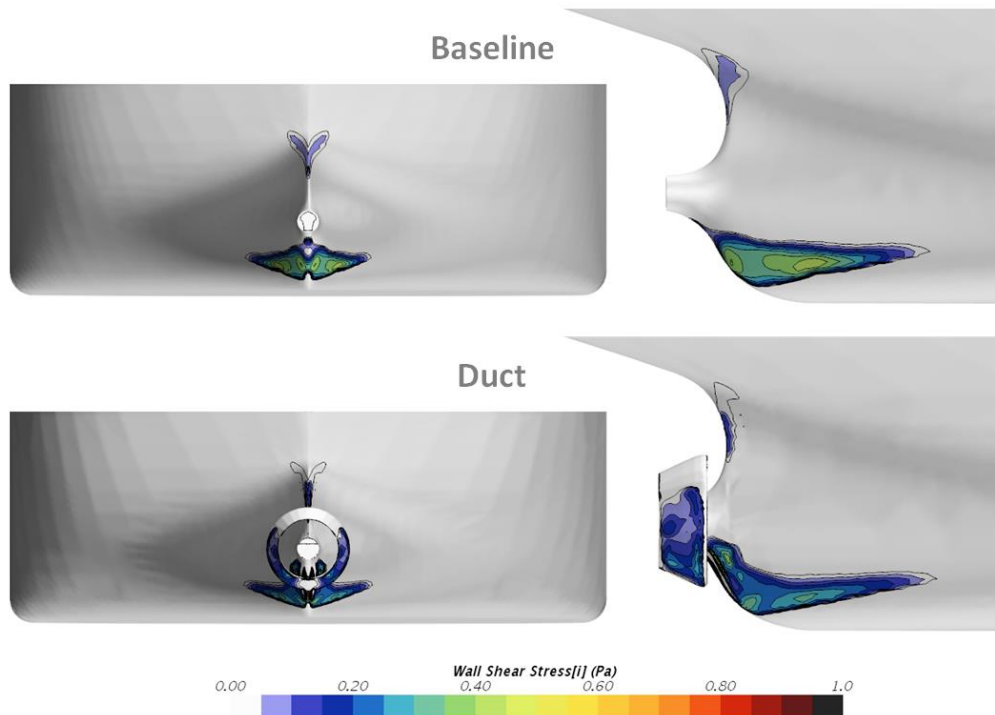


Figure 100. Wall Shear Stress: Towing (*Flow Separation Comparison*)

The Wall Shear Stress analyses between the geometries in towing conditions are presented in Figure 100 with values higher than 0, indicating regions of flow separation. Although a large separation area appeared on the JBC hull with duct, the magnitude of separation was higher on the JBC without duct. It is evident that the baseline hull without duct experiences stronger separation of flow. This was further confirmed when analysing the wake at different planes upstream of the duct, highlighting the reduced extents of separation around the ship hull (Figure 101). Furthermore, as can be seen in Figure 100, the flow field around the duct in towing conditions showed a significant area of separation on the duct itself.

When analysing the limiting streamlines at the stern of the bulk carrier in the absence of the duct and propeller, an area of recirculation just below the bossing was present. Figure 102 demonstrates that these effects are reduced once the duct is installed. For the purpose of clarity, the duct was not included in the respective figure.

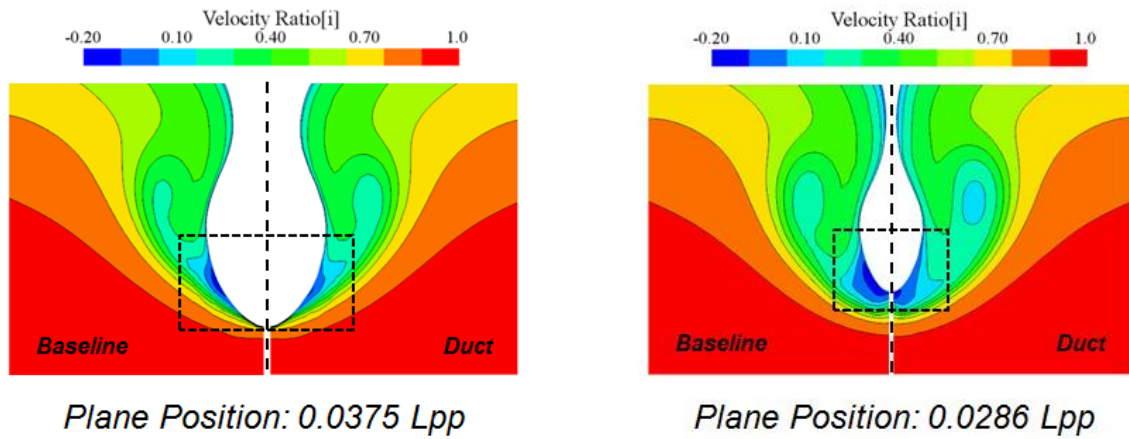


Figure 101. Wake Velocity Distribution (*Flow separation Comparison*)

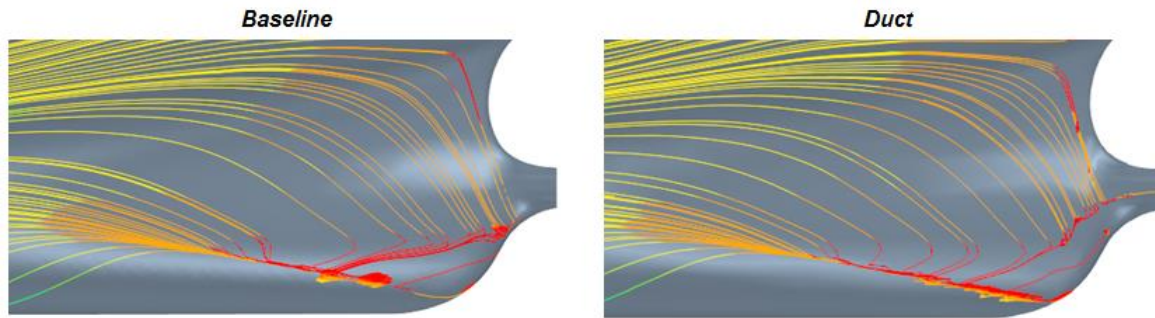


Figure 102. Limiting Streamlines for Baseline Design and Duct Design without Duct Visualisation: *Towing*

On the other hand, with the presence of the rotating propeller, as exhibited in Figure 103, the flow separation that was evident in Figure 100 on the underside of the stern hull just below boss cap level, is no longer visible. That being said, very slight separation occurs just below the boss cap at the keel. This behaviour was minimised with the introduction of the duct. These effects are also visible using limiting streamlines as seen in Figure 104. The self-propulsion conditions have also pronounced flow separation at the stern valley, with the duct having no effect on the flow behaviour in this region. One further observation is that the separation on the Energy Saving Duct itself has reduced significantly with the presence of the propeller. This would probably indicate that the propeller induced effects have altered the angle of attack of the flow onto the duct reducing flow detachment.

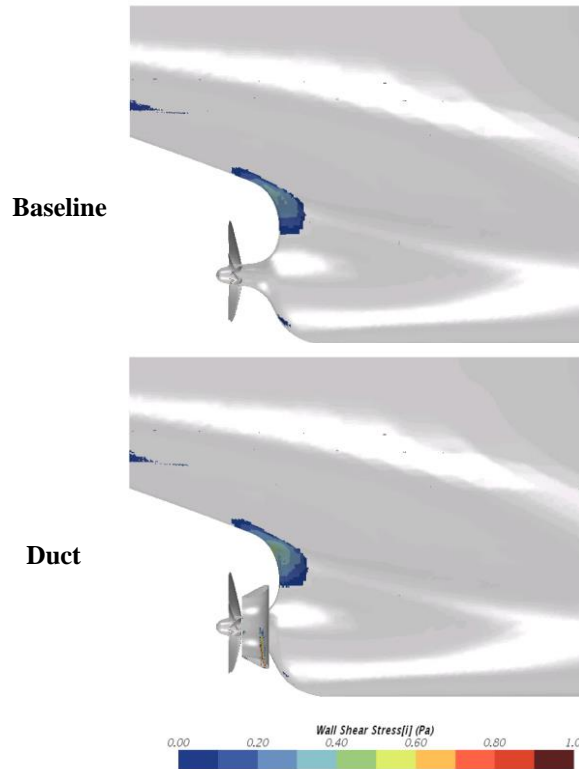


Figure 103. Wall Shear Stress: Self-Propulsion (Flow Separation Comparison)

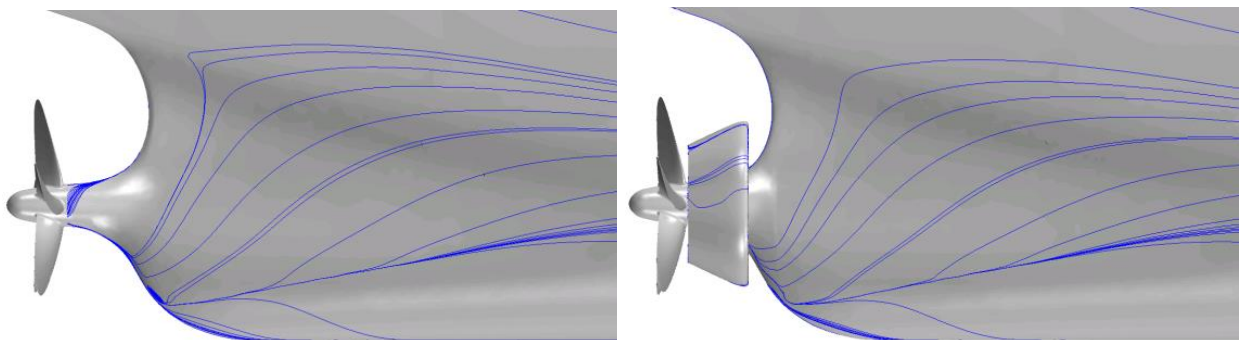


Figure 104. Limiting Streamlines for Baseline Design and Duct Design: *Self-Propulsion*

The separation of flow on the duct as seen in Figure 100 is confirmed in Figure 105, which presents the velocity flow vectors around the duct in towing conditions. The probable cause behind this behaviour, is that the angle of attack of the flow is so large, such that the stall angle is exceeded causing the flow to separate. However, with the introduction of the propeller, separation on the duct is no longer evident as depicted in Figure 106, which presents the velocity flow vectors around the duct in propeller conditions from the top view. It is assumed that the induced effects of the propeller alter the angle of attack such that the critical angle is no longer exceeded.

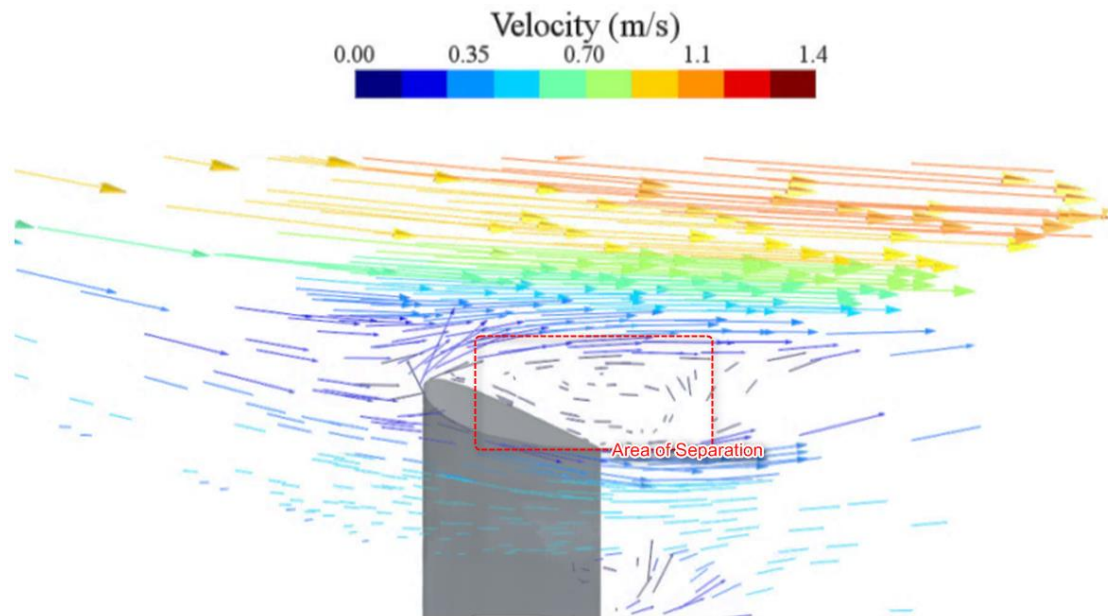


Figure 105. - Separation Around Duct at Maximum Width of the Duct

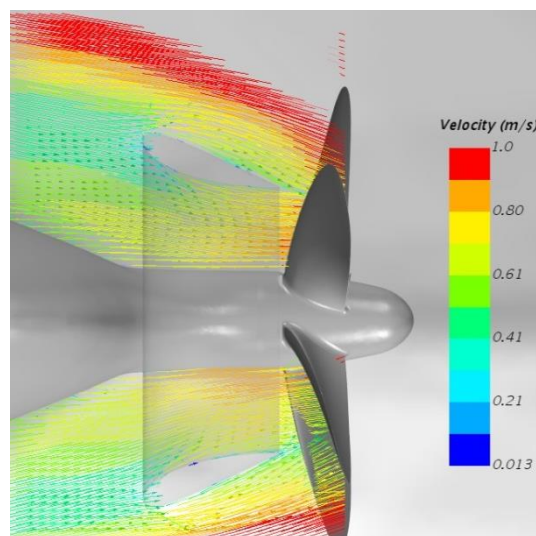


Figure 106. Velocity Flow Vectors (Top View)

Together with the analyses of the flow vectors, it was also possible to look into and investigate the function of the duct. Flow vectors were also analysed in profile view as exhibited in Figure 107 and pressure regions classified according to the velocity magnitude. It can be seen that the top part of the duct is generating a lift in the desired direction due to the pressure difference behaviour as defined in foil theory. However, the bottom part of the duct is producing an undesired lift in the opposite direction. This explains why when taking the whole duct into consideration, the net force is acting in the opposite direction to that of vessel motion, thus acting as added resistance as explained in Table 57. This explains why some new ESD designs, such as the “Kawasaki SDS-F”, make use of a semi duct, which they claim produces a thrust.

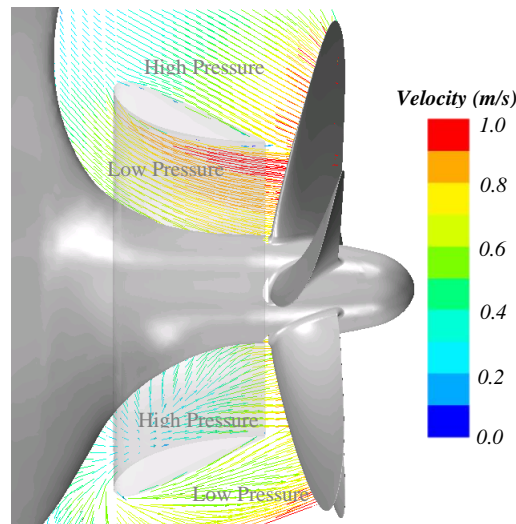


Figure 107. Velocity Flow Vectors (Profile View)

Assessing the kinetic energy losses in a ship's far wake field, where the static pressure is completely recovered, can provide meaningful information on the type of energy recovery and saving; axial or transverse energy (Wald, June 1965). However, as suggested by Dang et al. (2015), numerical dissipation may become too strong in the far wake field and therefore the analyses must be carried out just behind the propeller. Although the static pressure right behind the propeller is not completely recovered, it is considered that the difference between the geometries would not be too significant thus still being able to give a good indication on the energy saving. Axial and transverse kinetic energy losses were thus computed at the APP for a cylindrical plane that was 15% greater than the propeller diameter for towing and self-propulsion simulations.

Table 65. Kinetic Energy Losses: Towing Conditions

K.E. Losses	Baseline Hull	Hull w/Duct	% Diff.
<i>Axial (K_{ax})</i>	0.00249	0.00255	+ 2.43
<i>Transverse (K_{tr})</i>	0.00034	0.00022	- 37.02
<i>Total (K_{Total})</i>	0.00283	0.00276	- 2.34

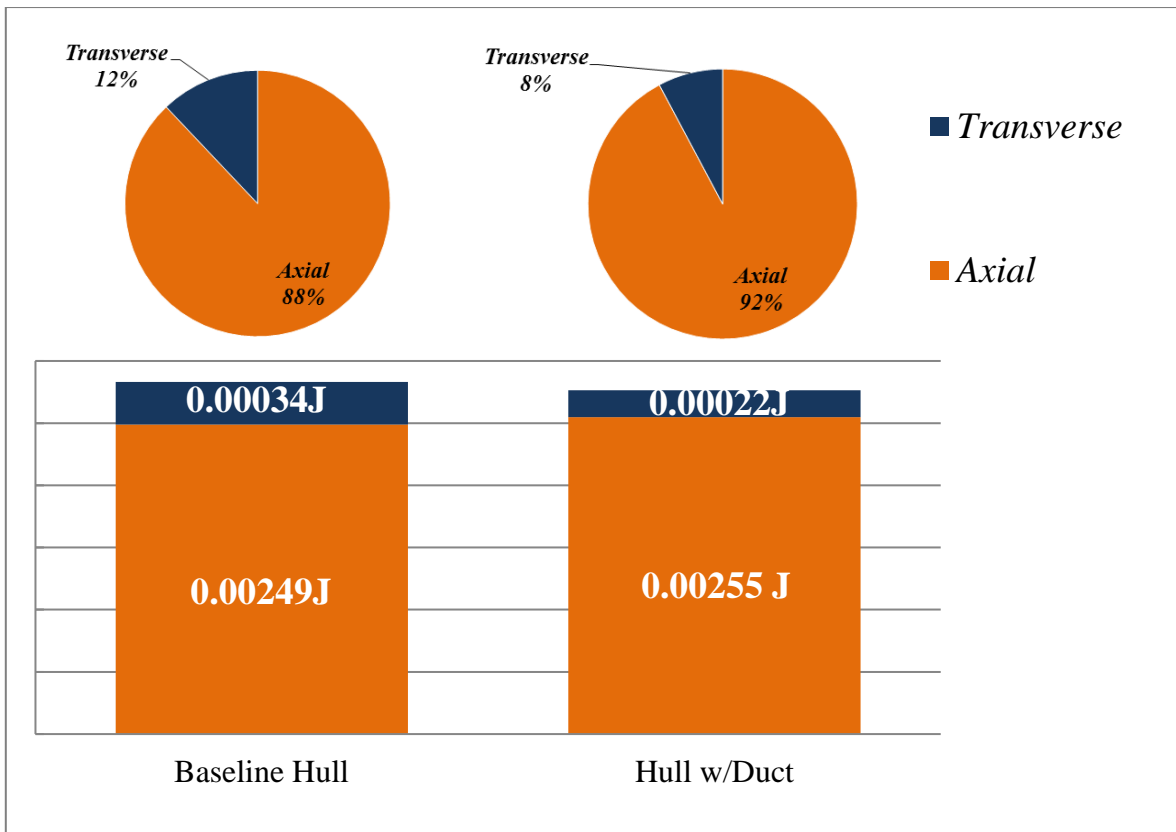


Figure 108. Kinetic Energy Losses: *Towing Conditions*

In contrast to the resistance simulations, where axial losses were the most significant (Table 65), it can be seen that for the self-propulsion simulations, the transverse energy losses were the most prominent (Table 66). This is only natural due to the introduced rotational flow of the propeller in the slipstream. In towing conditions, the ESD (duct) increased the axial losses but reduced the transverse losses as demonstrated in Table 65. However, in propelled conditions, the duct geometry produces less axial as well as transverse energy to the slipstream. That being said, the energy differences between the baseline hull and the ducted hull are not directly comparable since they respectively have different delivered power.

Table 66. Kinetic Energy Losses: *Self-Propulsion Conditions*

K.E. Losses	Baseline Hull	Hull w/Duct	% Diff.
<i>Axial</i> (K_{ax})	0.00149	0.00139	-6.98
<i>Transverse</i> (K_{tr})	0.00565	0.00505	-10.65
<i>Total</i> (K_{Total})	0.00715	0.00644	-9.88

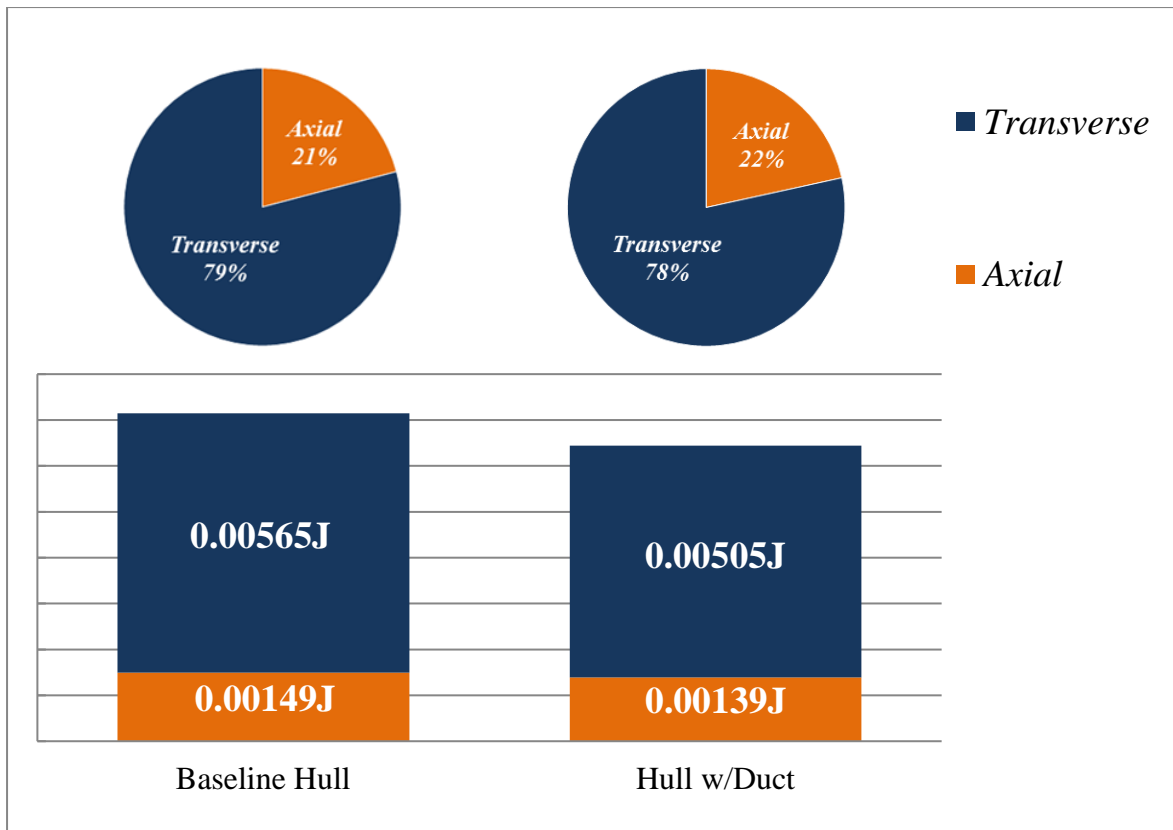


Figure 109. Kinetic Energy Losses: *Self-Propulsion Conditions*

8.3.2 ESD Investigation at Full Scale

The next step in this investigation deals with the analysis of the performance of the JBC vessel at full-scale both with and without the duct. This was carried out by going through most of the pre-defined ESD analysis checklist. This section presents the major findings and outcomes. The impact of the ESD is particularly studied and highlighted. All the simulations were carried out using the state of the art CFD procedure outlined in Chapter 4. The layout of the following report (information) will take a similar approach as presented in section 8.3.1 with the study firstly focusing on the performance of the vessel in the absence of the propeller and then moving on to demonstrating and discussing the propulsive behaviour in self-propelled conditions.

At full scale, the towing resistance of the JBC with duct experiences an opposite behaviour in trend when compared to the model scale results. As demonstrated in Table 67, the introduction of the ESD has increased the resistance from 1081.51N to 1104.60N. Even though the wetted surface area is taken into account, one can also see a noticeable increase in the resistance coefficient (Table 67), from 1.94 to 1.97, thus showing a 1% increase. This indicates that the

duct is adding resistance and is not producing a net forward thrust. This magnitude of increase lies within simulation uncertainty, thus raising some doubts regarding impact. It was therefore deemed appropriate to later analyse and breakdown the force components individually.

Table 67. Performance: Towing

Parameter		Without ESD	With ESD
U	[ms] : Ship Speed	7.4566	7.4566
R_T	[kN] : Towing Resistance	1081.51	1104.60
$CT (x10^{-3})$	[m] : Total Resistance Coefficient	1.94	1.97

Proceeding to the self-propulsion performance analyses, the results are presented in Table 68. Looking at the overall general performance, the duct did not prove beneficial at full scale. The ESD increased the delivered power requirement by 0.77% from 11548 kW to 11637 kW. The reduced rpm of the propeller did not make up for the increase in torque that produced a higher power value requirement. Since the power difference is probably within the numerical uncertainty error, the ESD performance cannot be clearly determined. That being said, a distinctive benefit from the ESD function at full scale cannot be outlined. These remarks are well in agreement with Visonneau et al. (2016) who describe the device as an ineffective energy saving device. It could very well be that this duct was designed for model-scale conditions. Examining the performance even further, installation of the duct had barely any effect on the propeller efficiency, which improved slightly from 0.698 to 0.708. Similar to the model scale simulations, the relative rotative efficiency was not affected. The duct reduced the open water efficiency but improved the hull efficiency leading to an ever so slightly improved propeller efficiency. This increment in propeller efficiency did not make up for the increase in resistance. With regards to the open water efficiency, a new propeller with less pitch would probably result in an OW efficiency increase and therefore, since the duct modifies the inflow, the geometry of the propeller should be designed to suit the ESD.

Although the duct condition produced a non-desired reduced thrust deduction term (1-t), the major benefit coming from the hull efficiency, which surged from 1.13 to 1.20, was mainly derived from the increase in the wake fraction (w_t). An increase in the wake fraction indicates that less work is done by the propeller in delivering the required thrust hence indicating that the propeller performance has improved. This benefit was outweighed by the reduced open water efficiency that decreased from 0.60 to 0.57. Furthermore, it can be said that the slight increment in propulsive efficiency did not outweigh the added resistance the duct introduced into the system, thus leading to a higher delivered power requirement.

Table 68. Performance: Self-Propulsion

Parameter			Without ESD	With ESD
U	[ms]	: Ship Speed	7.4566	7.4566
R_{TSP}	[kN]	: Self-Propulsion Resistance	1428.98	1477.48
D	[m]	: Propeller Diameter	8.12	8.12
n	[rps]	: Propeller Revolution Rate	1.28	1.27
T	[kN]	: Propeller Thrust	1427.61	1479.50
Q	[kNm]	: Propeller Torque	1436.94	1464.06
K_T		: Thrust Coefficient	0.196	0.207
K_Q		: Torque Coefficient	0.024	0.025
$I-t$: Thrust Deduction Term	0.76	0.75
J		: Advance Ratio	0.48	0.45
$K_{Q,ow}$: Torque Coefficients Open Water	0.025	0.026
V_a	[m/s]	: Advance Velocity	4.98	4.62
$I-w_t$: Mean Velocity Ratio	0.67	0.62
η_{ow}		: Open Water Efficiency	0.60	0.57
η_R		: Relative Rotative Efficiency	1.03	1.03
η_H		: Hull Efficiency	1.13	1.20
η_D		: Propulsive Efficiency	0.698	0.708
P_d	[kW]	: Delivered Power	11547.53	11636.68

The force components were broken down and analysed for both the towing as well as the self-propulsion full-scale conditions as presented in Table 69, Table 70 and Table 71. When taking into consideration the non-propelled setup (Table 69), the inclusion of the duct geometry resulted in no major changes to the total shear resistance. However, the ESD configuration reduced the pressure resistance on the bare hull geometry (from 269kN to 249kN), but the duct itself introduced a pressure resistance (44kN) that outweighed the benefit gained from the reduced hull pressure resistance resulting in an overall increased total resistance (1105kN).

This behaviour contradicts that of model-scale performance whereby the duct minimally reduces the overall towing resistance of the vessel due to a difference in the viscous pressure resistance generated by the ESD. Although the duct at model-scale reduces the viscous pressure resistance of the bare hull by around 4% whereas the full-scale technology reduces the viscous

resistance by 7%, the duct itself introduces a viscous pressure drag that is less than 1% of the total retrofitted resistance in contrast to the 4% that is generated at full scale. Meanwhile, the shear contribution ratio of the duct is very similar at both scales sitting at about 0.12%.

Table 69. Resistance Breakdown: Towing

	Baseline Resistance			Retrofitted ESD/s		
	Shear (kN)	Pressure(kN)	Total(kN)	Shear (kN)	Pressure(kN)	Total(kN)
Bare Hull	812.24	269.28	1081.51	811.00	248.62	1059.63
Duct	-	-	-	1.32	43.65	44.97
Total	812.24	269.28	1081.51	812.33	292.27	1104.60

Table 70. Resistance Breakdown: Self-Propulsion

	Baseline Resistance			Retrofitted ESD/s		
	Shear (kN)	Pressure(kN)	Total(kN)	Shear (kN)	Pressure(kN)	Total(kN)
Bare Hull	824.89	781.11	1605.99	825.02	723.35	1548.37
Duct	-	-	-	4.42	97.65	102.08
Boss Cap	0.46	-177.48	-177.02	0.38	-173.36	-172.97
Total	825.34	603.64	1428.98	829.83	647.65	1477.48

In summary, although the ESD has a better effect on the reduction of the bare hull resistance at full scale, the ESD generates a much higher drag ratio at full scale resulting in a negative net performance. Self-propulsion conditions experience similar behaviour, as demonstrated in Table 70. As can be seen in Table 71, the thrust and torque produced by the propeller, increase with the inclusion of the duct, which is not the case in the model scale scenario. Once again, it is good to point out that these values cannot be compared since the propeller is working under different conditions.

Table 71. Thrust and Torque Breakdown: Self-Propulsion

	Baseline		Baseline with ESDs	
	Thrust (N)	Torque (Nm)	Thrust (N)	Torque (Nm)
Propulsion System Blades	1427.61	1436.94	1479.50	1464.06
Total	1427.61	1436.94	1479.50	1464.06

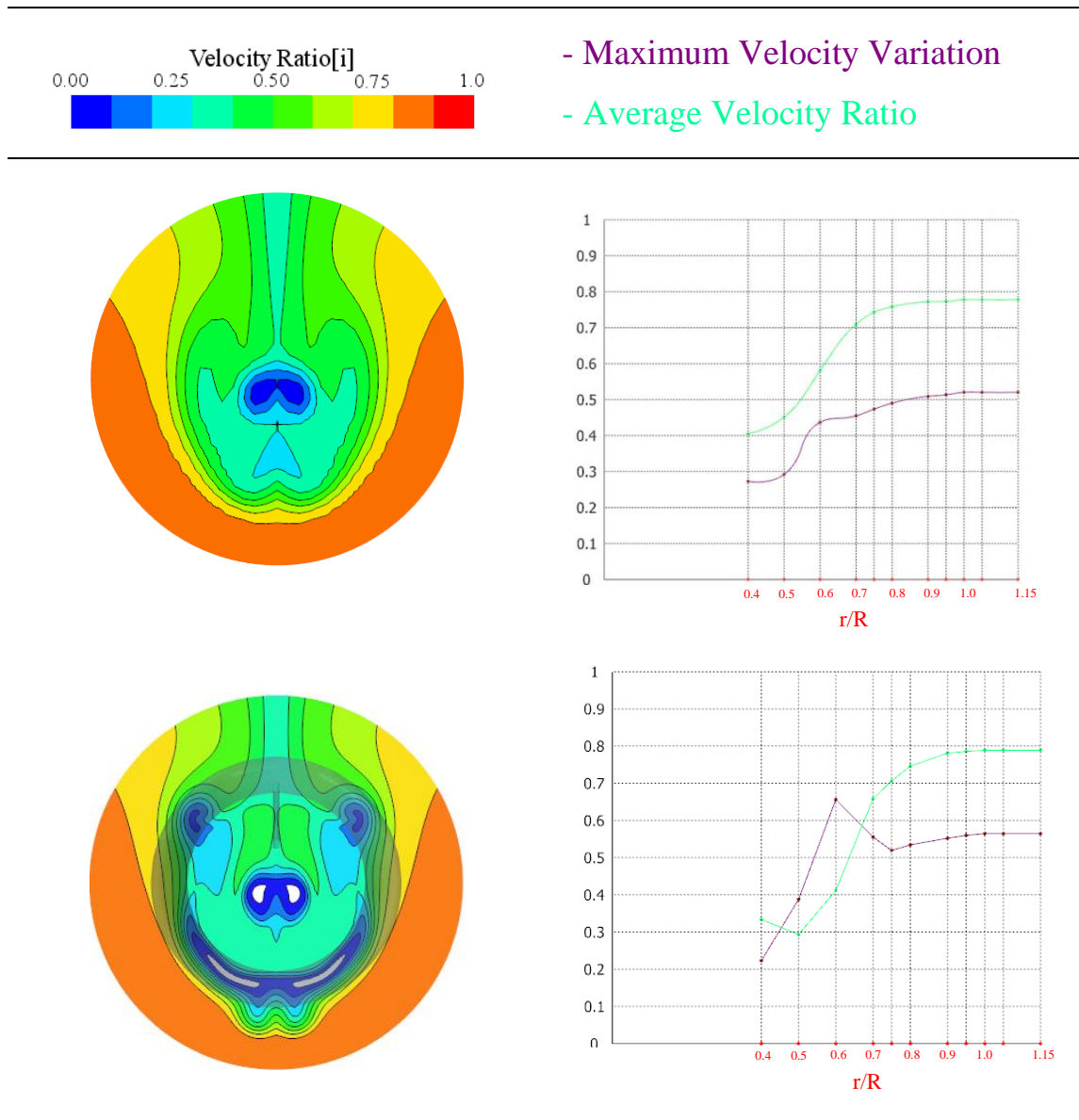
The axial wake analysis was carried out in a similar manner to the model case study whereby the developed WAT tool was used to provide valuable insight into the fluid flow behaviour in the wake region. Tables 26 to 30 present meaningful data together with informative figures for enhanced explanation and understanding of the flow behaviour.

Similar to the model scale conditions, the inclusion of the duct increased the wake fraction (from 0.296 to 0.331) and produced a higher wake non-uniformity (0.446 to 0.522). This implies that the duct increases the hull efficiency at the expense of a reduced wake non-uniformity that is more susceptible to hull vibrations. This increment in wake fraction corroborates the information presented in Table 68. By carrying out detailed analyses of the wake using the developed WAT tool (Table 73), it can be understood that the duct in towing conditions increased the non-uniformity at the inner radii and slightly reduced the non-uniformity at outer radii. Moreover, it also reduced the velocity ratio at lower radii. However, the influence of the duct decreased the velocity variation on the outer radii, which could be desirable for the reduction of vibration and cavitation risk. It was also evident that stagnated/reversed flow inside the wake region is less dominant at full scale.

Table 72. Full-Scale Wake Analyses @ Propeller Plane (Towing)

Parameter		Without ESD	With ESD
<i>Taylor Wake Fraction</i>	$[w_t]$	0.296	0.331
<i>Non- Wake Uniformity</i>	$[\Delta w]$	0.446	0.522

Table 73. Flow Field Behaviour @ Propeller Plane (Towing)



With regards to the wake analyses in self-propulsion conditions at 0.0168 LPP in the x direction, Table 74 outlines that the installation of the duct increased the wake fraction from 0.213 to 0.239 (around 10.9 %), which is similar to the 10.5% increment at model scale. This would, in turn, improve the hull efficiency since the parameter is directly proportional to the propulsive efficiency. However, installation of the duct increased the wake non-uniformity from 0.463 to 0.524 (+13.2%). This increment is quite significant.

Table 74. Full-Scale Wake Analyses @ 0.0168Lpp (Self-Propulsion)

Parameter		Without ESD	With ESD
Taylor Wake Fraction	$[w_t]$	0.213	0.239
Non- Wake Uniformity	$[\Delta w]$	0.463	0.524

Table 75. Full-Scale Flow Filed behaviour @ 0.0168Lpp (Self-Propulsion)

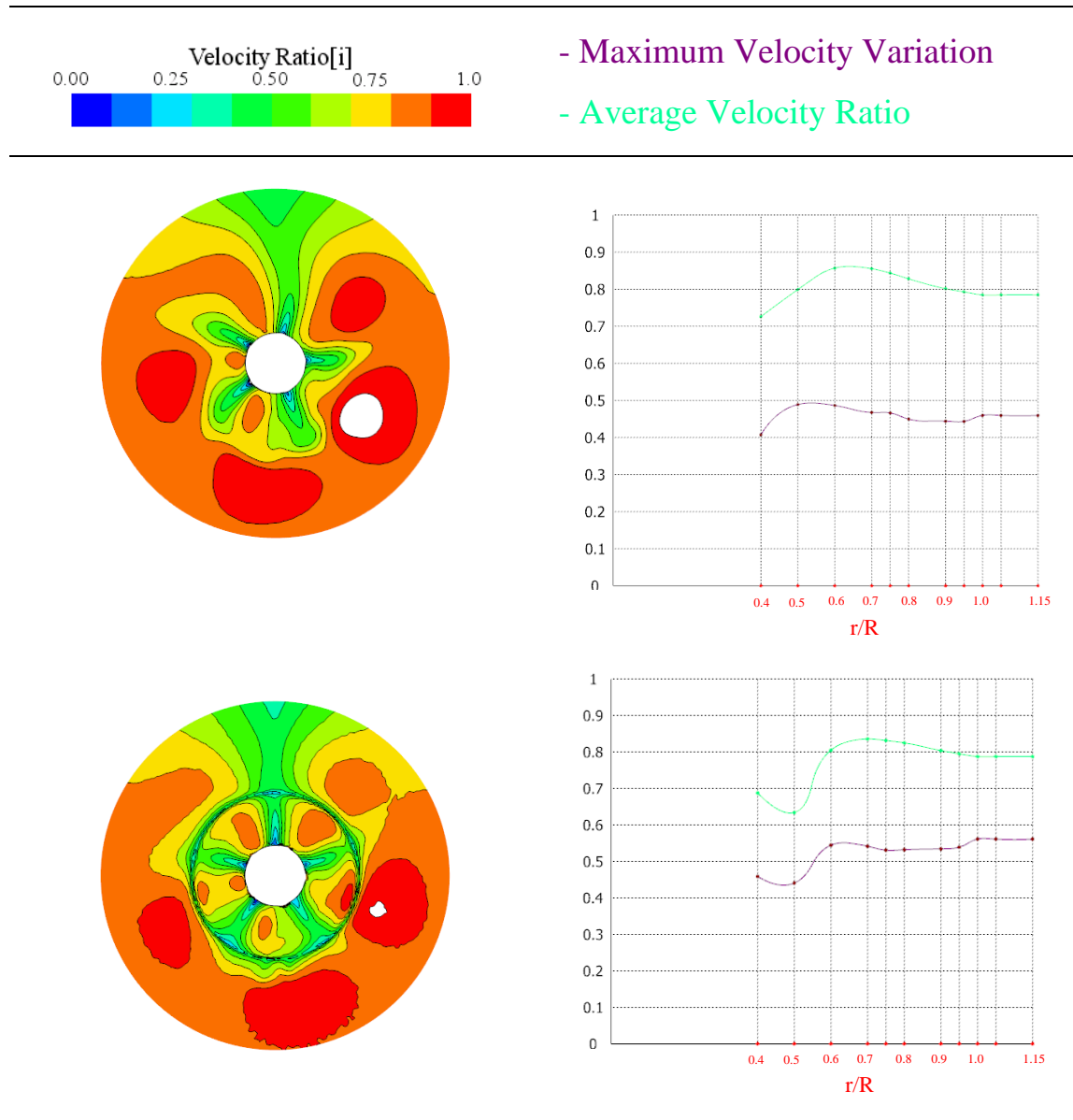
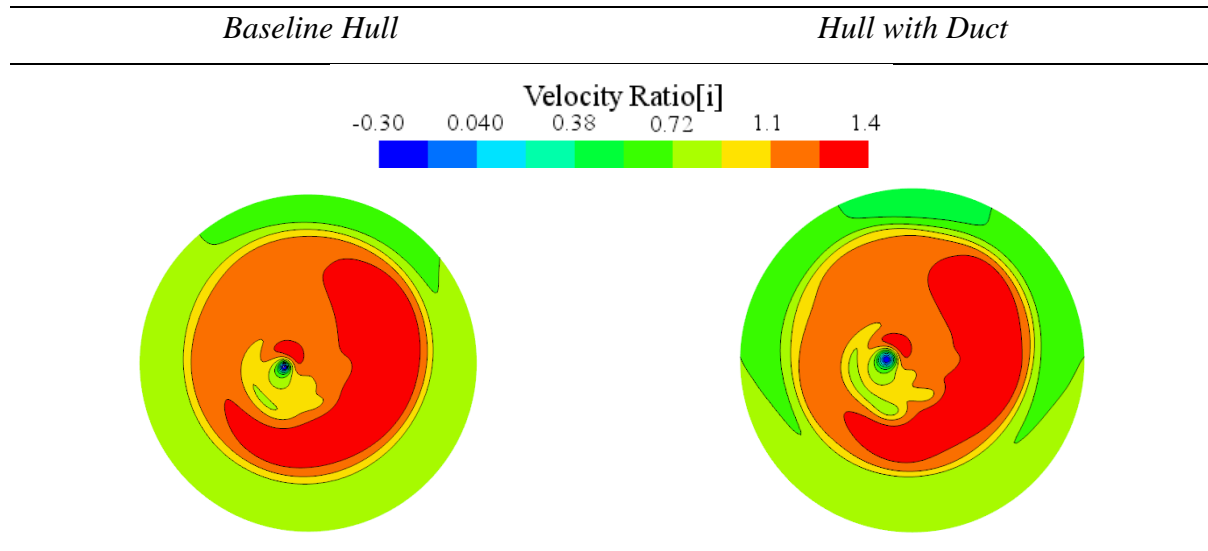


Table 75 demonstrates that the duct particularly reduced the velocity ratio as well as the wake non-uniformity at $r/R=0.5$, which is just behind the trailing edge of the duct. However, it produces a higher wake non-uniformity at higher radii and also a reduced velocity ratio at neighbouring radii $0.6 r/R$ and $0.7 r/R$. Meanwhile, the fluid flow just behind the propeller is

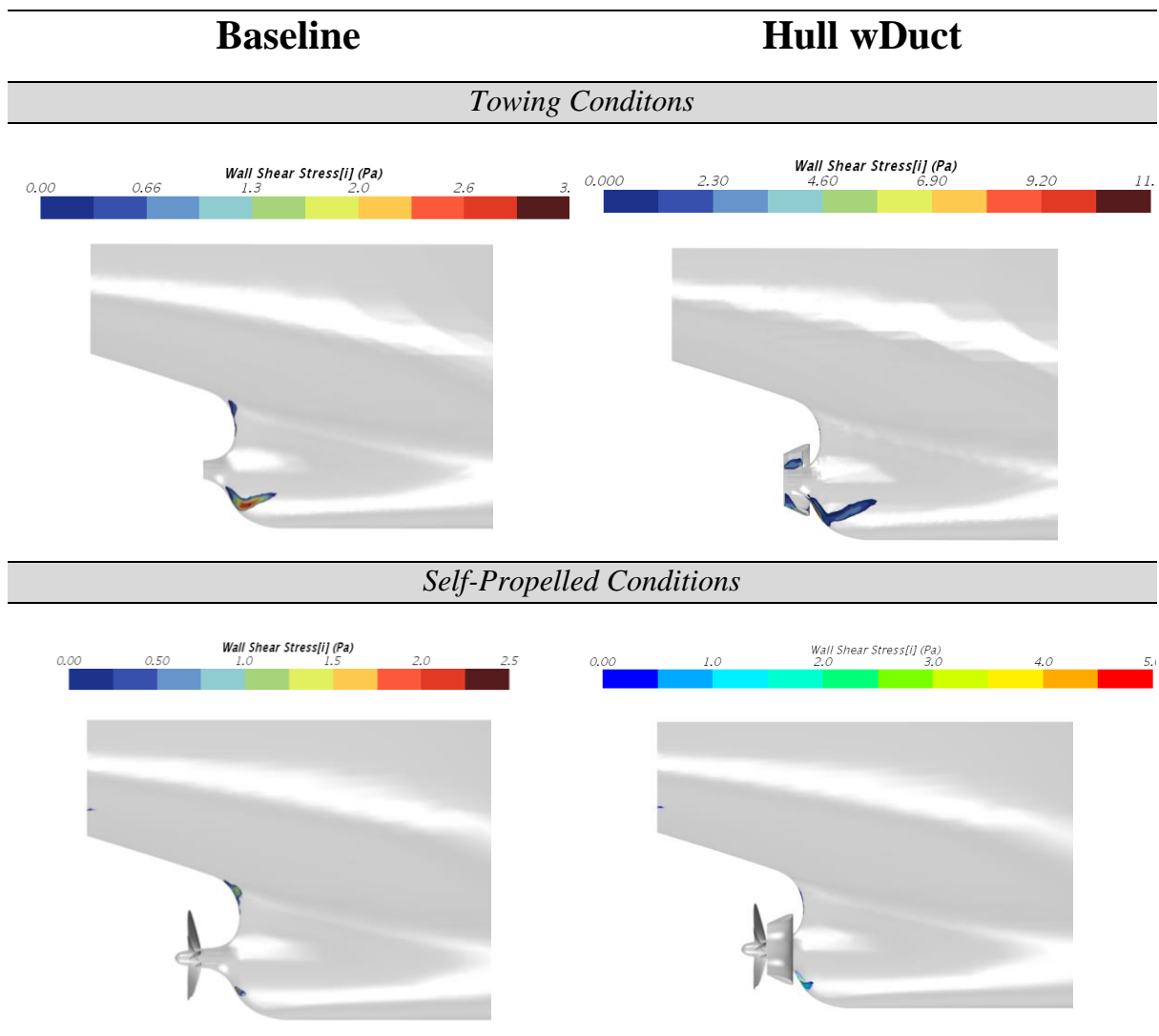
presented in Table 76, with not many differences evident from a visual aspect. The energy balance at the post-propeller plane is later investigated to provide better indications for these criteria.

Table 76. Full- Scale Flow field behaviour Post-Propeller (*Self-Propulsion*)



In full-scale conditions, due to the difference in Reynolds number, the separation effects are insignificant as demonstrated via wall shear stress analyses in Table 77. At model scale, this was not the case (Figure 100), with a significant area of separation on both the hull and the duct. For this particular case study, Table 77 outlines that the duct reduces the small area of separation that happens at the stern valley and barely has any effect on the separation that occurs just below the boss cap at the keel

Table 77. Full-Scale Wall Shear Stress Analyses



The velocity flow vectors around the duct were also analysed to identify the direction of the force generated by different parts of the ESD. The magnitude of the velocity vector indicates regions of high and low pressures around the foil, implying the force direction based on foil theory. The duct cross-section from the bottom view, as depicted in Figure 110, demonstrated that the velocity flow on each side of the foil is similar, thus not creating a significant force in any direction. With regards to the profile (side) view of the duct, as presented in Figure 111, due to the pressure distribution, it can be said that the bottom foil generates a drag. In contrast to the model scale assembly, the foil at the top section produces similar velocity magnitudes on either side, thus not giving any particular indication to whether it is producing a thrust or a drag. Furthermore, it is assumed that the magnitude of the force would be minor. Therefore, one assumes that the relative net drag ratio of the duct to the whole system is larger at full scale

i.e. the contribution of the duct drag is higher. Hence, going back to the force breakdown table (Table 70), it was calculated that the duct generates 1.6% of the total resistance at model scale with the same analysis increasing to 6.9% at full scale.

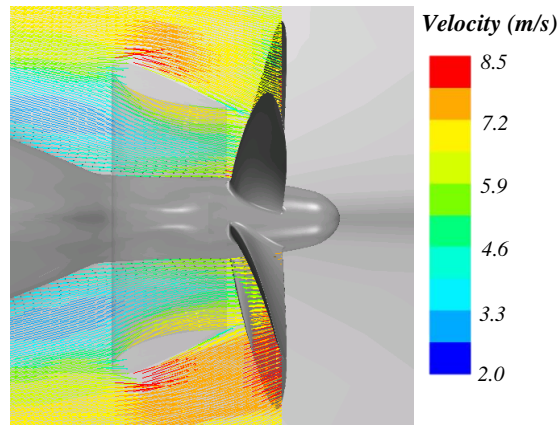


Figure 110. Full-Scale Velocity Flow Vectors (*Bottom View*)

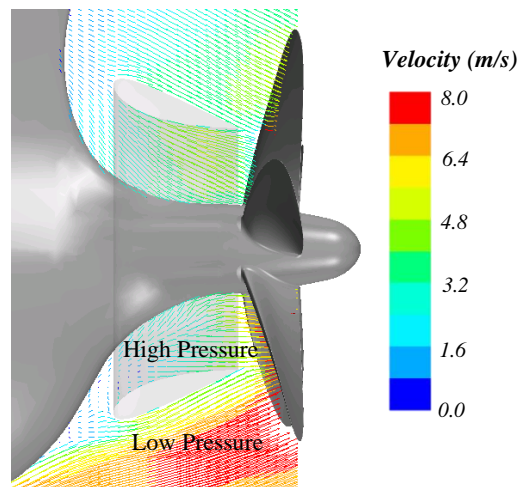


Figure 111. Full-Scale Velocity Flow Vectors (*Profile View*)

Axial and transverse kinetic energy losses were also computed and assessed at the APP for a cylindrical plane that was 15% greater than the propeller diameter for towing and self-propulsion simulations at full scale. Similar to the model scale results, axial losses were primarily dominant for the resistance simulations, whereas transverse energy losses were the most prominent for the self-propellers simulations (Table 78 and Table 79). In towing conditions, the ESD increased the axial losses but reduced the transverse losses as demonstrated in Table 78. That being said, the net KE losses were still increased with the use

of duct indicating a detrimental performance. In contrast to the model scale results (Table 65), the ESD introduces significant axial losses. A 10.5% increase in comparison to the 2.43 % at model scale. Furthermore, the reduction of the transverse kinetic energy at full scale was lower than that at model scale (-11.72 %, -37.02 % respectively).

The biggest difference was identified in the propelled conditions where the axial losses, as well as the transverse losses, both increased with the use of the technology device (Table 79). This had the total opposite behaviour in model scale environments where both parameters were simultaneously reduced (Table 80). Thus, it could be said that kinetic energy losses in self-propelled conditions with duct also indicated a negative impact. These results are well in agreement with the performances outlined in this section.

Table 78. Kinetic Energy Losses: Towing Conditions

K.E. Losses	Baseline Hull	Hull w/Duct	% Diff.
<i>Axial (K_{ax})</i>	2.21430	2.44690	+ 10.5
<i>Transverse (K_{tr})</i>	0.97510	0.86080	- 11.72
<i>Total (K_{Total})</i>	3.18940	3.30770	3.71

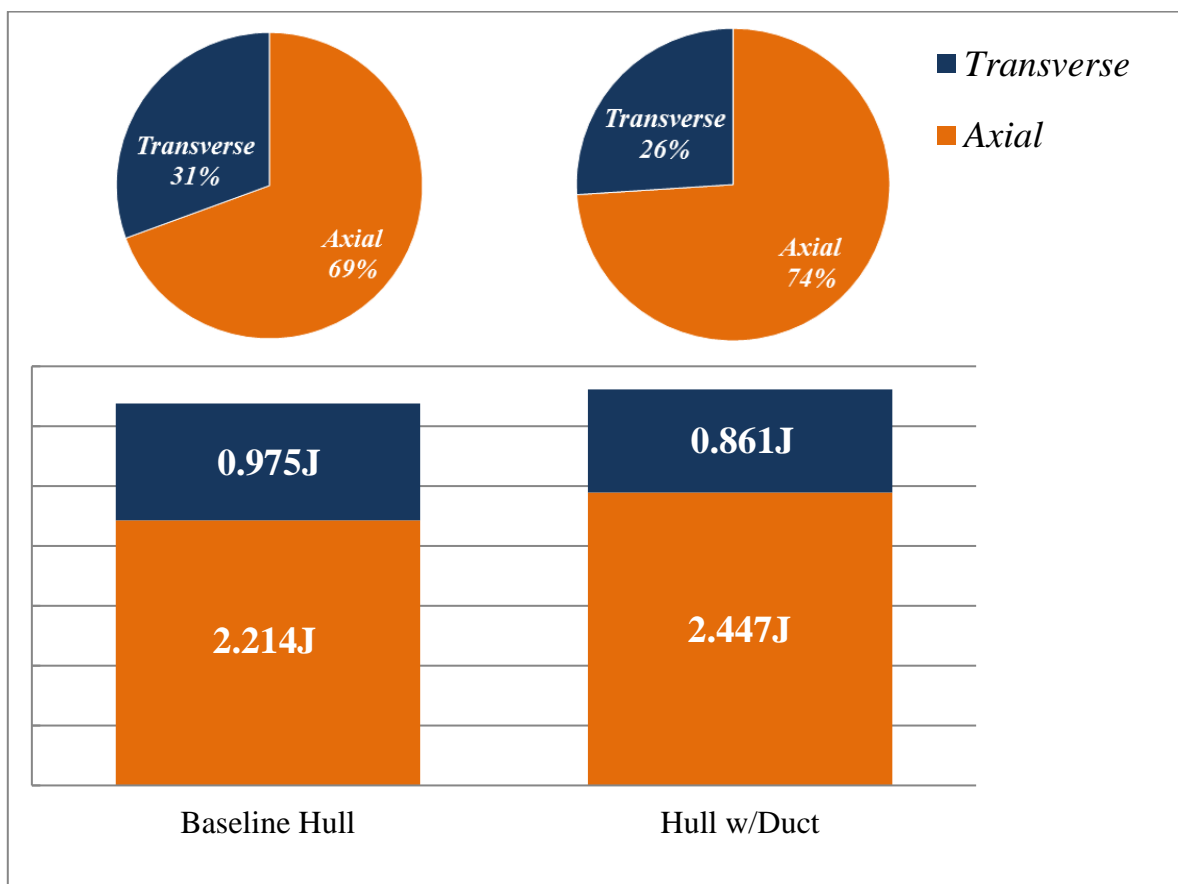


Figure 112. Kinetic Energy Losses: Towing Conditions

Table 79. Kinetic Energy Losses: *Self-Propulsion Conditions*

K.E. Losses	Baseline Hull	Hull w/Duct	% Diff.
Axial (K_{ax})	3.47780	3.63660	4.57
Transverse (K_{tr})	7.19180	7.56710	5.22
Total (K_{Total})	10.66960	11.20370	5.01

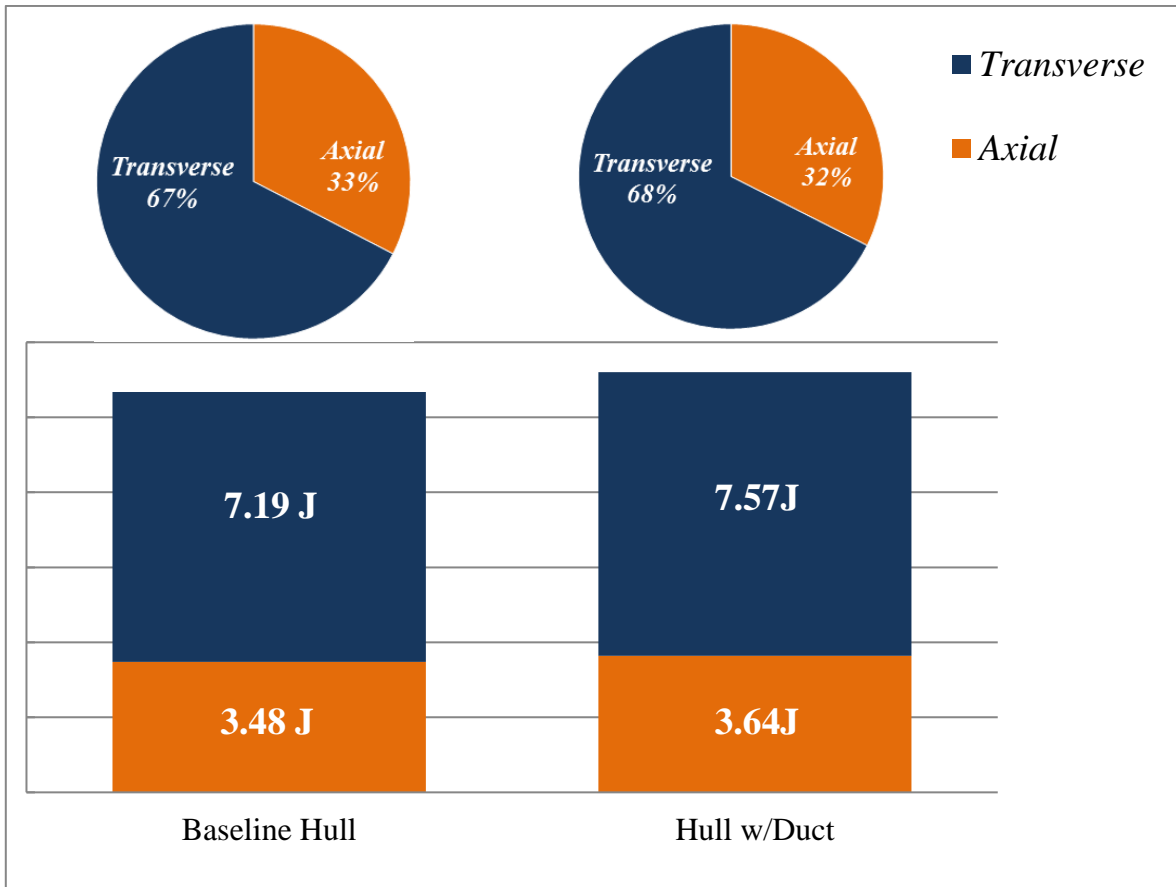


Figure 113. Kinetic Energy Losses: *Self-Propulsion Conditions*

Table 80. Kinetic Energy Losses: *Model-Scale vs Full -Scale*

K.E. Losses	Model-Scale % Diff.	Full-Scale % Diff.
Axial (K_{ax})	-6.98	4.57
Transverse (K_{tr})	-10.65	5.22
Total (K_{Total})	-9.88	5.01

8.4 Chapter Summary and Conclusion

This chapter presents and describes in great detail, a study that was carried out to identify the main contributors to hydrodynamic ship performance variations between different scale environments. Therefore, CFD methods were used to simulate the performance of the Japan Bulk Carrier (JBC), with and without the duct, both in model and full-scale conditions.

The study is made up of three modules (sections). Firstly, it compares the fluid flow behaviour of the hull without duct at both model and full- scale. It then moves on to analysing the impact of the duct on the ship performance at model scale. Similarly, the chapter finishes off by investigating the impact of the duct at full-scale conditions. The main differences between the two scale environments are clearly highlighted and outlined below, thus contributing further to scientific research.

In the absence of the duct or any energy saving device, the propeller efficiency and performance parameters vary at different scales, mainly due to the change in hull efficiency as a result of a diverse wake fraction. This re-confirms outcomes from previous research, whereby the difference in Reynolds numbers alters the fluid flow behavior and the boundary layer thickness ratio produces a different wake fraction.

With regards to impact of the duct at model scale, it seems that the duct itself is producing a minimal drag both in towing and self-propulsion conditions. However, its presence has a beneficial effect on the bare hull resistance (mainly pressure resistance). Whilst CFD indicates that the difference in total resistance is minimally reduced, the highest benefit is achieved through the enhanced propeller performance that is reflected in the hull efficiency as a result of the wake fraction. This was further verified using wake analyses and the study of energy losses. However, installation of the duct increased the non-wake uniformity. This might increase the risk of propeller excited vibrations or propeller cavitation and is probably worth looking into further.

At full scale, the towing resistance of the JBC with duct experiences an opposite behaviour in trend when compared to the model scale results by increasing the resistance by a slight margin. Looking at the overall general performance in self-propulsion, the duct did not prove beneficial at full scale. The ESD slightly increased the delivered power requirement. Installation of the duct produced an insignificant increase in the propulsive efficiency. This increment in propeller efficiency did not make up for the increase in resistance the duct itself has introduced. Although

the ESD configuration reduced the pressure resistance on the bare hull geometry, the duct itself introduced a significant pressure resistance that outweighed the benefit gained from the reduced hull pressure resulting in an overall increased total resistance. When comparing to the model-scale condition, the ESD has a better effect on the reduction of the bare hull resistance at full scale. However, the ESD itself generates a much higher drag ratio at full scale resulting in a negative net performance.

Taking all the above into account, one can conclude that the duct improves the wake fraction of a vessel both in model and full-scale conditions (not necessarily the power performance). For this to be effective in the overall performance, this benefit, hull efficiency, should outweigh the resistance of the duct itself. Therefore, the foil of the duct, needs to be specifically optimized to produce the least possible resistance or generate a thrust and the reference propeller redesigned accordingly. Only then would the duct prove beneficial. It is evident that the performance of the duct in a nominal wake field is completely different from that in an effective wake field. A duct should always be analysed and designed to function in an effective wake as this will be its normal operating conditions.

This study addresses a hot topic within the marine industry regarding the impact of scale effects in different environments with a particular focus on duct installations. Although this topic is not new to the industry and has been studied extensively, its science was always considered challenging with some areas that have never been fully understood or exploited. In that respect, with better simulation methods and more detailed post- processing capabilities available, the subject deserved further investigation using newer methods. With that motive in mind, this study carried out the above approach using state-of- the- art CFD procedures as highlighted in chapter 4. With regards to future recommendations, it is encouraged to re-investigate this subject with any further developments in CFD and computing capabilities. This would allow for further understanding and discoveries.

In conclusion, this chapter has successfully demonstrated the performance differences, both in towing and self-propulsion conditions, of a ducted case study vessel in different scale environments. Furthermore, the main discrepancies are outlined and discussed for justification. The study has thus contributed to the body of knowledge in this regard.

9 Analysing ESD Combinations

9.1 Introduction

As previously outlined in Chapter 2, there are a number of research questions regarding the installation of a multiple ESD on a vessel in a full-scale environment. Do these devices provide an enhanced benefit when combined or do they interrupt and interact the flow regimes, functions and working principles of one another? Another topic of discussion is whether the propulsive impacts are directly cumulative. All these questions have provided good bases for motivation to carry out the work in this chapter. The main idea behind the study is to shed more light on this subject using the current state of the art methods and contribute to the body of knowledge in the ESD community.

The research was carried out by investigating all possible combinations between the PBCF, Stator Fins and Duct on the RSBC bulk carrier. These were analysed in full-scale environments by investigating their impact on performance, wake characteristics and pressure excited vibrations. The end goal is to address the research questions and contribute knowledge to the marine industry. Where possible, most of the ESD analytical process and checklist developed for this thesis was also carried out for all the respective combinations. The idea is to adopt and transfer all the knowledge and skills from the previous chapters to carry out this novel study with the highest standard and quality.

This chapter will briefly explain the approach and methodology carried out together with any assumptions and considerations outlined. Furthermore, personal input and feedback is provided regarding the whole process and procedure. The chapter then moves on to outlining the propulsive performance of each combination, together with any relevant discussion. Although most of the analysis checklist was carried out for all the simulations, not all the results are presented. Major findings and results relevant to conclusions would be presented in reference for discussion and remarks. That being said, all configurations are analysed in great detail, investigating performance breakdown, wake flow characteristics, pressure excited vibrations and more.

In summary, this chapter addresses a key issue in the marine industry, ESD combinations. The use of Energy Saving Devices to improve propulsive efficiency is not new to the industry. The necessity for further improvements has directed research to either develop new ESD designs or combine well-established ESD devices. However, not all technologies can be used in parallel for enhanced benefits. Each technology has its own function and therefore cannot be easily paired with another device of similar function. The different combinations and configurations of ESD devices that are compatible with each other, are not well-established within the research community and require further investigation.

This study has been devised in such a way to address this topic and contribute to the body of knowledge by analysing the combination of three popular technologies; PBCF, Stator Fins and a Pre-Duct on the RSBC vessel. Furthermore, this study will demonstrate an approach on how to analyse different ESD combinations for a particular vessel. The research and findings of this case study are presented and discussed together with any concluding remarks outlined.

9.2 Approach & Methodology

The numerical approach and CFD methods carried out for the analyses of the different ESD combinations follows along the methodology outlined in Chapter 4. The RSBC geometry was the baseline ship hull that was used to install the different ESD combinations. This hull was presented in chapter three of this thesis. With regards to the selection of ESD combinations, it was decided to analyse 3 of the most common technologies in the marine industry, namely, Propeller Boss cap Fins (PBCF), Pre-Swirl Stators (PSS) and Wake Equalising Ducts (WED). These three devices will be installed simultaneously in all the possible combinations as follows:

Table 81. ESD Combinations

--	Baseline
1.	PBCF
2.	DUCT
3.	STATORS
4.	PBCF & DUCT
5.	PBCF & STATORS
6.	DUCT & STATORS
7.	PBCF& DUCT & STATORS

Please note that the conditions are colour coded for better understanding and identifying the results. Figure 115 represents all three ESD geometries respectively. It is also demonstrated that the surface mesh outlining these devices were refined in order to accurately capture the flow behaviour around the technologies. That particular PBCF form was selected since it is the actual geometry installed on the real ship that is represented by the RSBC hull. The form of this PBCF was provided by a source that cannot be disclosed and is unfortunately not of the best quality.

Furthermore, virtual open water propeller tests that were carried out using CFD procedures indicated a reduction in open water efficiency with the use of the propeller boss cap fins. That being said, such devices can still prove to be beneficial helping reduce the hub vortex as demonstrated in Chapter 6.

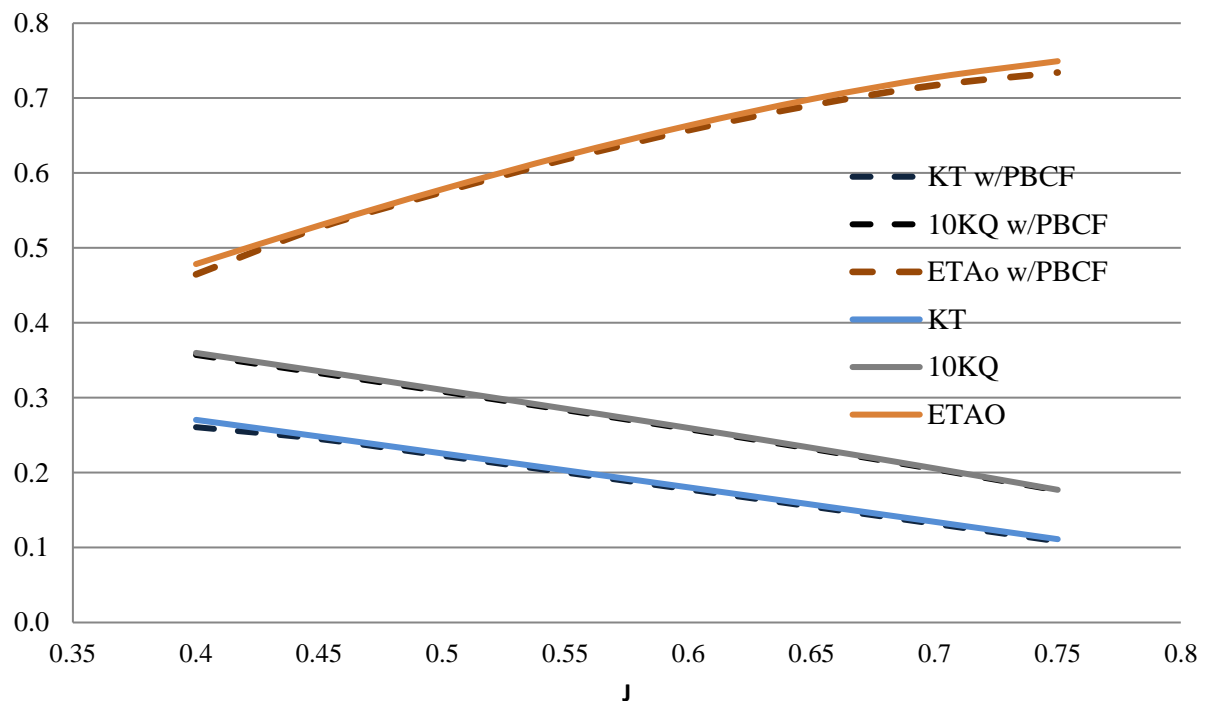


Figure 114. Open Water Tests

Before presenting and discussing the results for the study, it is worth outlining a few general remarks that should be kept in mind. These are as follows:

- Some of the ESD combinations produced significant dynamic forces. So it was not so easy to average out the results. Computing a mean of the solution was thus carried out by experience and in the best way possible.

- Due to averaging of the results, the solution might not be very accurate, but this method is a good means of comparing the different ESD combinations and provides a good basis for when improved CFD solutions are available for such scenarios.

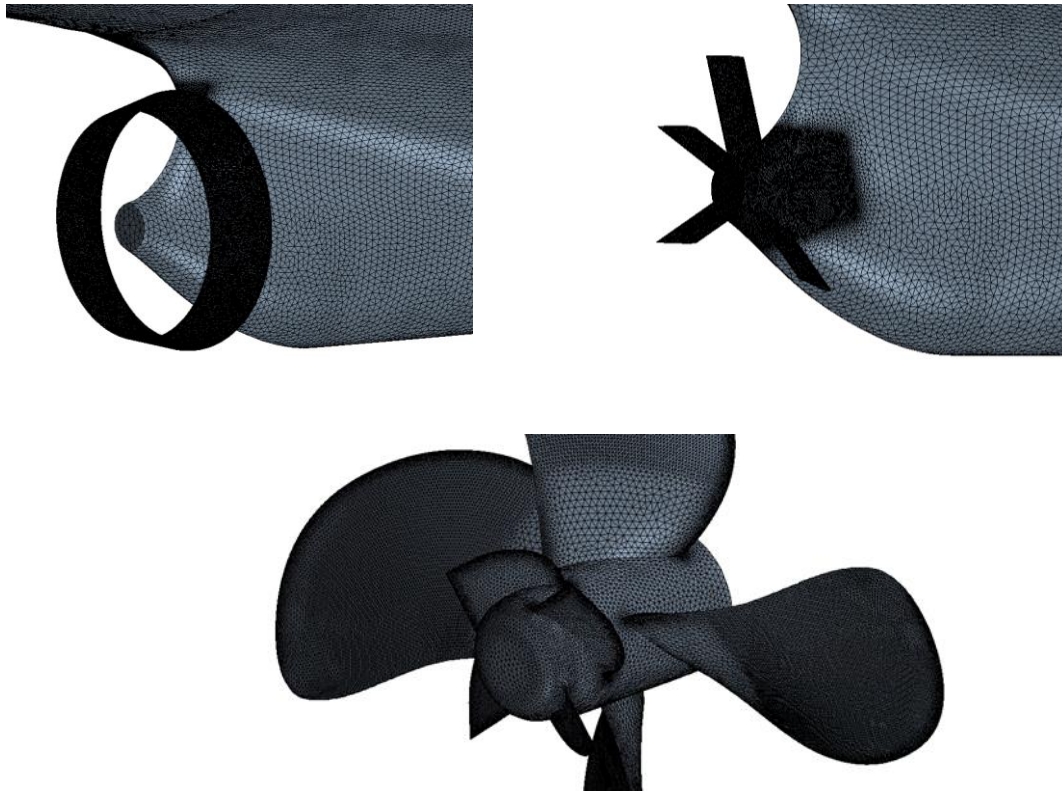


Figure 115. ESD Geometry

9.3 Towing performance Analyses: Resistance

When analysing the performance of a hull-propeller system, it is also crucial to investigate the forces generated by the individual components. This gives an indication to the source of improvement or detrimental performance. This study has thus analysed and looked into the breakdown of forces both with and without the presence of the propeller. Therefore, Table 82 indicates the breakdown of forces for each component in towing conditions, whilst Table 83 indicates the aforementioned in self-propelled conditions.

The Duct and Stators were considered to be part of the hull system whilst the PBCF was considered to be part of the propulsion system, which is why the latter do not feature in the

towing simulations. Therefore, excluding the baseline hull condition, towing conditions were run for three combinations:

- Duct Only
- Stator Only
- Duct & Stator

When looking at the overall resistance for all towing conditions as exhibited in Table 82, it is noted that all the installed ESD devices increased the drag of the vessel. It was further demonstrated that the duct component as well as the fins produced a thrust when performing independently. They both however have a detrimental effect on the resistance of the hull, due to the increase in drag and the resultant effect is not beneficial. When these Energy Saving Devices are combined, the duct no longer produces a thrust while the stator fins produce a higher thrust. That being said, the resultant drag is increased by around 6%.

At this stage, it would be worthwhile investigating the reason behind the incremental resistance of the hull itself when installing these devices. It is therefore useful to look into the breakdown of resistance between the different geometries by analysing the pressure and shear resistance, as demonstrated in Table 83.

Table 82. Resistance Breakdown: Towing

Resistance (N)								
	--	1.	2.	3.	4.	5.	6.	7.
Condition	Baseline	PBCF	Duct	Stators	PBCF + Duct	PBCF + Stators	Duct + Stators	PBCF + Duct + Stators
Base Hull	284683	284683	301624	290216	301624	290216	304819	304819
Duct	-	-	-3510	-	-3510	-	3137	3137
Stators	-	-	-	-3403	-	-3403	-5035	-5035
Total (N)	284683	284683	298114	286813	298114	286813	302921	302921
Diff %			+4.71	+0.75	+4.71	+0.75	+6.41	+6.41

When looking into the hull & duct geometry configuration, the duct has a beneficial effect on the shear resistance of the hull but also has a detrimental effect on the Pressure of the hull. The duct itself obviously generates a shear resistance due to the wetted surface area but produced a beneficial thrust due to the pressure effects. The benefits of the duct itself do not outweigh the undesired effects resulting in an overall higher resistance by a slight margin.

With regards to the Hull & Stators geometry arrangement, in a similar manner, the stator fins reduce the shear resistance of the hull, but increase the pressure resistance of the hull from 38884 to 50534N as demonstrated in Table 83. The fins themselves generate an insignificant shear drag but also generate thrust due to the pressure differences around the foils. The overall effects in towing conditions are minor, with no significant improvements or detrimental performance.

Meanwhile, when installing both ESDs together on the baseline hull, it can be noted that the presence of the stator fins deteriorated the thrust performance of the duct and the presence of the duct enhanced the thrust performance of stator fins. That being said, this arrangement has produced the highest resistance output from all four conditions.

It is important to outline that no ESD had a positive overall contribution in towing conditions. As a general outlook, it can be said that the ESD components both add shear resistance due to the added wetted surface area. However, they produce a beneficial pressure effect that outweighs the added shear drag. That being said, this improvement is not sufficient. The ESD devices significantly increase the pressure resistance of the hull component which overshadows the beneficial effects of the ESD themselves. Furthermore, when combining the devices, the beneficial effect of the Duct disappears, and the overall resistance increases significantly.

Table 83. Understanding Resistance in Towing

	Baseline Hull			Hull & Duct		
Resistance (N)	Shear (N)	Pressure (N)	Total (N)	Shear (N)	Pressure (N)	Total (N)
Base Hull	245799	38884	284683	239659	61965	301624
Duct	-	-	-	2334	-5844	-3510
Stators	-	-	-	-	-	-
Total (N)	245799	38884	284683	241993	56121	298114
	Hull & Stators			Hull & Duct & Stators		
Resistance (N)	Shear (N)	Pressure (N)	Total (N)	Shear (N)	Pressure (N)	Total (N)
Base Hull	239682	50534	290216	239673	65146	304819
Duct	-	-	-	2291	847	3137
Stators	587	-3990	-3403	599	-5634	-5035
Total (N)	240269	46544	286813	242549	60372	302921

9.4 Propelled Performance Analyses: Resistance, Thrust & Torque

Table 84. Resistance, Thrust and Torque Breakdown: *Self-Propulsion*

Resistance (N)								
	--	1.	2.	3.	4.	5.	6.	7.
Base Hull	399476	400721	430780	415163	435002	417411	444662	448717
Duct			-29072	-	-29083	-	-22669	-23819
Stators	-	-	-	-5403	-	-5479	-1112	-1067
Total (N)	399476	400721	401708	409760	405919	411932	420882	423830
Diff %	--	+0.3	+0.6	+2.6	+1.6	+3.1	+5.4	+6.1
Thrust (N)								
	--	1.	2.	3.	4.	5.	6.	7.
Prop. Blades	388425	390948	391207	395344	398623	403446	406946	413170
Hub	11926	13256	13154	14895	14101	14923	14698	15044
PBCF	-	-4731	-	-	-3635	-6221		-5701
Total (N)	400351	399473	404362	410240	409089	412149	421644	422514
Diff %		-0.2	+1.0	+2.5	+2.2	+2.9	+5.3	+5.5
Torque (N-m)								
	--	1.	2.	3.	4.	5.	6.	7.
Prop. Blades	343474	343050	352185	341972	354887	345081	354019	355829
Hub	13735	14736	5555	8748	7493	6919	7603	5386
PBCF	-	3779	-	-	-24	5028		4480
Total (N)	357209	361565	357741	350720	362356	357028	361622	365695
Diff %		1.2	0.1	-1.8	1.4	-0.1	1.2	2.4

Table 84 gives a detailed breakdown of the resistance, thrust or torque generated by the different parts in self-propulsion conditions. As displayed in the table, one can find the hull system components in the resistance section and the propulsion parts under the “Thrust” and “Torque” headers. It is good to note that any positive values under “Resistance” represent drag while a negative indicates a thrust. Similarly, a positive value under the “Thrust” header indicates a thrust and a negative value a drag.

All ESD combinations result in increased total drag. This will be later discussed in detail when analysing Table 85. Similarly, all ESD combinations resulted in an increased thrust except for condition 1 (PBCF only). This indicated that the PBCF (1) on its own had a detrimental effect on the Torque. However, when pairing the PBCF with any of the other ESD devices (combinations 4,5 and 7), these have a beneficial impact on the Thrust. While the duct (2) produced an enhanced thrust generation, the stators (3) delivered higher thrust forces. It can also be said that when installed in parallel, they produce an even higher thrust generation.

The different conditions resulted in various torque generation with no evident behaviour patterns. However, the following relations could be deduced. The installation of PBCF (1) increases torque generation. However, while the duct (2) has no particular effect on Torque, the Stators (3) reduce torque generation. That is why the combination of PBCF and DUCT (4) result in reduced Torque values. The installation of both the PBCF and Stators (5) in conjunction produces no difference since the ESDs cancel each other's effects. The duct diminishes the beneficial reduction of Torque produced by the stators (6). All ESDs installed together result in the worst possible scenario.

Table 85. Understanding Resistance in Self-propulsion

	Baseline Hull			1. PBCF		
Resistance (N)	Shear (N)	Pressure (N)	Total (N)	Shear (N)	Pressure (N)	Total (N)
Base Hull	253641	145834	399476	253732	146989	400721
Duct	-	-	-	-	-	-
Stators	-	-	-	-	-	-
Total (N)	253641	145834	399476	253732	146989	400721
	2. Duct			3. Stators		
Resistance (N)	Shear (N)	Pressure (N)	Total (N)	Shear (N)	Pressure (N)	Total (N)
Base Hull	253560	177220	430780	253504	161659	415163
Duct	2585	-31657	-29072	-	-	-
Stators	-	-	-	708	-6111	-5403
Total (N)	256146	145562	401708	254212	155548	409760

	4. PBCF & Duct			5. PBCF & Stators		
Resistance (N)	Shear (N)	Pressure (N)	Total (N)	Shear (N)	Pressure (N)	Total (N)
Base Hull	253795	181207	435002	253665	163746	417411
Duct	2573	-31656	-29083	-	-	-
Stators	-	-	-	711	-6190	-5479
Total (N)	256368	149551	405919	254376	157556	411932
	6. Duct & Stators			7. PBCF & Duct & Stators		
Resistance (N)	Shear (N)	Pressure (N)	Total (N)	Shear (N)	Pressure (N)	Total (N)
Base Hull	253798	190864	444662	254064	194653	448717
Duct	2594	-25262	-22669	2596	-26415	-23819
Stators	724	-1836	-1112	718	-1785	-1067
Total (N)	257116	163766	420882	257377	166453	423830

Table 85 has been developed to demonstrate and understand the resistance of all the self-propelled conditions. It is noted that the PBCF has no significant contribution to the resistance. In propelled conditions, the beneficial impact of the duct or stators on the shear resistance of the base hull is no longer identified (when compared to towing conditions). However, the detrimental effect on its pressure resistance is still in effect.

Furthermore, when the duct and stators components are installed independently, they both produce a thrust. This, however, does not outweigh the detrimental effects on the base hull for overall improved performance. On the other hand, when these ESDs are installed in parallel in self-propelled conditions, their counterpart presence both have a negative effect on the thrust generated by the components themselves, i.e., they produce more thrust when installed independently. It is good to highlight that the thrust of the duct increases significantly in propelled conditions when compared to its respective condition in the absence of the propeller.

As can be seen in Table 85, the baseline hull still provides the least total resistance. This indicates that although the technologies are producing a thrust, none of the ESD arrangements are having a beneficial impact on the overall drag. This, in turn, does not imply that they are not effective. Other factors that contribute to propulsive performance need to be analysed and looked into.

9.5 Analyses of ESD Behaviour

It was deemed to be appropriate to further investigate, the behaviour of the Energy Saving Devices. The technologies were thus analysed by looking into the drag or thrust generated by the different components of section. As shown in Table 86, the duct and stator fins are analysed in 4 parts. These have been displayed in Figure 116 for better understanding for the reader.

Table 86. ESD Analyses (*Drag*)

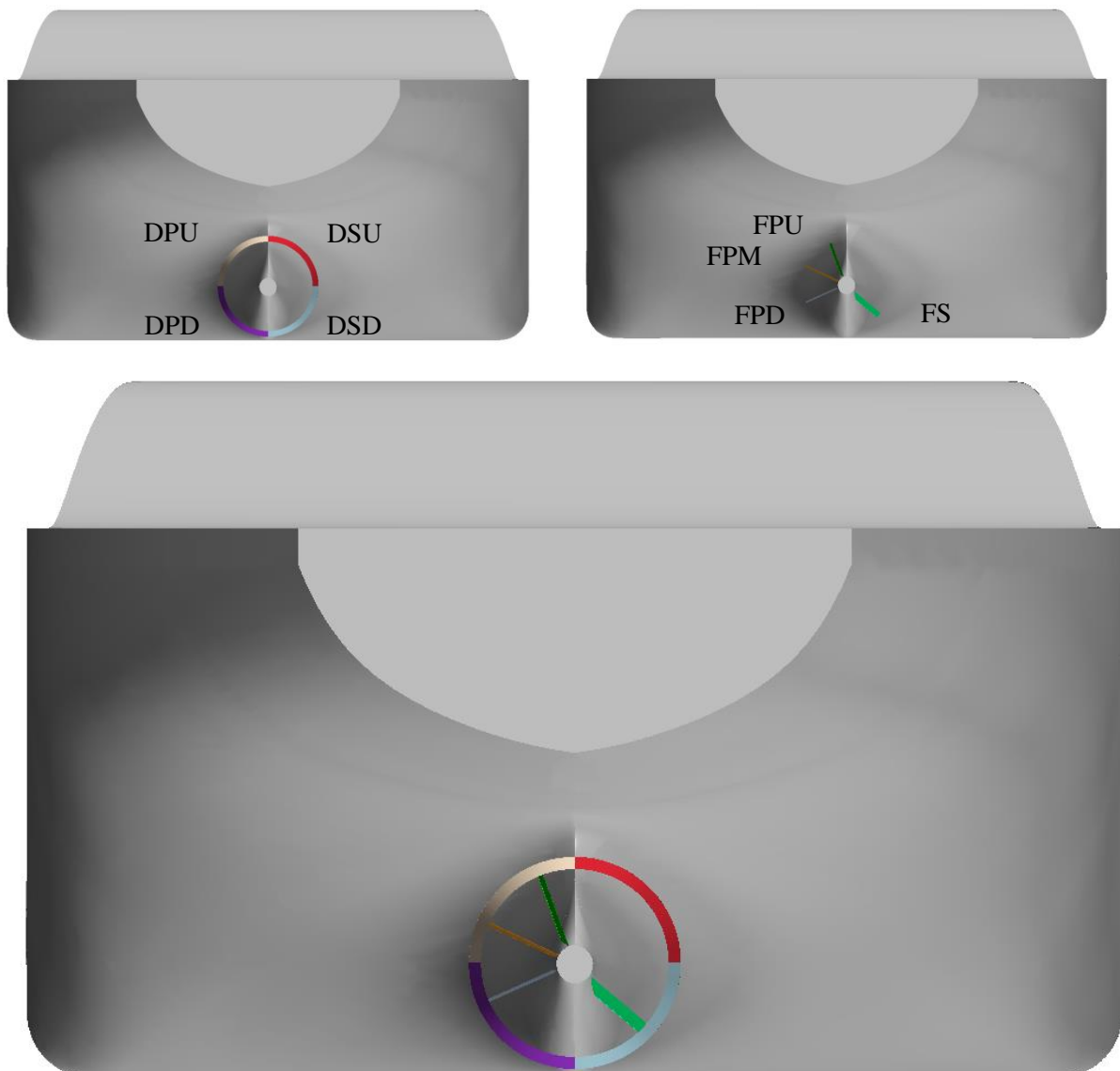
Condition	Components		Towing	Self-Propulsion
			<i>N</i>	<i>N</i>
Duct	Duct Port Up	<i>DPU</i>	4190	1400
	Duct Starboard Up	<i>DSU</i>	4300	1000
	Duct Port Down	<i>DPD</i>	-6000	-15200
	Duct Starboard Down	<i>DSD</i>	-6000	-16300
Stators	Fin Port Up	<i>FPU</i>	-1524	-1200
	Fin Port Middle	<i>FPM</i>	-1676	-3600
	Fin Port Down	<i>FPD</i>	-1503	-2100
	Fin Starboard	<i>FS</i>	1300	1500
Duct & Stators	Duct Port Up	<i>DPU</i>	4337	1305
	Duct Starboard Up	<i>DSU</i>	4600	1308
	Duct Port Down	<i>DPD</i>	-4600	-14572
	Duct Starboard Down	<i>DSD</i>	-1200	-10710
	Fin Port Up	<i>FPU</i>	-2300	-1623
	Fin Port Middle	<i>FPM</i>	-2100	-2895
	Fin Port Down	<i>FPD</i>	-1635	-1645
	Fin Starboard	<i>FS</i>	1000	5051

When considering the different parts of the duct as depicted in Table 86, one notes that the upper side of the duct produces a drag while the bottom section of the duct produces a thrust (negative drag value). In self-propulsion, the duct proved to be more effective. This is because the upper portion of the duct produced less drag, and the bottom part of the duct generated more thrust when compared to the towing condition.

On the other hand, when looking into the stators, it is noted that the fins on the port side of the vessel are producing a thrust while the fins on the starboard side are producing a drag. The middle and bottom fins on the port side become more effective in propelled conditions. The starboard fin is thus not properly designed and ineffective.

When both technologies are installed in conjunction in towing environments, the fins cause the bottom part of the duct to generate less thrust but the presence of the duct causes the upper and middle fin on the starboard side to generate more thrust. Similar behaviour is not exhibited in self-propelled conditions with some fins performing better and others worse. One significant difference when both ESDs are installed in parallel in propelled conditions, is the increase in resistance of the stator on the starboard side.

Figure 116. Duct & Fin Components



9.6 Propulsive Performance Analyses

Ultimately, for enhanced efficiency or better performance, the vessel is required to propel the ship forward at reduced power for the same speed. Reduced power output would, in turn, require less fuel consumption and minimise pollutants and emissions. Table 87 presents the propulsive performance for all the different ESD fitted combinations studied in this chapter. Since power is a factor of torque and propeller revolutions, requiring a lower rpm value or producing a reduced torque can achieve a performance benefit.

The table outlines that condition 3, (stators only), provided the best propulsion performance resulting in a 5% power reduction which is relatively significant. It is worth mentioning that a negative sign indicates a power reduction and positive values indicating that more power is required. The PBCF-Stator (condition 5) configuration produced the second-best performance providing around 2.2% power reductions. The worst conditions proved to be the PBCF- Duct combination requiring 1.95% more delivered power. The rest of the conditions mostly vary within 1% of the baseline performance.

Power can also be determined as a factor of propulsive efficiency. The latter is deduced via a combination of three other efficiencies (relative rotative efficiency, hull efficiency and open water efficiency). These were analysed to identify the source of benefits or detrimental effects for all the different conditions. While these criteria can be analysed for all the different conditions, for the purpose of this study, we will look into the two conditions that provided significant benefits (condition 3 & 5).

As previously mentioned, the condition that provided the best propulsive efficiency from all the ESD combinations is condition 6 (Duct & Stators) with a value of 0.63 followed by conditions 7 (PBCF, Duct & Stators) and 3 (Stators) both having a value of 0.62. It is good to note that a common denominator of all three conditions is the stators which indicate their beneficial contribution to the propulsion efficiency as an Energy Saving Device. That being said, the duct in conjunction with the stators provide the best propulsive efficiency but not the best propulsive performance or power output as indicated in Table 87.

Table 87. Propulsion Performance Analyses

Condition	Baseline	1.PBCF	2. Duct	3. Stators	4. PBCF & Duct	5. PBCF & Stators	6. Duct & Stators	7. PBCF & Duct & Stators
V _S	6.43	6.43	6.43	6.43	6.43	6.43	6.43	6.43
R _T	284682.97	284682.97	298113.60	286812.93	298113.60	286812.93	302921.12	302898.00
R _{SP}	399475.50	400721.00	401708.14	409760.00	405919.00	411931.65	420881.91	423830.31
t	0.29	0.29	0.26	0.30	0.27	0.30	0.28	0.28
1-t	0.71	0.71	0.74	0.70	0.73	0.70	0.72	0.72
T	400350.65	399473.43	404361.72	410239.50	409089.00	412148.72	421644.17	422513.53
T	357209.00	361565.06	357740.90	350720.40	362356.00	357027.86	361622.08	365695.17
KT	0.1865	0.1858	0.1884	0.2043	0.1887	0.2005	0.2051	0.2035
KQ	0.0291	0.0294	0.0291	0.0305	0.0292	0.0304	0.0308	0.0308
n	1.40	1.40	1.40	1.35	1.41	1.37	1.37	1.38
FD	-875.15	1247.57	-2653.58	-479.50	-3170.00	-217.07	-762.26	1316.78
V _A	0.59	0.58	0.58	0.55	0.58	0.55	0.55	0.54
KQ _{ow}	0.03	0.03	0.03	0.03	0.03	0.03	0.03	0.03
V _a	4.69	4.66	4.66	4.23	4.63	4.30	4.27	4.27
wt	0.27	0.28	0.28	0.34	0.28	0.33	0.34	0.34
1-wt	0.73	0.72	0.72	0.66	0.72	0.67	0.66	0.66
η _{ow}	0.65	0.64	0.65	0.62	0.64	0.62	0.62	0.61
η _R	0.92	0.91	0.92	0.94	0.93	0.93	0.94	0.93
η _H	0.97	0.98	1.02	1.06	1.01	1.04	1.08	1.08
η _D	0.58	0.58	0.61	0.62	0.60	0.60	0.63	0.62
DHP (kW)	3137.69	3178.22	3142.36	2979.32	3198.83	3068.80	3108.29	3159.38
+/- More Power (%)	--	1.29	0.15	-5.05	1.95	-2.20	-0.94	0.69

Power is a function of the product of towing resistance with the ship velocity divided by the propulsive coefficient. This indicates that although condition 6 provides the best propulsive efficiency, the gain in towing resistance is significant, thus limiting the power reduction or power savings. This, in turn, indicates that the best power savings would be achieved by a candidate that ideally produces a better propulsive efficiency at no or minimal expense of towing resistance gain. Although condition 6 (Duct and Stators), provides the best propulsive efficiency, the duct produces a significant increase in resistance, thus not providing the best overall performance. On the other hand, condition 3, Stators, produced the second-best propulsive efficiency at little expense of added resistance, thus providing the best performance requiring the least power.

It is worth studying the conditions further and understanding the reasons behind the improvements. Propulsive efficiency is directly proportional and a function of the open water efficiency, the relative rotative efficiency and the hull efficiency with the latter being dependant on the thrust deduction fraction and the wake fraction.

The results displayed in Table 87 indicate that the stators tended to reduce the open water efficiency and the advance velocity into the propeller. Meanwhile, the PBCF and Duct technologies had an insignificant effect on the advance velocity and open water efficiency. Although the improvements are minimal, the stators tended to increase the relative rotative efficiency. No apparent or obvious correlation could be made with the other technologies and their impact on the relative rotative efficiency.

Both the duct and the stators, when used individually or in conjunction, have resulted in an increase in hull efficiency. The increase in hull efficiency could be either due to an increase in the thrust deduction term $(1 - t)$ and/or a reduction in the velocity ratio $(1 - w)$. Results from Table 87 indicated that the duct tended to reduce the thrust deduction fraction while the stators increased the parameter in question. On the other hand, the Stators reduced the velocity ratio $(1-w)$ with the duct having no significant effect on this criterion.

The reduction of the thrust deduction fraction by the duct condition explains the increase in resistance the technology introduces (with respect to the baseline condition) in towing conditions. This increment in resistance in self-propulsion conditions for the duct is not as significant. The reasons for this behaviour is explained earlier in this chapter. Therefore, the duct condition produces a lower thrust deduction fraction resulting in a higher $1-t$ (thrust deduction term).

With regard to the stators conditions, although the stators do not change the towing resistance significantly when compared to the baseline condition, they require a higher thrust to propel the vessel forward at the desired speed (higher propelled resistance). This can also be verified with the lower advance ratio required and reduced open water efficiency. The increase in required thrust results in a higher thrust deduction fraction (t), and consequently the $1-t$ is reduced. However, the reduced advance ratio has a beneficial effect on the wake fraction of the system. The reduced advance velocity into the propeller indicates an increase in the wake fraction (w), thus reducing the velocity ratio ($1-w$). This benefit outweighs the detrimental effects of the thrust deduction fraction producing an overall improved hull efficiency.

Since the propeller performance of the Duct condition is very similar to that of the baseline condition, there was little or no impact on the wake fraction. Thus, it can be said that the benefits of the duct are coming from the benefits of the thrust deduction fraction.

The higher wake fraction (w) produced by the stators implies that the velocity ratio ($1-w$) is lower. This indicates that the velocity of the fluid into the propeller plane is lower than that of the baseline condition. The stators are thus having a significant effect on the boundary layer.

This observation or deduction is quite interesting because the stators in towing conditions, as indicated in Table 88 produce a lower wake fraction (w) at the propeller plane. It is also worth mentioning that the wake analyses at the propeller plane in self-propulsion conditions was not possible due to the presence of the geometry. Analyses were only carried out aft of the propeller, which also indicate an increase in the mean wake fraction, but it is hard to make a direct deduction or correlation from these results. Nevertheless, the results in Table 87 indicate an increase in w in self-propulsion conditions and reduced velocity ratio. Therefore, it can be said that the stators are behaving differently between Towing and Self-propulsion conditions. This can be further investigated by analysing the resistance of the technology in both conditions. Table 86 presents the resistance/thrust generated by the stators in towing or self-propulsion conditions. It exhibits that the Thrust produced by the stators in self-propulsion conditions is 5400N while the thrust in towing environments is 3403N. It could very well be that the presence of the propeller is changing the angle of attack of the flow thus making the foils of the stator work more efficiently hence leading to a reduction in the advance velocity. This is to be further investigated.

In summary, the Duct combinations enhance the propulsive efficiency because it produces a lower thrust deduction fraction and has no impact on the wake fraction, thus improving the hull

efficiency. The stators, on the other hand, enhance the propulsive efficiency because the benefits achieved through a higher wake fraction outweigh the detrimental effects of the undesired higher thrust deduction fraction. Furthermore, the stators reduce the open water efficiency but increase the relative rotative efficiency.

When combining these technologies together, the performance is very similar to that of the Stators condition. However, the reduction of the thrust deduction fraction of the duct dominates. Therefore, the duct produces a lower thrust deduction fraction while the stators increase the wake fraction, thus providing an even higher hull efficiency and overall better propulsive efficiency. That being said, these combined technologies do not provide the best power performance due to the high resistance caused by the duct in towing conditions.

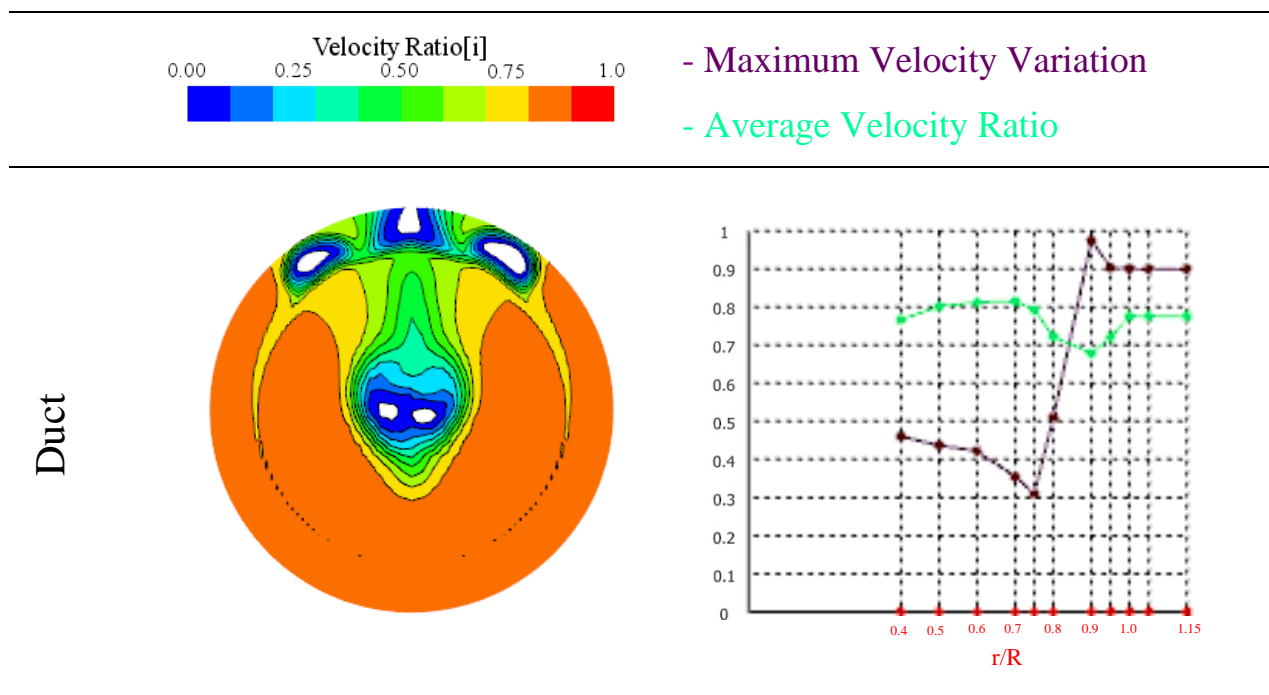
9.7 Wake Analyses

Towing

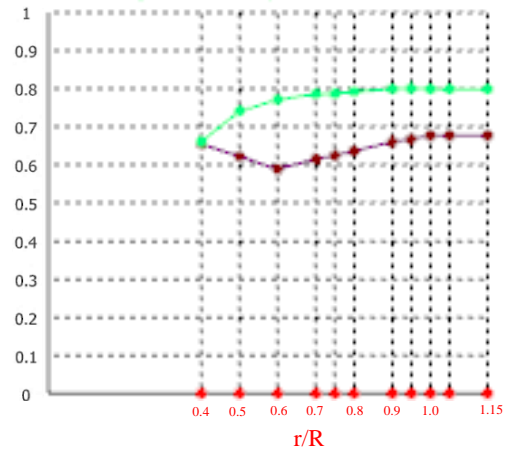
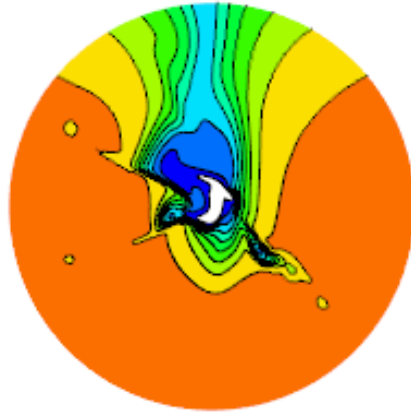
Table 88. Wake Analyses @ propeller Plane (*Towing*)

Parameter		Duct	Stators	Duct & Stators
Taylor Wake Fraction	$[w_t]$	0.257	0.238	0.275
Non- Wake Uniformity	$[\Delta w]$	0.62	0.64	0.815

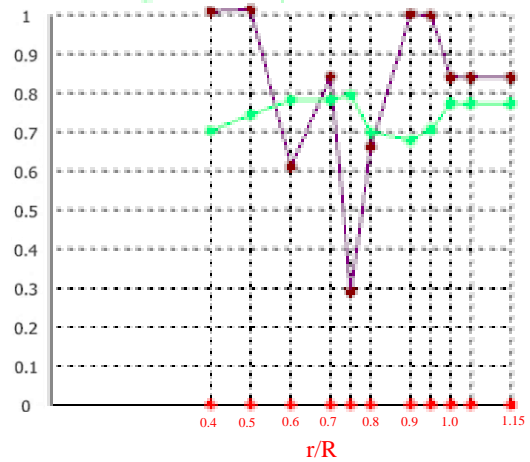
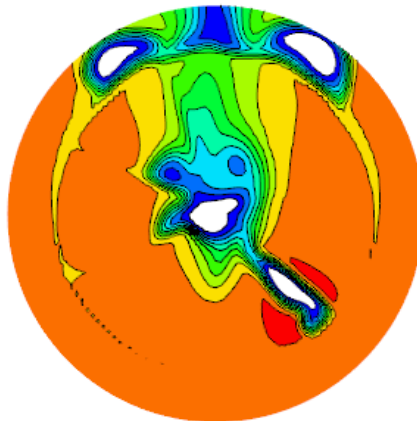
Table 89. Flow Field Behaviour @ Propeller Plane (*Towing*)



Stators



Duct & Stators



Axial wake analyses were carried out for both the towing conditions as well as the self-propelled conditions. The developed WAT tool (Maasch et al., 2019) was used to analyse the flow field past the hull and provide valuable insight into the wake region. The wake was analysed at the propeller plane for the towing condition and the results presented in Table 88 and Table 89. Due to the presence of the technologies and the propeller, the data was extracted at a location post the propeller for the self-propelled condition. Results for the latter are depicted in Table 90. Such analyses can shed light on the energy that is leaving the ship-system, which is preferred to be kept at a minimum for more efficient designs. That being said, no direct correlations or deductions can be made since the analyses focuses solely on the axial velocities. As explained in the previous chapter, the energy depends on the velocity components of the three different directions.

In the absence of the propeller (in towing environments), the duct produced a higher wake fraction when compared to the stators. However, when these two technologies are installed in parallel, these produced the highest wake fraction, which contribute towards an enhanced hull

efficiency. That being said, this combination (Duct + Stators) produced the highest non-uniformity in the wake and this might increase the risk of propeller excited vibrations or cavitation.

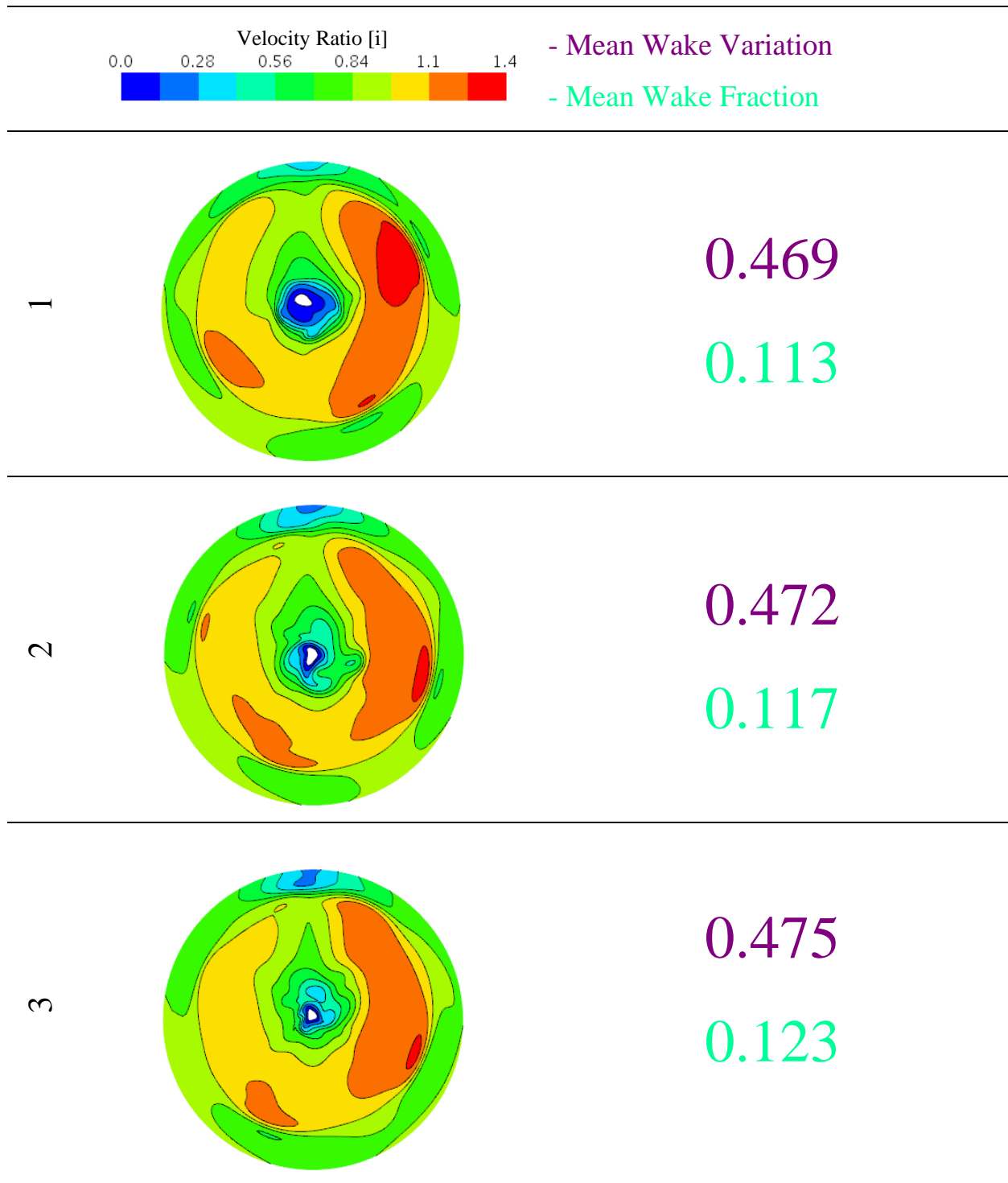
Analysing the flow field further, the plots for the Duct condition indicate that the duct introduces a sudden decrease in velocity at $r/R= 0.9$. Further to this, one can notice the swirling/reversed flow at the upper region of the wake, which is located above the trailing edge of the duct. This could lead to critical issues with cavitation and pressure excited vibrations.

On the other hand, the stators produced a more uniform flow and more constant velocity variation as can be seen in the table. However, it can be observed that the velocity dips at $r/R= 0.4$ and that the velocity change at the Top Dead Centre of the wake is more critical since the fluid flow rapidly increases with an increase in angle (from blue to yellow).

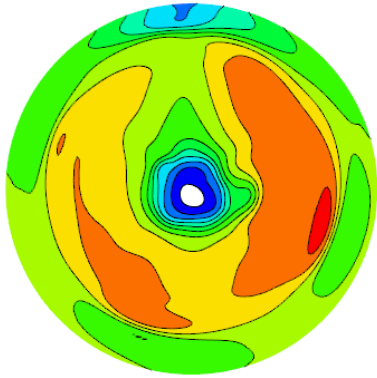
This just goes to show that the “Maximum Velocity Variation” and the “Average Velocity Ratio” plots do not provide sufficient information. These values do not present the behaviour or change of the flow within the same radius over varying angles. That is why it was also important to analyse the graphical images included in the table. When the technologies were installed in parallel, the non-uniformity of the wake increased significantly. The swirling flows produced by the Duct were still present and the stator on the starboard side seemed to have also generated an additional swirling flow in this condition.

Diverting the attention to the self-propelled systems, the condition involving the stators (condition 3) produced the highest mean wake fraction, but it also produced the highest wake variations. However, the fins can be seen to reduce the velocity ratio peaks that are represented by the red regions on the starboard side and represented by the orange colour on the port side. It was hard to come to any deductions or conclusions from the rest of the conditions. This would be better investigated by computing the K.E. losses. However, due to time constraints, this was not possible for this study and would be outlined for future recommendations

Table 90. Flow Field Behaviour @ Post- Propeller Plane (*Self-Propulsion*)



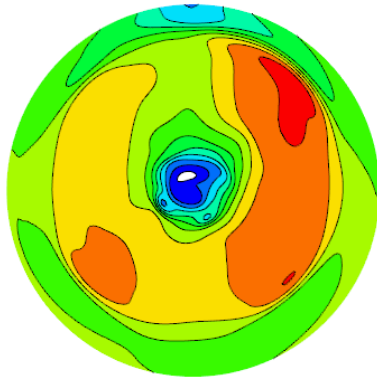
4



0.453

0.112

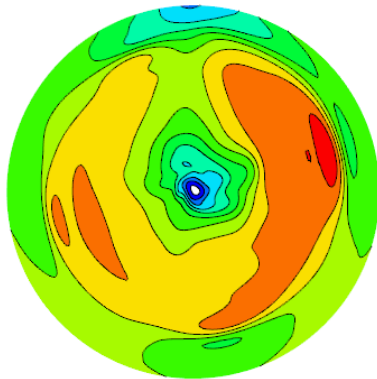
5



0.486

0.119

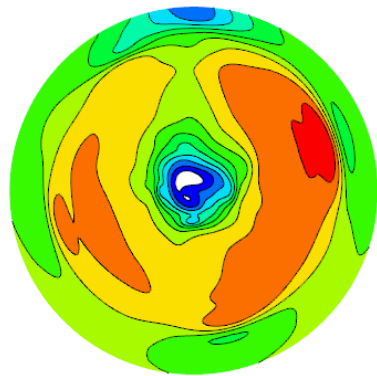
6



0.458

0.121

7



0.475

0.113

9.8 Chapter Summary and Conclusion

This chapter presents and describes in great detail, a study that was carried out to investigate the performance differences that various ESD combinations provide when installed on board a vessel. Therefore, the chapter addresses research questions related to the installation of multiple energy-saving devices. More specifically, whether the devices provide an enhanced benefit, or if they interrupt and interact with the flow regimes, functions and working principles of one another. Furthermore, whether the propulsive impacts are directly cumulative when installed simultaneously.

The research was carried out by investigating the installation of all possible combinations of the following technologies; Propeller Boss Cap Fins (PBCF), Stator Fins and the Wake Equalising Duct. This amounted to seven different conditions, including the baseline vessel with no technology installed.

The analyses were carried out using state-of-the-art CFD procedures, as explained in Chapter 4 of this thesis. Furthermore, the study followed the ESD analyses checklist that was previously outlined in this thesis to analyse all the different conditions. That being said, some of the methods in the procedure were not carried out due to time constraints and are highlighted to be examined in future work for more thorough analyses. However, this study is thorough with lots of detail on the topics that were addressed on the list.

Key findings indicated that the propulsive impacts are not directly cumulative. The technologies do interrupt and interact with flow regimes and functions of one another. However, it can be said that the installation of a combination of devices can provide enhanced benefit if the devices are allowed to contribute to improved efficiency through their designed function simultaneously. Preferably, their working principles and design function should be separate and different in order for them to be compatible. The goal here is to bring the best of both worlds with each device contributing to different parameters of propulsive efficiency or enhancing each other's weak points.

In this particular study, it was deduced that the Duct technology enhances the hull efficiency by reducing the thrust deduction fraction (t) and has no impact on the wake fraction. Meanwhile, the stators improve the hull efficiency because the benefits achieved through a higher wake fraction, outweigh the detrimental effects of the undesired higher thrust deduction fraction. When these two technologies are installed in parallel, the system maintains and

produces the higher wake fraction of the stators while also being able to maintain a lower thrust deduction fraction of the duct. Therefore, this combination provided an even higher hull efficiency and best overall propulsive efficiency from all the conditions. In this scenario, the devices improved separate components of the hydrodynamic system. One could also highlight that the duct contributed to avoiding the stators' weak point of producing a higher thrust deduction fraction. However, this condition did not provide the best power output.

Although the Duct + Stators combination provided the best propulsive efficiency, it was the Stators conditions that required the least power to run at design speed. This indicates that the gain in hull efficiency achieved by the duct did not outweigh the additional overall drag it created. Therefore, in an ideal case scenario, the best power savings would be achieved by a candidate that ideally produces a better propulsive efficiency at no or minimal expense of resistance gain. It would be interesting to analyse the performance of the system if the duct was replaced with a semi-duct.

It can be said that the Stators proved to be the best technology by augmenting the hull efficiency at minimal expense of drag. It also seems to produce the most uniform wake flow. However, its wake and flow regime impact require further analyses and justification.

It is worth mentioning that the PBCF of this particular study did not provide any benefit due to the increase in generated torque, indicating that it is not cancelling the hub vortex. It is not justifiable to conclude that this particular technology does not function properly. It was merely designed poorly for this particular vessel. Chapter 6 of this thesis has clearly and successfully indicated the benefits of propeller boss cap fins. This just shows how important it is that the devices are customised and designed accordingly and not bought off-the-shelf. It is also good to point out that the deductions and conclusion highlighted for this chapter are merely based on these specific designs. The purpose of this chapter is not to outline the best technologies or combinations but to indicate the performance impact/behaviour of installing devices simultaneously and the approach to how they should be analysed. It is highly recommended that an ESD or combination of these technologies to be customised and analysed for guaranteed and enhanced benefit prior to installation.

In summary, this chapter has successfully demonstrated the performance differences when installing a combination of Energy Saving Devices (ESD). The main discrepancies are highlighted reasoned and discussed. Future work has also been outlined for further justification. The key findings in this study have contributed to the body of knowledge.

10 Discussion

10.1 Introduction

This chapter presents a discussion and analysis of the various studies conducted for this PhD. The research aims and objectives achieved are presented in Section 10.2. The following section (Section 10.3) consists of a general discussion highlighting the important remarks, findings and deductions gathered from the various studies together with novelties and contributions made by this PhD. The final section (Section 10.4) provides future recommendations.

10.2 Achievement of Research Aims and Objectives

The main aim of this PhD, as outlined in the first chapter, is to improve the development of hull forms of large ships for energy-efficient transportation. More specifically, the objective is to propose an intelligent state-of-the-art methodology and process in order to enhance the hull-propeller interaction of a vessel. This was achieved using numerical techniques, optimisation procedures and high-performance computing to identify optimal stern designs for particular vessels as well as any necessary Energy Saving Device/s that could help improve the stern flow characteristics and hence the energy efficiency of the ship.

The overall aim was achieved by carrying out a number of research objectives that were addressed by different studies outlined in their respective chapters. Each objective, along with the method used to achieve it, is described in this section and the important findings are analysed in section 10.3.

1) *To carry out an extensive literature review on hull-propeller interaction modelling techniques and design methods to improve the performance, including the modification of stern forms and use of ESDs in order to identify gaps in the literature.*

A literature and critical review were carried out and presented in Chapter 2 by covering all aspects of hull-propeller interaction, fluid dynamics and Energy Saving Devices. Following this process, research questions and gaps in the literature were identified and outlined accordingly in the introduction. (See Chapter 2. “Literature Review” for more details)

2) *To validate and verify numerical procedures of ship performance analyses in towing and self-propulsion conditions to accurately measure performance criteria and capture wake characteristics as well as wave cut analyses.*

This study has successfully validated and verified the numerical procedures that were used to analyse propellers in open water test conditions and ship performance in towing as well as self-propelled environments. The numerical methods that are demonstrated herein have been used to carry out various investigations in this PhD. study. This thesis also demonstrates the benefits of the recently introduced numerical curvature corrected (CC) turbulence models, which have also been incorporated in the well-established V&V procedures exhibiting monotonic convergence with good accuracy. The use of the curvature correction models significantly improved wake flow behaviour prediction accuracy also being able to capture vortical structures. This had no adverse effect on the resistance prediction but improved the accuracy of trim and sinkage values.

3) *To develop and demonstrate a practical full-scale stern form optimisation procedure and evaluate whether it can be considered to be a feasible alternative to computationally expensive full-scale self-propulsion optimisations.*

This study successfully demonstrated a viable method, which could be used to conduct a developed state-of-the-art ship stern optimisation procedure. This was achieved through the analysis of a total of 55 hull designs in full-scale conditions using CFD techniques. Since full-scale optimisation procedures of self-propulsion simulations are time-consuming and computationally expensive, the objective was to understand whether the methodology outlined in this chapter could be considered to be a suitable alternative/approach.

This was realised by running a multi-objective procedure of a ship in towing conditions with the aim to predict, analyse and improve both the resistance and wake quality (wake fraction and non-wake uniformity) parameters of the vessel. Forty designs were first investigated using a quasi-random batch method to understand the trends between the different parameters. A further 15 variants were examined using response surfaces to optimise the parameters. The most promising 3 candidates were those, which produced the least resistance and exhibited good wake behaviour in towing conditions. These were further analysed in self-propulsion conditions. The idea and reason behind this approach was to determine whether, the optimised parameters in towing conditions could provide valuable information, insight, relations and tendencies into the propulsive performance of the design candidate, thereby reducing efforts in analysing various design variants in self-propulsion conditions.

In summary, the multi-objective optimisation process was successful in enhancing the vessel performance in towing conditions by improving the drag and wake quality parameters. Therefore, it can be concluded that the vessel characteristics in towing conditions were effectively improved using state-of-the-art methodology. However, findings from this study indicated that the nominal wake characteristics of a vessel in the absence of a propeller do not provide significant indication/relations to the propulsive performance of the vessel. More details are outlined later on in this chapter.

4) To analyse the physics behind PBCF in a full-scale environment and contribute to understanding the function and working principles of such a retrofitting technology. Furthermore, a state-of-the-art full-scale PBCF optimisation procedure using high fidelity methods in open water conditions is to be proposed and demonstrated.

An optimisation process was successfully demonstrated using a validated and verified numerical technique to analyse 120 different PBCF designs in open water full-scale conditions. The proposed optimisation methodology can be applied to different case studies and modified to suit different scenarios.

Most of the previous research carried out experimental tests or numerical simulations at model scale. The PBCF analyses in this study were carried out in full-scale to improve predictions and avoid scaling effects. The performance and function of the PBCF in full-scale environments were studied and analysed. The major outcomes from this study are indicated in section 10.3 below.

5) *To analyse the influence of ESDs in different scales (i.e. full-scale and model-scale) and to develop a systematic ESD performance analytical process.*

This study has successfully demonstrated and outlined the performance differences of duct-retrofitted vessels in different scale environments i.e. model and full-scale scenarios. The main differences are outlined and discussed in Chapter 8, thus contributing to the body of knowledge.

In order to conduct this study, the flow behaviour of the hull without a duct was investigated under different scale scenarios. The impact of the retrofitted duct on vessel performance was then analysed at both scale environments independently, i.e. comparing the vessel with and without duct at model-scale and also comparing the impact of the duct at full-scale. The differences between the two were then outlined and highlighted contributing further to science. The details of the outcomes can be found in Section 10.3 below.

6) *To develop a further understanding of ESD combination effects in-full scale environments by investigating their impact on performance, wake characteristics and pressure excited vibrations.*

In order to further understand the science of installing multiple Energy Saving Devices on board ships simultaneously and the respective ship performance, research in this thesis was tailored and devised in such a way to address this topic and contribute to the body of knowledge. This was carried out by investigating three particular technologies on a bulk carrier vessel, namely, propeller boss cap fins (PBCF), Stator Fins and a Duct. A total of seven conditions were simulated and analysed using the same methodology outlined in Chapter 4. For more realistic and enhanced accurate predictions, these conditions were analysed in full-scale environments by investigating their impact on performance, wake characteristics and pressure excited vibrations. The results from this study were thoroughly analysed and discussed. Important findings are highlighted in Section 10.3. It can be said that this study successfully managed to address some important research questions and contribute knowledge to the marine industry.

10.3 General Discussion with Novelties and Contributions to the Field (addresses Research Questions)

1) What are the benefits of applying and implementing the newly available curvature correction feature for ship performance simulation and wake prediction?

This thesis has highlighted the shortcomings of the commonly used eddy-viscosity models (EVM) to model fluid turbulence. Such methods failed to accurately capture wake behaviour and characteristics as discussed in Chapter 4. Therefore, this study has demonstrated the benefits of adopting the recently introduced and developed curvature corrected (CC) turbulence models. These models significantly improve the prediction of wake characteristics at little expense. Such methods have also been validated and verified to ensure reliability. To the best of my knowledge, no literature has yet been published demonstrating validation and verification procedures with the use of the curvature corrected turbulence models in virtual towing and self-propulsion tests. This chapter has contributed to knowledge in the shipping industry by carrying out well-established V&V procedures with the use of the CC $k-\omega$ turbulence model.

2) Considering that optimisation techniques using full-scale self-propulsion simulations are not feasible, what can be considered a viable compromise and alternative to such methods? What would the outcome of a multi-objective stern form optimisation using full-scale towing simulations to improve the drag and wake field characteristics concurrently be? Would the performance of the optimal design candidate provided by the optimisation process improve in self-propulsion conditions? Can such a solution be considered a good alternative? What are the pros and cons of such a process?

This study has contributed to the body of knowledge by investigating the feasibility, practicality and functionality of developed procedures and processes to efficiently optimise the hull-propeller interaction of a vessel.

Firstly, an efficient and practical multi-objective optimisation method was designed and outlined to improve the performance of a ship in the absence of a propeller. Following thorough research, this optimisation approach was adopted from other case studies and applied to the hull in question. Results proved successful, hence validating the methodology and paving the way for studies similar in nature that could adopt the bases of the approach. The results provided information and insight on the trends and relations between the performance

parameters, thus providing a more in-depth understanding of the science behind stern form characteristics of a vessel. This research helped in developing a better understanding of hull-propeller interaction by investigating relations between drag and wake quality parameters together with the impact of different stern form designs.

Furthermore, this study investigated whether beneficial wake behaviour and characteristics in towing conditions could provide valuable insight into improving self-propelled performance. The motive behind such research was to provide alternative solutions to running various computationally intensive CFD simulations of full-scale vessels in self-propelled conditions. This would provide a compromise and allow for the running of most design variants in towing conditions that are less expensive and thereby, minimising the number of propelled simulations. Unfortunately, outcomes from this study have indicated that the quality of nominal wakes (with no propeller) could not provide any indication to the respective propulsive performance thus contributing to the body of knowledge in this respect. Therefore, the proposed approach could not be considered an alternative solution to optimisation procedures running full-scale CFD designs. That being said, such bold statements require further verification.

That being said, optimisation of the towing resistance rendered significant benefits in propelled conditions. Therefore, it can be deduced that the optimisation of resistance in towing conditions as outlined in this chapter is a beneficial process in hull design.

3) Extensive research on PBCF has been carried out at model-scale. What are the actual energy savings and benefits from installing PBCF in full-scale conditions and how do they function in such environments?

Research in this thesis indicated that propeller boss caps fins (PBCF) produce less gains at full scale (in open water environment) than previously predicted at model scale. The best PBCF candidate produced 1.3% performance improvement compared to that of a propeller without PBCF. Previous studies have claimed higher efficiency gains with the installations of PBCF. This study confirms and demonstrates that the PBCF reduces the hub vortex thus indicating benefits of the technology. Key findings indicate that the benefits do not come from the thrust of the fins themselves but the interaction effects that enhance the performance of the propeller blades and boss cap altogether. The significant differences come from the blades themselves, generating higher thrust and torque. The installation of the fins introduced a drag but reduced the torque of the system. The boss cap goes from creating drag to producing a thrust. Outcomes

from this study have been published in the following paper (Mizzi et al., 2017). The optimised PBCF design from this research is not optimal for all case scenarios, and each particular ship-propeller system is a case study in itself requiring a similar optimisation study to the one outlined in this study.

4) *With the use of more currently available analyses techniques, what can be further deduced regarding the differences in ESD function and working principles between different scale environments?*

No Duct Scale Comparison

In the absence of the duct, the full-scale ship produced a smaller propulsive efficiency to the corresponding model scale vessel. The change in wake fraction and subsequent hull efficiency discrepancy is what contributed most to the difference. This re-confirms outcomes and findings from the literature that outlines the difference in Reynolds numbers at different scales. Moreover, it alters the fluid flow behaviour resulting in a reduced boundary layer thickness ratio, thus producing a reduced wake fraction. Detailed wake analyses indicated that wake characteristics are significantly different at full-scale, thereby, generating higher wake non-uniformity around the top dead centre once again.

Duct Impact at Model-Scale

With regards to the function of the duct at model scale, the ducted hull in towing condition produced an insignificant decrease in resistance than the hull geometry with no ESD. Although the duct is producing a drag, this detrimental effect is being outweighed by the benefit the duct imposes on the viscous pressure resistance of the bare hull. It was also observed that the presence of the duct produced a reduction in flow separation and a reduction in energy lost to the slipstream. When analysed in propelled conditions, the technology indicated an improved power performance. This benefit was outlined to be sourcing from the improved hull efficiency due to the higher wake fraction. Flow vectors around the duct were also analysed in detail. The top part of the duct was generating a lift in the desired direction whilst the bottom part of the duct was producing an undesired lift in the opposite direction i.e. drag. This confirms and explains why some ESDs make use of a semi duct since it is thought they produce a thrust.

Duct Impact at Full-Scale

That being said, the duct exhibited different performance behaviour at full-scale. According to this study, the technology was not found to be beneficial in such scale environments. The resistance in towing conditions provided an increment with the inclusion of the duct. Moreover, the installation of the duct produced an insignificant improvement to the propulsive efficiency. This slight benefit was outweighed by the increment in resistance which led to a higher delivered power requirement. Thorough analyses identified that although the ESD reduced the bare resistance of the hull, the duct itself generated a much higher drag and drag ratio resulting in an overall larger resistance value. The function of the duct was thus analysed in order to better comprehend the underlying issue. Similar to the results obtained under model scale conditions, the bottom part of the foil was generating a drag. However, in contrast to the model scale assembly, the foil section at the top did not produce any drag or thrust, resulting in an overall larger resistance value.

5) *What are the effects and influences of installing two or more ESDs on a vessel in a full-scale environment?*

While researching for this thesis, it was noted, that it is indeed possible to achieve benefits when installing a combination of Energy Saving Devices in full-scale environments. However, it does not necessarily mean that a combination of devices is better than using one particular technology. It was deduced that the technologies should be customised according to the vessel for enhanced benefits. Designs that are bought off-the-shelf are best avoided. Not all technologies can be installed in parallel. The technologies that work best together are the ones that have different functions and that focus on improving different aspects of the propulsive efficiency interdependently. This study has successfully outlined and demonstrated the performance differences when installing a combination of Energy Saving Devices (ESD). The main discrepancies are highlighted reasoned and discussed in 7). The key findings in this study have contributed to the body of knowledge.

6) *Can the use of current CFD capabilities shed more light on this subject since it is a definite necessity in the ESD community?*

Advanced CFD techniques and enhanced computational power have allowed for further understanding on this subject. Using the methodology outlined in Chapter 4 of this thesis and most of the procedures from the ESD analyses checklist defined in chapter 7, a thorough

analysis was carried out on various ESD combinations to further enhance the understanding and address the research questions on the subject.

The continuous improvement of enhanced CFD techniques and the development of LES & DES procedures would definitely allow for more accurate ship performance predictions. This, in turn, would allow for further understanding of ESD functions. Furthermore, an increase in computational power would support more design variants and configurations to be analysed.

7) Using current state-of-the-art techniques and analyses, what are the impacts of these retrofitting technologies when installed simultaneously in relation to power performance and wake characteristics?

A total of seven different conditions/combinations were analysed to understand the impact/function of each technology device and the interaction with each of the other technologies. This study indicated that the function of the duct improved the hull efficiency by mean of reducing the thrust deduction fraction whilst having no impact on the wake fraction. On the other hand, the stators enhanced the hull efficiency by producing a higher wake fraction and an undesired reduction in the thrust deduction term. However, the benefits achieved through the augment in wake fraction outweigh the detrimental effects of the thrust deduction fraction, thus providing an overall positive benefit.

When the above technologies were installed in parallel, the hydrodynamic system produced a higher wake fraction, due to the function of the stators, while also being able to maintain a lower thrust deduction fraction, as a result of the duct, thus providing the best overall propulsive efficiency. The different technologies improved different components of the propulsive efficiency and hydrodynamic system. It can be said that the duct contributed towards preventing a higher thrust deduction factor which is generally produced by stators.

Although the duct and stators combination provided the highest propulsive efficiency from all the various combinations, it was not the condition that provided the best power performance. It was the Stators (on their own) condition that required the least power to run at design speed, hence indicating the best performance. This indicates that the gain in hull efficiency achieved by the duct did not outweigh the additional drag it created. Therefore, in an ideal case scenario, the best power savings would be achieved by a candidate that ideally produces a better propulsive efficiency at no or minimal expense of towing resistance gain.

It can be said that the Stators proved to be the best technology by augmenting the hull efficiency at minimal expense of drag. It also seems to produce the most uniform wake flow. However, its wake and flow regime impact require further analyses and justification.

On a different note, the PBCF investigated for this study did not provide any benefit. It is not justifiable to conclude that this particular technology does not function properly. It was merely designed poorly for this particular vessel.

With regards to wake characteristics in towing conditions, the duct condition introduces reversed flow while the stators seem to produce a more uniform flow and more constant velocity variation. When these technologies were installed in parallel, they produced the highest non-uniformity in the wake flow increasing the risk of propeller excited vibrations. The swirling flows produced by the duct were still present and the stator on the starboard side seemed to have also generated an additional swirling flow in this condition. In the presence of the propeller, it was hard to come to any deductions or conclusions regarding the wake flow requiring further investigation.

8) Do ESD technologies influence, interrupt or interact with the flow regimes, functions and working principles of one another? Are the energy savings directly cumulative and are there any adverse consequences?

Key findings in this case study indicate that the savings for each technology are not directly cumulative when installed in parallel. Furthermore, the flow regimes and functions of the different ESD do affect and interact with one another. As previously mentioned in 'Research Question 7' above, this study indicated that the stators, alone, tend to produce a higher wake fraction and an undesired reduction in the thrust deduction term. When installing the stators in conjunction with the duct, the combined system produced a high wake fraction (due to stators) while also maintaining a lower thrust deduction fraction (due to duct) thus providing the best overall propulsive efficiency. The adverse consequence here is that the duct produced a significant additional drag that reduced the benefit.

Therefore, it can be said that, with careful design and optimisation, the installation of a specific or a particular combination of devices can provide enhanced performance. The devices should be selected in such a way that each technology targets or improves different aspects of the propulsive efficiency parameters. That being said, one should also take into consideration that

the different parameters of propeller efficiency are dependant and influence each other. In other words, the best compromise should be sought.

Therefore, the combined ESDs should be allowed to contribute towards the improved efficiency though their designed function simultaneously. In other words, it would not be efficient to install a configuration of technologies that have the same function and target the same parameter. When designing an ESD configuration, the objective should be to bring the best out of each technology with each device contributing to different parameters of propulsive efficiency or enhancing each other's weak points. Since this study has indicated that ESDs influence the impact on one another when installed in parallel, it is better to optimise and analyse them in combination. For maximum benefit, the author proposes to first optimise the technology individually, to achieve the highest individual contribution. This is to be followed by optimising the combinations as a whole.

10.4 Future Study Recommendations

Recommendations for future study are now specified for the various case studies that were carried out for this PhD research.

Numerical Performance of Hull Propeller Characteristics

The V&V methods and procedures that were carried out using the adopted curvature correction model were conducted using hull geometries with no ESD installed. It is recommended that carrying out the V&V procedures for the ESD retrofitted hulls would provide further insight into the accuracy of the solver when studying Energy Saving Devices. Furthermore, it is foreseen that refining the mesh further for the full-scale simulations would improve wake flow prediction characteristics. This would require more computational power, which will probably be more readily available in the future.

Hull-Stern Optimisation

Since this study showed that nominal wake characteristics could not provide any insight into self-propelled behaviour, it would be interesting to carry out a similar multi-objective study with the aim to reduce propelled resistance and improve effective wake characteristics using simplified propeller methods such as the actuator disk.

Physics behind PBCF

With regards to the study addressing the physics behind PBCF, this could be further extended by adding more design variables to the optimisation procedure thus investigating a more varied range of PBCF geometries. A particular deduction made from this study indicated that the benefits of PBCF did not come from the fins themselves but from the interaction effects between the blades, hub and fins resulting in performance differences. This area requires further investigation and justification. Such an optimisation procedure could also be altered to identify a geometry that provides maximum energy efficiency as well as a reduction in hub vortex cavitation, thus taking a multi-objective optimisation approach and by implementing cavitation simulation in the numerical model. Although PBCF were analysed in self-propulsion conditions in Chapter 9, these were poorly designed and require further investigation when designed accordingly and placed in a realistic wake environment.

ESD Performance Impact at different scale Environments & ESD Combination Analyses

With regards to the chapters in question, it is highly recommended that these studies are re-investigated in the future once CFD techniques and computational power are further developed, allowing more accurate predictions and simulations. Simulating the roughness effects of hull, propellers and ESDs would further extend the fidelity of the numerical model and provide a better understanding of hull-propeller interaction and performance of ESDs.

For the more imminent future, since the post-processing of the results for these studies did not cover all the methods outlined in the pre-defined 'ESD analyses checklist' due to time constraints. Future research could focus on further examining the results using all the methods outlined in the list. Furthermore, it is recommended that different scale magnitudes and different technology combinations are investigated for verification. This would allow for further understanding and discoveries.

10.5 Chapter Summary and Conclusion

In summary, this chapter describes how the research aims and objectives were achieved through the various studies carried out for this thesis. This has been presented along with a general discussion highlighting the important remarks and findings together with any state-of-the-art contributions to the field, which were clearly demonstrated and listed. Suggestions and opportunities for future studies have also been provided.

11 Conclusion & Summary

11.1 Introduction

The overall aim of this thesis was to contribute to the body of knowledge of the marine industry by focusing on the hydrodynamic performance of ships to enhance their energy efficiency. This would aid in making a greener environment whilst at the same time reducing the operational costs for the ship owner. It is not very common that such requisites go hand in hand providing a win-win situation. It is in our best interests to take advantage of such a situation and do our best to achieve such goals.

Following a thorough literature review and identifying the statement of the problem, various research gaps/questions were outlined. It was decided to focus the research strategy on two key areas, namely, energy-efficient ship design/performance and Energy Saving Devices (ESDs). A series of objectives were thus developed accordingly to address the shortlisted research questions.

11.2 Conclusions

This PhD. was devised in a way to develop a better understanding of the stern-flow behaviour, hull-propeller interaction and the use of ESDs on commercial ships. Following a carefully designed research strategy, as outlined in Chapter 1, which was successfully carried out by the author of this thesis, key findings and outcomes from this study have aided and contributed to the field of knowledge as follows.

- The implementation of the newly available curvature correction feature into the CFD model has been successfully validated and verified, also demonstrating its enhanced wake prediction capabilities.
- This research has successfully demonstrated and developed a state-of-the-art stern form multi-objective optimisation procedure. This study provides a better understanding of hull-propeller interaction by investigating relations between drag and wake quality parameters, together with the impact of stern form design variants on the performance.

- This multi-objective optimisation rendered significant benefits when analysing the vessel in the absence of the propeller providing better drag performance.
- On the other hand, the wake parameters that were taken into consideration during this process could not provide any insight/ relations to the propelled performance. Therefore, it was deduced that such a method could not be considered a feasible alternative to the computationally expensive optimisation of full-scale vessels in self-propulsion conditions. That being said, this requires further study and verification.
- This study contributed to the field of knowledge by further analysing and understanding the physics and working principles behind PBCF in full-scale conditions. Research in this thesis indicated that propeller boss caps fins (PBCF) produce less gains at full scale in open water environment than previously predicted at model scale. However, the study confirms and demonstrates that the PBCF reduces the hub vortex thus indicating benefits of the technology. Furthermore, this case study has demonstrated a developed automated PBCF optimisation procedure that could be adopted and applied to different technologies within the sector.
- Outcomes from this thesis indicated that the difference in Reynolds numbers at different scales alters the fluid flow behaviour. This corroborates findings from the literature. It is therefore expected that energy saving technologies perform differently at different scales. This was investigated and demonstrated in this PhD. The installation of a duct device was analysed both in model and full-scale scenarios. The performance differences were clearly highlighted accordingly, thereby, providing a better understanding of the subject. According to this study, the duct in question, proved beneficial at model-scale but was ineffective at full-scale. This has demonstrated the importance of analysing technologies in full-scale environments.
- Outcomes from this research indicated that the installation of a combination of multiple Energy Saving Devices could be beneficial if designed properly. The flow regimes and functions of the different ESDs do affect and interact with one another and therefore their performance is not directly cumulative. The technologies that work best together are the ones that have different functions and working principles, and that focus on improving different aspects of the propulsive efficiency interdependently. The

technologies should be selected in such a way that each device targets or improves different aspects of the propulsive efficiency parameters.

11.3 Chapter Summary and Conclusion

The author believes that this PhD. has successfully addressed various research gaps and contributed to the marine industry by enhancing knowledge on the hydrodynamic performance of vessels and the use of Energy Saving Devices. This thesis has also outlined various methodologies that could be adopted and developed further for other research.

References

- ABS 2013. Ship energy efficiency measures: Status and guidance.
- ABT, C., BAE, S. D., BIRK, L. & HARRIES, S. 2001. Parametric hull form design- a step towards one week ship design. 8th International Symposium on Practical Design of Ships and Other Floating Structures Shanghai, China.
- ADAMS, B. M., EBEIDA, M. S., ELDRED, M., GERACI, G., JAKEMAN, J. D., A, K., JASON A, M., LAURA P, M., SWILER, L., STEPHENS, J. A., VIGIL, D. M., WILDEY, T. M., BOHNHOFF, W., DALBEY, K., EDDY, J., FRYE, J., HOOPER, R. W., HU, K. T., HOUGH, P. D., KHALIL, M., EM, R. & RUSHDI, A. 2017. Dakota, a multilevel parallel object-oriented framework for design optimization, parameter estimation, uncertainty quantification, and sensitivity analysis: Version 6.6 user's manual. *Sandia National Laboratories, Tech. Rep. SAND2014-4633*.
- AKTAS, B., ATLAR, M., TURKMEN, S., SHI, W., SAMPSON, R., KORKUT, E. & FITZSIMMONS, P. 2016. Propeller cavitation noise investigations of a research vessel using medium size cavitation tunnel tests and full-scale trials. *Ocean engineering*, 120, 122-135.
- ARCHIE-WEST. *Esprc funded archie-west high performance computer* [Online]. Available: <http://www.archie-west.ac.uk/> [Accessed].
- AROLLA, S. & DURBIN, P. 2012. Incorporating rotation and curvature effects in scalar eddy viscosity models. *42nd aiaa fluid dynamics conference and exhibit*. American Institute of Aeronautics and Astronautics.
- AROLLA, S. & DURBIN, P. 2013a. Assessing the effects of streamline curvature on the aerodynamics of circulation control airfoil. *51st aiaa aerospace sciences meeting including the new horizons forum and aerospace exposition*. American Institute of Aeronautics and Astronautics.
- AROLLA, S. K. & DURBIN, P. A. 2013b. Modeling rotation and curvature effects within scalar eddy viscosity model framework. *International Journal of Heat and Fluid Flow*, 39, 78-89.
- AROLLA, S. K. & DURBIN, P. A. 2014. A rotation/curvature correction for turbulence models for applied cfd. *Progress in Computational Fluid Dynamics, an International Journal*, 14, 341-351.
- ATLAR, M. & PATIENCE, G. 1998. An investigation into effective boss cap designs to eliminate propeller hub vortex cavitation. *Proceedings of the 7th International Symposium on Practical Designs of Ship and Mobile Units* The Hague, Netherlands. 757-769.

- ATLAR, M., WANG, D. & GLOVER, E. 2007. Experimental investigation into the impact of slipstream wash of a podded propulsor on the marine environment. *Proceedings of the Institution of Mechanical Engineers, Part M: Journal of Engineering for the Maritime Environment*, 221, 67-79.
- BAKER, T. J. 1989. Automatic mesh generation for complex three-dimensional regions using a constrained delaunay triangulation. *Engineering with Computers*, 5, 161-175.
- BERTRAM, V. 2011. *Practical ship hydrodynamics (second edition)*, Butterworth-Heinemann.
- BHUSHAN, S., ALAM, M. F. & WALTERS, D. K. 2013. Evaluation of hybrid rans/les models for prediction of flow around surface combatant and suboff geometries. *Computers & Fluids*, 88, 834-849.
- BHUSHAN, S., CARRICA, P., YANG, J. & STERN, F. 2011. Scalability studies and large grid computations for surface combatant using cfdship-iowa. *The International Journal of High Performance Computing Applications*, 25, 466-487.
- BHUSHAN, S., XING, T., CARRICA, P. & STERN, F. 2009. Model-and full-scale urans simulations of athena resistance, powering, seakeeping, and 5415 maneuvering. *Journal of Ship Research*, 53 SRC - GoogleScholar, 179-198.
- BIRK, L., CLAUSS, G. N. F. & LEE, J. Y. 2004. Practical application of global optimization to the design of offshore structures. 567-579.
- BLAUROCK, J. 1983. Propeller plus vane wheel, an unconventional propulsion system. *International Symposium on Ship Hydrodynamics and Energy Saving El Pardo*.
- BLAUROCK, J. 1990. An appraisal of unconventional aftbody configurations and propulsion devices. *Lips Propeller Symposium 7th Netherlands*.
- CAMPANA, E. F., PERI, D., TAHARA, Y. & STERN, F. 2006. Shape optimization in ship hydrodynamics using computational fluid dynamics. *Computer Methods in Applied Mechanics and Engineering*, 196, 634-651.
- CAPONE, A., ALVES PEREIRA, F., MAIOCCHI, A. & DI FELICE, F. 2019. Analysis of the hull wake of a twin-screw ship in steady drift by borescope stereo particle image velocimetry. *Applied Ocean Research*, 92, 101914.
- CARLTON, J. 2018. *Marine propellers and propulsion*, Butterworth-Heinemann.
- CARLTON, J. S. 2001. The propulsion of large container ship. Proceedings Symposium on Mega-Container Ship in Future, the Kansai Society of Naval Architects Kobe, Japan.

- CARLTON, J. S. 2007. 5-the wake field. *Marine propellers and propulsion (second edition)*. Oxford: Butterworth-Heinemann.
- CARRICA, P. M., HUANG, J., NOACK, R., KAUSHIK, D., SMITH, B. & STERN, F. 2010. Large-scale des computations of the forward speed diffraction and pitch and heave problems for a surface combatant. *Computers & Fluids*, 39, 1095-1111.
- CARRICA, P. M., WILSON, R. V., NOACK, R. W. & STERN, F. 2007. Ship motions using single-phase level set with dynamic overset grids. *Computers & Fluids*, 36, 1415-1433.
- CASTRO, A. M., CARRICA, P. M. & STERN, F. 2011. Full scale self-propulsion computations using discretized propeller for the kriso container ship kcs. *Computers & Fluids*, 51, 35-47.
- CD-ADAPCO 2014. User guide star-ccm+, version 9.02.011.
- CELIK, F. 2007. A numerical study for effectiveness of a wake equalizing duct. *Ocean Engineering Vol pp*, 34 2138-2145.
- CELIK, F. & GUNER, M. 2007. Energy saving device of stator for marine propellers. *Ocean Engineering Vol pp*, 34, 850-855.
- CELIK, I. B., GHIA, U., ROACHE, P. J., FREITAS, C. J., COLEMAN, H. & RAAD, P. E. 2008. Procedure for estimation and reporting of uncertainty due to discretization in cfd applications. *Journal of Fluids Engineering*, 130, 078001-078001-4.
- CHEN, B. Y., REED, A. M., KIM, K. H. & A. 1989. A vane-wheel propulsor for a naval auxiliary. *Ship Hydromechanics Department, Research and Development Report*. David Taylor Research Center.
- CHEN, P.-F. & HUANG, C.-H. 2002. An inverse hull design problem in optimizing the desired wake of ship. *Journal of Ship Research*, 46, 138-147.
- CHUNG, T. 1978. Finite element analysis in fluid dynamics. *NASA STI/Recon Technical Report A*, 78.
- CONSULTANTS, W. A., SIRENHA, HSVA, FLOWTECH, VTT, TECHNOLOGY, I. C. O. S., LLOYD, G. & ESPANOLES, A. 2002. Best practices guidelines for marine applications of computational fluid dynamics. *MARNET-CFD Report*.
- CRAFT, T. 2010. Near-wall modelling. *MSc Fluid Mechanics*.
- DACLES-MARIANI, J., ZILLIAC, G. G., CHOW, J. S. & BRADSHAW, P. 1995. Numerical/experimental study of a wingtip vortex in the near field. *AIAA Journal*, 33, 1561-1568.

- DANG, J., CHEN, H., DONG, G., PLOEG, A. V. D., HALLMANN, R. & MAURO, F. 2011. An exploratory study on the working principles of energy saving devices (esds). Symposium on Green Ship Technology Wuxi, China.
- DANG, J., HAO, C., RUEDA, L. & WILLEMSSEN, H. 2015. Integrated design of asymmetric aftbody and propeller for an aframax tanker to maximize energy efficiency. Fourth International Symposium on Marine Propulsors (smp '15) Austin, Texas, USA.
- DATE, J. C. & TURNOCK, S. R. 1999. *A study into the techniques needed to accurately predict skin friction using rans solvers with validation against froude's historical flat plate experimental data*, Southampton, UK, University of Southampton, Department of Ship Science.
- DE JONGH, M., OLSEN, K., BERG, B., JANSEN, J., TORBEN, S., ABT, C., DIMOPOULOS, G., ZYMARIS, A. & HASSANI, V. 2018. High-level demonstration of holistic design and optimisation process of offshore support vessel. Marine Design XIII, Volume 1: Proceedings of the 13th International Marine Design Conference (IMDC 2018), June 10-14, 2018, Helsinki, Finland. CRC Press, 203.
- DHAKAL, T. P. & WALTERS, D. K. 2009. Curvature and rotation sensitive variants of the k- ω sst turbulence model. 2221-2229.
- DI MASCIO, A., BROGLIA, R. & MUSCARI, R. 2007. On the application of the single-phase level set method to naval hydrodynamic flows. *Computers & Fluids*, 36, 868-886.
- DNV GL 2015. Hhi and dnv gl take a fresh look at grims vane wheel.
- DONG, S. & SHEN, J. 2010. An unconditionally stable rotational velocity-correction scheme for incompressible flows. *J. Comput. Physics*, 229, 7013-7029.
- DONG, S. & SHEN, J. 2012. A time-stepping scheme involving constant coefficient matrices for phase-field simulations of two-phase incompressible flows with large density ratios. *Journal of Computational Physics*, 231, 5788-5804.
- DYNE, G. 1995. The principles of propulsion optimization.
- FANG, I., CHENG, F., INCECIK, A. & CARNIE, P. 2013. Global marine trends 2030. London.
- FERZIGER, J. H. & PERIC, M. 2002. *Computational methods for fluid dynamics*, Springer.
- FLETCHER, C. A. 2012. *Computational techniques for fluid dynamics 2: Specific techniques for different flow categories*, Springer Science & Business Media.
- FRIENDSHIP SYSTEMS Friendship framework user manual.

- FUNENO, I. 2002. On viscous flow around marine propellers, hub vortex and scale effect. Japan: The Kansai Society of Naval Architects.
- FUREBY, C. 2008. Towards the use of large eddy simulation in engineering. *Progress in Aerospace Sciences*, 44, 381-396.
- GALLAGHER, P., MARCER, R., BERHAULT, C. & SALVATORE, F. 2009. Best practice guidelines for the application of computational fluid dynamics in marine hydrodynamics.
- GATIN, I. 2019. Cfd in the marine industry: Today and tomorrow.
- GEARHART, W. S. & MCBRIDE, M. W. 1989. Performance assessment of propeller boss cap fin type device. *St Johns Newfoundland Canada 22nd American Towing Tank Conference*.
- GENNARO, G. & GONZALEZ-ADALID, J. 2012. Improving the propulsion efficiency by means of contracted and loaded tip (clt) propellers. Athens.
- GHASSEMI, H. 2009. Hydrodynamic performance of coaxial contra-rotating propeller (ccrp) for large ships. *Polish Maritime Research Vol 16 pp*, 1, 22-28.
- GHASSEMI, H., MARDAN, A. & ARDESHIR, A. 2012. Numerical analysis of hub effect on hydrodynamics performance of propellers with inclusion of pbcf to equalize the induced velocity. *Polish Maritime Research*, 19.
- GHOSE, J. & GHOSE, R. 2004. *Basic ship propulsion*.
- GIRAULT, V. & RAVIART, P.-A. 2012. *Finite element methods for navier-stokes equations: Theory and algorithms*, Springer Science & Business Media.
- GÓMEZ, A. G. 1990. *Predicción y análisis de la configuración de la estela en buques de una hélice*. Universidad Politécnica de Madrid.
- HAN, J., KIM, J., SEO, J. & HWANGBO, M. 2006. Application of flow control devices to improve propeller cavitation performances. 9th Symposium on Practical Design on Ships and Other Floating Structures, PRADS2004 Lübeck-Travemünde.
- HAN, S., LEE, Y.-S. & CHOI, Y. B. 2012. Hydrodynamic hull form optimization using parametric models. *Journal of Marine Science and Technology*, 17, 1-17.
- HANNINEN, S. & MIKKOLA, T. 2006. Computation of ship-hull flows at model-and full-scale reynolds numbers. Numerical Ship Hydrodynamics Seminar, Maritime Institute of Finland, Turku.

- HANS-JURGEN HEINKE, K. H.-R. 2011. Investigation of scale effects on ships with a wake equalizing duct or with vortex generator fins. Second International Symposium on Marine Propellers Hamburg, Germany.
- HANSEN, H. R. & DINHAM-PEREN, T. 2014. Eedi challenges in the design of large slow-speed ships. London,UK.
- HANSEN, H. R., DINHAM-PEREN, T. & NOJIRI, T. 2011. Model and full scale evaluation of a 'propeller boss cap fins' device fitted to an afromax tanker. Second International Symposium on Marine Propulsors Hamburg Germany.
- HARRIES, S. 2015. Practical shape optimisation using cfd. *Friendship Systems*.
- HARRIES, S., ABT, C. & BRENNER, M. 2015. Upfront cad - parametric modeling techniques for shape optimisation. EUROGEN 2015 Glasgow, UK.
- HARRIES, S., ABT, C. & HOCHKIRCH, K. 2004. Modeling meets simulation-process integration to improve design. Sonderkolloquium zu Ehren der Professoren Hagen, Schluter und Thiel Germany.
- HARVALD, S. A. 1950. *Wake of merchant ships*, Danish Technical Press.
- HEINKE, H.-J. & HELLWIG-RIECK, K. 2011. Investigation of scale effects on ships with a wake equalizing duct or with vortex generator fins. Second International Symposium on Marine Propellers Hamburg, Germany.
- HELLSTEN, A. 1998. Some improvements in menter's k-omega sst turbulence model. *29th aiaa, fluid dynamics conference*. American Institute of Aeronautics and Astronautics.
- HILLEARY, R. R. 1966. The tangent search method of constrained minimization. Naval Postgraduate School Monterey Calif.
- HINO, T., OHASHI, K. & KOBAYASHI, H. 2010. Flow simulations using navier-stokes solver surf. Proceedings of Gothenburg 2010 Workshop on Numerical Ship Hydrodynamics.
- HIRT, C. W. & NICHOLS, B. D. 1981. Volume of fluid (vof) method for the dynamics of free boundaries. *Journal of Computational Physics*, 39, 201-225.
- HOEKSTRA, M. 1975. Prediction of full scale wake characteristics based on model wake survey. *International Shipbuilding Progress*, 22, 204-219.
- HOEKSTRA, M. 1999. *Numerical simulation of ship stern flows with a space-marching navier-stokes method*. Delft University of Technology.

- HOLLENBACH, U. & REINHOLZ, O. 2010. Hydrodynamic trends in performance optimization. *11th International Symposium on Practical Design of Ships and Other Floating Structures pp Rio de Janeiro Brazil*, 391-401.
- HOOIJMANS, P., HOLTROP, J. & WINDT, J. 2010. Refitting to save fuel and new approaches in the design of newbuildings. *11th International Symposium on Practical Design of Ships and Other Floating Structures pp Brazil*, 724-733.
- HSIN, C.-Y., LIN, B. H. & LIN, C.-C. 2009. The optimum design of a propeller energy saving device by computational fluid dynamics. *Computational Fluid Dynamics*.
- HUANG, F., WANG, L. & YANG, C. 2015/7/27/ 2015. Hull form optimization for reduced drag and improved seakeeping using a surrogate-based method. ISOPE: International Society of Offshore and Polar Engineers.
- HUANG, F. & YANG, C. 2016. Hull form optimization of a cargo ship for reduced drag. *Journal of Hydrodynamics, Ser. B*, 28, 173-183.
- HUANG, J., CARRICA, P. M. & STERN, F. 2007. Coupled ghost fluid/two-phase level set method for curvilinear body-fitted grids. *International Journal for Numerical Methods in Fluids*, 55, 867-897.
- HUANG, T. T. & GROVES, N. C. 1980. Effective wake: Theory and experiment. 13th ONR Symposium.
- HUANG, T. T., WANG, H. T., SANTELLI, N. & GROVES, N. C. 1976. Propellers/stern/boundary-layer interaction on axisymmetric bodies: Theory and experiment. David W Taylor Naval Ship Research and Development Center.
- HUSE, E. 1974. Effect of afterbody forms and afterbody fins on the wake distribution of single-screw ships.
- IMO 2009. Second imo ghg study 2009. London, UK.
- IMO. 2014. Guidelines on the method of calculation of the attained energy efficiency design index (eedi) for new ships. Annex 5, Resolution MEPC.245(66).
- IMO 2015. Third imo greenhouse gas study 2014. International Maritime Organisation (IMO).
- IPCC 2008. Climate change 2007: Synthesis report. *In: REISINGER, C. W. T. R. K. P. A.* (ed.). Geneva, Switzerland: Choice Reviews Online 45.
- ISO 2015. Guidelines for the assessment of speed and power performance by analysis of speed trial data. International Organisation for Standardization (ISO).

- ITTC 1999. Performance, propulsion 1978 ittc performance prediction method. *ITTC-Recommended Procedures*. International Towing Tank Conference.
- ITTC 2011a. Practical guidelines for ship cfd applications. International Towing Tank Conference (ITTC).
- ITTC 2011b. The specialist committee on scaling of wake field. 26th International Towing Tank Conference Rio De Janeiro, Brazil.
- JENS RING NIELSEN, K. W. S., EGE LUNDGREN, FARSHAD FAGHANI 2012. Combined kappel propeller and rudder bulb system for improved propulsion efficiency. Motorship Propulsion & Emissions Conference Hamburg, Germany.
- JOHANNSEN, C. 2000. Recent considerations on dealing with propeller induced hull pressure pulses. International Conference on ship and shipping research, NAV2000 Venice.
- KASSINOS, S. C., LANGER, C. A., KALITZIN, G. & IACCARINO, G. 2006. A simplified structure-based model using standard turbulence scale equations: Computation of rotating wall-bounded flows. *International Journal of Heat and Fluid Flow*, 27, 653-660.
- KAWAMURA, T., OUCHI, K. & NOJIRI, T. 2012. Model and full scale cfd analysis of propeller boss cap fins (pbcf). *Journal of Marine Science and Technology*, 17, 469-480.
- KEHR, Y.-Z. 1986. Hydrodynamische analyse des leitrads diss. *Berlin*.
- KELLET, P., TURAN, O. & INCECIK, A. 2013. A study of numerical ship underwater noise prediction. *Ocean Engineering*.
- KHORASANCHI, M., DAY, S., TURAN, O., INCECIK, A. & TURKMEN, S. 2013. What to expect from the hydrodynamic energy saving devices. Low Carbon Shipping Conference London.
- KIM, H. & YANG, C. 2010. A new surface modification approach for cfd-based hull form optimization. *Journal of Hydrodynamics, Ser. B*, 22, 520-525.
- KIM, H. & YANG, C. 2013/6/30/ 2013. Design optimization of bulbous bow and stern end bulb for reduced drag. Alaska, USA. ISOPE: International Society of Offshore and Polar Engineers.
- KIM, H., YANG, C., KIM, H. & CHUN, H.-H. 2009/1/1/ 2009. Hydrodynamic optimization of a modern container ship using variable fidelity models. ISOPE: International Society of Offshore and Polar Engineers.

- KIM, J.-H., CHOI, J.-E., CHOI, B.-J. & CHUNG, S.-H. 2014. Twisted rudder for reducing fuel-oil consumption. *International Journal of Naval Architecture and Ocean Engineering*, 6, 715-722.
- KIM, K., LEER-ANDERSEN, M., WERNER, S., ORYCH, M. & CHOI, Y. 2013. Hydrodynamic optimization of pre-swirl stator by cfd and model testing. *International shipbuilding progress*, 60, 233-276.
- KLUIJVEN, P. C., KWAKERNAAK, L., ZOETMULDER, F., RUIGROK, M. & BONDT, K. Contra-rotating propellers. Maritime Symposium Rotterdam: Rotterdam Mainport University of Applied sciences.
- LAMBOS MARITIME SERVICES LTD 2013. Marine efficiency systems at "slow steaming" conditions.
- LARSSON, L., STERN, F. & BERTRAM, V. 2003. Benchmarking of computational fluid dynamics. *Journal of Ship Research*, vol. 47, pp 63-81.
- LARSSON, L., STERN, F. & VISONNEAU, M. 2014. *Numerical ship hydrodynamics. An assessment of the gothenburg 2010 workshop*, Springer Netherlands.
- LAUNDER, B. E., REECE, G. J. & RODI, W. 1975. Progress in the development of a reynolds-stress turbulence closure. *Journal of Fluid Mechanics*, 68, 537-566.
- LAUNDER, B. E. & SPALDING, D. B. 1974. The numerical computation of turbulent flows. *Computer Methods in Applied Mechanics and Engineering*, 3, 269-289.
- LEE, J.-H., KIM, M.-C., SHIN, Y.-J. & KANU, J.-G. 2017. Study on performance of combined energy saving devices for container ship by experiments. Fifth International Symposium on Marine Propulsion smp'17 Finland.
- LEE, S.-K., HSIEH, Y.-F. & ZHOU, Z. 2012. Propeller energy loss reutilization for full form ship propulsion. 11th Conference on Computer and IT Applications in the Maritime Industries, COMPIT'12 Liege.
- LOCKLEY, P., JARABO-MARTIN, A., SHARMA, K. & HILL, J. 2011. Ship efficiency: The guide, s.L.: Fathom.
- LÜBKE, L. & ABDEL-MAKSOUUD, M. 2002. Berechnung des nachstromfeldes der großausführung. *Jahrbuch der Schiffbautechnischen Gesellschaft*, 96.
- LÜBKE, L. O. 2005. Numerical simulation of the flow around the propelled kcs. CFDWS05 Tokyo, Japan. 9-11.
- M. GAD-EI-HAK & BANDYOPADHYAY, P. R. 1989. Reynolds number effects in wall-bounded flows. *Applied Mechanics Reviews*, 47, 307-365.

- MAASCH, M., MIZZI, K., ATLAR, M., FITZSIMMONS, P. & TURAN, O. 2019. A generic wake analysis tool and its application to the japan bulk carrier test case. *Ocean Engineering*, 171, 575-589.
- MACCORMACK, R. & PAULLAY, A. 1972. Computational efficiency achieved by time splitting of finite difference operators. *10th aerospace sciences meeting*. American Institute of Aeronautics and Astronautics.
- MANI, M., LADD, J. A. & BOWER, W. W. 2004. Rotation and curvature correction assessment for one-and two-equation turbulence models. *Journal of Aircraft*, 41, 268-273.
- MARCUM, D. 1995. Generation of unstructured grids for viscous flow applications. *33rd aerospace sciences meeting and exhibit*. American Institute of Aeronautics and Astronautics.
- MCDONALD, P. 1971. The computation of transonic flow through two-dimensional gas turbine cascades. *ASME*, 71-89.
- MENTER, F. R. 1994. Two-equation eddy-viscosity turbulence models for engineering applications. *AIAA Journal*, 32, 1598-1605.
- METCALF, B., LONGO, J., GHOSH, S. & STERN, F. 2006. Unsteady free-surface wave-induced boundary-layer separation for a surface-piercing naca 0024 foil: Towing tank experiments. *Journal of Fluids and Structures*, 22, 77-98.
- MEWIS, F. & GUIARD, T. 2011. Mewis duct-new developments, solutions and conclusions. *Second International Symposium on Marine Propulsors Hamburg Germany*.
- MIZZI, K., DEMIREL, Y. K., BANKS, C., TURAN, O., KAKLIS, P. & ATLAR, M. 2017. Design optimisation of propeller boss cap fins for enhanced propeller performance. *Applied Ocean Research*, 62, 210-222.
- MIZZI, K., KIM, M., TURAN, O. & KAKLIS, P. 2015. Issues with energy saving devices and the way forward. *Shipping in Changing Climates Glasgow*.
- MOCKROS, L. F. 1962. *The significance of vorticity, vortex motion, and dissipation in turbulent fluid flows*, University of California, Berkeley.
- MORGANS, R., DALLY, B., NATHAN, G., LANSPEARY, P. & FLETCHER, D. 1999. Application of the revised wilcox (1998) k- ω turbulence model to a jet in co-flow. *Second International Conference on CFD in the Mineral and Process Industries Melbourne, Australia*.
- NISHIYAMA, S., SAKAMOTO, Y. & T., D. W. 1990. Development of contra-rotating propeller systems for junco-a 000 carrier. *Trans SNAME 98*, 37 SRC - GoogleScholar.

- NMRI. 2015. *A workshop on cfd in ship hydrodynamics* [Online]. <http://www.t2015.nmri.go.jp/announcement.html>: National Maritime Research Institute, Yokohama National University, Chalmers University of Technology, IIHR, ECN, KRISO. [Accessed].
- NOWACKI, H. 2001. On the development of ship hydrodynamics in the 20th century. *100 jahre schiffbautechnische gesellschaft*. Berlin, Heidelberg: Springer Berlin Heidelberg.
- NOWACKI, H. & SHARMA, S. D. 1971. Free-surface effects in hull propeller interaction. Department of Naval Architecture and Marine Engineering, Univeristy of Michigan.
- ODABASI, A. Y. & FITZSIMMONS, P. 1978. Alternative methods for wake quality assessment. *International Shipbuilding Progress*, 25.
- OH, K.-J. & KANG, S.-H. 1992. Full scale reynolds number effects for the viscous flow around the ship stern. *Computational Mechanics*, 9, 85-94.
- OK, J.-P. 2004. *Numerical investigation of scale effects of schneekluth's duct*, Arbeitsbereiche Schiffbau der Techn. Univ.
- OUCHI, K., KAWASAKI, T., TAMASHIMA, M. & KOIZUKA, H. 1990. Research and development of pbcf (propeller boss cap fins) : Novel energy-saving device to enhance propeller efficiency. *Naval architecture and ocean engineering*, 28, 39-47.
- PAPANIKOLAOU, A. 2010. Holistic ship design optimization. *Computer-Aided Design*, 42, 1028-1044.
- PARK, J.-H., CHOI, J.-E. & CHUN, H.-H. 2015a. Hull-form optimization of ksuezmax to enhance resistance performance. *International Journal of Naval Architecture and Ocean Engineering*, 7, 100-114.
- PARK, S., OH, G., HYUNG RHEE, S., KOO, B.-Y. & LEE, H. 2015b. Full scale wake prediction of an energy saving device by using computational fluid dynamics. *Ocean Engineering*, 101, 254-263.
- PARSONS, M. G. 2009. Applications of optimization in early stage ship design. *Ship Science and Technology*, 3, 9-32.
- PELLEGRINI, R., SERANI, A., BROGLIA, R., DIEZ, M. & HARRIES, S. 2018. Resistance and payload optimization of a sea vehicle by adaptive multi-fidelity metamodeling. 2018 AIAA/ASCE/AHS/ASC Structures, Structural Dynamics, and Materials Conference. 1904.
- PERI, D., ROSSETTI, M. & CAMPANA, E. F. 2001. Design optimization of ship hulls via cfd techniques. *Journal of Ship Research*, 45, 140-149.

- PIOMELLI, U. 2008. Wall-layer models for large-eddy simulations. *Progress in Aerospace Sciences*, 44, 437-446.
- PIOMELLI, U. & BALARAS, E. 2002. Wall-layer models for large-eddy simulations. *Annual review of fluid mechanics*, 34, 349-374.
- PRESS, W., TEUKOLSKY, S., VETTERLING, W. & FLANNERY, B. 2007. *Numerical recipes 3rd edition: The art of scientific computing*, Cambridge University Press.
- PRINS, H. J., FLIKKEMA, M. B., SCHUILING, B., XING-KAEDING, Y., VOERMANS, A. A. M., MÜLLER, M., COACHE, S., HASSELAAR, T. W. F. & PABOEUF, S. 2016. Green retrofitting through optimisation of hull-propulsion interaction – grip. *Transportation Research Procedia*, 14, 1591-1600.
- QUEUTEY, P., GUILMINEAU, E., VISONNEAU, M., WACKERS, J. & DENG, G. 2016. *Rans and hybrid rans-les simulations around the japan bulk carrier of the tokyo 2015 cfd workshop*.
- RICHARDSON, L. & GANT, J. A. 1927. F, the deferred approach to the limit. *Transactions of the Royal Society of London*, 226 SRC - GoogleScholar, 636-646.
- RICHARDSON, L. F. 1910. The approximate arithmetical solution by finite differences of physical problems involving differential equations, with an application to the stresses in a masonry dam. *Transactions of the Royal Society of London*, 210, 307-357.
- RICHARDSON, L. F. 1911. The approximate arithmetical solution by finite difference of physical problems involving differential equations, with an application to the stresses in a masonry dam. *Transactions of the Royal Society of London*, 210 SRC - GoogleScholar, 459-490.
- RIJPKEMA, D., STARKE, B. & BOSSCHERS, J. 2013. Numerical simulation of propeller-hull interaction and determination of the effective wake field using a hybrid rans-bem approach. Third International Symposium on Marine Propulsors, SMP2013. Tasmania, Australia.
- RIZZI, A. W. & INOUE, M. 1973. Time-split finite-volume method for three-dimensional blunt-body flow. *AIAA Journal*, 11, 1478-1485.
- ROACHE, P. J. 1998. *Verification and validation in computational science and engineering*, Hermosa.
- ROSENFELD, M., KWAK, D. & VINOKUR, M. 1991. A fractional step solution method for the unsteady incompressible navier-stokes equations in generalized coordinate systems. *Journal of Computational Physics*, 94, 102-137.

- RUTUNDI, C. F. 1934. Trials of the training ship *cristoforo colombo* with two screws on a common axis. *Trans Institution of Naval Architects*.
- SAMPSON, R. 2008. Presentation of ship wakes. School of Marine Science and Technology: Newcastle University.
- SASAJIMA, H. & TANAKA, I. 1966. On the estimation of wakes of ships. *Proceedings of the 11th ITTC*.
- SASAKI, N. & PATIENCE, G. 2005. Evolution of high efficiency propeller with new blade section. Motorship conference.
- SCHUILING, B. 2013. The design and numerical demonstration of a new energy saving device. 16th Numerical Towing Tank Symposium. 141-146.
- SCHUILING, B. & TERWISGA, T. V. 2016. Energy analysis of a propeller in open water using a rans method. 24th International HISWA Symposium on Yacht Design and Yacht Construction Amsterdam, Netherlands.
- SCHULZE, R. 1995. *Nabenkappenflossen fur schiffspropeller*. Potsdam, Germany: Potsdam Model Basin (SVA).
- SHARMA, R. & SHA, O. P. 2005. Practical hydrodynamic design of bulbous bows for ships. *Naval Engineers Journal*, 117, 57-76.
- SMIRNOV, P. E. & MENTER, F. R. 2009. Sensitization of the sst turbulence model to rotation and curvature by applying the spalart–shur correction term. *Journal of Turbomachinery*, 131, 041010-041010-8.
- SPALART, P. & ALLMARAS, S. 1992. A one-equation turbulence model for aerodynamic flows. *30th aerospace sciences meeting and exhibit*. American Institute of Aeronautics and Astronautics.
- SPALART, P. R. & SHUR, M. 1997. On the sensitization of turbulence models to rotation and curvature. *Aerospace Science and Technology*, 1, 297-302.
- STARKE, A., WINDT, J. & RAVEN, H. C. 2006. Validation of viscous flow and wake field predictions for ships at full scale. Proc. 26th Symposium on Naval Hydrodynamics Rome, Italy.
- STEPHENS, D. & MOHANARANGAM, K. 2010. Turbulence model analysis of flow inside a hydrocyclone. *Progress in Computational Fluid Dynamics, an International Journal*, 10, 366-373.

- STERN, F., HWANG, W. S. & JAW, S. Y. 1989. Effects of waves on the boundary layer of a surface-piercing flat plate: Experiment and theory. *Journal of Ship Research*, 33, 63-80.
- STERN, F., KIM, H., ZHANG, D., TODA, Y., KERWIN, J. & JESSUP, S. 1994. Computation of viscous flow around propeller-body configurations: Series 60 cb. *Journal of Ship Research*, 38, 137-157.
- STERN, F., WANG, Z., YANG, J., SADAT-HOSSEINI, H., MOUSAVIRAAD, M., BHUSHAN, S., DIEZ, M., YOON, S.-H., WU, P.-C., YEON, S. M., DOGAN, T., KIM, D.-H., VOLPI, S., CONGER, M., MICHAEL, T., XING, T., THODAL, R. S. & GRENESTEDT, J. L. 2015. Recent progress in cfd for naval architecture and ocean engineering. *Journal of Hydrodynamics, Ser. B*, 27, 1-23.
- STERN, F., WILSON, R. & SHAO, J. 2006. Quantitative v&v of cfd simulations and certification of cfd codes. *International Journal for Numerical Methods in Fluids*, 55, 1335-1355.
- STERN, F., WILSON, R. V., COLEMAN, H. W. & PATERSON, E. G. 2001. Comprehensive approach to verification and validation of cfd simulations—part 1: Methodology and procedures. *Journal of Fluids Engineering*, 123, 793-802.
- STERN, F., YANG, J., WANG, Z., SADAT-HOSSEINI, H., MOUSAVIRAAD, M., BHUSHAN, S. & XING, T. 2012. Computational ship hydrodynamics: Nowadays and way forward. 29th Symposium on Naval Hydrodynamics Gothenburg, Sweden.
- STERN, F., YOO, S. Y. & PATEL, V. C. 1988. Interactive and large-domain solutions of higher-order viscous-flow equations. *AIAA Journal*, 26, 1052-1060.
- STOPFORD, M. 2008. Maritime economics.
- SUZUKI, K., SASAKI, N. & KAWAMURA, T. 2017. *Resistance and propulsion*.
- SVA. 2011. Potsdam propeller test case. SVA Model Basin.
- TAHARA, Y., PERI, D., CAMPANA, E. F. & STERN, F. 2008. Computational fluid dynamics-based multiobjective optimization of a surface combatant using a global optimization method. *Journal of Marine Science and Technology*, 13, 95-116.
- TAHARA, Y. & STERN, F. 1996. A large-domain approach for calculating ship boundary layers and wakes and wave fields for nonzero froude number. *Journal of Computational Physics*, 127, 398-411.
- TAHARA, Y., STERN, F. & ROSEN, B. 1992. An interactive approach for calculating ship boundary layers and wakes for nonzero froude number. *Journal of Computational Physics*, 98, 33-53.

- TAHARA, Y., WILSON, R. & CARRICA, P. 2005. Comparison of free-surface capturing and tracking approaches in application to modern container ship and prognosis for extension to self-propulsion simulator. Proc. of CFD Workshop Tokyo, Japan. 9-11.
- TAO, R., XIAO, R., YANG, W. & WANG, F. 2014. A comparative assessment of spalart-shur rotation/curvature correction in rans simulations in a centrifugal pump impeller. *Mathematical Problems in Engineering*, 2014, 9.
- TERWISGA, T. V. May 2013. On the working principles of energy saving devices. 3rd International Symposium on Marine Propulsors Tasmania, Australia. 5-8.
- TEZDOGAN, T., DEMIREL, Y. K., KELLETT, P., KHORASANCHI, M., INCECIK, A. & TURAN, O. 2015. Full-scale unsteady rans cfd simulations of ship behaviour and performance in head seas due to slow steaming. *Ocean Engineering*, 97, 186-206.
- THOMPSON, J. F., WARSI, Z. U. & MASTIN, C. W. 1985. *Numerical grid generation: Foundations and applications*, North-holland Amsterdam, Elsevier Science Ltd.
- TRUESDELL, C. 1953. 2 measures of vorticity. *Journal of Rational Mechanics and Analysis*, 2, 173-217.
- VISONNEAU, M. 2005 2005. A step towards the numerical simulation of viscous flows around ships at full scale - recent achievements within the european union project effort. Royal Institute of Naval Architecture Marine CFD Southampton, France.
- VISONNEAU, M., DENG, G. B., GUILMINEAU, E., P.QUETHEY & WACKERS, J. September 2016 2016. Local and global assessment of the flow around the japan bulk carrier with and without energy saving devices at model and full scale. 31st Symposium on Naval Hydrodynamics Monterey, California.
- VON DER STEIN, N. 1996. 12 jahre schneekluth-zuströmdüse. *HANSA*, no. 7.
- WACKERS, J., KOREN, B., RAVEN, H. C., VAN DER PLOEG, A., STARKE, A. R., DENG, G. B., QUEUTEY, P., VISONNEAU, M., HINO, T. & OHASHI, K. 2011. Free-surface viscous flow solution methods for ship hydrodynamics. *Archives of Computational Methods in Engineering*, 18, 1-41.
- WALD, Q. June 1965. Performance of a propeller in a wake and the interaction of propeller and hull. *Journal of Ship Research*.
- WALLIN, S. & JOHANSSON, A. V. 2000. An explicit algebraic reynolds stress model for incompressible and compressible turbulent flows. *Journal of Fluid Mechanics*, 403, 89-132.
- WANG, H.-H. & DEPARTMENT, M. I. T. 1985. *Hub effects in propeller design and analyses*. PhD, Massachusetts Inst. of Tech. Cambridge Dept. of Ocean Engineering.

- WANG, J., YU, H., ZHANG, Y. & CAI, R. 2010. Numerical simulation of viscous wake field and resistance prediction around slow-full ships. *Chinese Journal of Hydrodynamics*, 25, 648-654.
- WANG, Z.-Z., XIONG, Y., WANG, R., SHEN, X.-R. & ZHONG, C.-H. 2015. Numerical study on scale effect of nominal wake of single screw ship. *Ocean Engineering*, 104, 437-451.
- WANG, Z., YANG, J., KOO, B. & STERN, F. 2009. A coupled level set and volume-of-fluid method for sharp interface simulation of plunging breaking waves. *International Journal of Multiphase Flow*, 35, 227-246.
- WIGLEY, W. 1935. Ship wave-resistance. Progress since 1930. *Trans. Inst. Nav. Architects*, 77, 223-236.
- WILCOX, D. 1998. *Turbulence modelling for cfd*, La Canada, California, DCW Industries Inc.
- WILSON, R., JI, L., KARMAN, S., HYAMS, D., SREENIVAS, K., TAYLOR, L. & WHITFIELD, D. 2008. Simulation of large amplitude ship motions for prediction of fluid-structure interaction. Proceedings of the 27th Symposium on Naval Hydrodynamics, ONR, Seoul.
- YANG, J. & STERN, F. 2009. Sharp interface immersed-boundary/level-set method for wave-body interactions. *Journal of Computational Physics*, 228, 6590-6616.
- YANG, X.-S. 2014. *Nature-inspired optimization algorithms*, Elsevier.
- ZHANG, P., ZHU, D. X. & LENG, W. H. 2008. Parametric approach to design of hull forms. *Journal of Hydrodynamics*, 20, 804-810.
- ZHANG, Z.-R. 2010. Verification and validation for rans simulation of kes container ship without/with propeller. *Journal of Hydrodynamics, Ser. B*, 22, 932-939.
- ZONDERVAN, G., HOLTROP, J., WINDT, J. & TERWISGA, T. V. 2011. On the design and analysis of preswirl stators for single and twin screw ships. Second International Symposium on Marine Propulsors Hamburg, Germany. Potsdam Germany Potsdam Model Basin SVA.

Research Outputs

The following publications were generated throughout the timespan of the PhD studies related to this thesis.

Journal Papers

1. **MIZZI, K.**, DEMIREL, Y. K., BANKS, C., TURAN, O., KAKLIS, P. & ATLAR, M. 2017. Design optimisation of Propeller Boss Cap Fins for enhanced propeller performance. *Applied Ocean Research*, 62, 210-222.
2. MAASCH, M., **MIZZI, K.**, ATLAR, M., FITZSIMMONS, P. & TURAN, O. 2019. A generic wake analysis tool and its application to the Japan Bulk Carrier test case. *Ocean Engineering*, 171, 575-589.

Conference Papers

1. **MIZZI, K.**, KIM, M., TURAN, O. & KAKLIS, P. 2015. Issues with energy saving devices and the way forward. *Shipping in Changing Climates*. Glasgow.
2. **MIZZI, K.**, DEMIREL, Y.K., BANKS, C., TURAN, O., KAKLIS, P., 2014. PBCF design optimisation and propulsion efficiency impact. In: *Proceedings of the International Conference on Influence of EEDI on Ship Design*, RINA, 24 – 25 September 2014. London, UK.
3. **MIZZI, K.**, KELLETT P., DEMIREL, Y.K., MARTIN, R., TURAN, O., 2015. HPC and CFD in the marine industry: past, present and future. In: *Proceedings of Exascale Applications and Software Conference (EASC 2015)*, 21 – 23 April 2015. Edinburgh, UK.
4. KELLETT, P., **MIZZI, K.**, DEMIREL, Y. K. & TURAN, O. Investigating the Roughness Effect of Biofouling on Propeller Performance. *Shipping in Changing Climates*, 2015 Glasgow.